THREE-DIMENSIONAL FINITE ELEMENT ANALYSIS OF END-BEARING PILE GROUPS FOR NEGATIVE SKIN FRICTION ESTIMATION

A THESIS SUBMITTED TO
THE GRADUATE SCHOOL OF NATURAL AND APPLIED SCIENCES
OF
MIDDLE EAST TECHNICAL UNIVERSITY

BY

MEHMET İLÇİOĞLU

IN PARTIAL FULFILLMENT OF THE REQUIREMENTS
FOR
THE DEGREE OF MASTER OF SCIENCE
IN
CIVIL ENGINEERING

DECEMBER 2023

Approval of the thesis:

THREE-DIMENSIONAL FINITE ELEMENT ANALYSIS OF END-BEARING PILE GROUPS FOR NEGATIVE SKIN FRICTION ESTIMATION

submitted by **MEHMET İLÇİOĞLU** in partial fulfillment of the requirements for the degree of **Master of Science** i**n Civil Engineering, Middle East Technical University** by,

Prof. Dr. Halil Kalıpçılar
Dean, Graduate School of **Natural and Applied Sciences** _____

Prof. Dr. Erdem Canbay
Head of the Department, **Civil Engineering** _____

Assoc. Prof. Dr. Nabi Kartal Toker
Supervisor, **Civil Engineering, METU** _____

Examining Committee Members:

Prof. Dr. Erdal Çokça
Civil Engineering, METU _____

Assoc. Prof. Dr. Nabi Kartal Toker
Civil Engineering, METU _____

Prof. Dr. Kemal Önder Çetin
Civil Engineering, METU _____

Assoc. Prof. Dr. Nejan Huvaj Sarıhan
Civil Engineering, METU _____

Assoc. Prof. Dr. Cem Akgüner
Civil Engineering, TED University _____

Date: 11.12.2023

I hereby declare that all information in this document has been obtained and presented in accordance with academic rules and ethical conduct. I also declare that, as required by these rules and conduct, I have fully cited and referenced all material and results that are not original to this work.

Name Last name : Mehmet İlçioğlu

Signature :

ABSTRACT

THREE-DIMENSIONAL FINITE ELEMENT ANALYSIS OF END-BEARING PILE GROUPS FOR NEGATIVE SKIN FRICTION ESTIMATION

İlçioğlu, Mehmet
Master of Science, Civil Engineering
Supervisor: Assoc. Prof. Dr. Nabi Kartal Toker

December 2023, 193 pages

Negative skin friction (NSF) is a phenomenon which occurs when soil surrounding the piles settles more than piles due to consolidation. NSF may result in dragload and engineering problems such as: differential settlements, damage on the piles and foundation failure.

The conventional analytical methods assume that NSF fully mobilizes above a neutral plane where settlement in the pile and soil are equal; leading to overestimation of dragload. Although there are numerous studies in the literature to investigate the behavior of single piles under the influence of NSF, there are very limited investigations on the behavior of pile groups and more specifically end-bearing pile groups. The presence of adjacent piles complicates the evaluation of the effects of soil-pile interaction.

In this study a 3D finite element analysis (FEA) is initially conducted on a single pile based on a reference case study and model is validated against field measurements. Further FEA were performed to conduct parametric studies on pile and soil properties to understand the magnitude and distribution of NSF, dragload and the

influence of group effect. The results of FEA were compared with a conventional analytical method and tributary area method. Finally, a new equation is proposed for accurate predictions of the NSF without a need to perform FEA during challenging and rushed working conditions in the industry.

Keywords: Negative Skin Friction, Pile Groups, 3D Finite Element Analysis, End Bearing Piles

ÖZ

ÜÇ BOYUTLU SONLU ELEMANLAR ANALİZİ İLE UÇ TAŞIYICI KAZIK GRUPLARINDA NEGATİF ÇEPER SÜRTÜNMESİNİN HESAPLANMASI

İlçioğlu, Mehmet
Yüksek Lisans, İnşaat Mühendisliği
Tez Yöneticisi: Doç. Dr. Nabi Kartal Toker

Aralık 2023, 193 sayfa

Negatif çeper sürtünmesi (NÇS), konsolidasyon nedeniyle kazıkların etrafındaki toprağın kazıklardan daha fazla oturması durumunda ortaya çıkan bir olgudur. NÇS, çekme yükü, farklı oturmalar, kazıklarda hasar ve temel çökmesi gibi mühendislik sorunlarına neden olabilir.

Geleneksel analitik yöntemler, NÇS'nin nötr düzlem üstünde tamamen mobilize olduğunu varsayar, bu da çekiş yüklerinin fazla hesaplanmasına yol açar. Literatürde tekil kazıkların NÇS etkisi altındaki davranışlarını inceleyen çok sayıda çalışma bulunmasına rağmen, kazık gruplarının ve daha spesifik olarak uç taşıyıcı kazık gruplarının davranışları üzerine çok sınırlı sayıda araştırma bulunmaktadır. Yanal kazıkların varlığı nedeniyle, kazık gruplarında zemin-kazık etkileşiminin etkilerinin değerlendirilmesi, tekli kazıklara göre daha karmaşıktır.

Bu çalışmada, referans vaka çalışmasına dayalı olarak ilk olarak tekil bir kazık üzerinde 3 boyutlu sonlu elemanlar analizi (SEA) gerçekleştirilmiş ve model, saha ölçümlerine ile doğrulanmıştır. NÇS'nin büyüklüğünü ve dağılımını, sürükleme yüklerini ve grup etkisinin etkisini anlamak amacıyla kazık ve zemin özellikleri

üzerinde parametrik çalışmalar yürütmek için daha fazla SEA yapılmıştır. SEA'nın sonuçları geleneksel analitik yöntemle ve bağımlı alan yöntemiyle karşılaştırılmıştır. Son olarak, endüstrideki zorlu ve aceleci çalışma koşulları sırasında SEA yapmaya gerek kalmadan NÇS'nin daha iyi tahmin edilmesi için yeni bir denklem önerilmiştir.

Anahtar Kelimeler: Negatif Çeper Sürtünmesi, Kazık Grupları, 3B Sonlu Elemanlar Analizi, Uç Taşıyıcı Kazıklar

To My Wife and My Family

ACKNOWLEDGMENTS

First and foremost, I express my deepest gratitude to my esteemed advisor, Dr. Kartal Toker, whose expertise and passion for research have been an inexhaustible source of inspiration. Dr. Toker's invaluable insights, constructive feedback, and patient mentorship have significantly enriched my understanding of the subject matter and elevated the quality of this work. I am truly fortunate to have had the privilege of learning from such an accomplished scholar and mentor.

I am also immensely thankful to my mentor, Ramtin Hosseini-Kamal, for his pivotal role in granting me the opportunity to pursue this thesis. His unwavering belief in my potential and continuous support have been essential in balancing work responsibilities with academic pursuits. I am grateful for his understanding and encouragement throughout this demanding endeavor.

To my dearest wife, Duygu Tuysuz, I am profoundly thankful for her unwavering support, patience, and understanding throughout this challenging journey. Her boundless love, and constant encouragement have been my rock during moments of doubt and fatigue. I couldn't have asked for a more loving and understanding partner, and I dedicate this accomplishment to her unwavering presence in my life.

I must also acknowledge the support and encouragement from my family, friends, and colleagues who have cheered me on every step of the way. Their belief in my abilities has been a constant source of motivation and joy, and for that, I am eternally grateful.

Finally, I wish to express my gratitude to the University and all the faculty members who have contributed to my academic development. The enriching educational environment at the university has been crucial in nurturing my passion for research and fostering my intellectual curiosity.

TABLE OF CONTENTS

ABSTRACT v

ÖZ vii

ACKNOWLEDGMENTS x

TABLE OF CONTENTS xi

LIST OF TABLES xv

LIST OF FIGURES xvii

LIST OF ABBREVIATIONS xxix

LIST OF SYMBOLS xxx

CHAPTERS

1 INTRODUCTION 1

2 LITERATURE REVIEW 5

2.1 Mechanism of Negative Skin Friction 6

2.2 Analytical and Empirical Methods for Analyzing Skin Friction 6

2.2.1 The α-method 7

2.2.2 The β-method 8

2.2.3 The λ-method 10

2.2.4 The ρ-method 10

2.2.5 Estimation from in-situ test results 11

2.2.6 Numerical methods 13

2.3 Tributary Area Concept 17

2.4 Negative Skin Friction on Pile Groups 18

2.4.1 Numerical analysis of pile groups subjected to negative skin friction 19

2.4.2 Experimental findings of pile groups subjected to negative skin friction 20
2.4.3 Field tests on pile groups subjected to negative skin friction 21
3 VALIDATION WITH A SINGLE PILE CASE STUDY 23
3.1 Numerical Modelling with PLAXIS 23
3.1.1 Pile modelling 24
3.2 Model Validation 26
3.2.1 Reference case study 26
3.2.2 FEM mesh and boundary conditions 27
3.2.3 Constitutive models and material properties 30
3.2.4 Comparison between field measurements and analysis results 36
4 3D SIMULATIONS OF END BEARING PILE GROUPS - RESULTS AND DISCUSSIONS 39
4.1 Analysis Framework 39
4.1.1 Soil parameters 42
4.1.2 Naming convention of the piles 43
4.1.3 Analysis procedure 44
4.2 Analysis Mechanism 45
4.3 Soil and Pile Settlements 45
4.4 Change of NSF and Neutral Point due to Foundation Loading 48
4.5 Parametric Analyses of NSF and Dragload 51
4.5.1 The effect of pile diameter 52
4.5.2 The effect of pile length 55
4.5.3 The effect of pile spacing 57
4.5.4 The effect of number of piles in a pile array 59

4.5.5 The effect of pile position in a pile array 61
4.5.6 The effect of soil compressibility 64
4.5.7 The effect of soil cohesion 65
4.5.8 The effect of soil friction angle 67
4.5.9 The effect of interface coefficient 69
4.6 Comparison of the Results with Analytical Estimations 72
4.7 Comparison of 3D Results with 2D Axisymmetric Simulation of Tributary Area Method 75
4.8 New Method for Predictions of NSF 77
5 CONCLUSION AND RECOMMENDATIONS 85
REFERENCES 89
APPENDICES
A. Pile and Soil Settlements 99
B. Change of NSF and Neutral Point due to Foundation Loading 101
C. The Effect of Pile Diameter 106
D. The Effect of Pile Length 116
E. The Effect of Pile Spacing 132
F. The Effect of Number of Piles in a Pile Array 136
G. The Effect of Pile Position in a Pile Array 143
H. The Effect of Soil Compressibility Factor 153
I. The Effect of Soil Cohesion 157
J. The Effect of Soil Friction Angle 161
K. The Effect of Interface Coefficient 165
L. Comparison of the Results with Analytical Estimations 169

M. Comparison of 3D Results with 2D Axisymmetric Simulation of Tributary Area Method 178

N. The New Suggested Method for Predictions of NSF 187

LIST OF TABLES

TABLES

Table 3.1 Model parameters used for the pile. 31
Table 3.2 Model parameters used for the fill material and sand layer (Adopted after Drbe et al. (2016) and Liu et al. (2012)). 33
Table 3.3 Model parameters used for the compressible clay layers (Adopted after Drbe et al. (2016) and Liu et al. (2012)). 36
Table 3.4 Difference between the field measurements and calculated values for skin friction and dragload. 38
Table 4.1 Soil parameters used for the compressible layer – Soft soil - Undrained A 42
Table 4.2 Soil parameters used for the fill layer and bearing stratum – Linear elastic perfectly plastic - Drained 42
Table 4.3 Soil parameters used for the piles – Linear elastic – Non-porous 43
Table 4.4 Investigated pile & pile group dimension parameters. 51
Table 4.5 Investigated soil parameters. 51
Table 4.6 Comparison of dragload forces for outer piles for three different pile diameters between the β-method and FEA results. 74
Table 4.7 Comparison of dragload forces for inner piles for three different pile diameters between the tributary area method and FEA results for 5x5 pile array, s/D=6, L/D=20 and surcharge load of 100kPa. 77
Table 4.8 Comparison of dragload forces for each pile position for three different pile diameters between the proposed method and FEA results. 83
Table A.1 Comparison of dragload forces for each pile position for three different pile diameters between the β-method and FEA results, 5x5 array, s/D=3 and surcharge load of 50kPa. 171

Table A.2 Comparison of dragload forces for each pile position for three different pile diameters between the β-method and FEA results, 5x5 array, s/D=3 and surcharge load of 100kPa. 174
Table A.3 Comparison of dragload forces for each pile position for three different pile diameters between the β-method and FEA results, 5x5 array, s/D=6 and surcharge load of 100kPa. 177
Table A.4 Comparison of dragload forces for each pile position for three different pile diameters between the tributary area method and FEA results, 5x5 array, s/D=3 and surcharge load of 50kPa..... 180
Table A.5 Comparison of dragload forces for each pile position for three different pile diameters between the tributary area method and FEA results, 5x5 array, s/D=3 and surcharge load of 100kPa..... 183
Table A.6 Comparison of dragload forces for each pile position for three different pile diameters between the tributary area method and FEA results, 5x5 array, s/D=6 and surcharge load of 50kPa..... 186
Table A.7 Comparison of dragload forces for each pile position for three different pile diameters between the suggested method and FEA results, 5x5 array, s/D=3 and surcharge load of 100kPa..... 190
Table A.8 Comparison of dragload forces for each pile position for three different pile diameters between the suggested method and FEA results, 5x5 array, s/D=6 and surcharge load of 50kPa..... 193

LIST OF FIGURES

FIGURES

Figure 2.1 Discretization of the soil-pile system into one-dimensional elements and the representation of typical nonlinear load-transfer curves (After Kim et al., 2018). 15
Figure 2.2 Example tributary area conceptual figure from a hexagonal pile pattern after Auvinet and Rodriguez (2017). 17
Figure 2.3 Example NSF scenario sketch for a 3x3 pile group connected with a cap. 18
Figure 3.1 Embankment, instrumented piles, and ground monitoring systems. (After Indraratna et al., 1992). 26
Figure 3.2 Local numbering and positioning of nodes and integration points of a 10-node tetrahedral element. 27
Figure 3.3 The reference case study, 3D half-model finite element mesh. 28
Figure 3.4 2D view of the model which shows the boundary conditions, soil layers and groundwater table level. 30
Figure 3.5 Stress-strain behavior of elastic perfectly plastic model. 32
Figure 3.6 Yield surface of linear elastic perfectly plastic model in principal stress state. 32
Figure 3.7 The relationship between volumetric strain and mean stress. 34
Figure 3.8 The yield surface of the Soft Soil model projected into the p'-q plane. 34
Figure 3.9 Visualization of the complete yield surface of the Soft Soil model in principal stress space. 35
Figure 3.10 Comparison of ground settlements between the present FEA study and field measurements after Indraratna et al., 1992 at 0.25m away from the pile. 36
Figure 3.11 a) Skin friction distribution, b) Dragload distribution between the present FEA study and measured results after Indraratna et al., 1992 along the pile shaft. 37
Figure 4.1 Example 3D-FEA mesh & boundary conditions for 5x5 pile array. 40

Figure 4.2 Example for boundary conditions sensitivity analysis for 5x5 array, D=1.0m, s/D=3, L/D=20. 41
Figure 4.3 Pile arrangement for 5x5 array. 43
Figure 4.4 Pile arrangement for 3x3 array. 44
Figure 4.5 Calculated pile and soil settlements from FEA where D=1.0m, s/D=3, L/D=20, surcharge load=50kPa, soil compressibility factor λ*=0.04. 46
Figure 4.6 Pile settlements for different pile locations. 47
Figure 4.7 Change of NSF and NP due to foundation loading for the 5x5 array, D=1m, s/D=6, L/D=20, surcharge load=50kPa – Pile A. 48
Figure 4.8 Negative skin friction at the mid depth of bearing stratum for (a) zero, (b) 25% and (c) 100% ultimate load on pile cap. 49
Figure 4.9 Comparison of superposed shear stresses with 25% ultimate foundation loading after consolidation for the 5x5 array, D=1m, s/D=6, L/D=20, surcharge load=50kPa – Pile A. 50
Figure 4.10 NSF and dragload of Pile A in three different diameter cases for model conditions of 5x5 array, L=15m, s/D=3 and surcharge load of 50kPa. 52
Figure 4.11 NSF and dragload of Pile C in three different diameter cases for model conditions of 5x5 array, L=15m, s/D=3 and surcharge load of 50kPa. 53
Figure 4.12 NSF and dragload of Pile A in three different diameter cases for model conditions of 5x5 array, L=15m, s=4.5m and surcharge load of 50kPa. 54
Figure 4.13 NSF and dragload of Pile C in three different diameter cases for model conditions of 5x5 array, L=15m, s=4.5m and surcharge load of 50kPa. 55
Figure 4.14 NSF and dragload of Pile A in three different length cases for model conditions of 5x5 array, D=0.6m, s/D=3 and surcharge load of 50kPa. 56
Figure 4.15 NSF and dragload of Pile F in three different length cases for model conditions of 5x5 array, D=0.6m, s/D=3 and surcharge load of 50kPa. 57
Figure 4.16 NSF and dragload of Pile A in three pile spacing cases for model conditions of D=1.5m, L/D=20 and surcharge load of 100kPa. 58
Figure 4.17 NSF and dragload of Pile E in three pile spacing cases for model conditions of D=1.5m, L/D=20 and surcharge load of 100kPa. 59

Figure 4.18 NSF and dragload of Pile A in two different pile arrays for model conditions of D=0.6m, s/D=3, L/D=20 and surcharge load of 50kPa. 60
Figure 4.19 NSF and dragload of Pile C in two different pile arrays for model conditions of D=0.6m, s/D=3, L/D=20 and surcharge load of 50kPa. 61
Figure 4.20 NSF and dragload of different pile positions for model conditions of D=0.6m, s/D=6, L/D=20 and surcharge load of 50kPa. 62
Figure 4.21 NSF and dragload of different pile positions for model conditions of D=0.6m, s/D=6, L/D=20 and surcharge load of 100kPa. 63
Figure 4.22 NSF and dragload of three different soil compressibility factors of Pile B for D=1.0m, s/D=3, L/D=20 and surcharge load of 50kPa. 64
Figure 4.23 NSF and dragload of three different soil compressibility factors of Pile E for D=1.0m, s/D=3, L/D=20 and surcharge load of 50kPa. 65
Figure 4.24 NSF and dragload of three different soil cohesion of Pile B for model conditions of D=1.0m, s/D=3, L/D=20 and surcharge load of 50kPa. 66
Figure 4.25 NSF and dragload of three different soil cohesion of Pile C for model conditions of D=1.0m, s/D=3, L/D=20 and surcharge load of 50kPa. 67
Figure 4.26 NSF and dragload of three different soil friction angles of Pile A for model conditions of D=1.0m, s/D=3, L/D=20 and surcharge load of 50kPa. 68
Figure 4.27 NSF and dragload of three different soil friction angles of Pile E for model conditions of D=1.0m, s/D=3, L/D=20 and surcharge load of 50kPa. 69
Figure 4.28 NSF and dragload of three different pile-soil interface coefficient of Pile A for D=1.0m, s/D=3, L/D=20 and surcharge load of 50kPa. 70
Figure 4.29 NSF and dragload of three different pile-soil interface coefficient of Pile E for D=1.0m, s/D=3, L/D=20 and surcharge load of 50kPa. 71
Figure 4.30 Comparison of the NSF between FEA and the β-method for 5x5 pile array, s/D=6, L/D=20 and surcharge load of 50kPa – Pile A. 72
Figure 4.31 Comparison of the NSF between FEA and the β-method for 5x5 pile array, s/D=6, L/D=20 and surcharge load of 50kPa – Pile B. 73
Figure 4.32 Comparison of the NSF between FEA and the β-method for 5x5 pile array, s/D=6, L/D=20 and surcharge load of 50kPa – Pile D. 73

Figure 4.33 Comparison of the NSF between 3D FEA and 2D axisymmetric tributary area, 5x5 pile array, s/D=6, L/D=20 and surcharge load of 100kPa – Pile C. 75
Figure 4.34 Comparison of the NSF between 3D FEA and 2D axisymmetric tributary area, 5x5 pile array, s/D=6, L/D=20 and surcharge load of 100kPa – Pile E. 76
Figure 4.35 Comparison of the NSF between 3D FEA and 2D axisymmetric tributary area, 5x5 pile array, s/D=6, L/D=20 and surcharge load of 100kPa – Pile F. 76
Figure 4.36 Partial pile position coefficients for each pile in 5x5 array. 79
Figure 4.37 Comparison of NSF between the proposed method and FEA results for three different pile diameters – Pile A, 5x5 array, s/D=3 and surcharge load of 50kPa. 80
Figure 4.38 Comparison of NSF between the proposed method and FEA results for three different pile diameters – Pile B, 5x5 array, s/D=3 and surcharge load of 50kPa. 80
Figure 4.39 Comparison of NSF between the proposed method and FEA results for three different pile diameters – Pile C, 5x5 array, s/D=3 and surcharge load of 50kPa. 81
Figure 4.40 Comparison of NSF between the proposed method and FEA results for three different pile diameters – Pile D, 5x5 array, s/D=3 and surcharge load of 50kPa. 81
Figure 4.41 Comparison of NSF between the proposed method and FEA results for three different pile diameters – Pile E, 5x5 array, s/D=3 and surcharge load of 50kPa. 82
Figure 4.42 Comparison of NSF between the proposed method and FEA results for three different pile diameters – Pile F, 5x5 array, s/D=3 and surcharge load of 50kPa. 82
Figure A.1 Calculated pile and soil settlements from FEA where D=1.0m, s/D=3, L/D=20, surcharge load=50kPa, soil compressibility factor λ*=0.07. 99

Figure A.2 Calculated pile and soil settlements from FEA where D=1.0m, s/D=3, L/D=20, surcharge load=50kPa, soil compressibility factor λ*=0.10. 100
Figure A.3 Change of NSF and NP due to foundation loading for the 5x5 array, D=1m, s/D=6, L/D=20, surcharge load=50kPa – Pile B. 101
Figure A.4 Change of NSF and NP due to foundation loading for the 5x5 array, D=1m, s/D=6, L/D=20, surcharge load=50kPa – Pile C. 102
Figure A.5 Change of NSF and NP due to foundation loading for the 5x5 array, D=1m, s/D=6, L/D=20, surcharge load=50kPa – Pile D. 103
Figure A.6 Change of NSF and NP due to foundation loading for the 5x5 array, D=1m, s/D=6, L/D=20, surcharge load=50kPa – Pile E. 104
Figure A.7 Change of NSF and NP due to foundation loading for the 5x5 array, D=1m, s/D=6, L/D=20, surcharge load=50kPa – Pile F. 105
Figure A.8 NSF and dragload of Pile B in three different diameter cases for model conditions of 5x5 array, L=15m, s/D=3 and surcharge load of 50kPa. 106
Figure A.9 NSF and dragload of Pile D in three different diameter cases for model conditions of 5x5 array, L=15m, s/D=3 and surcharge load of 50kPa. 107
Figure A.10 NSF and dragload of Pile E in three different diameter cases for model conditions of 5x5 array, L=15m, s/D=3 and surcharge load of 50kPa. 108
Figure A.11 NSF and dragload of Pile F in three different diameter cases for model conditions of 5x5 array, L=15m, s/D=3 and surcharge load of 50kPa. 109
Figure A.12 NSF and dragload of Pile A in three different diameter cases for model conditions of 5x5 array, L=12m, s/D=6 and surcharge load of 100kPa. 110
Figure A.13 NSF and dragload of Pile B in three different diameter cases for model conditions of 5x5 array, L=12m, s/D=6 and surcharge load of 100kPa. 111
Figure A.14 NSF and dragload of Pile C in three different diameter cases for model conditions of 5x5 array, L=12m, s/D=6 and surcharge load of 100kPa. 112
Figure A.15 NSF and dragload of Pile D in three different diameter cases for model conditions of 5x5 array, L=12m, s/D=6 and surcharge load of 100kPa. 113
Figure A.16 NSF and dragload of Pile E in three different diameter cases for model conditions of 5x5 array, L=12m, s/D=6 and surcharge load of 100kPa. 114

Figure A.17 NSF and dragload of Pile F in three different diameter cases for model conditions of 5x5 array, L=12m, s/D=6 and surcharge load of 100kPa. 115
Figure A.18 NSF and dragload of Pile B in three different length cases for model conditions of 5x5 array, D=0.6m, s/D=3 and surcharge load of 50kPa. 116
Figure A.19 NSF and dragload of Pile C in three different length cases for model conditions of 5x5 array, D=0.6m, s/D=3 and surcharge load of 50kPa. 117
Figure A.20 NSF and dragload of Pile D in three different length cases for model conditions of 5x5 array, D=0.6m, s/D=3 and surcharge load of 50kPa. 118
Figure A.21 NSF and dragload of Pile E in three different length cases for model conditions of 5x5 array, D=0.6m, s/D=3 and surcharge load of 50kPa. 119
Figure A.22 NSF and dragload of Pile A in three different length cases for model conditions of 5x5 array, D=1.0m, s/D=3 and surcharge load of 50kPa. 120
Figure A.23 NSF and dragload of Pile B in three different length cases for model conditions of 5x5 array, D=1.0m, s/D=3 and surcharge load of 50kPa. 121
Figure A.24 NSF and dragload of Pile C in three different length cases for model conditions of 5x5 array, D=1.0m, s/D=3 and surcharge load of 50kPa. 122
Figure A.25 NSF and dragload of Pile D in three different length cases for model conditions of 5x5 array, D=1.0m, s/D=3 and surcharge load of 50kPa. 123
Figure A.26 NSF and dragload of Pile E in three different length cases for model conditions of 5x5 array, D=1.0m, s/D=3 and surcharge load of 50kPa. 124
Figure A.27 NSF and dragload of Pile F in three different length cases for model conditions of 5x5 array, D=1.0m, s/D=3 and surcharge load of 50kPa. 125
Figure A.28 NSF and dragload of Pile A in three different length cases for model conditions of 5x5 array, D=1.5m, s/D=3 and surcharge load of 50kPa. 126
Figure A.29 NSF and dragload of Pile B in three different length cases for model conditions of 5x5 array, D=1.5m, s/D=3 and surcharge load of 50kPa. 127
Figure A.30 NSF and dragload of Pile C in three different length cases for model conditions of 5x5 array, D=1.5m, s/D=3 and surcharge load of 50kPa. 128
Figure A.31 NSF and dragload of Pile D in three different length cases for model conditions of 5x5 array, D=1.5m, s/D=3 and surcharge load of 50kPa. 129

Figure A.32 NSF and dragload of Pile E in three different length cases for model conditions of 5x5 array, D=1.5m, s/D=3 and surcharge load of 50kPa. 130
Figure A.33 NSF and dragload of Pile F in three different length cases for model conditions of 5x5 array, D=1.5m, s/D=3 and surcharge load of 50kPa. 131
Figure A.34 NSF and dragload of Pile B in three pile spacing cases for model conditions of D=1.5m, L/D=20 and surcharge load of 100kPa. 132
Figure A.35 NSF and dragload of Pile C in three pile spacing cases for model conditions of D=1.5m, L/D=20 and surcharge load of 100kPa. 133
Figure A.36 NSF and dragload of Pile D in three pile spacing cases for model conditions of D=1.5m, L/D=20 and surcharge load of 100kPa. 134
Figure A.37 NSF and dragload of Pile F in three pile spacing cases for model conditions of D=1.5m, L/D=20 and surcharge load of 100kPa. 135
Figure A.38 NSF and dragload of Pile B in two different pile arrays for model conditions of D=0.6m, s/D=3, L/D=20 and surcharge load of 50kPa. 136
Figure A.39 NSF and dragload of Pile A in two different pile arrays for model conditions of D=1.0m, s/D=3, L/D=20 and surcharge load of 100kPa. 137
Figure A.40 NSF and dragload of Pile B in two different pile arrays for model conditions of D=1.0m, s/D=3, L/D=20 and surcharge load of 100kPa. 138
Figure A.41 NSF and dragload of Pile C in two different pile arrays for model conditions of D=1.0m, s/D=3, L/D=20 and surcharge load of 100kPa. 139
Figure A.42 NSF and dragload of Pile A in two different pile arrays for model conditions of D=1.5m, s/D=6, L/D=20 and surcharge load of 50kPa. 140
Figure A.43 NSF and dragload of Pile B in two different pile arrays for model conditions of D=1.5m, s/D=6, L/D=20 and surcharge load of 50kPa. 141
Figure A.44 NSF and dragload of Pile C in two different pile arrays for model conditions of D=1.5m, s/D=6, L/D=20 and surcharge load of 50kPa. 142
Figure A.45 NSF and dragload of different pile positions for model conditions of D=0.6m, s/D=3, L/D=20 and surcharge load of 50kPa. 143
Figure A.46 NSF and dragload of different pile positions for model conditions of D=0.6m, s/D=3, L/D=20 and surcharge load of 100kPa. 144

Figure A.47 NSF and dragload of different pile positions for model conditions of D=1.0m, s/D=3, L/D=20 and surcharge load of 50kPa. 145
Figure A.48 NSF and dragload of different pile positions for model conditions of D=1.0m, s/D=3, L/D=20 and surcharge load of 100kPa. 146
Figure A.49 NSF and dragload of different pile positions for model conditions of D=1.5m, s/D=3, L/D=20 and surcharge load of 50kPa. 147
Figure A.50 NSF and dragload of different pile positions for model conditions of D=1.5m, s/D=3, L/D=20 and surcharge load of 100kPa. 148
Figure A.51 NSF and dragload of different pile positions for model conditions of D=1.0m, s/D=6, L/D=20 and surcharge load of 50kPa. 149
Figure A.52 NSF and dragload of different pile positions for model conditions of D=1.0m, s/D=6, L/D=20 and surcharge load of 100kPa. 150
Figure A.53 NSF and dragload of different pile positions for model conditions of D=1.5m, s/D=6, L/D=20 and surcharge load of 50kPa. 151
Figure A.54 NSF and dragload of different pile positions for model conditions of D=1.5m, s/D=6, L/D=20 and surcharge load of 100kPa. 152
Figure A.55 NSF and dragload of three different soil compressibility factors of Pile A for model conditions of D=1.0m, s/D=3, L/D=20 and surcharge load of 50kPa. 153
Figure A.56 NSF and dragload of three different soil compressibility factors of Pile C for model conditions of D=1.0m, s/D=3, L/D=20 and surcharge load of 50kPa. 154
Figure A.57 NSF and dragload of three different soil compressibility factors of Pile D for model conditions of D=1.0m, s/D=3, L/D=20 and surcharge load of 50kPa. 155
Figure A.58 NSF and dragload of three different soil compressibility factors of Pile F for model conditions of D=1.0m, s/D=3, L/D=20 and surcharge load of 50kPa. 156
Figure A.59 NSF and dragload of three different soil cohesion of Pile A for model conditions of D=1.0m, s/D=3, L/D=20 and surcharge load of 50kPa. 157

Figure A.60 NSF and dragload of three different soil cohesion of Pile D for model conditions of D=1.0m, s/D=3, L/D=20 and surcharge load of 50kPa. 158
Figure A.61 NSF and dragload of three different soil cohesion of Pile E for model conditions of D=1.0m, s/D=3, L/D=20 and surcharge load of 50kPa. 159
Figure A.62 NSF and dragload of three different soil cohesion of Pile F for model conditions of D=1.0m, s/D=3, L/D=20 and surcharge load of 50kPa. 160
Figure A.63 NSF and dragload of three different soil friction angles of Pile B for model conditions of D=1.0m, s/D=3, L/D=20 and surcharge load of 50kPa. 161
Figure A.64 NSF and dragload of three different soil friction angles of Pile C for model conditions of D=1.0m, s/D=3, L/D=20 and surcharge load of 50kPa. 162
Figure A.65 NSF and dragload of three different soil friction angles of Pile D for model conditions of D=1.0m, s/D=3, L/D=20 and surcharge load of 50kPa. 163
Figure A.66 NSF and dragload of three different soil friction angles of Pile F for model conditions of D=1.0m, s/D=3, L/D=20 and surcharge load of 50kPa. 164
Figure A.67 NSF and dragload of three different pile-soil interface coefficients of Pile B for model conditions of D=1.0m, s/D=3, L/D=20 and surcharge load of 50kPa..... 165
Figure A.68 NSF and dragload of three different pile-soil interface coefficients of Pile C for model conditions of D=1.0m, s/D=3, L/D=20 and surcharge load of 50kPa..... 166
Figure A.69 NSF and dragload of three different pile-soil interface coefficients of Pile D for model conditions of D=1.0m, s/D=3, L/D=20 and surcharge load of 50kPa..... 167
Figure A.70 NSF and dragload of three different pile-soil interface coefficients of Pile F for model conditions of D=1.0m, s/D=3, L/D=20 and surcharge load of 50kPa..... 168
Figure A.71 Comparison of the NSF between FEA and the β-method for 5x5 pile array, s/D=3, L/D=20 and surcharge load of 50kPa – Pile A. 169
Figure A.72 Comparison of the NSF between FEA and the β-method for 5x5 pile array, s/D=3, L/D=20 and surcharge load of 50kPa – Pile B. 170

Figure A.73 Comparison of the NSF between FEA and the β-method for 5x5 pile array, s/D=3, L/D=20 and surcharge load of 50kPa – Pile D. 171
Figure A.74 Comparison of the NSF between FEA and the β-method for 5x5 pile array, s/D=3, L/D=20 and surcharge load of 100kPa – Pile A. 172
Figure A.75 Comparison of the NSF between FEA and the β-method for 5x5 pile array, s/D=3, L/D=20 and surcharge load of 100kPa – Pile B. 173
Figure A.76 Comparison of the NSF between FEA and the β-method for 5x5 pile array, s/D=3, L/D=20 and surcharge load of 100kPa – Pile D. 174
Figure A.77 Comparison of the NSF between FEA and the β-method for 5x5 pile array, s/D=6, L/D=20 and surcharge load of 100kPa – Pile A. 175
Figure A.78 Comparison of the NSF between FEA and the β-method for 5x5 pile array, s/D=6, L/D=20 and surcharge load of 100kPa – Pile B. 176
Figure A.79 Comparison of the NSF between FEA and the β-method for 5x5 pile array, s/D=6, L/D=20 and surcharge load of 100kPa – Pile D. 177
Figure A.80 Comparison of the NSF between 3D FEA and 2D axisymmetric tributary area, 5x5 pile array, s/D=3, L/D=20 and surcharge load of 50kPa – Pile C. 178
Figure A.81 Comparison of the NSF between 3D FEA and 2D axisymmetric tributary area, 5x5 pile array, s/D=3, L/D=20 and surcharge load of 50kPa – Pile E. 179
Figure A.82 Comparison of the NSF between 3D FEA and 2D axisymmetric tributary area, 5x5 pile array, s/D=3, L/D=20 and surcharge load of 50kPa – Pile F. 180
Figure A.83 Comparison of the NSF between 3D FEA and 2D axisymmetric tributary area, 5x5 pile array, s/D=3, L/D=20 and surcharge load of 100kPa – Pile C. 181
Figure A.84 Comparison of the NSF between 3D FEA and 2D axisymmetric tributary area, 5x5 pile array, s/D=3, L/D=20 and surcharge load of 100kPa – Pile E. 182

Figure A.85 Comparison of the NSF between 3D FEA and 2D axisymmetric tributary area, 5x5 pile array, s/D=3, L/D=20 and surcharge load of 100kPa – Pile F. 183
Figure A.86 Comparison of the NSF between 3D FEA and 2D axisymmetric tributary area, 5x5 pile array, s/D=6, L/D=20 and surcharge load of 50kPa – Pile C. 184
Figure A.87 Comparison of the NSF between 3D FEA and 2D axisymmetric tributary area, 5x5 pile array, s/D=6, L/D=20 and surcharge load of 50kPa – Pile E. 185
Figure A.88 Comparison of the NSF between 3D FEA and 2D axisymmetric tributary area, 5x5 pile array, s/D=6, L/D=20 and surcharge load of 50kPa – Pile F. 186
Figure A.89 Comparison of NSF between the suggested method and FEA results for three different pile diameters -Pile A, 5x5 array, s/D=3 and surcharge load of 100kPa..... 187
Figure A.90 Comparison of NSF between the suggested method and FEA results for three different pile diameters -Pile B, 5x5 array, s/D=3 and surcharge load of 100kPa..... 187
Figure A.91 Comparison of NSF between the suggested method and FEA results for three different pile diameters -Pile C, 5x5 array, s/D=3 and surcharge load of 100kPa..... 188
Figure A.92 Comparison of NSF between the suggested method and FEA results for three different pile diameters -Pile D, 5x5 array, s/D=3 and surcharge load of 100kPa..... 188
Figure A.93 Comparison of NSF between the suggested method and FEA results for three different pile diameters -Pile E, 5x5 array, s/D=3 and surcharge load of 100kPa..... 189
Figure A.94 Comparison of NSF between the suggested method and FEA results for three different pile diameters -Pile F, 5x5 array, s/D=3 and surcharge load of 100kPa..... 189

Figure A.95 Comparison of NSF between the suggested method and FEA results for three different pile diameters - Pile A, 5x5 array, s/D=6 and surcharge load of 50kPa. 190
Figure A.96 Comparison of NSF between the suggested method and FEA results for three different pile diameters - Pile B, 5x5 array, s/D=6 and surcharge load of 50kPa. 191
Figure A.97 Comparison of NSF between the suggested method and FEA results for three different pile diameters - Pile C, 5x5 array, s/D=6 and surcharge load of 50kPa. 191
Figure A.98 Comparison of NSF between the suggested method and FEA results for three different pile diameters - Pile D, 5x5 array, s/D=6 and surcharge load of 50kPa. 192
Figure A.99 Comparison of NSF between the suggested method and FEA results for three different pile diameters - Pile E, 5x5 array, s/D=6 and surcharge load of 50kPa. 192
Figure A.100 Comparison of NSF between the suggested method and FEA results for three different pile diameters - Pile F, 5x5 array, s/D=6 and surcharge load of 50kPa. 193

LIST OF ABBREVIATIONS

ABBREVIATIONS

CPT: Cone penetration test

FEA: Finite element analysis

FEM: Finite element method

NSF: Negative skin friction

OCR: Overconsolidation ratio

PMT: Pressuremeter test

SPT: Standard penetration test

SSM: Soft soil model

LIST OF SYMBOLS

SYMBOLS

A: Cross sectional area

C_c: Compression index

C_s: Swelling index

c_u: Undrained shear strength

D: Pile diameter

e_0: Initial void ratio

E: Elasticity modulus

f_s: Unit skin friction

G: Shear modulus

K: Bulk modulus

K_0: Earth pressure coefficient at rest

k: Permeability coefficient

L: Pile length

q_c: Cone resistance

q_s: Sleeve friction

R: Interface coefficient

s: Pile spacing

S: Soil settlement

z_p: Pile settlement

α: Empirical coefficient for estimation of skin friction

β: Analytical coefficient for estimation of skin friction

γ: Unit weight

δ': Effective interface friction angle

κ^*: Modified swelling index

λ: Empirical coefficient for estimation of skin friction

λ^*: Modified compression index

ν_{ur}: Poisson's ratio for unloading / reloading

ρ: Analytical coefficient for estimation of skin friction

σ_v': Effective vertical stress

ϕ': Effective soil friction angle

ψ: Dilatancy angle

CHAPTER 1

INTRODUCTION

Pile foundations are essential elements in supporting various structures, ranging from buildings and bridges to offshore platforms. These deep foundation elements are designed to transfer structural loads from the superstructure to deeper, more stable layers of the soil. The fundamental principle involves the mobilization of friction along the pile shaft, partially offsetting the downward force exerted on the pile. Nevertheless, specific circumstances may engender a differential settlement between the surrounding soil and the pile shaft, leading to a phenomenon known as Negative Skin Friction (NSF).

Negative skin friction, also known as negative pile skin friction or downdrag, occurs when the surrounding soil settles more than the piles themselves. This phenomenon may arise due to consolidation causes such as the lowering of the piezometric head, fill placement, or dissipation of excess pore water pressure during pile installation (Davisson, 1962). The consequences of NSF can lead to time-dependent compressive forces (dragload) and excessive pile settlements (downdrag), resulting in engineering challenges such as differential settlements, pile damage, and potential foundation failure (Matlock, 1970; Coyle & Castello, 1981).

Early observations of NSF, notably in the coastal plains of the Netherlands, revealed that structures supported by piles through soft strata experienced excessive settling, particularly when thick fill layers were introduced prior to pile installation. Pioneering studies by Terzaghi and Peck in 1948 documented instances of NSF-induced pile downdrag settlement, underlining the pivotal role of NSF in foundation design.

While sporadic reports of pile failure due to NSF emerged in the early 20th century, concerted research efforts began in the 1960s, notably culminating in significant field tests presented at the 7th International Conference on Soil Mechanics and Foundation Engineering in 1969. Since then, extensive knowledge has been amassed from laboratory and field tests. However, despite significant strides, the intricate mechanics of NSF remain elusive, and design methodologies continue to rely on empirical approaches (Fellenius, 1998). In practice, piles rarely operate solely under the influence of dragload; they commonly support both external loads and dragload concurrently. Moreover, piles are typically installed in groups, interconnected by robust pile caps beneath loaded columns.

While significant research has focused on the behavior of individual piles under the influence of NSF, the performance of pile groups is a more complex and less explored area (Chow et al., 1998). Pile groups, especially those connected with a pile cap (fixed head), introduce additional complexities in the soil-pile interaction due to the presence of adjacent piles (Randolph, 2003). Therefore, a comprehensive understanding of the behavior of pile groups under the effects of NSF is essential for ensuring the safe and efficient design of such foundation systems.

Traditional analytical methods or tributary area method are used to assess piles and pile groups under NSF often involve simplifying assumptions that may lead to overestimation of dragloads and misinterpretation of actual behavior (Meyerhof, 1963). In recent years, advancements in numerical analysis techniques, particularly the use of Finite Element Analysis (FEA), have revolutionized geotechnical engineering practices. FEA provides a powerful tool to model complex soil-structure interactions and accurately predict the behavior of piles and pile groups subjected to negative skin friction (Leoni & Sassu, 2018).

The primary objective of this thesis is to investigate the behavior of piles and pile groups under the influence of negative skin friction using Three-Dimensional Finite Element Analysis (3D FEA). The research aims to analyze the effects of NSF on individual piles in a multi-layered soil profile, validate the 3D FEA results against

existing field observations, and extend the analysis to study pile groups connected with a pile cap. The study focuses on understanding the influence of various parameters, including soil stiffness, strength, ultimate skin friction, pile-soil interface stiffness, and pile configuration, on the behavior of pile groups subjected to NSF. Additionally, sensitivity analyses will be conducted to explore the effects of group interaction on downdrag settlements and dragloads.

This thesis aims to contribute to geotechnical engineering literature by providing a comprehensive investigation of the effects of negative skin friction on bored piles and pile groups. The findings will enhance the understanding of soil-pile interaction in complex geotechnical settings and facilitate the design of more efficient and resilient pile foundations. Moreover, the study will highlight the advantages of using Finite Element Analysis for accurate and reliable assessments, paving the way for its wider application in geotechnical engineering practice. By enhancing our understanding of pile behavior and the benefits of using 3D FEA, this thesis aims to offer efficient, and more economical foundation design practices in geotechnical engineering by developing a new proposed method.

CHAPTER 2

LITERATURE REVIEW

The geotechnical phenomenon of Negative Skin Friction (NSF) on piles and pile groups is pivotal for the stability and functionality of foundation systems. NSF arises when a pile is inserted through a layer of soft soil undergoing consolidation, situated above more stable underlying substrates. As the soft soil consolidates, its settlement surpasses that of the pile, which usually bears a vertical load from the superstructure. Consequently, instead of providing support, the consolidating soft soil exerts a downward pull on the pile, resulting in NSF. The implications of NSF on pile behavior are twofold. Firstly, it leads to an escalation in the maximum load borne by the pile shaft, potentially subjecting the pile material to excessive stress, particularly in severe cases. Secondly, NSF induces additional settlement in the pile due to the downward drag, which can significantly impact the functionality of the superstructure.

For the secure and efficient design of deep foundations, a thorough comprehension of how piles and pile groups respond to NSF is essential. This comprehensive literature review scrutinizes the existing body of research dedicated to NSF on piles and pile groups. This encompasses a detailed exploration of the fundamental mechanisms driving NSF, an examination of various analytical methodologies employed to study it, an assessment of the empirical and experimental investigations shedding light on its characteristics, and a critical evaluation of how different configurations of pile groups influence NSF behavior. By synthesizing the insights gleaned from this extensive body of research, this review seeks to provide a robust basis for the subsequent analysis and discussion of NSF behavior.

2.1 Mechanism of Negative Skin Friction

Negative skin friction occurs when the surrounding soil consolidates more than the piles, resulting in additional compressive forces and downdrag. Several mechanisms contribute to the development of NSF.

The consolidation process of soft soil can be attributed to three common triggers: (1) the dissipation of excess pore water pressure resulting from pile driving, as discussed by Fellenius (1972); (2) the reduction of piezometric heads, leading to an augmentation of effective stress within the soft clay, as examined by Endo (1969), Inoue (1977), Auvinet and Hanell (1981), Yen et al. (1989), and Lee et al. (1998); and (3) the application of additional load on the ground surface, as observed in case studies by Johanessan and Bjerrum (1965), Brand (1975), Bozozuk (1981), and Indraratna et al. (1992). Well-documented instances from real-world projects compellingly demonstrate that the resulting downward drag forces on piles can be of sufficient magnitude to lead to excessive settlement of the piles. This has been extensively observed in studies conducted by Brand (1975), Inoue (1977), and Jacob and Kenneth (1997). In severe cases, it may even culminate in structural failure of the piles due to excessive stress, as reported in cases discussed by Chellis (1961), Kog (1987), Kog (1990), and (Davisson, 1993).

2.2 Analytical and Empirical Methods for Analyzing Skin Friction

Various methods for estimating skin friction around piles exist, including analytical and empirical approaches. The α-method utilizes a undrained strength coefficient (α) to estimate shaft resistance, while the β-method considers effective stress parameters for more realistic predictions. The λ-method combines total and effective stress approaches, correlating skin-friction with undrained shear strength and vertical effective stress. The ρ-method provides a structured approach for moderately overconsolidated clays, employing the skin-friction ratio (ρ) analogous to undrained strength ratio. In-situ tests like CPT and Piezocone CPT offer valuable data for

estimating skin friction. Advanced soil models, such as the Soft Soil creep model, have also been explored for improved accuracy in estimation. These methods collectively aid geotechnical engineers in designing and analyzing pile foundations, considering the complex interactions between piles and surrounding soils.

2.2.1 The α-method

The α-method represents a fully empirical approach, and its formulation for the unit skin friction is provided in Equation (2.1).

$$f_s = \alpha . c_u \tag{2.1}$$

The α-method employs an adhesion factor (α) and undrained shear strength (c_u) in its formulation, where α typically varies between 0.3 to 1.0 for bored piles and between 1 to 1.5 for displacement piles, with the possibility of higher values in stiff clays (Kezdi & Rethati, 1988).

However, in spite of its straightforwardness, the α-method has faced criticism from researchers due to its inconsistency, particularly with regards to the extensive variability in α values. For instance, when scrutinizing a field test involving piles subjected to NSF, Bozozuk (1972) determined that there existed minimal to no correlation between the negative skin friction applied to the pile and the in-situ shear strength of the soil. Little (1989) obtained the α value from his previously mentioned laboratory model test through two distinct approaches: by utilizing the initial measured shear strength of the soil at the outset of each loading stage, and by employing the calculated value of the undrained shear strength pertinent to the evolving degree of consolidation. When predicated on a consistent initial undrained shear strength, the deduced α value exhibited a wide dispersion ranging from 0.27 to 2.13. Considering the altered shear strength due to consolidation led to the computation of an "adhesion value," namely the α value, within a much narrower range of 0.29 to 0.58.

The α-method for estimating negative skin friction on piles has certain limitations and drawbacks. One of the main handicaps of the α-method is its simplicity, as it relies on a single coefficient (α) to estimate the reduction in shaft resistance due to negative skin friction. This simplistic approach may not accurately capture the complex behavior of the soil-pile system under such conditions, especially when dealing with nonlinear soil behavior or layered soil profiles. The α-method assumes a linear relationship between the increase in excess pore water pressure along the pile shaft and the corresponding reduction in shaft resistance. However, in reality, the relationship may not be linear especially during consolidation, and the actual behavior of the soil-pile system could deviate significantly from the assumptions of the α-method.

Consequently, more rational approaches, such as the effective stress method (β-method), are preferable for estimating skin-friction (f_s) since they account for excess pore pressures during consolidation, as highlighted by Azzouz et al. (1990). These methods allow for the estimation of stresses and soil properties surrounding the pile throughout its different stages of service life.

2.2.2 The β-method

The effective stress method (β-method) was initially introduced by Johannessen and Bjerrum in 1965 as an analytical approach primarily suitable for cohesionless soils. In this method, the calculation of pile skin friction (f_s) relies on effective stress considerations, and the formula for the maximum skin friction is expressed as Equation (2.2) following Burland's work in 1973.

$$f_s = \beta . \sigma'_v \tag{2.2}$$

In this equation, σ'_v represents the vertical effective stress acting on the surrounding soil, while β is an empirical factor influenced by the characteristics of the neighboring soil. The value of the β-coefficient is determined by using the following soil properties: internal friction angle (ϕ'), interface friction angle (δ'), and the over

consolidation ratio (OCR) according to Fellenius in 2008, and the expression for β is given in Equation (2.3).

$$\beta = M.tan\phi'(1 - sin\phi').OCR^{0.5} \quad (2.3)$$

where $M = tan\delta'/tan\phi'$.

The β coefficient exhibits variability based on the soil type, ranging from 0.2 to 0.25 for clay, 0.25 to 0.35 for silt, and 0.35 to 0.50 for sand.

Unlike the α-method, the β-method takes into account effective stress parameters, which are critical in determining the soil strength under negative skin friction conditions. By directly considering the effective stresses, the β-method provides a more realistic and accurate approach for estimating the reduction in shaft resistance. This is particularly important when dealing with cohesionless soils, where the effective stress plays a significant role in determining the soil's shear strength.

Upon initial examination, it may seem that numerous factors contribute to the variability of the β value; however, this variability is not as extensive as the individual components might imply. Researchers worldwide have reported consistent and narrowly ranged values. For instance, Johannesson and Bjerrum (1965) documented a range of 0.18 to 0.23 for soft to medium-soft clay based on field tests conducted in the Harbor of Oslo. Garlanger (1974) suggested that β values for clays could be considered within the range of 0.20 to 0.25 based on test analyses. Leung et al. (2004) obtained an average β value of 0.25 from centrifuge model experiments. Burland (1973) proposed an upper limit of 0.25 for soft clay, and the NAVFAC foundation design manual (1982) recommends a range of 0.20 to 0.25 for clay.

Overall, the β-method's incorporation of effective stress parameters and its ability to account for soil strength based on effective stresses make it a more reliable and robust method for estimating negative skin friction compared to the simplistic assumptions of the α-method. Its analytical approach provides a better representation

of the complex behavior of the soil-pile system under negative skin friction conditions. Additionally, consolidation is drainage process where effective stress changes, that is what β-method makes the most suited analytical approach for estimations of NSF.

2.2.3 The λ-method

The λ-method is an integrated approach that combines elements of both total stress and effective stress methods. It establishes a correlation between the skin-friction (f_s) and the undrained shear strength (c_u) along with the vertical effective stress (σ'_v). It is an empirical method developed from pile load tests. It is mainly used in marine installations (driven piles) in overconsolidated clays according to the Bowles, 1997. The equation for the λ-method is:

$$f_s = \lambda(\sigma'_v + 2c_u) \tag{2.4}$$

In this method, the skin-friction (f_s) is related to the undrained shear strength (c_u) and the mid-height vertical effective stress of a soil layer (σ'_v). The coefficient λ is derived through regression analysis using data from numerous pile tests.

2.2.4 The ρ-method

The ρ-method, developed by Azzouz et al. (1990), is an effective approach for estimating skin friction on single, vertical, rigid, cylindrical, and driven floating piles in moderately overconsolidated clays with overconsolidation ratios (OCR) ranging from 1 to 4. Unlike the α-method, which lacks accuracy in accounting for pile installation effects and soil properties, the ρ-method overcomes these limitations by incorporating realistic assumptions regarding drainage during pile penetration and axial loading (Azzouz et al., 1990). The key concept in the ρ-method is the skin-friction ratio, which is analogous to the undrained strength ratio (c_u/σ'). Through regression analysis based on extensive pile tests, the ρ-coefficient is obtained,

enabling the accurate estimation of skin friction in moderately overconsolidated clays (Azzouz et al., 1990; Randolph et al., 2008). This empirical approach offers a structured and reliable means of analyzing and predicting skin friction behavior in friction piles under challenging soil conditions, making it valuable in geotechnical engineering practice.

2.2.5 Estimation from in-situ test results

2.2.5.1 Cone penetration test method

The Cone Penetration Test (CPT) is a widely used in-situ testing method for measuring the resistance of soil to penetration by a cone-shaped probe. The test provides valuable information on the soil's properties, including unit skin friction along the pile shaft.

Although various researchers have suggested different empirical methods, the most commonly used method by Bustamante and Gianeselli's (1982) approach for estimations of unit skin friction is given below.

$$f_s = q_c/\alpha_f \tag{2.5}$$

Where q_c is cone resistance and α_f is side friction correlation coefficient and it is a function of soil and pile type.

2.2.5.2 Standard penetration test method

Standard Penetration Test (SPT) is the most widely used field test all over the world. However, in the literature, there is no widely used method for estimating pile bearing capacity with SPT data in European practice. SPT and unit side friction (f_s) and tip resistance (q_p) estimation methods are available in the US and partly in the Japanese literature. SPT-N values generally used for the side friction estimations are the average of the values measured along the pile length.

Schmertmann (1975) has suggested different correlation coefficients for unit skin friction estimations of driven piles according to the different soil types. The values for cohesive soils range from 0.04 to 0.05 in tsf (tons per square foot).

2.2.5.3 Pressuremeter test method

The pressuremeter test is a method based on the principle that a cylindrical cell (probe) placed in a vertical position in a borehole applies a uniformly distributed radial pressure to the well wall with the help of a flexible membrane. This cell is connected to the measurement unit on the ground surface with a tube or cable, and during the experiment, the applied pressure and deformations on the well wall are recorded. Therefore, stresses and unit deformations applied to the ground can be measured simultaneously. Based on the measured stress-deformation relationship, soil behavior can be determined in many aspects by applying the cavity expansion theory, assuming that the soil behaves linearly, isotropicly and elastically - fully plastic. As it is known, PMT technology is in an advantageous position in this respect, since the stresses applied to the ground and the unit deformations occurring in the ground cannot be defined in most field experiments.

Pressuremeter technology was developed by French Engineer Louis Menard in 1955. The experimental technique began to be widely used all over the world after the adoption of the empirical basic design criteria proposed by Menard. Different pressuremeter models have been developed over time. PMT can be applied on almost all types of soil and rocks. Test results are mainly used in determining the strength and deformation modulus parameters of soils and in bearing capacity and settlement calculations in foundation design.

Bustamante and Doix (1985) have developed an empirical methodology for the estimations of unit skin friction for the piled foundations where the unit and ultimate limits of skin friction changes according to the pile & soil types and construction methods.

2.2.6 Numerical methods

Salas and Belzunce (1965) introduced theoretical solutions based on Elastic theory, which assumes soil behavior as a Boussinesq half-space. The approach did not consider pile compressibility.

Poulos and co-workers (1989) utilized a simplified boundary element approach. This method discretizes the pile into small segments while treating the soil as an elastic continuum at the pile-soil interface. The approach is limited to end-bearing piles and employs a "mirror-image" technique.

Several other researchers developed numerical methods to analyze skin friction on piles. These methods vary in their soil modeling techniques. For instance, Lim et al. (1993) used a discrete element approach, while Wong and Teh (1995) employed hyperbolic soil springs. Chow et al. (1996) combined subgrade reaction with elastic theory.

Some studies embraced three-dimensional finite element methods to analyze NSF on piles. Indraratna and Balasubramaniam (1993) used the CRISP code, incorporating undrained and Biot-coupled consolidation models. The way shear stress was distributed along the pile shaft directly correlated with how the soil-pile interface, modeled with thin layer elements, behaved. Jeong and Kim (1998) used ABAQUS to study group effects on piles, but neglected slip at the pile-soil interface. Lee et al. (2002, 2004) employed ABAQUS to analyze NSF on piles and downdrag settlement in consolidating soil. Soil slippage at the interface between the pile and the soil has emerged as the pivotal factor influencing the creation of dragload and subsequently, the group effect. The group effect is contingent not just on the arrangement of the pile group but also on the soil's slippage along the pile-soil interface, primarily regulated by their interface friction coefficient and the settlement of the soil. Comodromos and Bareka (2005) used FLAC3D, a 3D geotechnical software, to investigate the effects of construction sequence on NSF in pile groups. It was shown that in fixed-head friction pile groups, the collective dragload effect is

notably higher compared to free-head end-bearing pile groups. Additionally, it was observed that if the embankment is built before the application of the foundation working load, the impact of negative skin friction is notably reduced compared to the scenario where this sequence is reversed.

2.2.6.1 The Load-transfer method

The behavior of skin friction estimations of individual piles under external loading conditions are governed by the load-transfer mechanism. Various methods and models have been developed and investigated to understand and estimate the load transfer along the pile shaft. These methods play a vital role in designing safe and efficient pile foundations.

The load-transfer method, as proposed by Brown et al. (1987) and described by a differential Equation (2.6), is a versatile and efficient technique used to analyze the response of individual piles to external loads. This method is particularly suitable for situations involving nonlinear soil behavior or layered soil conditions. It represents the soil-pile interface using zero-length springs, with their load-deformation behavior described by either the skin-friction or T-z curve, as shown in Figure 2.1, providing nonlinear models of soil reaction concerning displacement (z). Similarly, at the pile's base, another zero-length spring is represented, defined by either the end-bearing or Q-z curve, capturing the behavior of the soil-pile interaction at the pile base.

$$EA\frac{d^2z_p}{dz^2} = P.f_s \tag{2.6}$$

In the load-transfer equation, z_p represents the displacement of the pile or shaft at a specific depth, A denotes the cross-sectional area of the pile, E is the elasticity modulus of the pile, P represents the pile perimeter, and f_s indicates the unit skin friction of the soil at that particular depth.

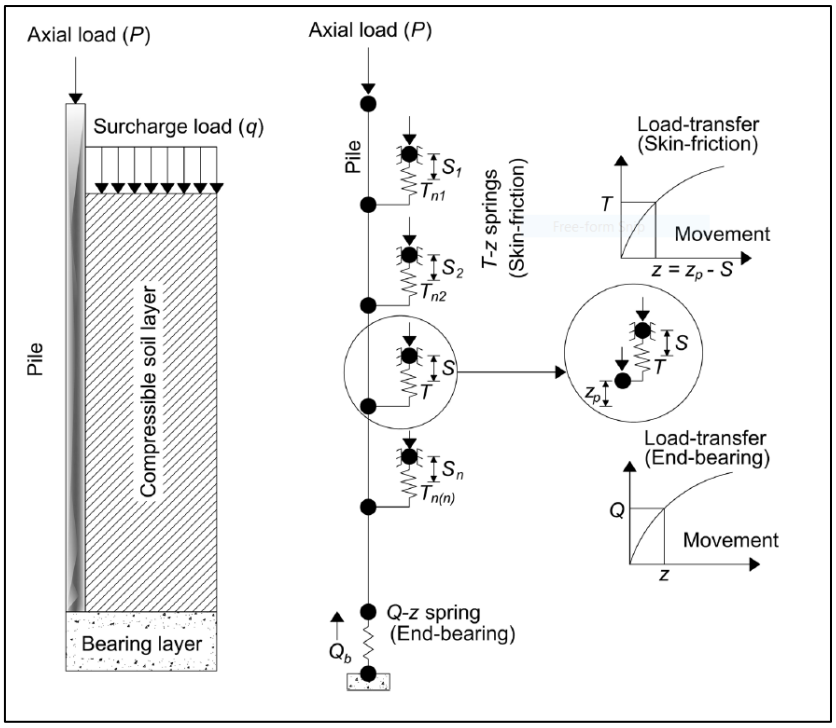

Figure 2.1 Discretization of the soil-pile system into one-dimensional elements and the representation of typical nonlinear load-transfer curves (After Kim et al., 2018).

The unit skin friction (f_s) in Equation (2.6) can be expressed as a function of the disparity between the settlements of the pile and the soil, denoted as z_p and S, respectively as shown in Equation (2.7).

$$f_s = f(z_p - S) \tag{2.7}$$

- ($S > z_p$), T=drag force
- ($S < z_p$), T=positive skin friction
- ($S = z_p$), T=0 (neutral plane)

Several researchers have investigated the load-transfer mechanism for pile skin friction using different methods and approaches. For instance, Vesic (1977) and Reese et al. (1974) proposed methods for estimating pile skin friction based on load-transfer curves obtained from field measurements and laboratory testing. Other researchers, such as Fellenius (1998), have developed methods using CPT data to estimate pile skin friction and other relevant soil parameters. Moreover,

Jamiolkowski et al. (1988) have explored the use of field load tests, both static and dynamic, to study pile load transfer behavior.

In summary, the load-transfer mechanism for pile skin friction is a complex phenomenon, and various methods, both empirical and analytical, have been developed to estimate pile skin friction based on soil-pile interaction characteristics. The three-dimensional pile model introduced by Kim et al. (2007) represents a significant advancement in accurately capturing the load transfer behavior, especially when lateral loads are involved. However, ongoing research and advancements in geotechnical engineering continue to improve our understanding of the load-transfer mechanism, leading to more reliable and efficient design practices for pile foundations.

2.2.6.2 Finite element method

Finite Element Method (FEM) represents progress beyond the load transfer method by enabling the incorporation of intrinsic soil properties into the models. The discretization of the soil-structure into elements facilitates modeling of complex problems, including intricate soil layering, geometry, and consolidation.

Due to the growing computational capabilities of modern computers and the widespread availability of advanced geotechnical software, the numerical analysis of NSF on piles has advanced significantly. This progression has transitioned from simplified methods developed in the 80s and 90s to the current utilization of 3-D Finite Element Method (FEM) simulations. This approach specifically addresses the inherently three-dimensional behavior of pile groups experiencing NSF. It incorporates sophisticated constitutive models to accurately represent the elasto-plastic behavior of soil, as well as the slip characteristics at the pile-soil interface.

2.3 Tributary Area Concept

The tributary area concept refers to the area of soil surrounding a pile that contributes to the development of NSF. When the soil settles due to consolidation, it imposes dragload on the adjacent piles. The tributary area concept helps estimate the zone of influence or the area of soil contributing to this dragload.

The tributary area concept serves as a fundamental method to estimate NSF distribution and dragload along the pile shaft. Schlosser et al. (1984) laid the theoretical foundation of this concept, highlighting its significance in understanding the distribution of NSF along pile shafts. The weight of fill within the tributary area serves as the upper limit for the dragload and analysis of one repeatable tributary cell may represents the inner piles. The size and shape of the tributary area may change according to the pile geometry, soil properties, magnitude of the settlement and pile pattern, but it can be considered as approximately circular with a radius equal to half of the pile spacing. Example tributary area conceptual figure from a hexagonal pile pattern after Auvinet and Rodriguez (2017) is presented in Figure 2.2.

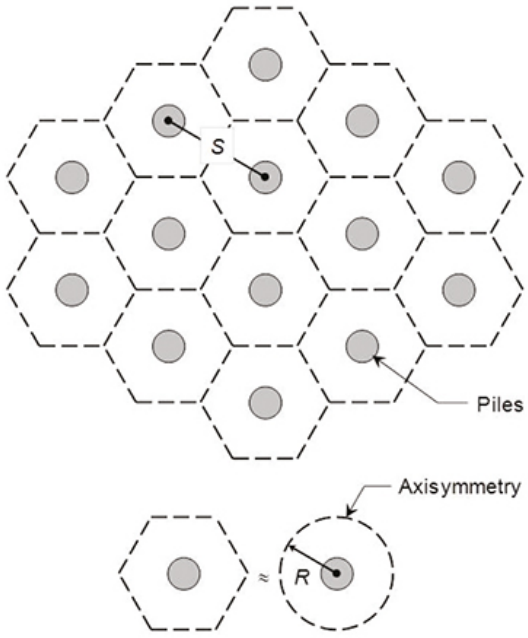

Figure 2.2 Example tributary area conceptual figure from a hexagonal pile pattern after Auvinet and Rodriguez (2017).

The tributary area concept assumes that the negative skin friction developed along the pile is related to the settlement of the soil around it. The tributary area is the area around the pile where the settlement contributes significantly to the development of NSF. Numerical and analytical approaches have also played a crucial role in estimating NSF using the tributary area concept. These methods, integrated into finite element analyses and analytical models, provide insights into the complex behavior of pile foundations subjected to NSF.

2.4 Negative Skin Friction on Pile Groups

The collective impact of NSF on pile groups has been acknowledged for a considerable period. Example sketch for NSF scenario around a pile group has been given in Figure 2.3.

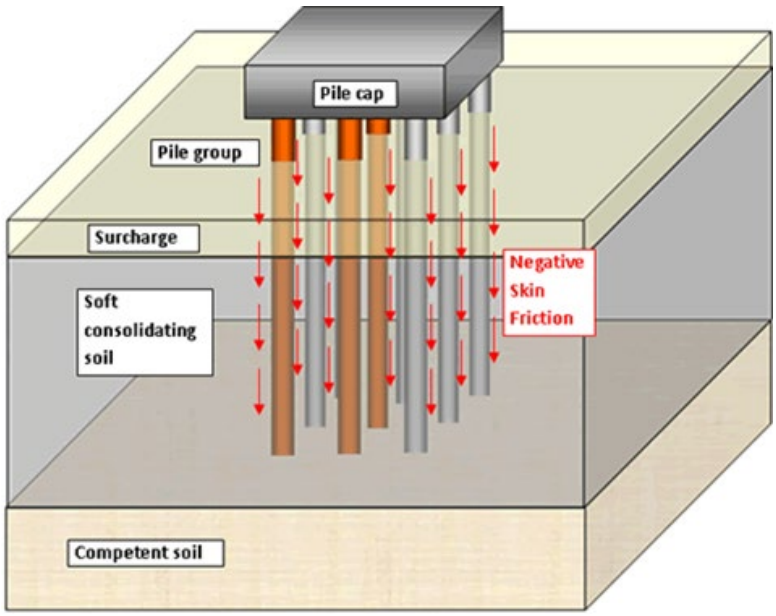

Figure 2.3 Example NSF scenario sketch for a 3x3 pile group connected with a cap.

However, it has generally been observed that in comparison to individual piles, there is a notable scarcity of field test data pertaining to NSF on pile groups. This scarcity can be attributed, in part, to the substantial costs associated with conducting large-scale field tests of this nature (Briaud et al. 1991; Teh and Wong, 1995; Ergun and

Sonmez, 1995; Lee, 2002). While various numerical methods have been put forth to predict NSF on pile groups over the years, their validation has been hindered by the limited availability of test data.

Rituraj and Rajesh (2022) have done a thorough review related to the effects of different pile and soil conditions on the NSF. This review is compiled from analytical, numerical, experimental, and field studies, all of which significantly contribute to grasping and integrating the influence of negative skin friction into design considerations. They have noted that there exist certain research gaps in the area of the NSF, and they have suggested conducting a large number of three-dimensional coupled consolidation analyses under various soil conditions for a better understanding of NSF.

2.4.1 Numerical analysis of pile groups subjected to negative skin friction

Comodromos and Bareka (2005) have done 3D-nonlinear analyses to investigate the effects of NSF on pile foundations and they have noted that if the embankment construction comes before applying the working load, the impact of negative skin friction is notably diminished compared to the opposite sequence. Moreover, they have also concluded that the impact of the dragload group effect is notably more pronounced in fixed-head piles compared to free-head piles, particularly with the commonly used 3.0D spacing but with an increased spacing of 6.0D, this effect became almost negligible.

Shahin et al. (2022) investigated the impact of pile spacing, pile arrangement, and number of piles on dragload estimations within a pile group affected by negative skin friction. Utilizing the PLAXIS 3D software, single piles, 2x2 pile configurations, and 3x3 pile arrangements with varying pile spacings were examined in a stratified soil environment. Results indicated that dragload reduction due to the group effect lessened with wider pile spacings. Additionally, central piles displayed the most substantial reduction in dragload within the group, followed by edge and corner piles.

Liang et al. (2023) have studied the effect of soil creep on the long term-development of NSF by a numerical analysis. They have noted that a high creep coefficient of the soil resulted in an increase in NSF and a descending trend of the neutral plane (NP). The delay in NSF onset induced by creep was observed, attributed to the increase in excess pore pressure during the early stage of consolidation. The NP position had varied drastically at the commencement of consolidation when considering creep. Ultimately, the study had proposed an exponential prediction model to reflect the time dependence of the NP location.

2.4.2 Experimental findings of pile groups subjected to negative skin friction

Zhang et al. (2021) conducted a series of model tests to examine the bearing characteristics of a pile group affected by groundwater levels. They explored the pile's axial force, negative skin friction, settlement, and soil pore pressure. Findings indicated that fluctuations in water levels, whether rising or falling, increased the axial force of the upper part of the pile but decreased it in the lower section. Both axial force and negative skin friction exhibited time-dependent characteristics. The magnitude of negative skin friction correlated positively with the pile head load, and the neutral plane shifted between 0.57 L to 0.64 L with changes in the water level. The soil demonstrated layer-wise settlement while pore water pressure change mirrored the pattern as the water level altered.

Shen et al. (2022) presented the findings from centrifuge model tests that investigated the impact of negative skin friction on piles embedded in soft clay and resting on dense underlying sand. It was observed that the negative skin friction generated along the pile increased as the soft clay settled, reaching its peak when full slippage between the pile and soil occurred. With the application of axial load, this locked-in negative skin friction decreased, gradually disappearing as the neutral plane progressively moved upward due to increased loading. However, when additional surcharge was placed on the clay surface, leading to more settlement,

downdrag forces were reinstated along the pile shaft, causing the neutral plane to shift downward. The study also explored the effects of negative skin friction developed in a group of piles.

Lee and Chen (2022) investigated the negative skin friction induced on piles due to settlements resulting from self-weight consolidation and a decrease in groundwater levels. The study involved the use of two instrumented model piles to measure axial force distribution within a pile group, subjected to an acceleration of 50 g. As the pile head settled more, the neutral point elevation shifted upward, resulting in reduced NSF. The mobilization of NSF decreased with reduced pile spacing and fewer piles. Inner piles exhibited less NSF compared to outer piles, but they would demonstrate similar NSF to isolated piles if the pile spacing exceeded six times the pile diameter. They proposed an assessment method for NSF on grouped piles, utilizing the concept of average effective numbers of piles, which showed reasonable agreement between analytical and model test results. They presented relationships between η_{ave} and n_{ave} for estimating total NSF in pile groups, providing insights applicable to engineering practices.

2.4.3 Field tests on pile groups subjected to negative skin friction

Okabe (1977) conducted field monitoring on a pile group comprising 38 piles, each with a diameter of 0.7 m and installed at a spacing of 2.2 times the pile diameter. Results showed significant negative skin friction on perimeter piles, but interior piles experienced negligible drag loads.

Keenan and Bozozuk (1985) studied a 3-pile group with a spacing of 4 pile diameters over 6.5 years. Piles were 32 m long, 324-mm diameter steel pipes driven through a granular test embankment into clayey silt. No group effect was observed.

Little (1993, 1994) conducted a full-scale test on two free-headed pile groups on a UK clay site. The site had soft to firm, normally consolidated estuarine clay with an average thickness of 15 m. The piles were steel tubular with a 406 mm diameter. One

group was driven above a dense gravel layer, while the other was driven into it. Negative skin friction was induced by a 2.5 m high embankment. Monitoring showed unexpected dragload patterns, particularly in the "friction pile group". The center pile experienced more dragload than anticipated, while the corner pile had the highest and it was about 1.3 times the edge pile. In the "end-bearing pile group", the center pile had the least dragload, contrary to expectations. This was attributed to insufficient pile penetration into the gravel layer. Also, it is noted that the NSF developed for the edge and corner piles was about the same.

CHAPTER 3

VALIDATION WITH A SINGLE PILE CASE STUDY

Accurate estimation of negative skin friction is essential to design safe and economical pile foundations. Traditional analytical methods assume that NSF is fully mobilized above the neutral plane, leading to overestimation of dragloads due to the requirement of large downdrag to fully mobilize the NSF on piles. However, in reality, slippage between the soil and piles may start before excessive settlements are observed in the soil stratum.

While numerous studies exist in literature investigating the behavior of single piles under the influence of NSF, limited research focuses on end-bearing pile groups connected to a pile cap (fixed head). The presence of adjacent piles complicates the evaluation of soil-pile interaction in pile groups. Therefore, a parametric study is necessary to understand the effects of soil stiffness, ultimate skin friction, pile-soil interface stiffness, and pile configuration on downdrag settlements, dragloads, and the influence of the group effect in pile groups.

In this study, 3D finite element analysis using PLAXIS software is conducted to analyze the effects of NSF on end-bearing piles in a multi-layered soil system. The results are compared and validated with previous studies. Furthermore, the study is extended to analyze pile groups connected to a pile cap to gain insights into the behavior of piles in a group under the influence of NSF.

3.1 Numerical Modelling with PLAXIS

Finite Element Method (FEM) involves discretizing a boundary value problem into interconnected finite elements, which can be one-dimensional (1-D), two-dimensional (2-D), or three-dimensional (3-D). The equations for each element are

formulated using shape and interpolating functions. By assembling these element equations, a global stiffness matrix is generated and solved to satisfy the prescribed boundary conditions.

The numerical investigation in this study employed the geotechnical Finite Element Method (FEM) software package, PLAXIS. Plaxis-3D is tailored for three-dimensional FEM analysis of deformation, stability, and groundwater flow in geotechnical scenarios.

To conduct a comprehensive numerical analysis of a pile foundation, it is essential to have appropriate constitutive models for the pile, and soil. The details of these models will be discussed in subsequent sections. Selection of PLAXIS is based on its extensive usage and its advanced constitutive models which replicate the non-linear and time-dependent behavior of soils. For simulating soil behavior, the Soft Soil model from PLAXIS anniversary edition version 22 is adopted. This specific model is recommended for analyzing compressible soils, making it well-suited for studying negative skin friction and pile settlement in cohesive soil conditions, which are the key focus areas of this research. Additionally, PLAXIS offers a user-friendly interface element to model the interaction between structures and soils, which proves pivotal in simulating negative skin friction at the pile-soil interface in this study.

Notably, PLAXIS segregates pore pressure into two components: hydrostatic pore pressure, defined by a specified water table, and excess pore pressure, regulated by the Biot (1941) and Biot (1955) consolidation process. While this treatment of pore pressure within a FEM domain might appear somewhat arbitrary in cases of abrupt water head changes, such as in deep excavations, it proves more suitable to have the pore pressure entirely governed by the Biot consolidation process.

3.1.1 Pile modelling

PLAXIS 3D offers two distinct methods for modelling piles: embedded pile, and volume elements. Among these methods, the embedded pile elements stand out due

to their ability to incorporate the interaction between the pile and soil with a continuous mesh between pile rows. As a result, they can more effectively simulate the effects of both axial and lateral loads on the pile's behavior (Brinkgreve, 2014). However, neither method considers pile driving or installation effects.

Within the embedded pile method, the ultimate skin resistance and bearing capacity are provided as input parameters rather than being derived as outputs of the numerical analysis. Advantages of embedded piles are given below:

- Efficient way to model different types of piles,
- Validated for axial loading, pile groups.

The limitations of embedded piles are as follows:

- Primarily for serviceability states,
- Mesh-dependency of results,
- Full bonding is considered in lateral movement.

This method does not allow direct input of interface properties such as the interface friction angle and interface stiffness parameters. Instead, these interface properties must be calibrated based on additional data and information.

The volume elements approach involves substituting the soil with pile material and introducing an interface between the pile and soil. This method has been chosen because it has several advantages as discussed below:

- Pile composed of volume elements or wall elements with pile properties,
- Massive piles or tubes (wall tubes).

The limitations of volume elements are as follows:

- Uses high number of elements,
- Limited number of piles are feasible,
- Mesh quality has to be checked thoroughly.

3.2 Model Validation

3.2.1 Reference case study

Indraratna et al. (1992) conducted extensive field measurements on two prestressed, precast concrete piles situated approximately 10 kilometers east of Bangkok, Thailand. One of these piles was coated with a layer of bitumen, while the other remained uncoated.

The telltale system was employed to monitor pile compression and movements. Hydraulic piezometers were strategically placed at distances of 0.5 and 1 meter from the pile shaft, and at depths of 4, 8, 12, 16, and 20 meters. Figure 3.1 provides an overview of the various components involved in the tests, including the embankment, instrumented piles, and ground monitoring systems.

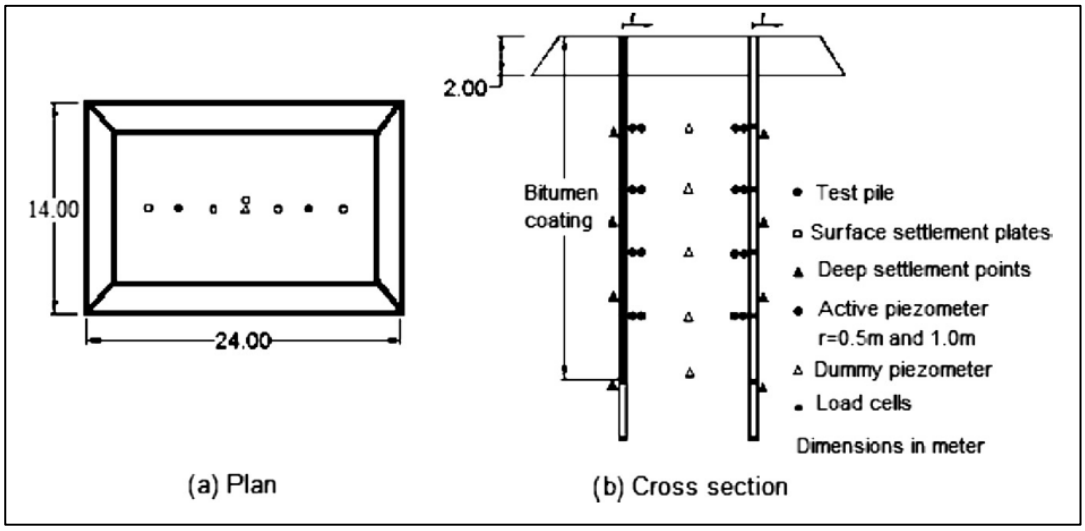

Figure 3.1 Embankment, instrumented piles, and ground monitoring systems. (After Indraratna et al., 1992).

Each of the instrumented piles was divided into six segments, with five segments measuring 4 meters in length and the uppermost one extending to 7 meters. A 24 by 12-meter embankment, constructed with 2:1 side slopes, was swiftly erected over the test area within 3 days, standing at a height of 2 meters. This embankment was crucial in generating negative skin friction.

Pile installation involved driving from 2 meters above to a final depth of 25 meters below the ground surface. The piles featured an inner diameter of 0.25 meters and an outer diameter of 0.4 meters.

In this particular study by Indraratna et al. (1992), five boreholes were drilled to a depth of 35 meters below the ground surface. The subsurface profile revealed distinct layers, including a weathered clay crust at the surface, followed by a soft clay layer extending to a depth of 16 meters. Beneath this was a medium stiff clay layer (4 meters thick), succeeded by a 3-meter stiff clay layer, overlying a sand layer. The water table was consistently found at a depth of 2 meters below the natural ground surface.

3.2.2 FEM mesh and boundary conditions

For the back-analysis, an equivalent half 3D-model focusing on a single pile was employed. The study utilized the PLAXIS finite element code. The soil clusters were replicated using 10-noded tetrahedral elements, which offer second-order interpolation for displacements and employ 4 Gauss points for numerical integration as illustrated in Figure 3.2.

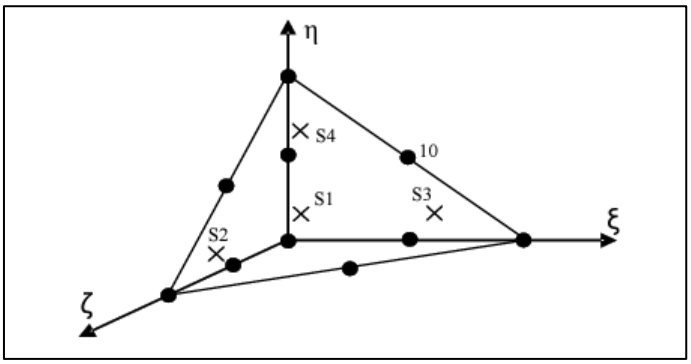

Figure 3.2 Local numbering and positioning of nodes and integration points of a 10-node tetrahedral element.

Compatible interface elements with three node line elements were employed to replicate the interaction between the pile and the soil. The volume elements method

was used to simulate the uncoated pile. As shown in Figure 3.3, the generated mesh is highly refined where significant stress gradients are expected, and half model is used for computational efficiency. Element size gradually increases towards the boundaries, aiming to reduce computational effort needed. However, it should be noted that Figure 3.3 is cropped for better presentation of the mesh sizes, and it does not represent the actual boundary conditions used in the model.

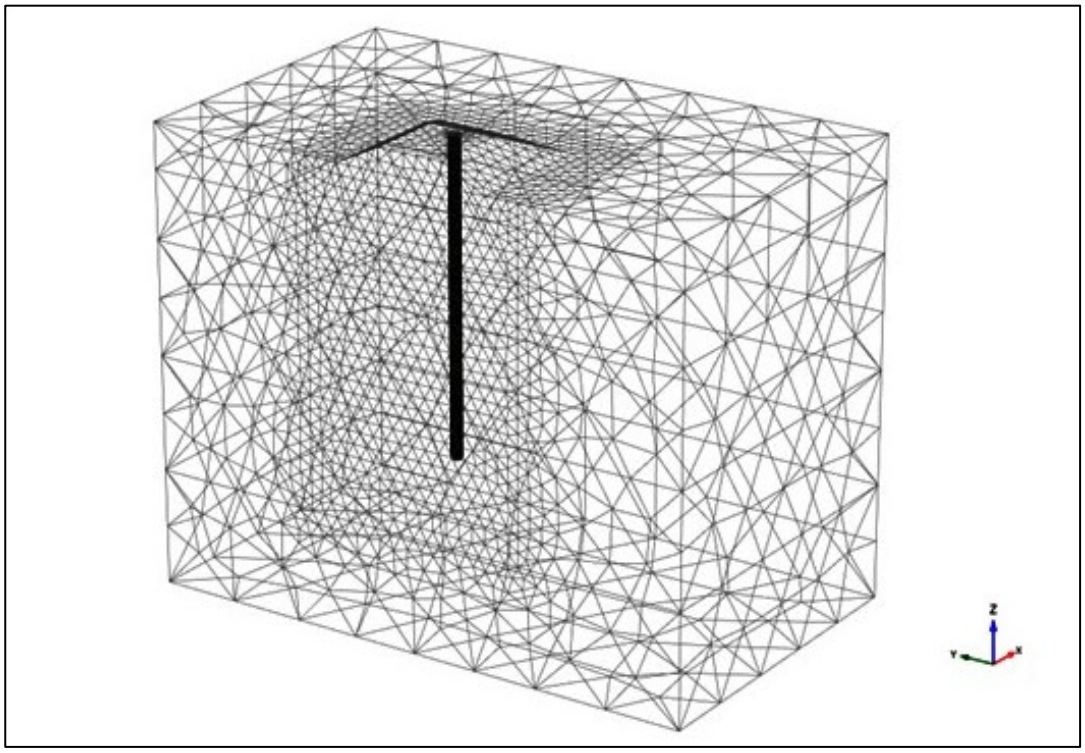

Figure 3.3 The reference case study, 3D half-model finite element mesh.

At the side boundaries of the model, roller supports allow settlements in the vertical direction, whereas the bottom boundary is fixed, and the top boundary remains free.

Early investigations into axially loaded piles operated under the assumption that the shear strains in the vicinity of a pile shaft were confined to a narrow zone approximately 5 to 10 cm adjacent to the pile (Burland, et al., 1966). At the pile-soil interface, the shear stress reached its peak, gradually diminishing with increasing distance from the pile shaft (Cooke, 1974). Randolph and Wroth (1978) proposed that beyond a certain influence radius, denoted as r_m, the shear stress became

negligible. They established that for a pile embedded in a uniform soil stratum, the influence radius, r_m, equated to 2.5L(1-ν), where L represents the length of the pile, and ν denotes the Poisson ratio of the soil. In the case of an end-bearing pile, r_m is determined as follows (Randolph and Wroth, 1978):

$$r_m = L\{0.25 + [2\rho(1-\nu) - 0.25]\xi\} \quad (3.1)$$

Where ρ is the ratio of shear modulus at half depth to the base of compressible soil layer and ξ is the ratio of shear modulus of compressible layer at base to shear modulus of the bearing stratum.

Assuming the homogeneity factor is set to one, a necessary effective radius of influence was determined to be 50 meters. However, the results of the analysis based on this 50-meter radius model indicated a settlement of 11 millimeters at the side boundary of the soil surface. This model radius value derived from Equation (3.1) proved inadequate due to the difference in loading conditions between the current analysis and Randolph and Wroth's formula. The formula was originally derived for a single pile without a surcharge, while in the current analysis, the dimensions of the embankment impact the radius of influence.

To ascertain the appropriate model radius, a sensitivity analysis was conducted. Increasing the radius beyond 60 meters had no significant effect on the maximum settlement value. Therefore, a radius of 60 meters was deemed appropriate. This selected model radius (horizontal axis length) of 60 meters is sufficiently large to mitigate any boundary effects on the analysis outcomes. The bottom boundary of the model is positioned at a depth of 40 meters below the ground surface, with a clearance between the pile toe and the bottom boundary equal to half of the pile length. 2D view of the model which shows the boundary conditions, soil layers and groundwater table level is presented in Figure 3.4.

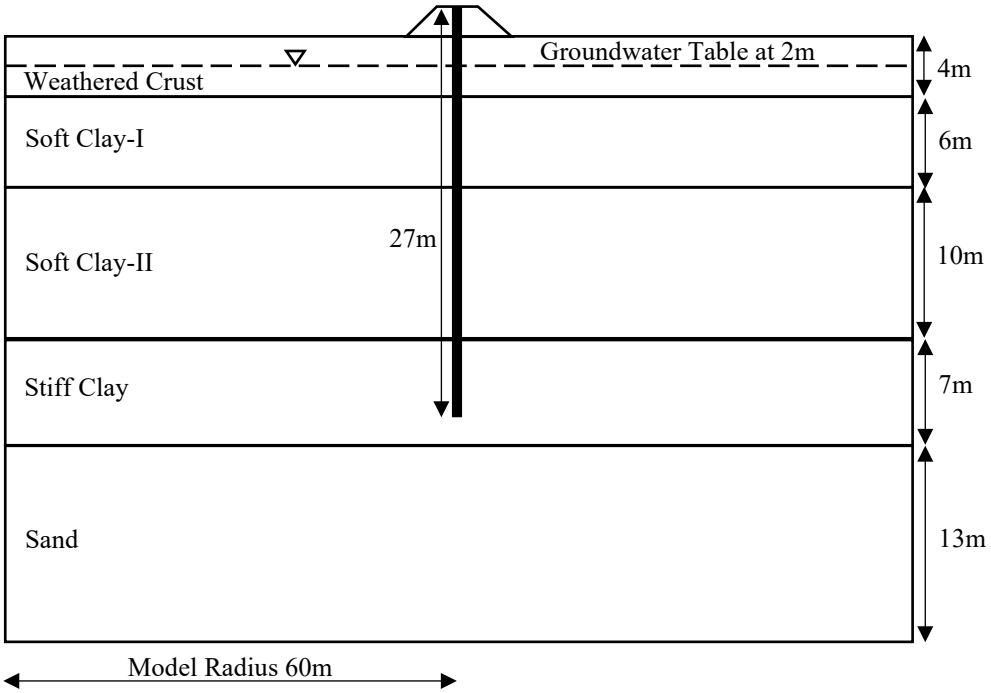

Figure 3.4 2D view of the model which shows the boundary conditions, soil layers and groundwater table level.

3.2.3 Constitutive models and material properties

PLAXIS provides a range of constitutive models and material properties. For the purpose of back-analysis the pile is represented by linear elastic model, linear elastic perfectly plastic constitutive soil model is used for embankment and sand layers and soft soil constitutive model is adopted for the clay layers. Interface elements are introduced between the pile and the soil to ensure complete interaction between them. The roughness of the interface element is determined by a strength reduction factor denoted as R_{int}.

The soil properties are adopted after Drbe et al. (2016) and Liu et al. (2012) based on the airport site at the east of Bangkok City and results of a parametric study respectively.

Strength tests revealed that the undrained shear strength fluctuated within the range of 20 - 45 kPa for the weathered clay layer and 16 - 38 kPa for the soft clay layer. The average undrained shear strength for the medium stiff to stiff clay layer was 45 kPa.

Index tests indicated that the water content in the weathered clay ranged from 40% above the water table to 55% below it. The water content in the soft clay layer varied at different depths, reaching up to 95% at certain levels. This layer showcased a liquid limit range of 70% – 100% and a plastic limit range of 25% – 40%. The compression index for the soft clay ranged between 1.1 - 1.3.

3.2.3.1 Linear elastic model

Linear elastic models characterize the behavior of a material by considering its elastic properties, such as shear modulus (G) and bulk modulus (K) to be constant with strain. These models are frequently used to represent the structural elements of the system that are not expected to approach yielding, such as steel or concrete components. The model parameters used for the pile are given below in Table 3.1.

Table 3.1 Model parameters used for the pile.

Material	E (kPa)	γ (kN/m^3)	ν
Pile	2.9 x 10^7	24.5	0.2

3.2.3.2 Linear elastic perfectly plastic constitutive soil model

Soil behavior exhibits non-linearity when exposed to changes in stress or strain. In reality, soil stiffness depends on factors such as stress levels, stress paths, and strain levels. PLAXIS incorporates these features in advanced soil models. However, for simplicity, the linear elastic perfectly plastic model is a commonly used linear elastic-perfectly plastic model that serves as an initial approximation of soil behavior. The linear elastic part of this model is based on Hooke's law of isotropic

elasticity, while the perfectly plastic part is founded on the linear elastic perfectly plastic failure criterion within a non-associated plasticity framework as shown in Figure 3.5.

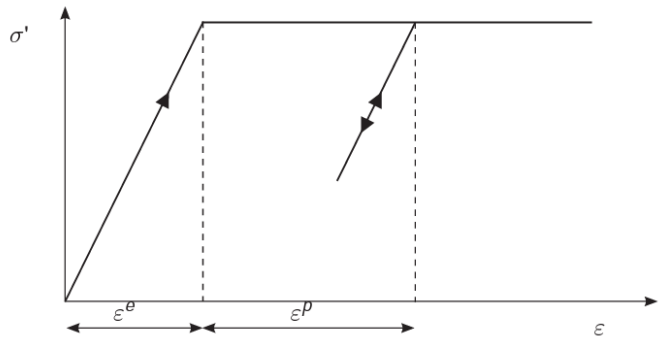

Figure 3.5 Stress-strain behavior of elastic perfectly plastic model.

Plasticity entails the development of irreversible strains. To determine whether plasticity occurs during a calculation, a yield function 'f' is introduced as a function of stress and strain. Plastic yielding is associated with the condition 'f=0', often visualized as a surface in the principal stress space (Figure 3.6). A perfectly plastic model is a constitutive model with a fixed yield surface, meaning the yield surface is fully defined by model parameters and remains unaffected by plastic straining. For stress states within the yield surface, the behavior is purely elastic, and all strains are reversible.

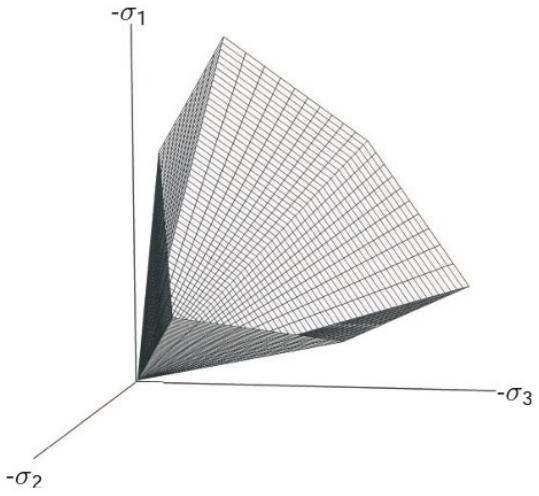

Figure 3.6 Yield surface of linear elastic perfectly plastic model in principal stress state.

The model parameters used for the embankment and sand layers are given below in Table 3.2.

Table 3.2 Model parameters used for the fill material and sand layer (Adopted after Drbe et al. (2016) and Liu et al. (2012)).

Material	E (kPa)	γ (kN/m^3)	ν	c' (kPa)	Φ' (°)
Fill	4.9x10^3	16.7	0.2	0.1	30
Sand	28x10^3	17.0	0.2	0.1	35

3.2.3.3 Soft soil constitutive model

The Soft Soil model (SSM) is derived from the Cam-clay model and is particularly suitable for analyzing nearly-normally consolidated clay, clayey silt, and peat soils characterized by high compressibility.

The Hardening Soil model is recognized for its effectiveness in addressing issues related to soft soils. While it proves highly effective for most soft soil scenarios, it may not be the best choice for very soft soils exhibiting high compressibility. For such soil scenarios, the use of SSM is preferred. Some features of SSM are given below:

- Stress dependent stiffness (logarithmic compression behavior).
- Differentiation between primary loading and following unloading-reloading phases.
- Retains memory of pre-consolidation stress.
- Shear failure behavior adheres to the Mohr-Coulomb criterion.

In the SSM, volumetric strains exhibit a logarithmic relationship with the mean effective stresses, which is expressed through specific equations (Figure 3.7, Equation (3.2), and Equation (3.3)) for virgin compression and unloading-reloading scenarios.

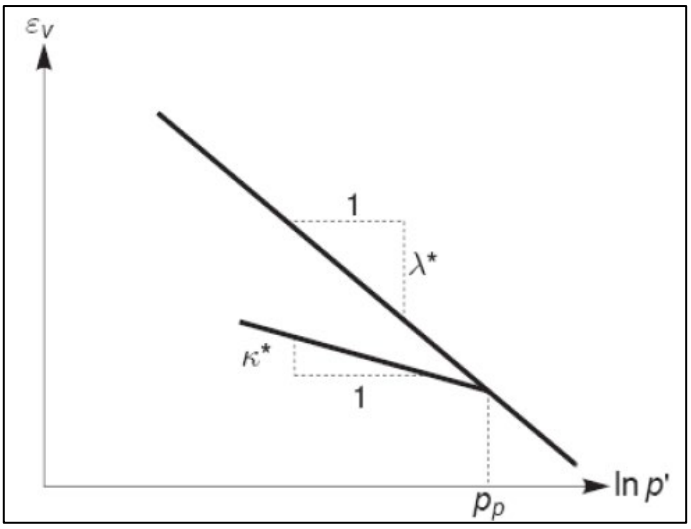

Figure 3.7 The relationship between volumetric strain and mean stress.

$$\varepsilon_v - \varepsilon_v^0 = -\lambda^* . \ln\left(\frac{\rho'}{\rho^0}\right) \tag{3.2}$$

$$\varepsilon_v - \varepsilon_v^0 = -\kappa^* . \ln\left(\frac{\rho'}{\rho^0}\right) \; if \; \rho' \leq p_p \tag{3.3}$$

In the SSM, the yield function takes the form of an ellipse, where the ellipse's height is determined by parameter M, and its width is influenced by parameter P_p (see Figure 3.8). As the yield surface expands, the soil state on the yield surface undergoes irreversible volumetric strain deformations, represented by movement along the primary compression line. Within the yield curve, the soil experiences reversible deformations, as described by the swelling lines.

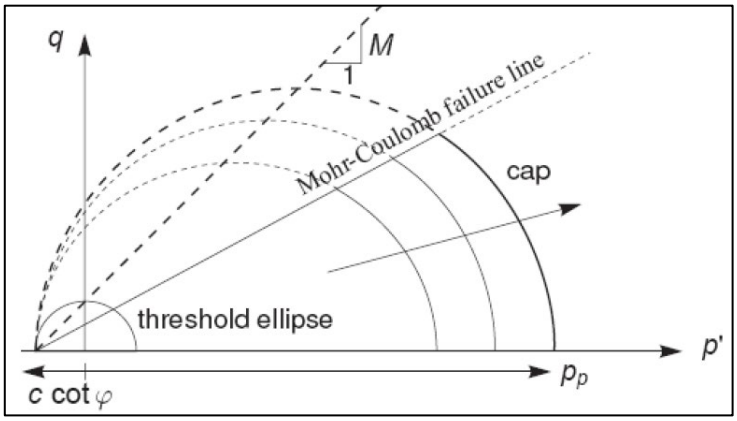

Figure 3.8 The yield surface of the Soft Soil model projected into the p'-q plane.

The primary input parameters for the Soft Soil model (SSM) include initial state parameters (K_0, overconsolidation ratio, or pre-overburden pressure), compression parameters (λ^*, κ^*, and v_{ur}), and strength parameters (φ', c', and ψ). These essential parameters are determined through isotropic triaxial tests. Additionally, the compression parameters can be derived from one-dimensional consolidation (oedometer) tests using C_c and C_s, as indicated in Equation (3.4) to (3.5), or through Cam-clay parameters, as shown in Equations (3.6) to (3.7).

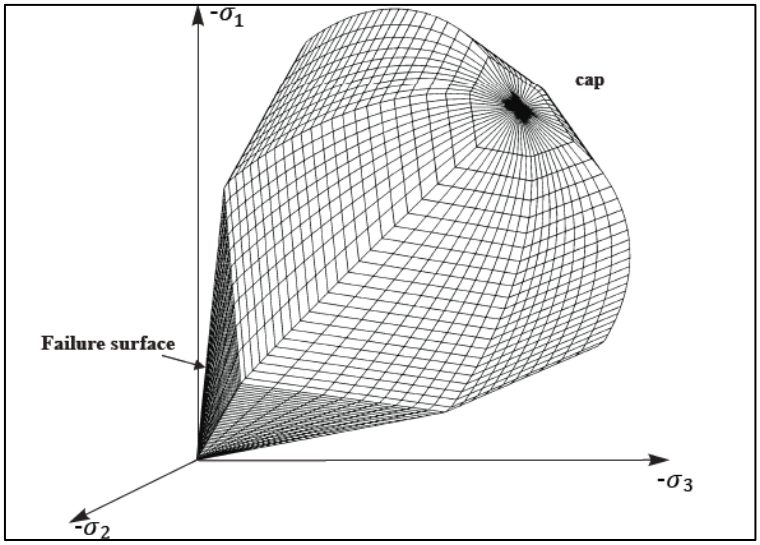

Figure 3.9 Visualization of the complete yield surface of the Soft Soil model in principal stress space.

$$\lambda^* = \frac{C_c}{2.3(1+e_0)} \tag{3.4}$$

$$\kappa^* \approx \frac{C_s}{2.3(1+e_0)} \tag{3.5}$$

$$\lambda^* = \frac{\lambda}{(1+e)} \tag{3.6}$$

$$\kappa^* = \frac{\kappa}{(1+e)} \tag{3.7}$$

The model parameters used for the clay layers (weathered crust, soft soils, and stiff clay) are given below in Table 3.3.

Table 3.3 Model parameters used for the compressible clay layers (Adopted after Drbe et al. (2016) and Liu et al. (2012)).

Material	γ (kN/m^3)	e_0	λ^*	κ^*	k (m/day)	OCR
Weathered Crust	16.7	1.8	0.065	0.019	$1.3x10^{-4}$	3
Soft clay - 1	14.7	2.8	0.135	0.022	$5.5x10^{-4}$	1.3
Soft clay - 2	16.7	2.4	0.095	0.019	$2.6x10^{-4}$	1.3
Stiff clay	18.6	1.2	0.053	0.012	$1.1x10^{-4}$	1.85

3.2.4 Comparison between field measurements and analysis results

The soil settlement measured 0.25m away from the pile after 265 days of embankment construction obtained from the FEA study is compared against the field measurements of Indraratna et al. (1992) in Figure 3.10. The results are matching reasonably well between the FEA study and field measurements. The ground surface settlement difference between the FEA result and field measurement is about 7mm.

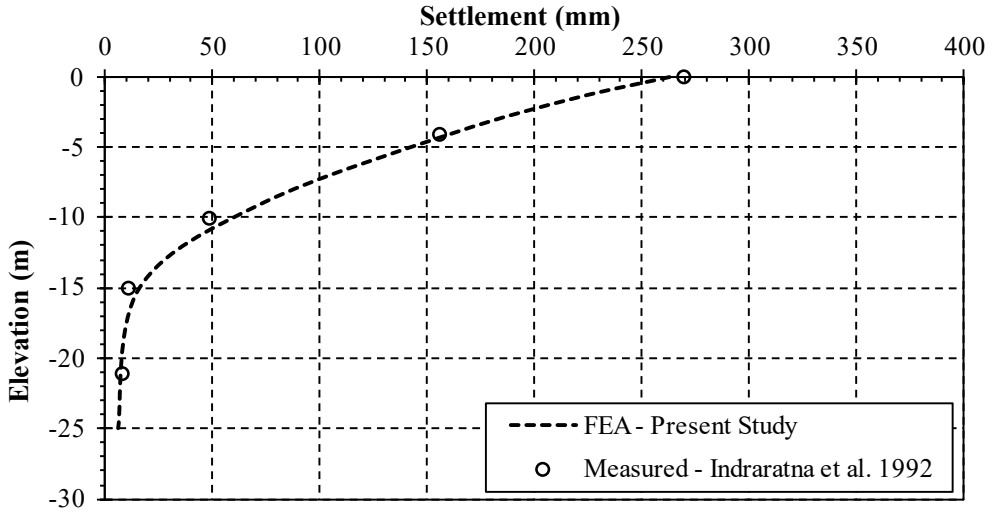

Figure 3.10 Comparison of ground settlements between the present FEA study and field measurements after Indraratna et al., 1992 at 0.25m away from the pile.

The Figure 3.11 illustrates the distribution of skin friction and dragload along the uncoated pile shaft for the current 3D FEA study and the recorded results after 265 days of embankment construction, as per Indraratna et al., 1992.

The skin friction values are obtained from the shear stresses along the pile interface and the dragload is calculated by hand. While the skin friction closely aligns with the measurements, there is a slight overestimation of the dragload along the pile shaft. This disparity is expected, as the present analysis does not account for the complex pile driving effects, particularly in the top 20m segment of the pile subjected to repeated driving-pullout processes. The difference between the measured and calculated values are presented in Table 3.4.

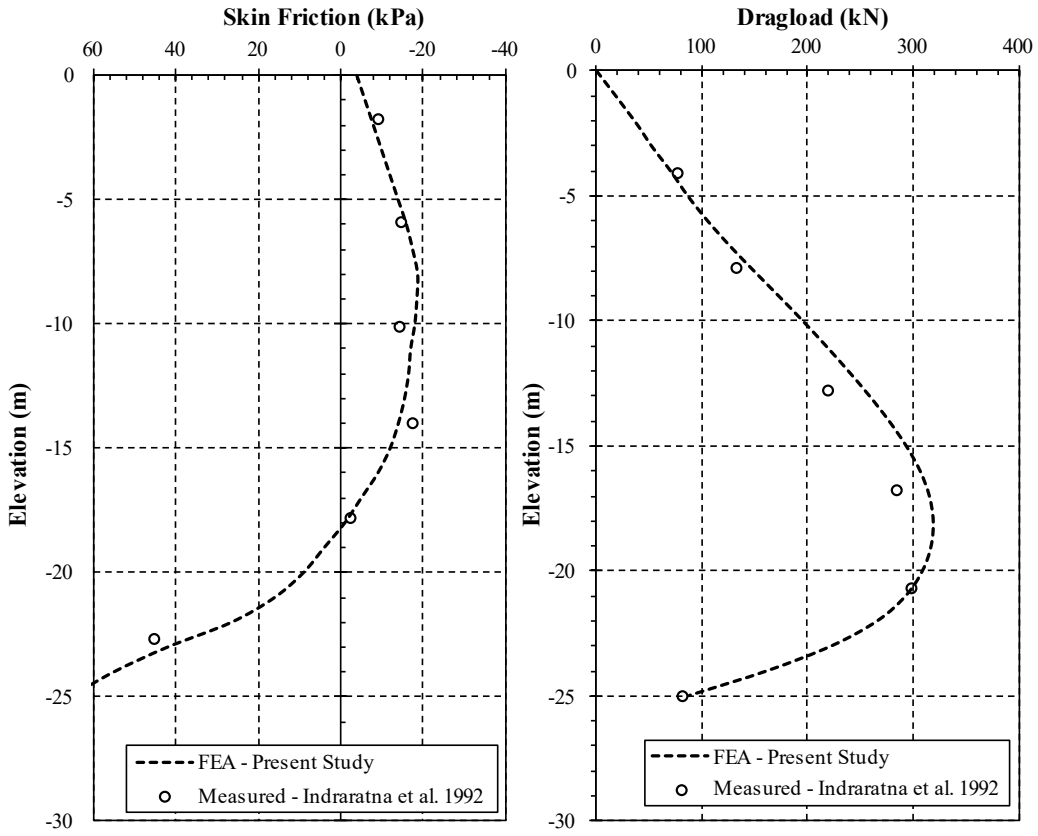

Figure 3.11 a) Skin friction distribution, b) Dragload distribution between the present FEA study and measured results after Indraratna et al., 1992 along the pile shaft.

Table 3.4 Difference between the field measurements and calculated values for skin friction and dragload.

Output	Measured Value	Calculated Value	Error (%)
Max. NSF (kPa)	17.5	18.7	6.9
Max. Dragload (kN)	298	319	7.0

The general agreement between the FEA results and the field measurements show that 3D FEA is a robust and capable tool for investigating the development of negative skin friction on the pile and pile groups.

CHAPTER 4

3D SIMULATIONS OF END BEARING PILE GROUPS - RESULTS AND DISCUSSIONS

4.1 Analysis Framework

In order to study the development and change of NSF of end-bearing pile groups connected with a pile cap, geotechnical engineering finite element software PLAXIS 3D is used in this thesis. Through application of surcharge loading over the full model area, NSF is produced around piles and examined in terms of distribution of NSF displacements of pile and soil, and dragload along the pile lengths. The development of NSF and dragload around the piles have been investigated by using different pile dimensions, spacings, and soil parameters.

The FEA model adopted for the investigation is a 3D quarter model. This choice provides efficient use of computational resources, allowing the simulation of the pile's response to external loads with reduced computation time compared to a full 3D model.

To ensure adequate discretization, the mesh utilized 10-noded tetrahedral elements for both the piles and soil. Vertical and horizontal interfaces were incorporated between the pile and soil, as well as at the pile tips, to capture the complexities of the pile-soil interaction. Example mesh and boundary conditions for a 5x5 pile group is presented in Figure 4.1.

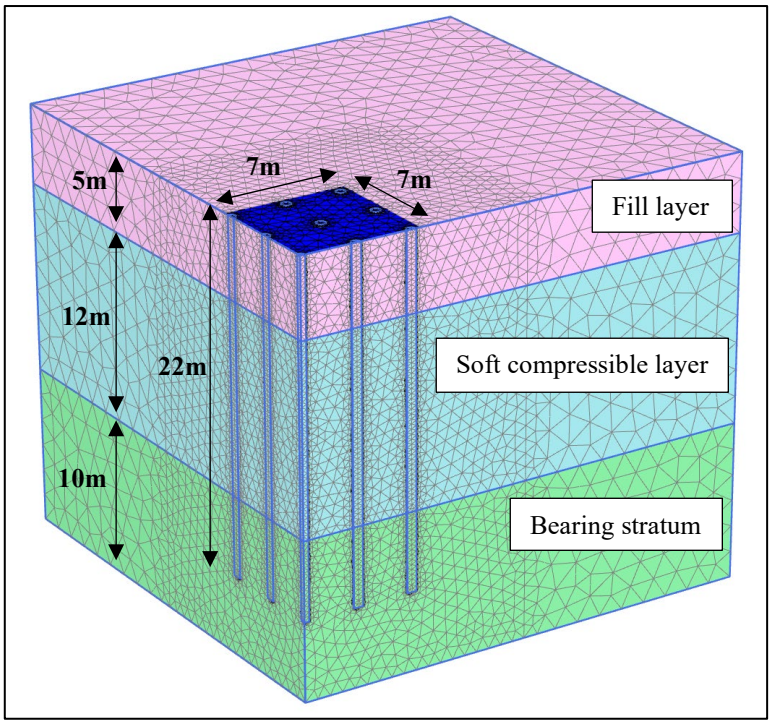

Figure 4.1 Example 3D-FEA mesh & boundary conditions for 5x5 pile array.

Horizontal constraints were applied to the lateral boundaries and this restraint prevented any lateral movement of the pile into the symmetry planes, accurately capturing interactions between the pile and surrounding soil.

For vertical deformations in the pile and surrounding soil, the lateral boundaries were left unconstrained in the vertical direction. This freedom accommodated settlements and uplifts, which are vital in assessing the pile's response to external loads.

The top and bottom boundary conditions were defined to establish a stable base for the model. The bottom boundary was fixed in both horizontal directions, while the top boundary was left unrestricted to permit free vertical deformation of the model.

Leveraging the symmetry of the problem, the symmetrical axes (X_{min} & Y_{min}) were fixed to optimize computational efficiency without compromising the essential pile behavior.

The global water level was set to align with the ground surface, providing accurate modeling of the groundwater table's impact on pile behavior. The top and bottom

boundaries were designed to allow for groundwater flow but due to use of the quarter-model, groundwater flow was not allowed into the symmetry axes. This consideration enabled realistic simulation of pore pressure distributions and interactions between the pile and surrounding soil under varying groundwater conditions.

After reviewing Randolph and Wroth (1978)'s equation (Equation (3.1)) the model width was selected as 2.5 times the length of the pile in soft bearing stratum to adequately account for relevant soil-pile interactions.

Sensitivity checks were performed to validate the chosen boundary conditions and confirm their efficacy in simulating realistic pile behavior under the influence of negative skin friction and external loads. An example sensitivity analysis case has been given in Figure 4.2 with a soft bearing layer thickness of 20m which is underlaid by a bearing stratum.

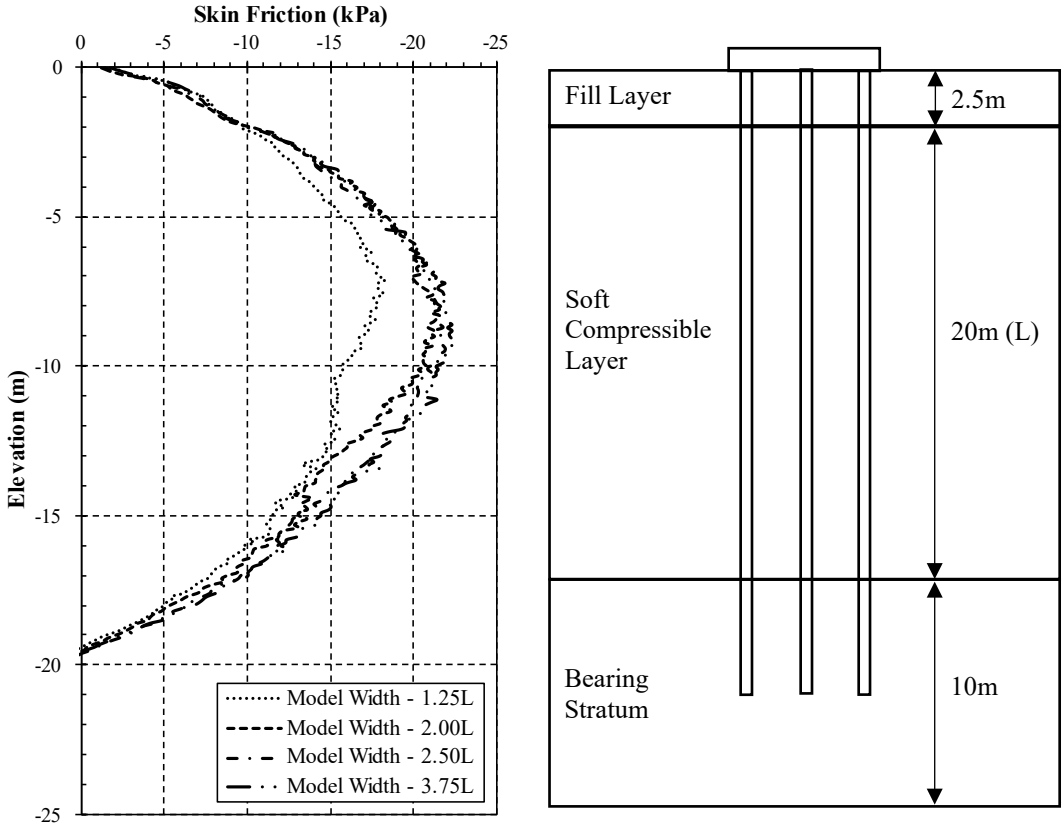

Figure 4.2 Example for boundary conditions sensitivity analysis for 5x5 array, D=1.0m, s/D=3, L/D=20.

The validation process demonstrated that the adopted model dimensions and boundary conditions yield consistent and reliable results, enhancing confidence in the numerical analysis outcomes.

In conclusion, the selection and implementation of appropriate boundary conditions are crucial in conducting reliable and efficient finite element analysis. The chosen 3D quarter model, along with prescribed boundary conditions, successfully captured the load transfer mechanisms and deformations within the pile foundation system. The findings underscore the significance of considering boundary conditions to ensure a realistic representation of pile-soil interactions and the reliable serviceability of the foundation system.

4.1.1 Soil parameters

The soil parameters used for the compressible soft clay layer (Soft Soil – Undrained A), freely draining bearing stratum/fill layer (Linear elastic perfectly plastic – Drained) and pile(s) (Linear elastic – Nonporous) which are adopted in the analyses are given in Table 4.1 to Table 4.3 respectively.

Table 4.1 Soil parameters used for the compressible layer – Soft soil - Undrained A

Material	**γ (kN/m^3)**	**e_0**	**λ^***	**κ^***	**k (m/day)**	**R_{int}**
Soft Compressible Layer	18.0	0.9	0.05	0.01	8.6×10^{-4}	0.7

Table 4.2 Soil parameters used for the fill layer and bearing stratum – Linear elastic perfectly plastic - Drained

Material	**E (kPa)**	**γ (kN/m^3)**	**ν**	**c' (kPa)**	**Φ' (°)**
Fill	5.0×10^3	20.0	0.2	0.1	30
Bearing Stratum	1.0×10^5	23.0	0.2	0.1	35

Table 4.3 Soil parameters used for the piles – Linear elastic – Non-porous

Material	E (kPa)	γ (kN/m^3)	ν
Pile / Pile Cap	3.5 x 10^7	25.0	0.2

It should be noted that although the properties of the pile cap are the same as reinforced concrete piles, it is modelled as plate element. The thickness of the pile cap varies equal to the pile diameter and the dimensions of the pile cap vary half pile diameter higher than the outer pile edge at each different FEA model.

4.1.2 Naming convention of the piles

Pile group arrangement of 5x5 and 3x3 arrays are shown in Figure 4.3 and Figure 4.4 respectively.

The pile locations for 5x5 array are as follows:

- Corner pile: A
- Edge piles: B & D
- Inner piles: C & E
- Center pile: F

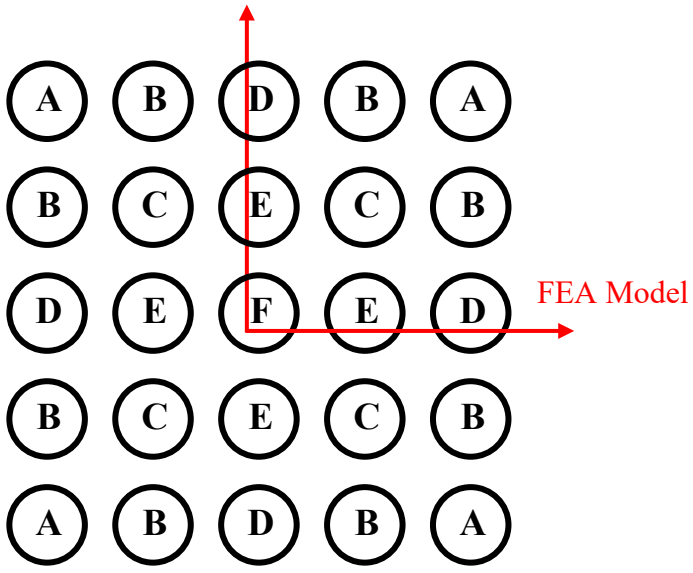

Figure 4.3 Pile arrangement for 5x5 array.

The pile locations for 3x3 array are as follows:

- Corner pile: A
- Edge pile: B
- Center pile: C

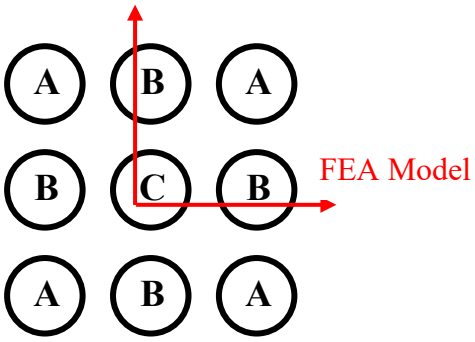

Figure 4.4 Pile arrangement for 3x3 array.

Traditionally (Poulos and Davis, 1980) the pile naming convention is done starting from outer to inner piles. However, in the case of 5x5 pile array, locations of Pile C and Pile D have been changed for direct comparison between the 5x5 and 3x3 arrays.

4.1.3 Analysis procedure

The model is divided into three different construction phases. The first phase is the initial stage where K_0 procedure was used for generating the effective soil stresses and pore water pressure with automatic lateral earth pressure coefficient due to flat horizontal layer arrangement.

An intermediate consolidation calculation step was included in the analysis for the construction of fill layer and piles within a 0.1-day time period.

In the final stage consolidation calculation was applied until minimum excess pore pressure is reached.

4.2 Analysis Mechanism

In situations where the fill/embankment layer is constructed over soft compressible layer, the interaction among piles, soil, and pile cap in a grouped foundation becomes notably intricate compared to typical scenarios. Various studies confirm a consistent alteration in negative skin friction (NSF) behavior between individual piles and pile groups. The soil displacement surrounding a pile group differs from the displacement observed in outer soil, owing to the shielding effect of outer piles.

Furthermore, NSF varies among corner, edge, and center piles, with corner and edge piles typically experiencing greater NSF and deeper neutral point positions compared to center piles. However, usually in the case of end-bearing piles, the location of the neutral point is at the layer boundary between soft compressible layer and bearing stratum unless the compressible layer is sufficiently thick for surcharge load to become negligible within the layer itself. Hence, in order to investigate and better understand the NSF behavior around pile groups, a parametric analysis has been conducted. After changing a single parameter at a time in multiple pile configuration, pile dimension and loading conditions, the effects of each parameter have been examined.

4.3 Soil and Pile Settlements

The pile/soil settlements calculated for the chosen finite element model with D=1.0m, s/D=3, L/D=20, surcharge load=50kPa, soil compressibility factor λ^*=0.04, are presented in Figure 4.5. It should be noted that the presented graphs are the same plot with different settlement axis scales.

This figure shows that the calculated maximum soil settlement is ~50cm more than the soil settlements observed in the soil under the pile cap for an end-bearing pile group connected with a pile cap. It is also observed that pile settlement was only limited to ~1mm for Pile C.

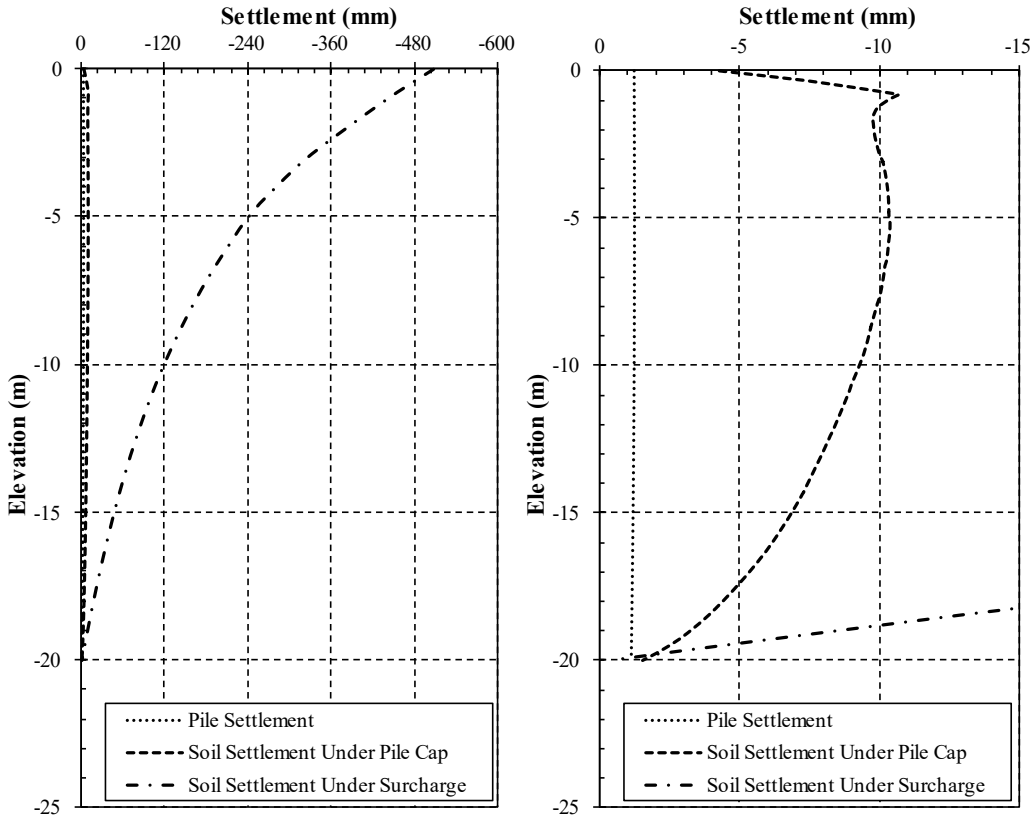

Figure 4.5 Calculated pile and soil settlements from FEA where D=1.0m, s/D=3, L/D=20, surcharge load=50kPa, soil compressibility factor λ*=0.04.

The difference between the soil and pile settlements were further presented in Appendix A where different soil compressibility factors were adopted for each finite element model. It is observed that with the increasing soil compressibility factor, the settlements observed in the soil also increase whereas the pile settlements slightly decrease causing higher NSF development on the pile surfaces. It is also observed that this change is more evident for the inner piles than the outer piles.

In Figure 4.6 pile settlements for different pile locations plotted against each other for the 5x5 pile array.

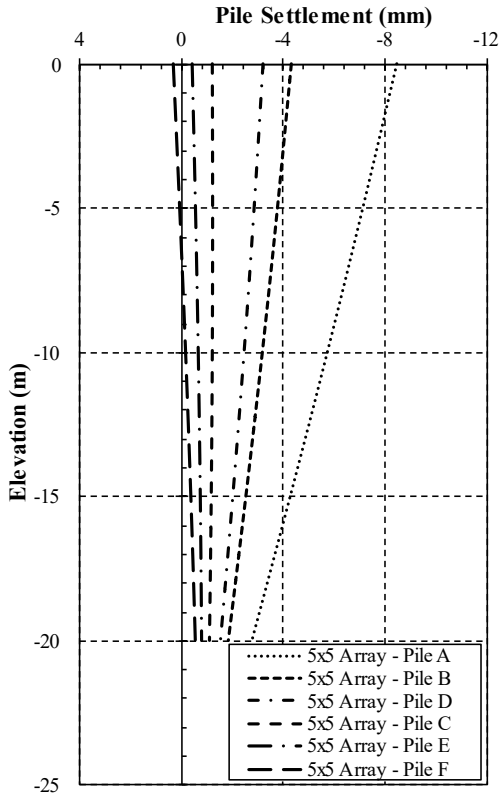

Figure 4.6 Pile settlements for different pile locations.

Based on the results presented in Figure 4.6, maximum pile settlement changes between the corner and center piles as ~8 to 1mm respectively. It is observed that outer piles (A, B & D) settle more than the inner piles (C, E & F). It is also acknowledged that for the outer piles, settlements decrease gradually from the ground surface to bearing stratum whereas the exact opposite is noted for the inner piles which means that inner piles are in tension. Although this is not commonly observed in the literature, there are instances in Poulos and Davis's (1980) elastic solutions with inner piles in tension.

Based on the results presented in Appendix A, the rate of change in the settlements along the pile lengths also increases with increasing soil compressibility factor.

4.4 Change of NSF and Neutral Point due to Foundation Loading

This thesis aims to investigate the NSF behavior of the individual piles in end-bearing pile groups connected with a pile cap. Therefore, the neutral point (NP) is located near the bottom of the soft compressible layer level (top of bearing stratum). However, in the actual site conditions, after the development of the NSF, foundation is further loaded with superstructure loads and hence it causes a shift on the position of the NP and the magnitude of the NSF exerted on the piles due to the increase in the overburden stresses. This phenomenon is presented in Figure 4.7 for Pile A and the other pile locations are given in Appendix B.

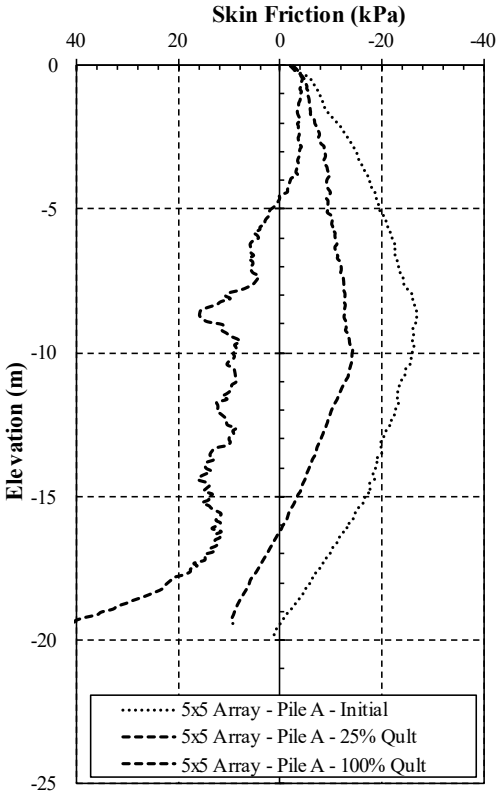

Figure 4.7 Change of NSF and NP due to foundation loading for the 5x5 array, D=1m, s/D=6, L/D=20, surcharge load=50kPa – Pile A.

In this FEA model the foundation has undergone consolidation under the surcharge load of 50kPa at the initial stage and then the foundation is loaded until 25% and 100% of the ultimate limit capacity in separate stages.

As it can be seen from Figure 4.7, the location of the NP shifts from 19.2m to 16m and 4.5m under 25 and 100% ultimate foundation load respectively. It is also observed that the maximum NSF reduces by 47% and 84% for 25% and 100% ultimate foundation loading states respectively. A similar phenomenon is also noted by Fellenius (1998), and it is concluded that liveloads and dragloads should not be combined.

Based on the results presented in Appendix B, the shift of the location of NP increases from inner to outer piles in the order of: F – E – C – D – B – A for 25% ultimate foundation loading stage. Although, the shift of the location of NP is also observed in the same order for the 100% ultimate loading state, this shift is not as severe as the 25% ultimate loading state. This difference is visualized by PLAXIS outputs given in Figure 4.8 where shear stresses around the piles at the mid depth of the soft compressible layer. In Figure 4.8, red color presents negative skin friction and blue color represents the positive skin friction.

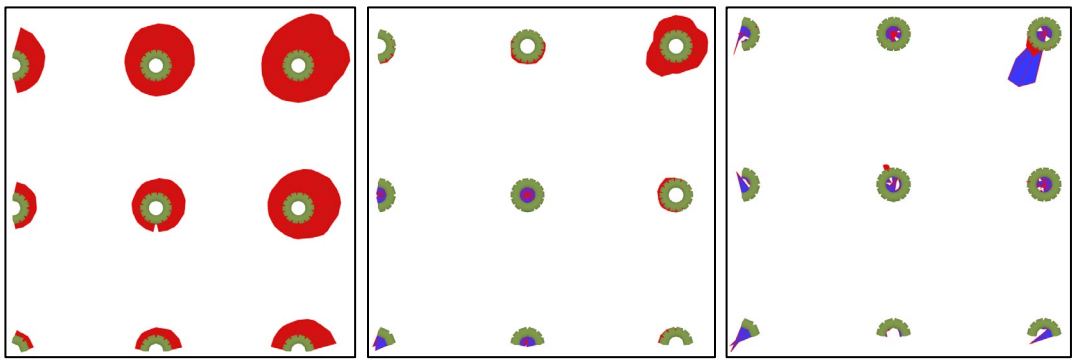

a b c

Figure 4.8 Negative skin friction at the mid depth of bearing stratum for (a) zero, (b) 25% and (c) 100% ultimate load on pile cap.

Figure 4.8 indicates that at 25% ultimate loading state outer piles are still under the influence of NSF whereas the inner piles show positive skin friction response which clearly indicates a clear change of the position of the NP. However, in the case of 100% ultimate loading state all piles are in the positive skin friction regime showing NSF disappears at the ultimate limit state, so it only affects serviceability (i.e. settlement) analyses.

In order to understand the effect of foundation loading on the NSF distribution and magnitude, the foundation load has been applied to the pile cap prior to the consolidation of the soft compressible layer. The results then have been superposed with the initial full NSF without structural load and compared with the 25% ultimate foundation loading stage after consolidation as shown in Figure 4.9.

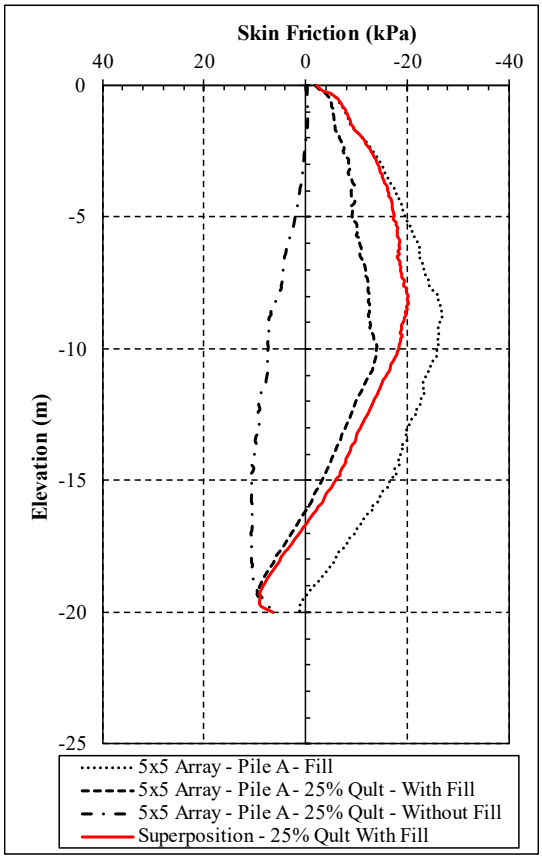

Figure 4.9 Comparison of superposed shear stresses with 25% ultimate foundation loading after consolidation for the 5x5 array, D=1m, s/D=6, L/D=20, surcharge load=50kPa – Pile A.

Based on the comparison of the results between the two cases, it is observed that shear stresses cannot be combined, and the effect of foundation loading (decrease in the NSF magnitude) is higher than the expected shear stress increase along the pile perimeter.

4.5 Parametric Analyses of NSF and Dragload

The NSF and dragload of an end-bearing pile group can be influenced by several parameters. These influencing factors can be grouped into two main categories: dimension parameters of pile & pile group and soil parameters. The parameters investigated in these two different categories for the purpose of this study are tabulated in Table 4.4 and Table 4.5.

Table 4.4 Investigated pile & pile group dimension parameters.

Pile Diameter (m)	0.6	1.0	1.5
Pile Length (m)	L/D=15	L/D=20	L/D=25
Pile Spacing (m)	s/D=3	s/D=6	-
Pile Array	Single	3x3	5x5
Pile Position	The effect of pile position within the pile group		

It should be noted that all combinations of pile and pile group dimension parameters tabulated above have been modelled for the parametric analyses.

In soil parameter investigations, the presented model parameters in Chapter 4.1.1 were chosen as the base model and each parameter varied up and down while the others kept constant as shown in Table 4.5.

Table 4.5 Investigated soil parameters.

Parameter	**Reference Case**	**Parameter Variation**
Soil Compressibility (λ^*)	0.07	0.04 - 0.10
Cohesion (kPa)	7	2 - 12
Friction Angle (°)	28	24 - 32
Pile-Soil Interface	0.7	0.5 - 1.0

4.5.1 The effect of pile diameter

The effect of pile diameter has been investigated for two different cases and the same conclusion has been made for both of them. The percentile difference in the NSF increases from outer to inner piles where the highest difference is observed at the smaller diameter piles. Although, the NSF is higher for the smaller diameter piles due to the reduction in the surface area of the pile in contact with the soil for the outer piles, the dragload for the smaller diameter piles also starts to increase from outer to inner piles caused by the significant difference observed in the NSF for the inner piles. Two example figures have been provided in Figure 4.10 and Figure 4.11 for visualization of this occurrences whereas the rest of the figures presented in Appendix C.

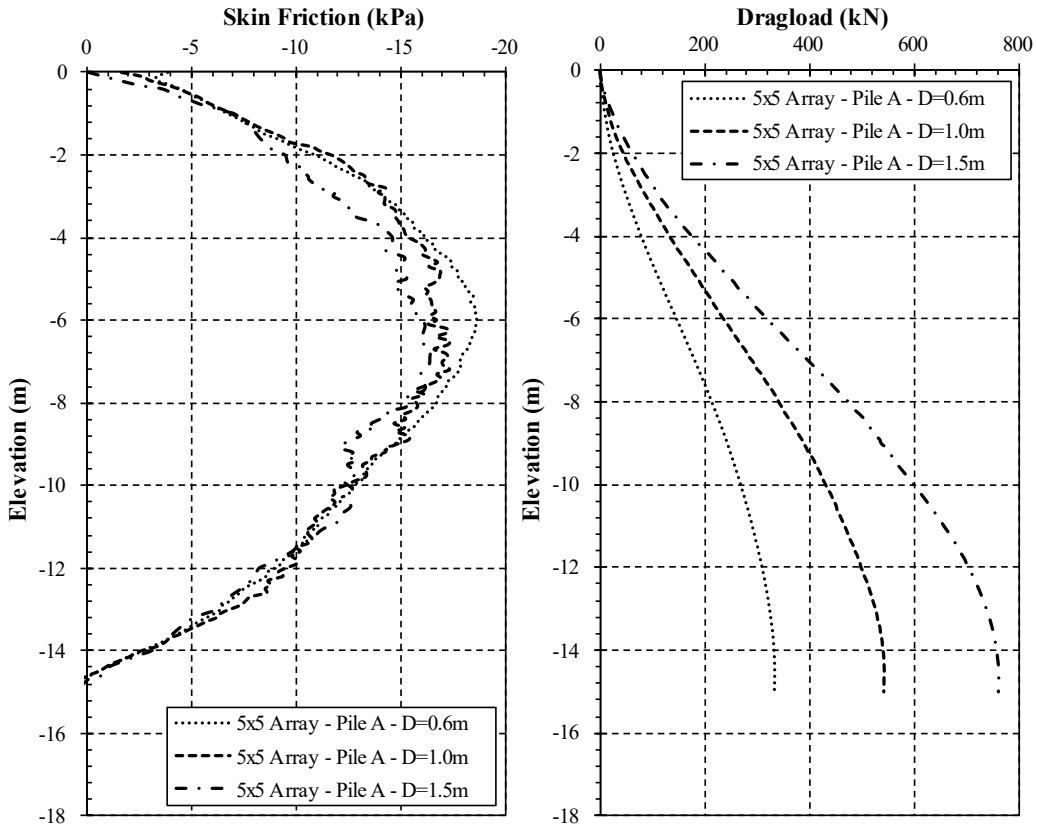

Figure 4.10 NSF and dragload of Pile A in three different diameter cases for model conditions of 5x5 array, L=15m, s/D=3 and surcharge load of 50kPa.

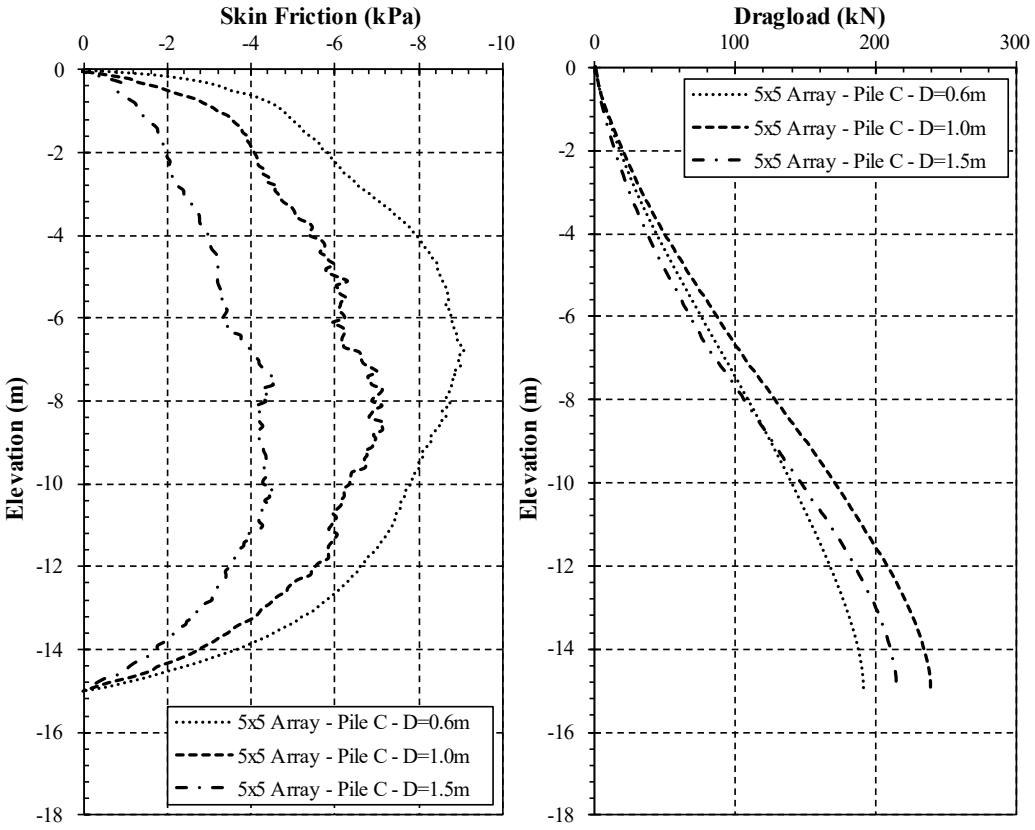

Figure 4.11 NSF and dragload of Pile C in three different diameter cases for model conditions of 5x5 array, L=15m, s/D=3 and surcharge load of 50kPa.

It should be noted that the pile spacings have been normalized with pile diameter for these two analysis cases, but this means that the pile group block area also increases with pile diameter. To investigate this phenomenon, another analysis has been performed where the pile positions are kept at the same locations with changing pile spacings for each pile diameter case. The results of this analysis have been presented for Pile A & Pile C for comparison in Figure 4.12 and Figure 4.13.

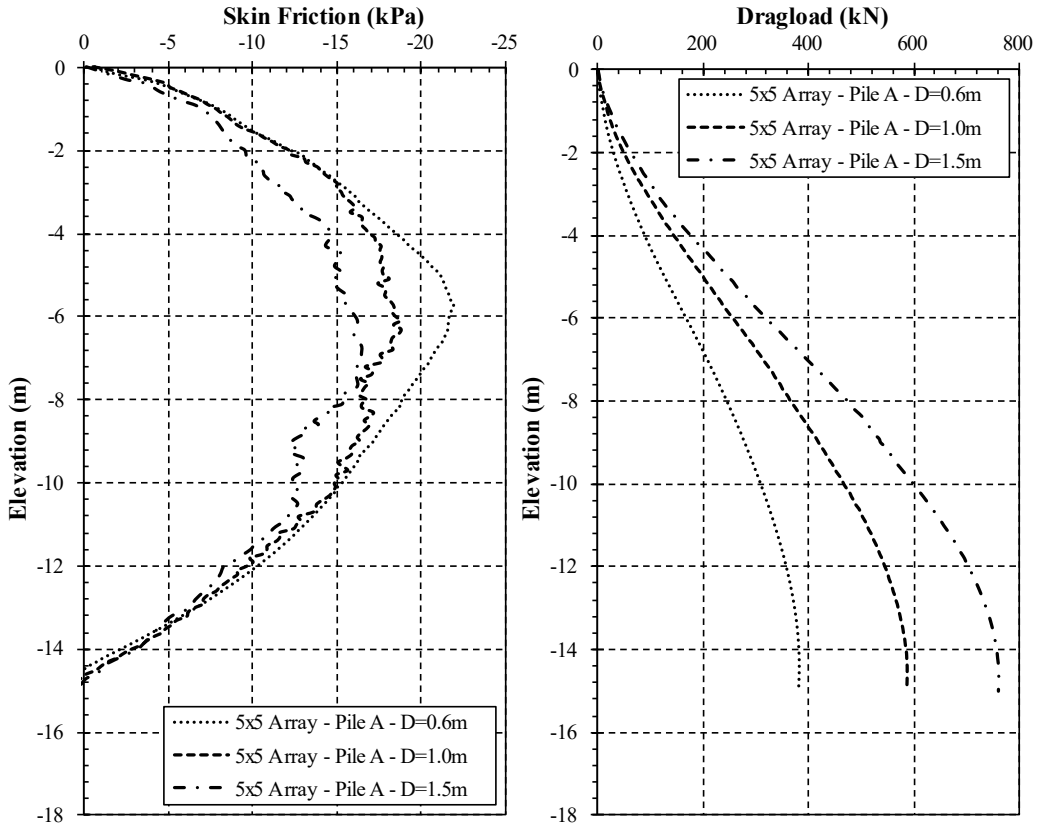

Figure 4.12 NSF and dragload of Pile A in three different diameter cases for model conditions of 5x5 array, L=15m, s=4.5m and surcharge load of 50kPa.

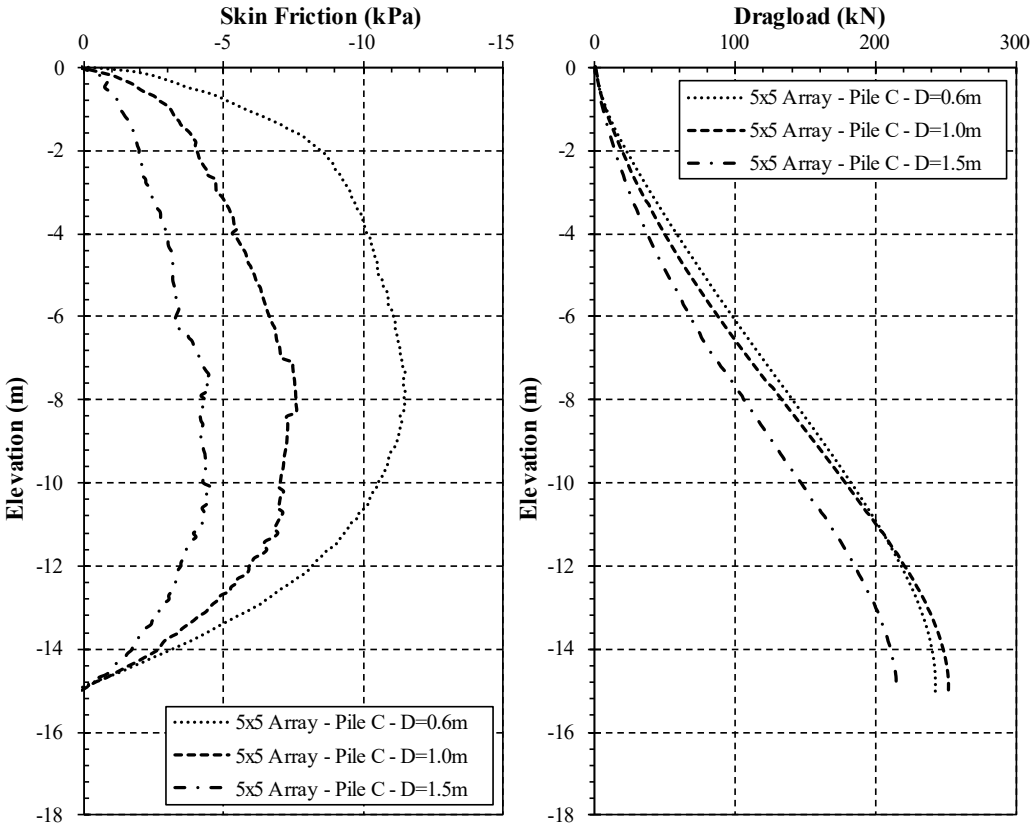

Figure 4.13 NSF and dragload of Pile C in three different diameter cases for model conditions of 5x5 array, L=15m, s=4.5m and surcharge load of 50kPa.

When different analysis cases were assessed, it is understood that the change of the NSF is not influenced by the distance from edge of the pile cap but instead it is affected by the distance between the adjacent piles. As the pile diameter increases, the distance between adjacent piles is reduced and as the piles starting from outer to inner piles are influenced by surrounding piles.

4.5.2 The effect of pile length

To understand the effect of pile length on the NSF and dragload behavior, three different analyses were performed for normalized pile lengths of 15D, 20D and 25D for the end-bearing pile groups connected with a pile cap. The analysis results

indicate that there is a direct correlation between the depth of full NSF mobilization and pile length, hence also the total dragload.

It is also acknowledged that shape of the NSF distribution along the pile length changes from outer to inner piles such that the maximum NSF is observed at greater depths for inner piles as shown in two example cases of Pile A and Pile F presented in Figure 4.14 and Figure 4.15, respectively. The rest of the figures for this analysis set are given in Appendix D.

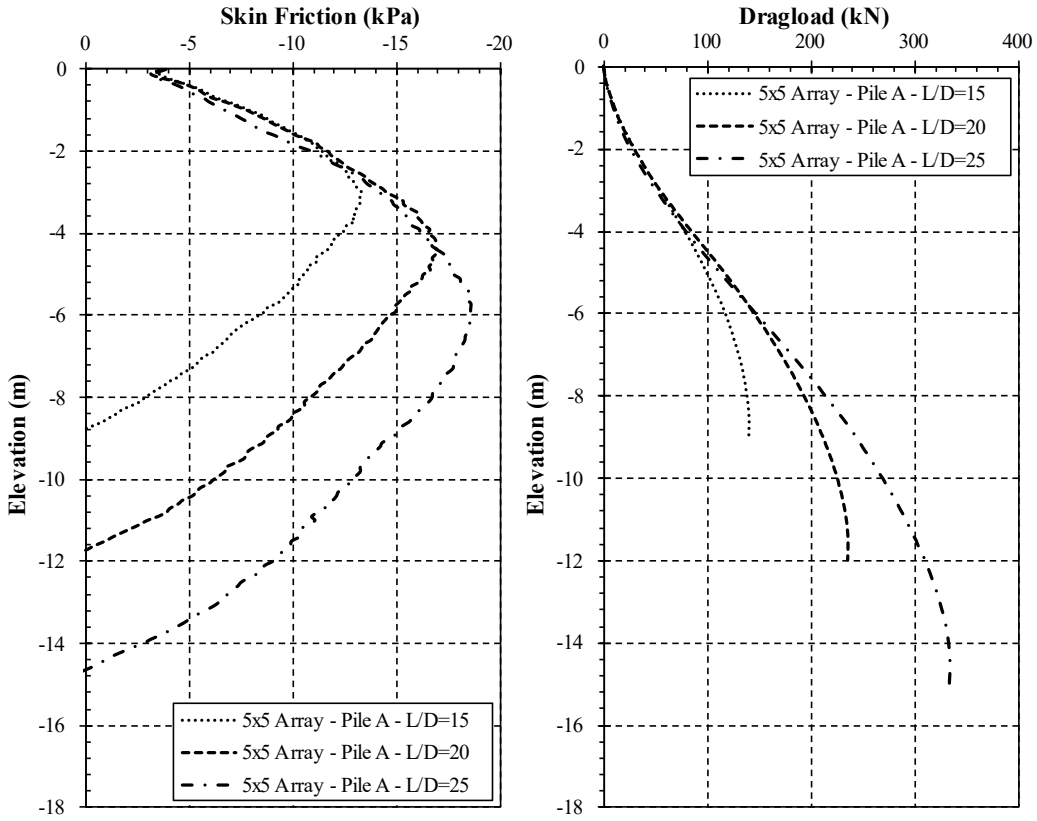

Figure 4.14 NSF and dragload of Pile A in three different length cases for model conditions of 5x5 array, D=0.6m, s/D=3 and surcharge load of 50kPa.

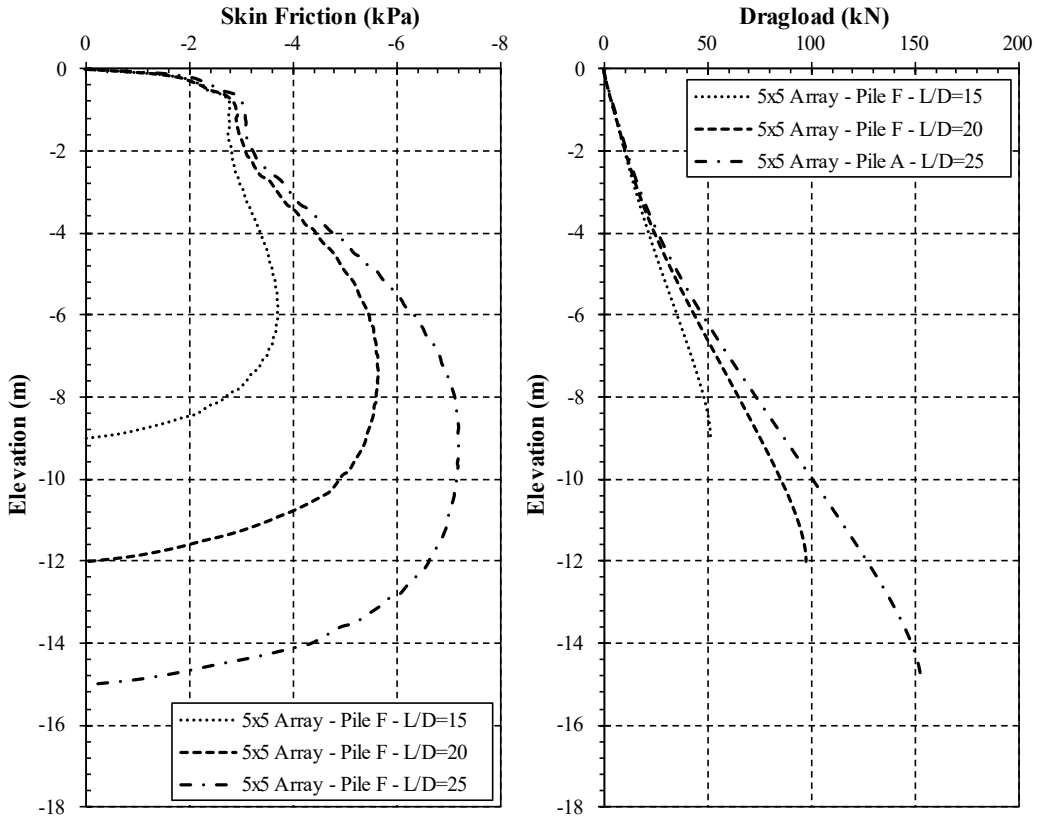

Figure 4.15 NSF and dragload of Pile F in three different length cases for model conditions of 5x5 array, D=0.6m, s/D=3 and surcharge load of 50kPa.

4.5.3 The effect of pile spacing

In order to investigate the effect of pile spacing, three analysis cases (s/D=3, s/D=6 and single pile) were examined. Although, pile spacing has an effect on the magnitude of the NSF (and hence the total dragload exerted on the piles) between the s/D=3 & 6 cases, it is not as severe as the difference observed in between the single pile and the individual pile in a pile group. This is mainly due to the effect of surrounding piles and load distribution within a pile group. Two example cases are plotted for Piles A and E in Figure 4.16 and Figure 4.17, respectively whereas the remaining figures are provided in Appendix E.

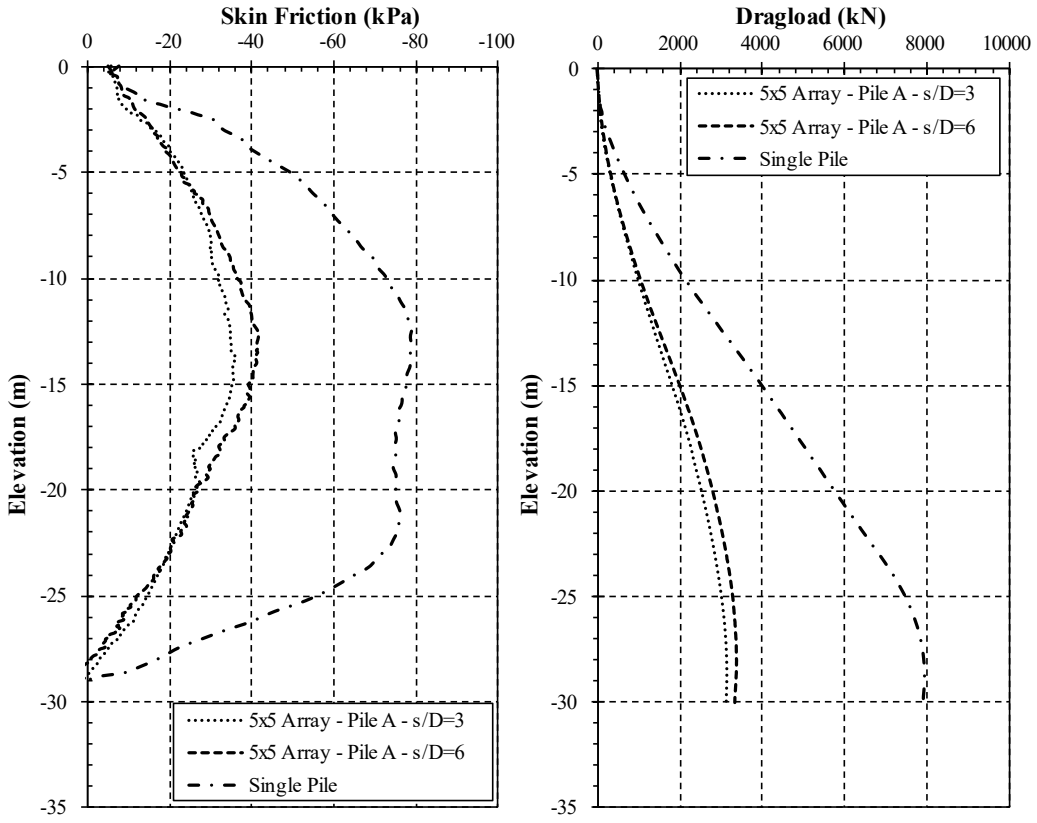

Figure 4.16 NSF and dragload of Pile A in three pile spacing cases for model conditions of D=1.5m, L/D=20 and surcharge load of 100kPa.

As it can be seen from Figure 4.16, increase in the pile spacing from 3D to 6D has increased the maximum NSF by 13% for Pile A whereas there is a 54% to 47% reduction in the maximum NSF between the single pile and 3D and 6D spacings respectively.

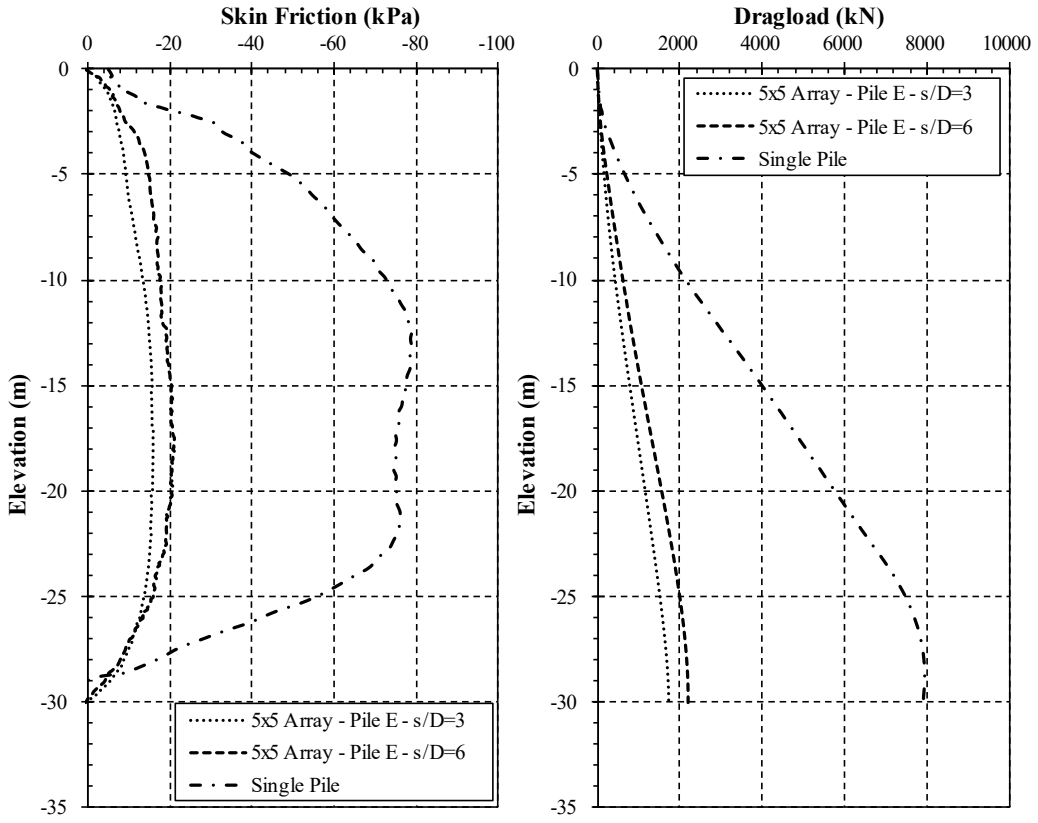

Figure 4.17 NSF and dragload of Pile E in three pile spacing cases for model conditions of D=1.5m, L/D=20 and surcharge load of 100kPa.

Figure 4.17 indicates that for inner piles, the pile spacing effect is not localized to the middle of the pile length as in the case of the outer piles. The difference in the NSF between the 3D and 6D pile spacings distributed all along the pile length.

4.5.4 The effect of number of piles in a pile array

The surcharge load distribution has a significant effect on the magnitude of the NSF and its distribution along the pile length as discussed briefly in Section 4.5.3. However, to explore this effect in detail 3x3 and 5x5 pile array groups have been investigated for different pile diameters and surcharge loads, and results have been given in Appendix F. The analyses have shown that the maximum NSF increases as the number of piles in a pile array decrease. Additionally, the position of the

maximum NSF (the turning point) shifts to greater depths. Moreover, when the outer and inner piles were compared, this change in the magnitude and position of the NSF increases from outer to inner piles, hence consequently the total dragload increases too. Two example figures are presented in this section to discuss the results in Figure 4.18 and Figure 4.19 for Piles A and C respectively.

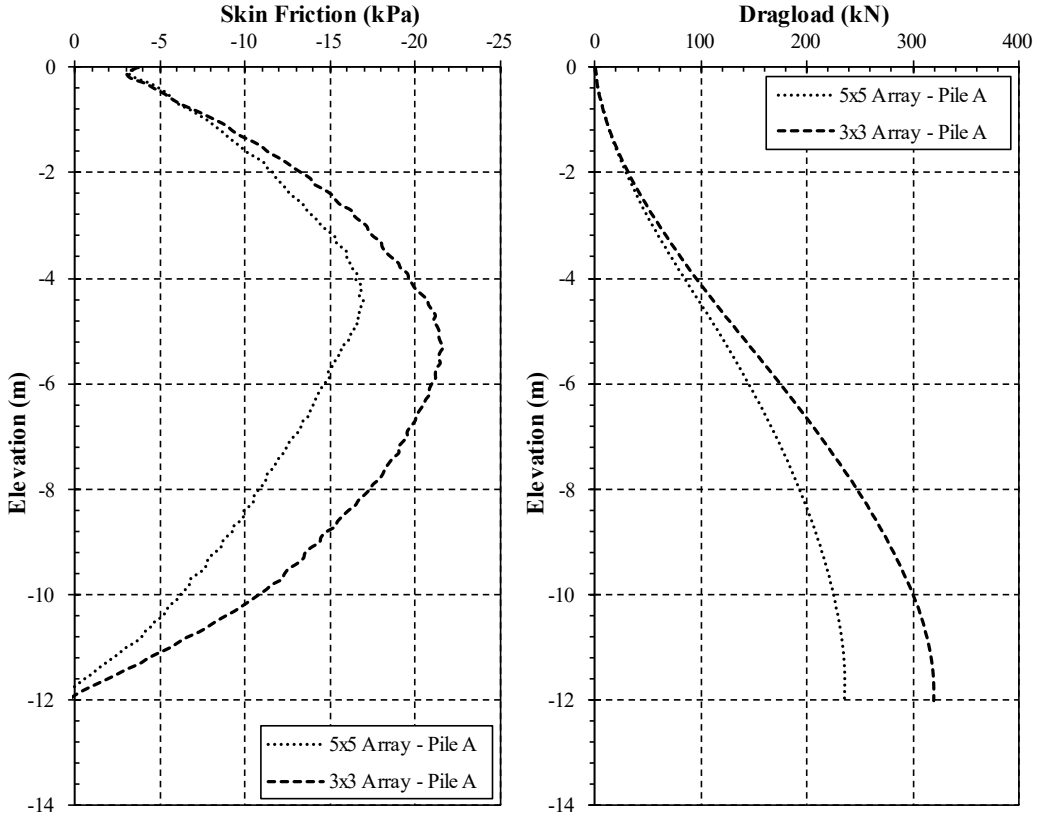

Figure 4.18 NSF and dragload of Pile A in two different pile arrays for model conditions of D=0.6m, s/D=3, L/D=20 and surcharge load of 50kPa.

As presented in Figure 4.18, the maximum NSF increases by 21% as the number of piles decreases from 25 to 9 for the corner Pile A. It should be noted that the turning point of the NSF shifts from 4.5m depth to 5.3m.

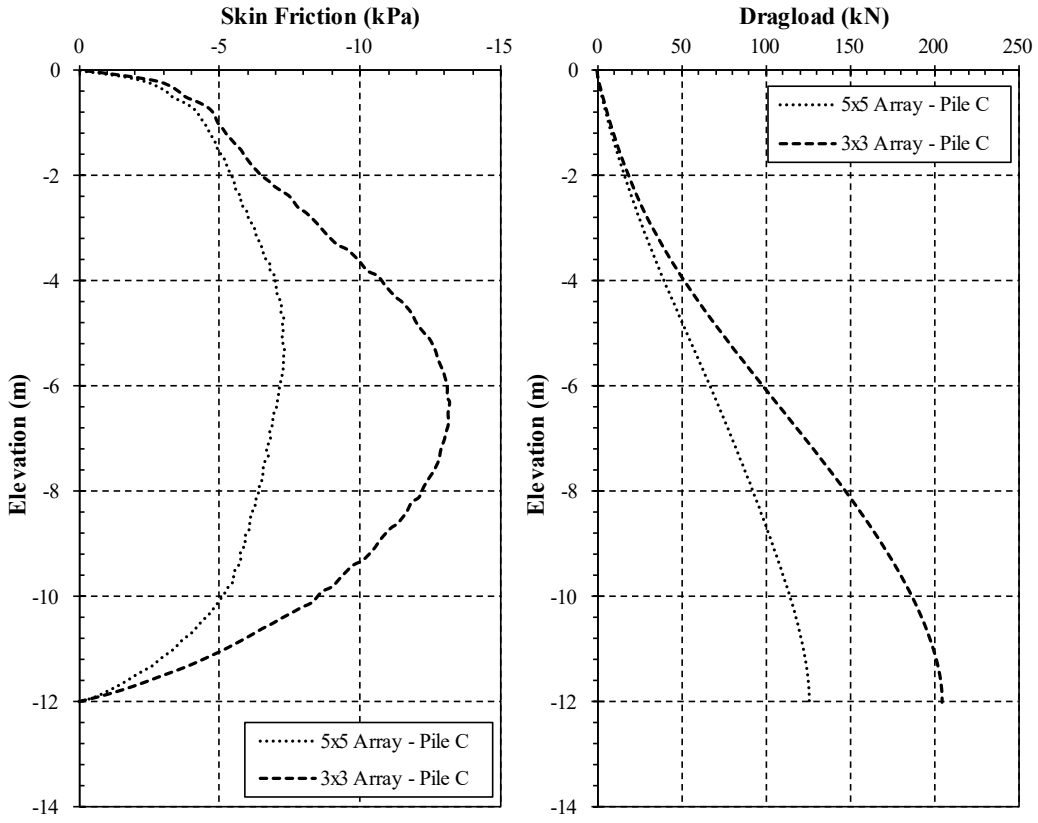

Figure 4.19 NSF and dragload of Pile C in two different pile arrays for model conditions of D=0.6m, s/D=3, L/D=20 and surcharge load of 50kPa.

When the inner Pile C is examined, it is observed that the change in magnitude of NSF has increased by 82% and the turning point of the maximum NSF has changed from 5.1m depth to 6.5m when the array is changed from 5x5 to 3x3.

4.5.5 The effect of pile position in a pile array

A total of 12 analyses have been examined to understand the NSF behavior and dragload forces acting on the pile for different diameter, spacing and surcharge load cases. It has been observed that slope of the NSF distribution along the pile length and the turning point of the NSF decreases from outer to inner piles. It is also noted that the location of the NP shifts slightly towards the ground surface in the same

order. The example case for D=0.6m, s/D=6 and surcharge load of 50kPa is presented in Figure 4.20 and the remaining analysis results have been given in Appendix G.

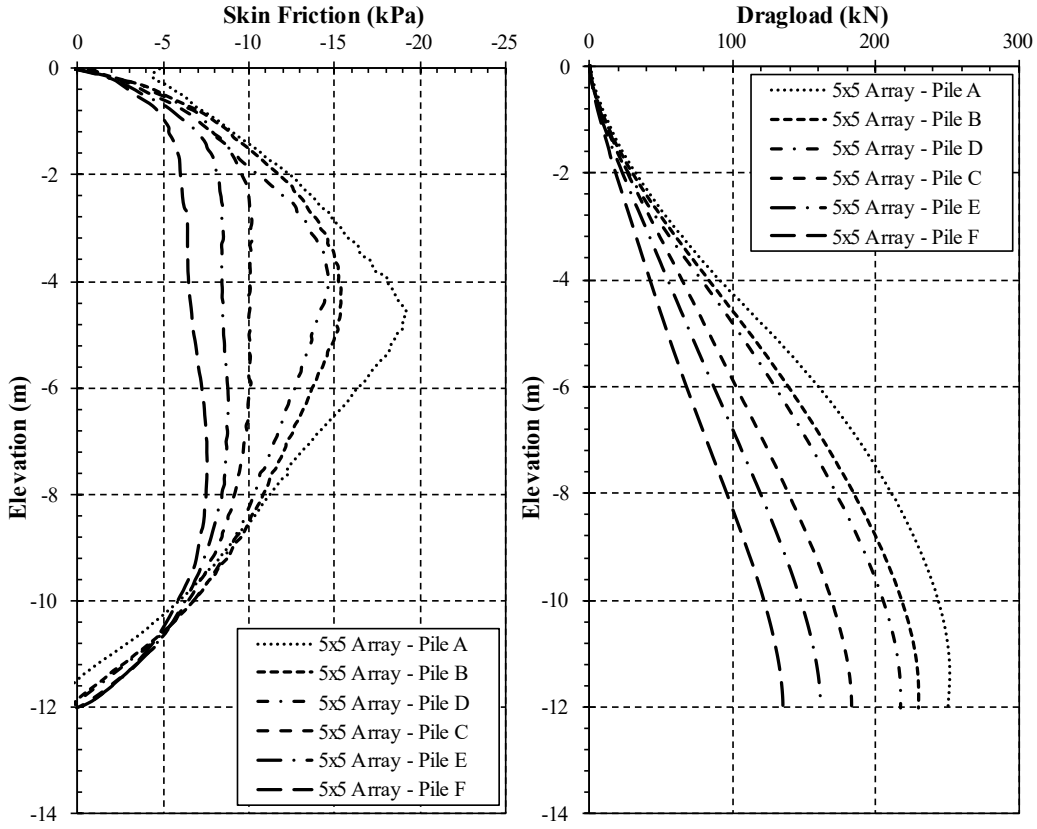

Figure 4.20 NSF and dragload of different pile positions for model conditions of D=0.6m, s/D=6, L/D=20 and surcharge load of 50kPa.

As it can be seen from Figure 4.20, the maximum NSF and the total dragload exerted on the piles decreases from corner to edge, inner and center piles in the following order of the pile naming convention: A – B – D – C – E – F.

Additionally, in order to investigate the effect of surcharge load on the NSF behavior acting along the pile length, 100kPa surcharge load has been applied on the model and the results are presented in Figure 4.21.

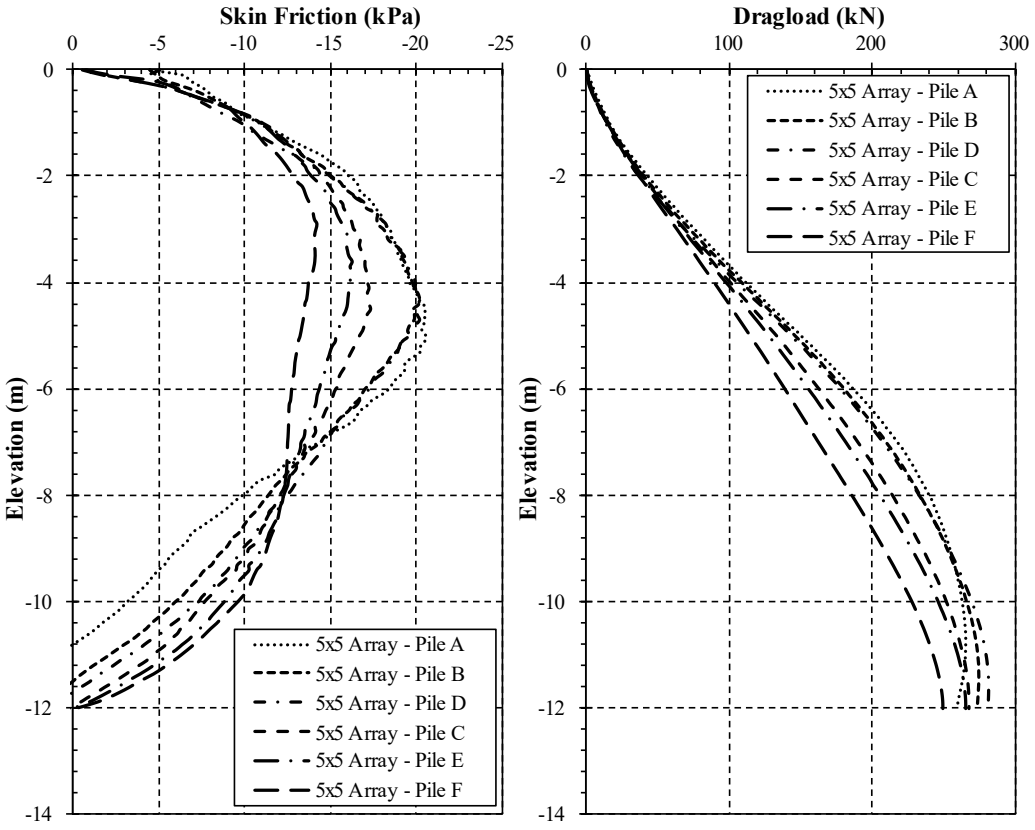

Figure 4.21 NSF and dragload of different pile positions for model conditions of D=0.6m, s/D=6, L/D=20 and surcharge load of 100kPa.

When the surcharge load is increased from 50kPa to 100kPa, it is noticed that the difference of the magnitude of the NSF between the piles decreased. On the other hand, NSFs increase for all piles where the change is higher from outer to inner piles.

It is noted that with increasing surcharge load, NSF distribution along the pile length of inner and outer piles got similar. It should also be noted that increase in the surcharge load has shifted NP location towards the ground surface much more drastically which is beneficial considering the decrease in the total dragload forces acting on the piles.

4.5.6 The effect of soil compressibility

In order to examine the effect of soil compressibility on the NSF and dragload behavior for the end-bearing piles connected with a cap, three different soil compressibility factors (λ^*): 0.04, 0.07 and 0.10 have been chosen which are corresponding to C_c of 0.17, 0.30 and 0.43 for the same initial void ratio (e_0) of 0.9. The two example cases are presented in Figure 4.22 and Figure 4.23 for Piles B and E respectively where the rest of the analyses results are given Appendix H.

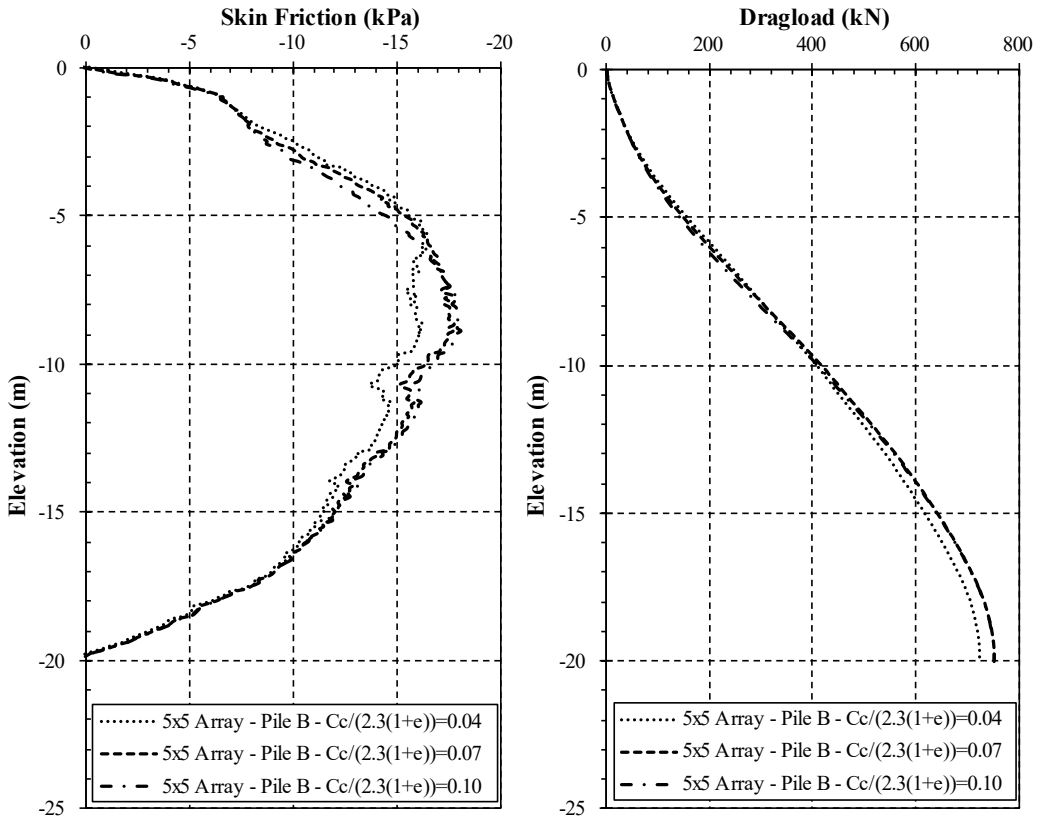

Figure 4.22 NSF and dragload of three different soil compressibility factors of Pile B for D=1.0m, s/D=3, L/D=20 and surcharge load of 50kPa.

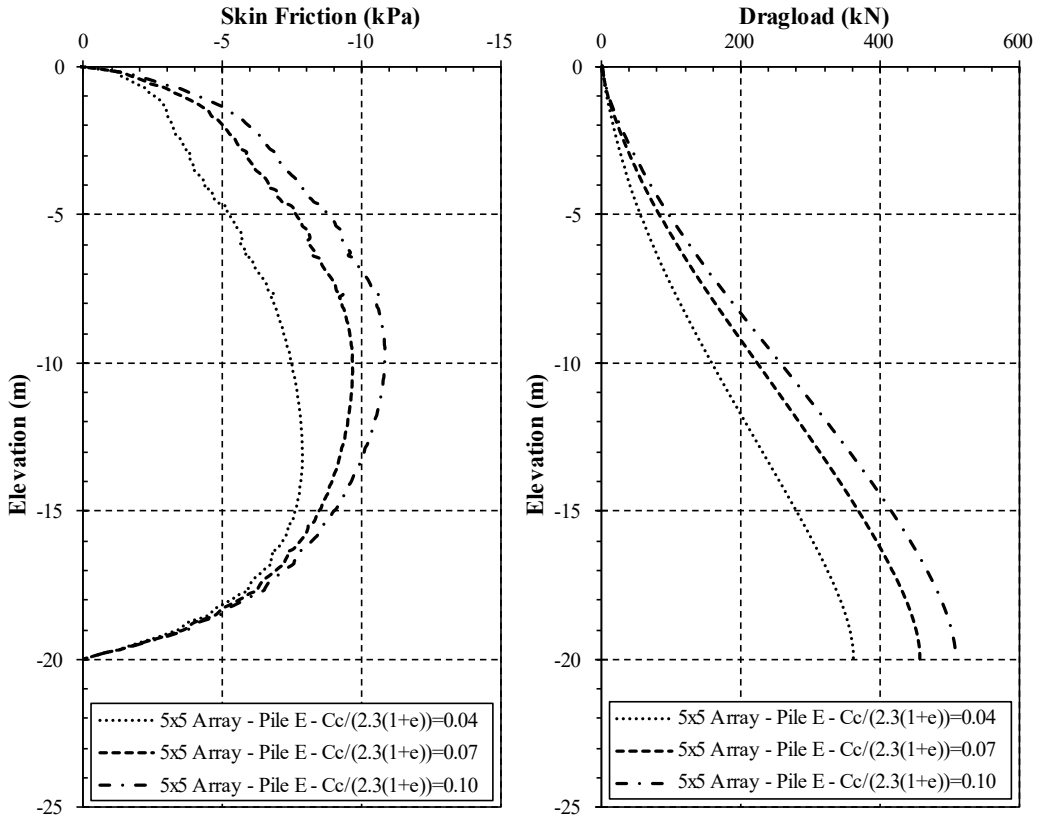

Figure 4.23 NSF and dragload of three different soil compressibility factors of Pile E for D=1.0m, s/D=3, L/D=20 and surcharge load of 50kPa.

The results of the analyses show that the change of the magnitude of the NSF and dragload is greater for the inner piles than the outer piles which already are taking NSF fully. It is also observed that with the increasing soil compressibility factor the turning point of maximum NSF shifts towards the top of the pile for the outer piles, whereas it shifts toward the tip for the inner piles.

4.5.7 The effect of soil cohesion

The effect of soil cohesion of the NSF behavior and the total dragload forces on the end-bearing pile group has been looked into by changing the effective cohesion by 2, 7 and 12 kPa. The results of two example pile positions have been presented in

Figure 4.24 and Figure 4.25 for Piles B and C respectively whereas the remaining analysis results have been provided in Appendix I.

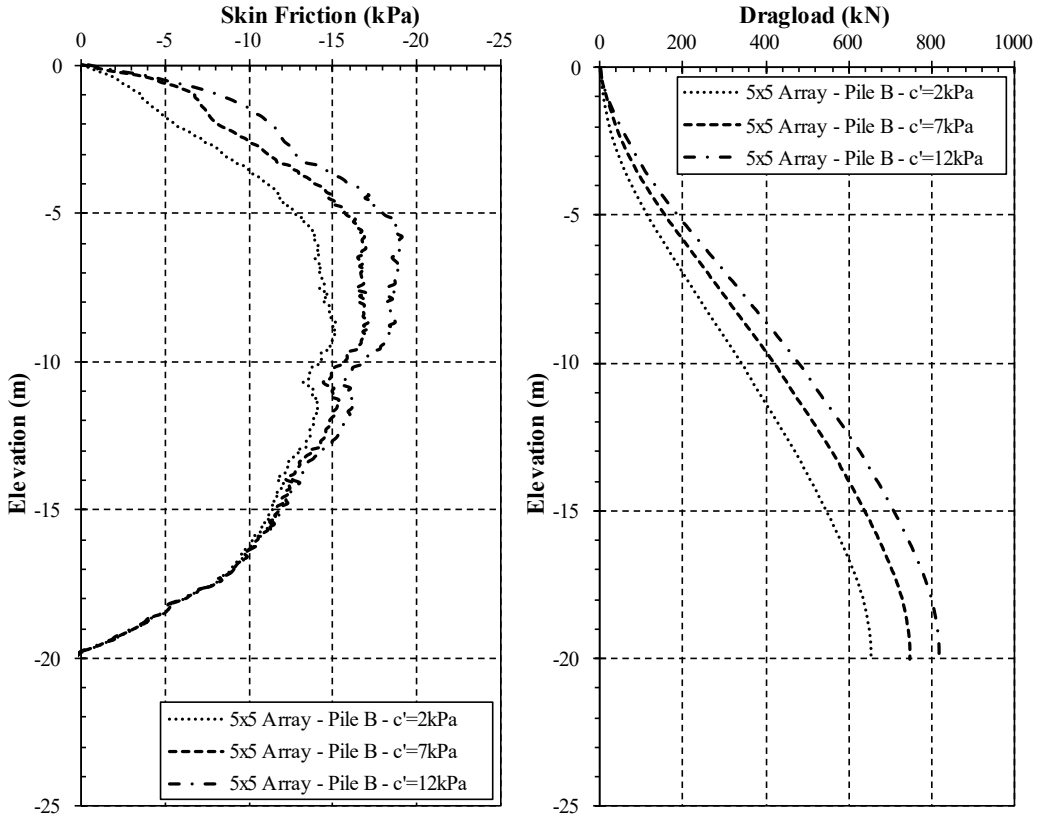

Figure 4.24 NSF and dragload of three different soil cohesion of Pile B for model conditions of D=1.0m, s/D=3, L/D=20 and surcharge load of 50kPa.

As it can be seen from Figure 4.24, the cohesion affects the NSF for approximately 80% of the pile length starting from the top part of the pile while no change is observed towards the tip of the pile/start of the bearing stratum.

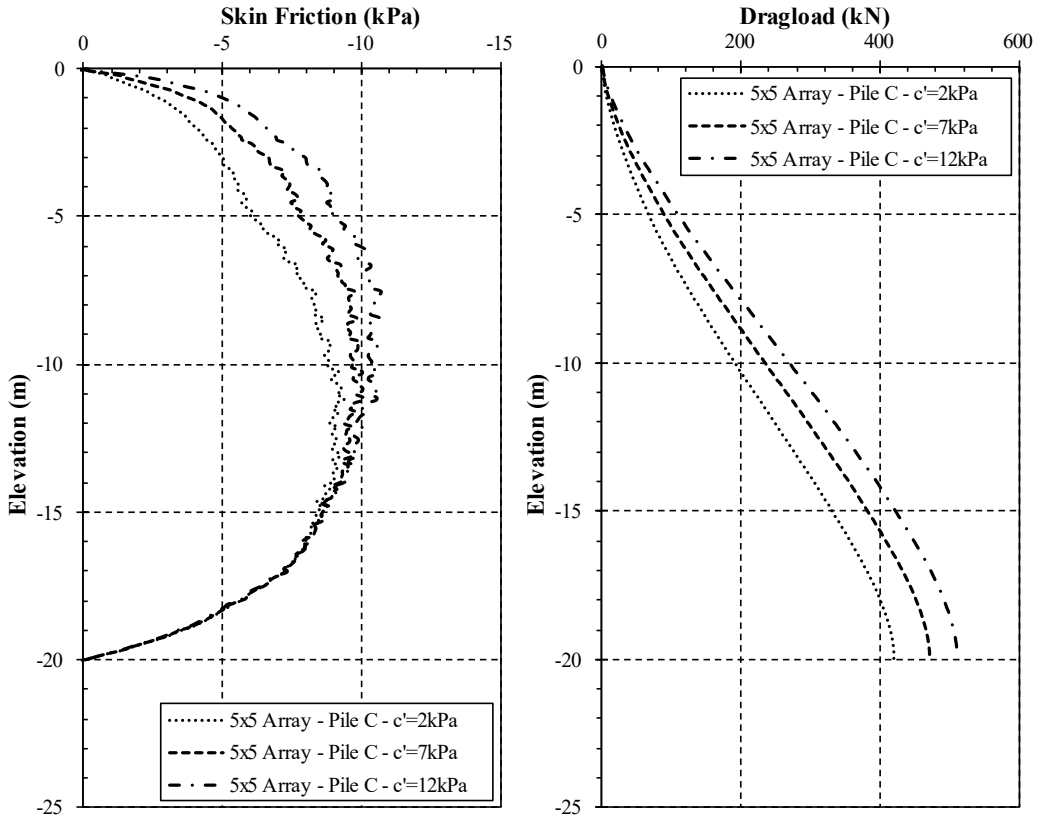

Figure 4.25 NSF and dragload of three different soil cohesion of Pile C for model conditions of D=1.0m, s/D=3, L/D=20 and surcharge load of 50kPa.

By comparison of Figure 4.24 and Figure 4.25, it is observed that the change in the NSF and the dragload is similar for all piles regardless of their position in the pile group.

4.5.8 The effect of soil friction angle

Long term effective friction angle of the soft clay usually changes between 24 to 32° and the effect of this change has been investigated by running three different FEA models and setting the friction angles to 24, 28 and 32°. The analysis results of two different pile positions are illustrated in Figure 4.26 and Figure 4.27 for Piles A and E, while the remainder of the analysis results are provided in Appendix J.

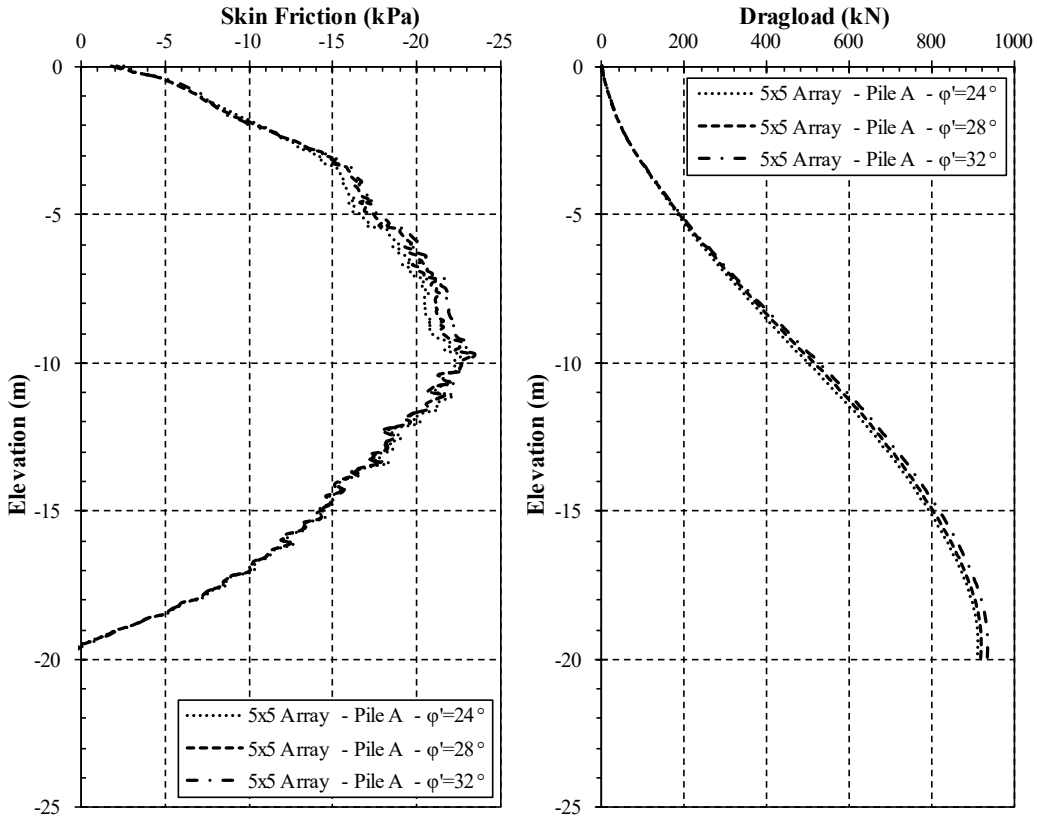

Figure 4.26 NSF and dragload of three different soil friction angles of Pile A for model conditions of D=1.0m, s/D=3, L/D=20 and surcharge load of 50kPa.

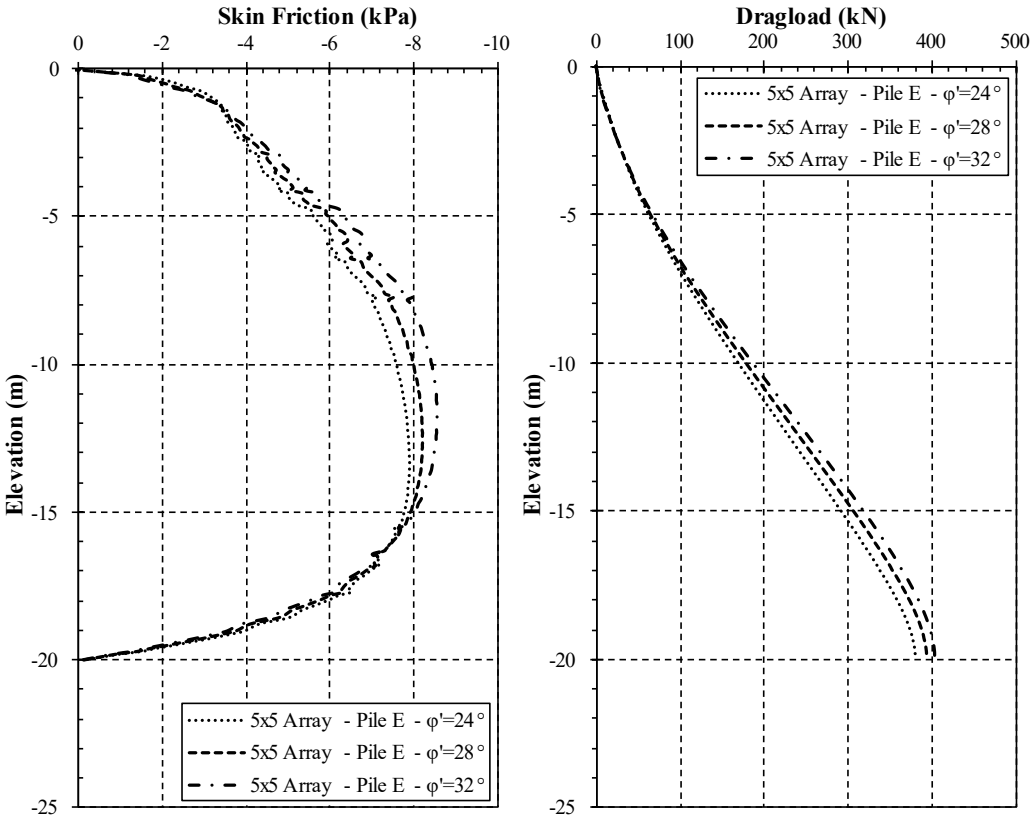

Figure 4.27 NSF and dragload of three different soil friction angles of Pile E for model conditions of D=1.0m, s/D=3, L/D=20 and surcharge load of 50kPa.

The analysis results have revealed that there is a negligible change in magnitude of the NSF and the total dragload exerted on the pile length regardless of the pile position in the pile arrangement.

4.5.9 The effect of interface coefficient

The interaction between a pile and the adjacent soil significantly influences the load-bearing capacity of a pile foundation. The FEA model computes the shearing force by multiplying the shear strength with an interface coefficient represented by R_{int}. For the purpose of this study three different analyses have been performed for different R_{int} values of 0.5, 0.7 and 1.0. The example pile position results of the analyses have been presented in Figure 4.28 and Figure 4.29 for better understanding

and the interpretation of the results whereas results of the rest of the analyses are provided in Appendix K.

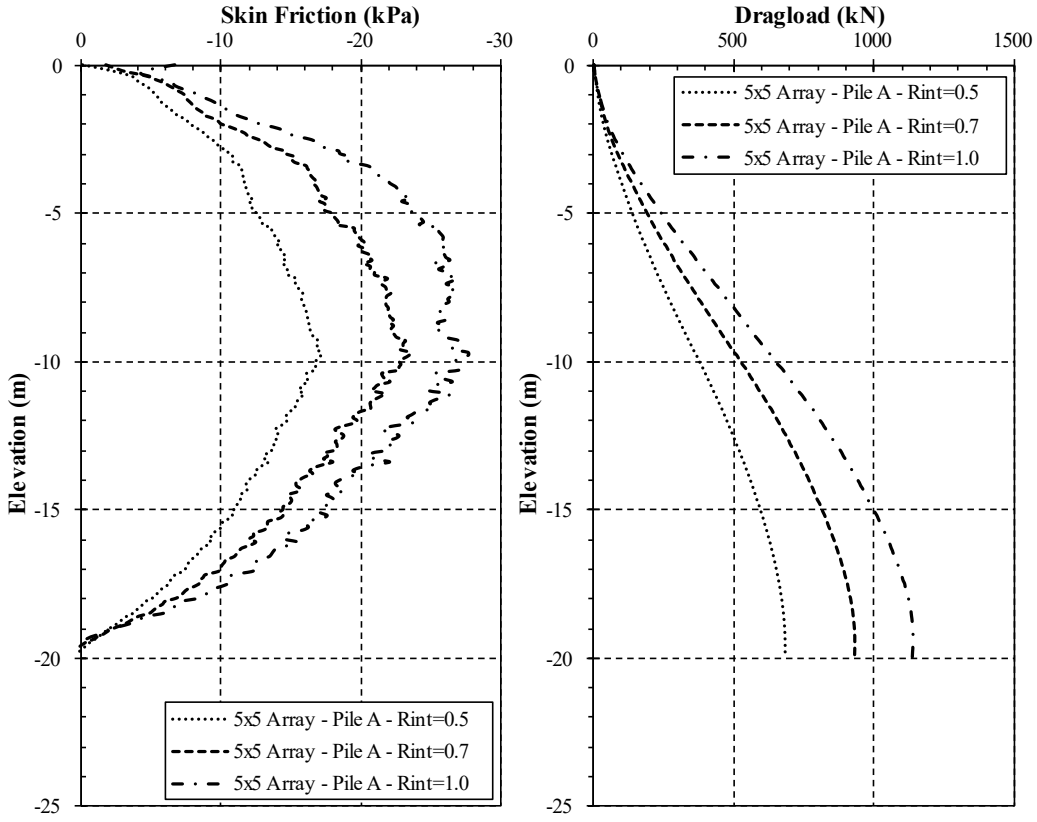

Figure 4.28 NSF and dragload of three different pile-soil interface coefficient of Pile A for D=1.0m, s/D=3, L/D=20 and surcharge load of 50kPa.

Based on Figure 4.28, the pile-soil interface coefficient correlates with the magnitude of the NSF and consequently the total dragload forces acting on the pile shaft for the outer piles. As R_{int} controls the ultimate skin friction, it also directly affects NSF for corner piles which are at their ultimate limit state as far as skin friction is concerned.

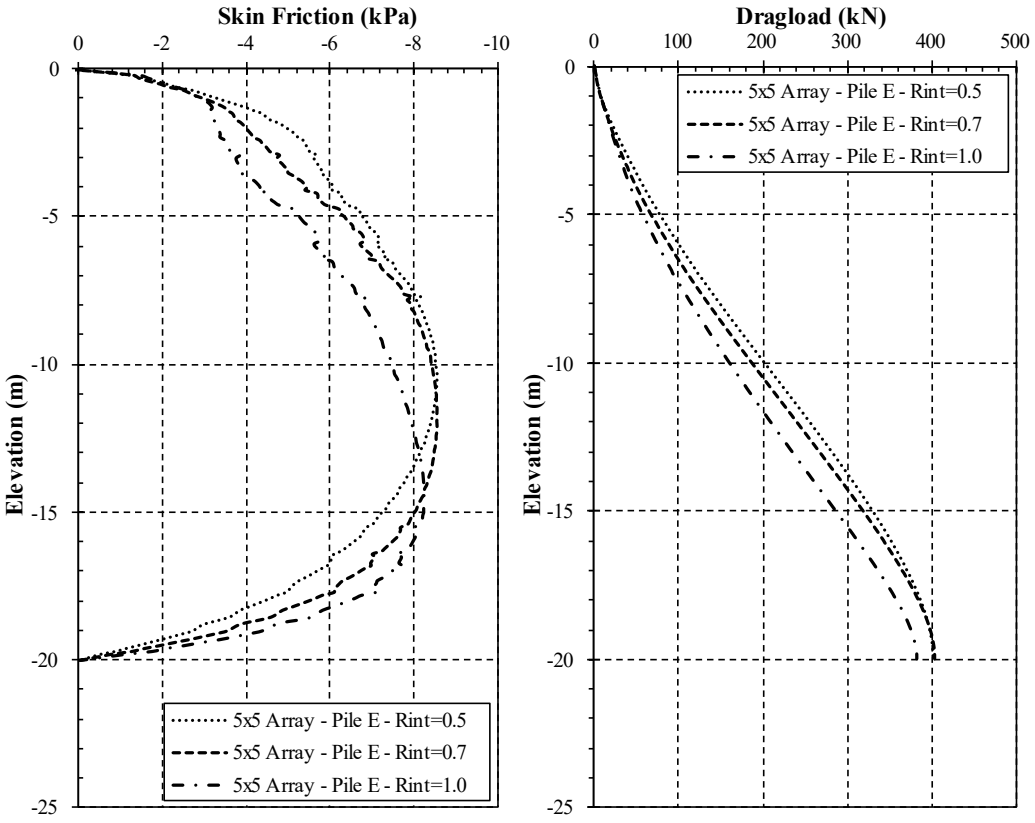

Figure 4.29 NSF and dragload of three different pile-soil interface coefficient of Pile E for D=1.0m, s/D=3, L/D=20 and surcharge load of 50kPa.

The plotted results of inner Pile E in Figure 4.29 have showed that the maximum NSF does not change with increasing R_{int} which means that the inner piles do not reach the capacity. It is also noted that as the pile-soil interface coefficient increases the position of the maximum NSF and hence turning point moves towards the pile tip.

4.6 Comparison of the Results with Analytical Estimations

It is previously discussed that unlike the other analytical methods, the β-method takes into account effective stress parameters, which are critical in determining the soil strength under negative skin friction's drained conditions. By directly considering the effective stresses, the β-method provides a more realistic and accurate approach for estimating the reduction in shaft resistance. Hence, the β-method has been chosen to compare the finite element analysis model results for outer piles by normalizing all the pile group dimensions with the pile diameter. These findings are illustrated in Figure 4.30 to Figure 4.32 for the 5x5 pile array. It should be noted that comparisons between the β-method and FEA results are not provided for the inner piles because the β-method is not capable of considering the group effects within a pile group.

The β-method formula used for the NSF comparisons against the FEA results are given in Equation (4.1).

$$NSF = K tan\delta * \{q * tan\phi' + c' - [\sigma' * tan\phi']\} \quad (4.1)$$

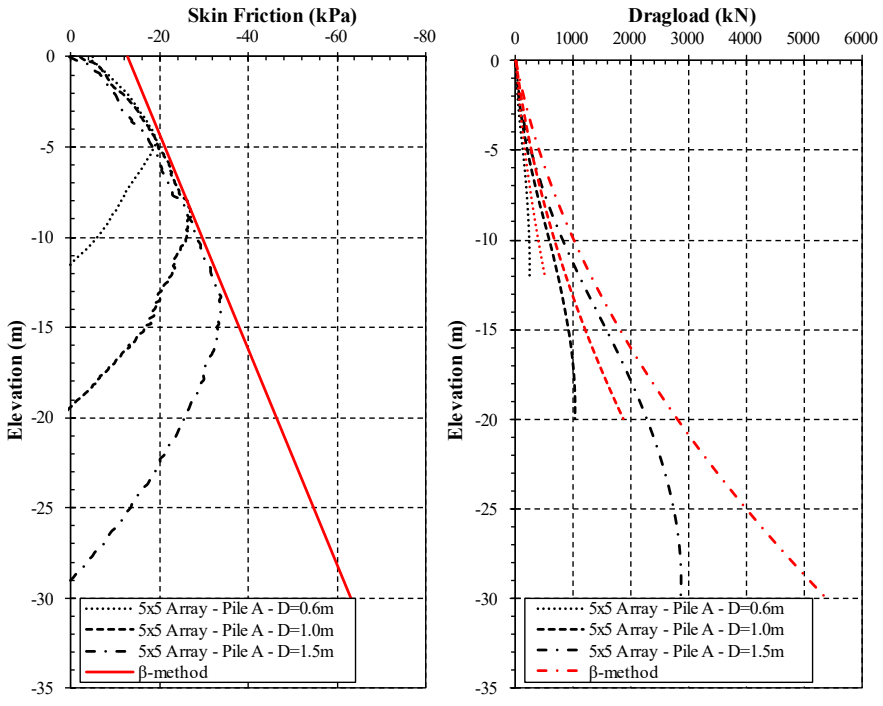

Figure 4.30 Comparison of the NSF between FEA and the β-method for 5x5 pile array, s/D=6, L/D=20 and surcharge load of 50kPa – Pile A.

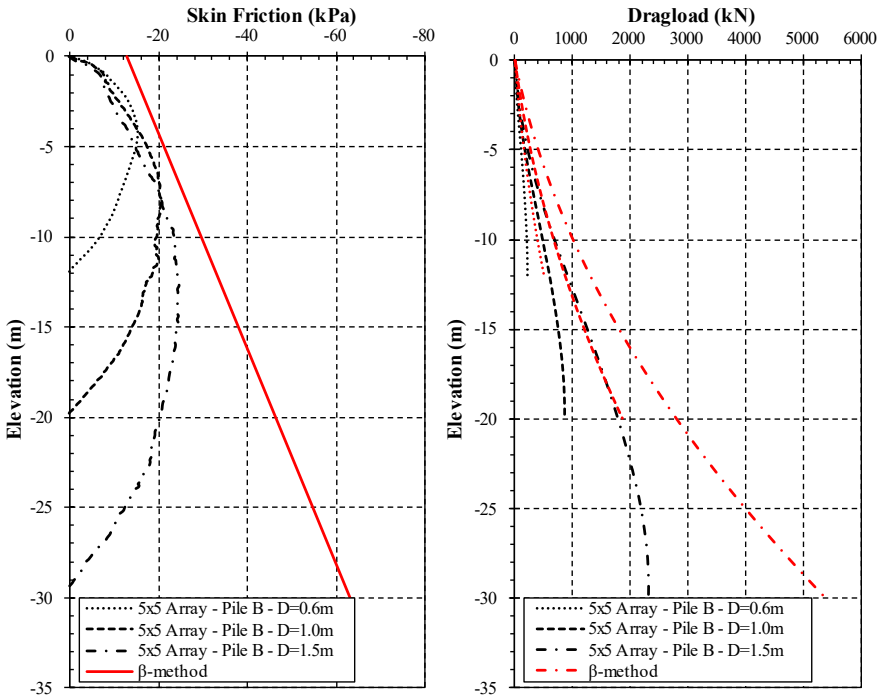

Figure 4.31 Comparison of the NSF between FEA and the β-method for 5x5 pile array, s/D=6, L/D=20 and surcharge load of 50kPa – Pile B.

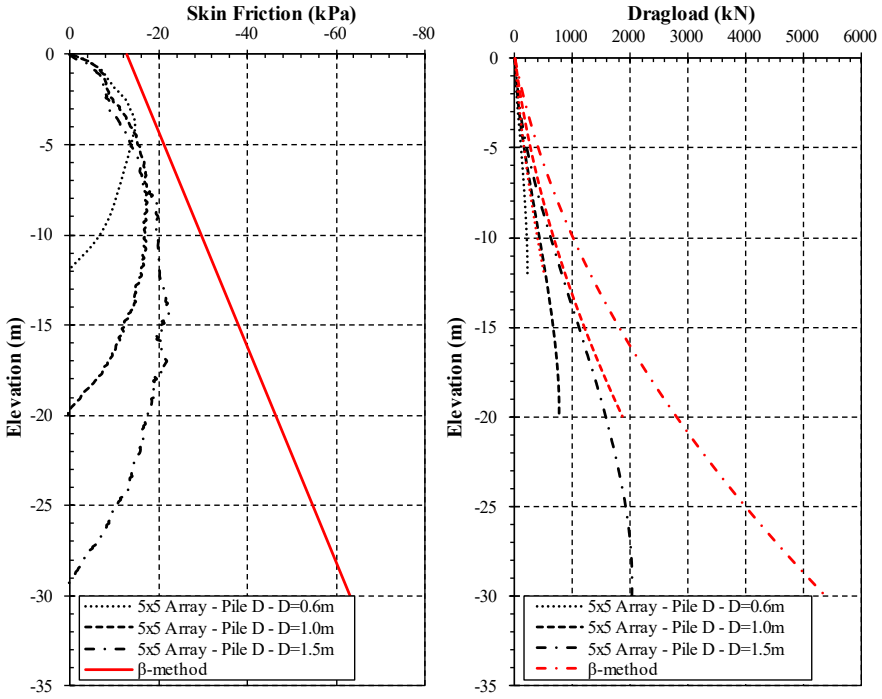

Figure 4.32 Comparison of the NSF between FEA and the β-method for 5x5 pile array, s/D=6, L/D=20 and surcharge load of 50kPa – Pile D.

When the results of outer piles are compared between the FEA and the β-method, it is observed that the estimation of the maximum NSF for corner Pile A matches reasonably well and there is a slight overestimation for edge piles B and D. The remaining comparisons between the all-normalized FEA cases and the β-method estimations are presented in Appendix L.

It is also observed that while the β-method continues to increase towards the pile tip due to increase in the overburden stresses, findings of the FEA show a decrease in the NSF after a certain pile length, beyond which the difference between settlements of piles and soil is smaller. This situation would cause the overestimation of the calculated total dragload forces.

Based on the NSF distributions presented in Figure 4.30 to Figure 4.32, the total dragload exerted on outer pile has been calculated for both the β-method and the FEA results. The comparison of the results have shown in Table 4.6 along with the percentile difference whereas the remaining tables are given in Appendix L.

Table 4.6 Comparison of dragload forces for outer piles for three different pile diameters between the β-method and FEA results.

Pile-#	Dragload (kN)						Percentile Difference (%)		
	FEA Results			β-Method					
	D=0.6m	D=1.0m	D=1.5m	D=0.6m	D=1.0m	D=1.5m	D=0.6m	D=1.0m	D=1.5m
Pile-A	250	1028	2868	521	1867	5385	108	82	88
Pile-B	230	864	2307	521	1867	5385	127	116	133
Pile-D	217	770	2022	521	1867	5385	140	142	166

The provided comparison table of dragloads between the FEA results and the β-method indicate that there is an overestimation of the calculated dragloads and it is generally higher than 100% for outer piles. It is also noticed that the observed difference is higher for the edge piles than the corner pile. This difference could be caused by the incapability of neighboring effect considerations in the β-method.

4.7 Comparison of 3D Results with 2D Axisymmetric Simulation of Tributary Area Method

The NSF for the piles that are not located at the edge of a pile group cannot be determined by the β-method since the inner piles are not in contact with the outer soil area that settles more. The NSF and dragload estimations for the inner piles are only influenced by the surcharge (or weight of the fill) within each individual cell area. Hence, the tributary area method has been used to calculate the NSF and the dragload for the inner and center piles.

For the purpose of this comparison, 2D axisymmetric FEA is used to calculate the NSF behavior and magnitude for tributary area estimations and the model width is chosen as half of the pile spacing for each scenario. The comparison of the results is presented from Figure 4.33 to Figure 4.35 for a 5x5 pile array, s/D=6, L/D=20, surcharge load of 100 kPa and for Piles C, E and F respectively whereas the remaining figures are given in Appendix M.

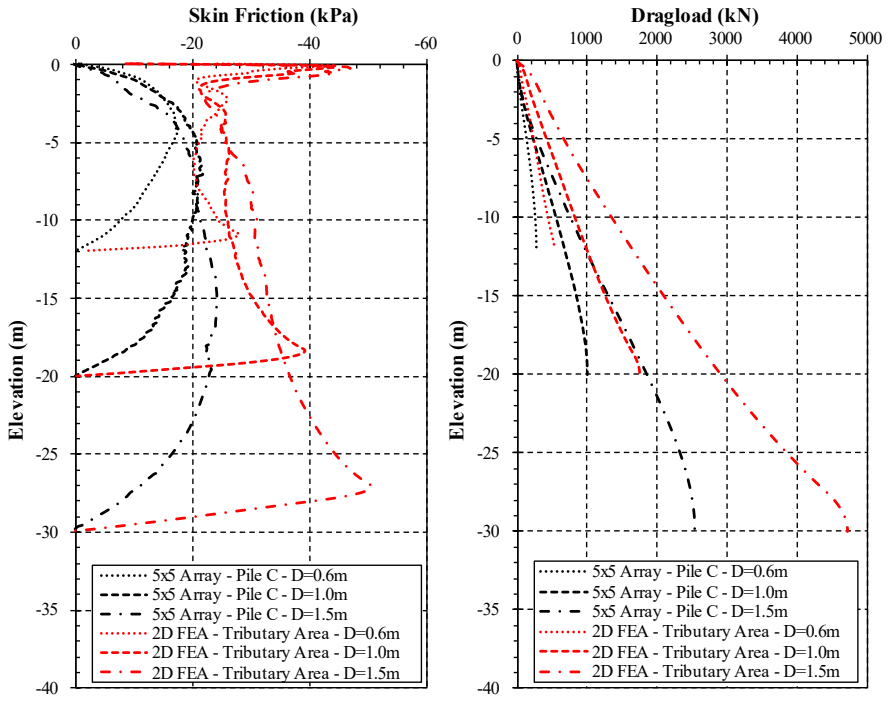

Figure 4.33 Comparison of the NSF between 3D FEA and 2D axisymmetric tributary area, 5x5 pile array, s/D=6, L/D=20 and surcharge load of 100kPa – Pile C.

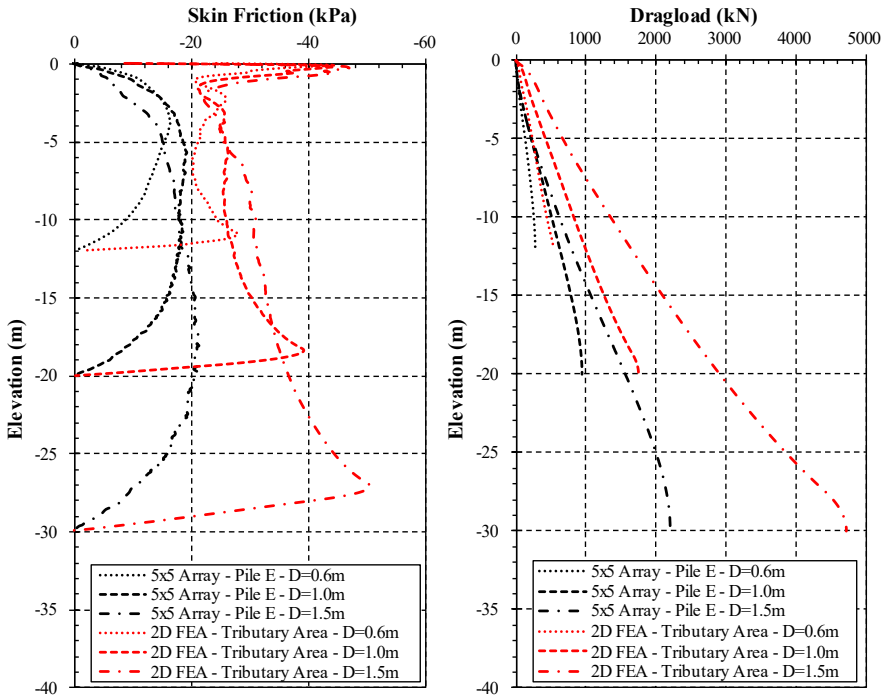

Figure 4.34 Comparison of the NSF between 3D FEA and 2D axisymmetric tributary area, 5x5 pile array, s/D=6, L/D=20 and surcharge load of 100kPa – Pile E.

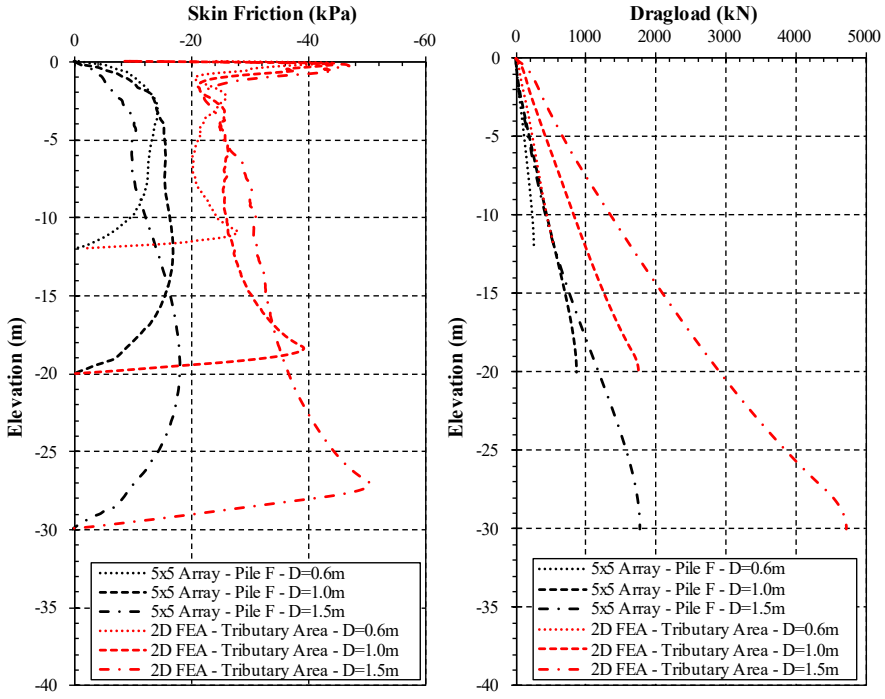

Figure 4.35 Comparison of the NSF between 3D FEA and 2D axisymmetric tributary area, 5x5 pile array, s/D=6, L/D=20 and surcharge load of 100kPa – Pile F.

Based on the provided comparisons between the FEA results and tributary area method, it is observed that NSF distribution does not match well. Moreover, the tributary area method overestimates the magnitude of the NSF. When the results for s/D=3 are inspected, it is seen that NP location may shift towards the ground surface and full mobilization of NSF may not happen. Hence, the amount of dragload exerted on the piles can be underestimated for s/D=3 spacing, but for s/D=6 spacing, the dragloads are overestimated due to higher NSF around the inner piles.

The comparison of the calculated dragload results are shown in Table 4.7 along with the percentile differences for this pile array whereas the remaining tables are given in Appendix M.

Table 4.7 Comparison of dragload forces for inner piles for three different pile diameters between the tributary area method and FEA results for 5x5 pile array, s/D=6, L/D=20 and surcharge load of 100kPa.

Pile-#	Dragload (kN)						Percentile Difference (%)		
	3D FEA			2D Axisymmetric					
	D=0.6m	D=1.0m	D=1.5m	D=0.6m	D=1.0m	D=1.5m	D=0.6m	D=1.0m	D=1.5m
Pile-C	267	1002	2533	522	1752	4711	96	75	86
Pile-E	265	934	2197	522	1752	4711	97	88	114
Pile-F	250	854	1777	522	1752	4711	109	105	165

4.8 New Method for Predictions of NSF

Finite element analysis remains a robust and capable method for predictions of negative skin friction (NSF) in pile foundations. However, its efficacy diminishes when dealing with multiple pile foundations or when conducting consolidation assessments with numerous piles, significantly prolonging the analysis duration. In real-world project scenarios where time constraints are critical, the computational demands of finite element analysis may render it less favorable for immediate application, especially in projects involving numerous pile foundations.

This new suggested method addresses the demand within the industry by proposing an alternative analytical formulation specifically tailored for estimating NSF within 5x5 end-bearing pile groups interconnected via a pile cap. Unlike conventional methods, this new approach integrates critical factors such as soil characteristics, overburden stresses, pile length within the soft compressible layer, pile diameter, spacing between piles, and the respective positions of piles within the 5x5 group. By considering these parameters collectively, this method aims to offer a more comprehensive and accurate prediction of NSF and total dragload forces exerted on the piles, catering to the nuanced requirements of multi-pile foundation designs. The formula is given below in Equation (4.2) with the definitions of the inputs. The equation has been formulated by using the principles of β-method and, trial and error process to fit the existing data.

Firstly, in order to match the NSF at the ground level surcharge part is divided by 5. Secondly, another depth factor introduced into the overburden stress part of the formula to get a parabolic shape and it is correlated with the pile length in the compressible layers together with two other constants. Then, spacing, diameter and surcharge load have been introduced into the formula to match the maximum NSF and the turning point of the NSF distribution by a trial and error. Finally, partial pile position coefficient is included in the formula to account for different pile positions within the pile group.

$$NSF_{5x5} = Ktan\delta \ * \eta \ * \left\{ \frac{q * tan\phi'}{5} + c' - \left[\sigma' * \left(1 + \frac{1.05z}{L} \right) * \left(2.4 + 0.17\frac{s}{D} - D + \frac{q}{100} \right) * tan\phi' \right] \right\} \quad (4.2)$$

Where;

$Ktan\delta$: Coefficient of horizontal earth pressure multiplied with pile-soil interface factor.

η: Partial pile position coefficient.

q: Surcharge load (kPa).

ϕ': Effective friction angle (°).

c': Effective soil cohesion (kPa).

σ': Effective stress (kPa).

z: Depth (m).

L: Pile length in soft compressible layer (m).

s: Pile spacing (m).

D: Pile diameter (m).

Partial pile position coefficient (η) for each pile in 5x5 array is shown in Figure 4.36.

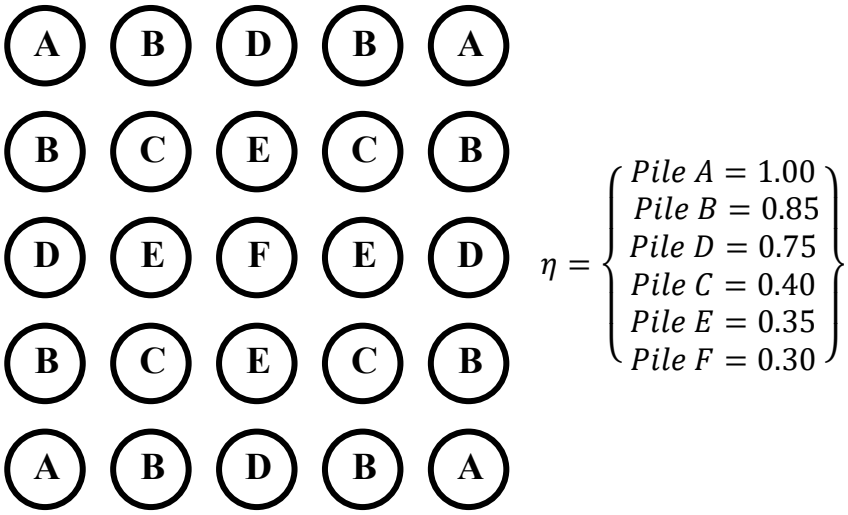

Figure 4.36 Partial pile position coefficients for each pile in 5x5 array.

The example compative graphs of NSF distribution along the pile length betweeen the proposed method and FEA results for s/D=3, L/D=20 and surcharge load of 50 kPa for 0.6, 1.0 and 1.5m diameters at each pile positions have been presented from Figure 4.37 to Figure 4.42 whereas the remaining plots have been given in Appendix N.

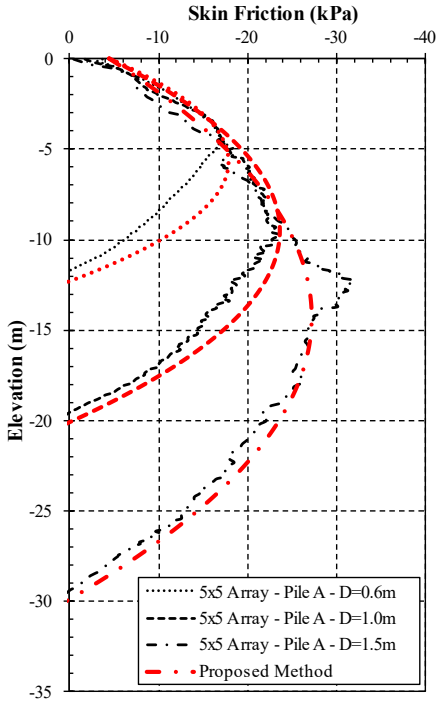

Figure 4.37 Comparison of NSF between the proposed method and FEA results for three different pile diameters – Pile A, 5x5 array, s/D=3 and surcharge load of 50kPa.

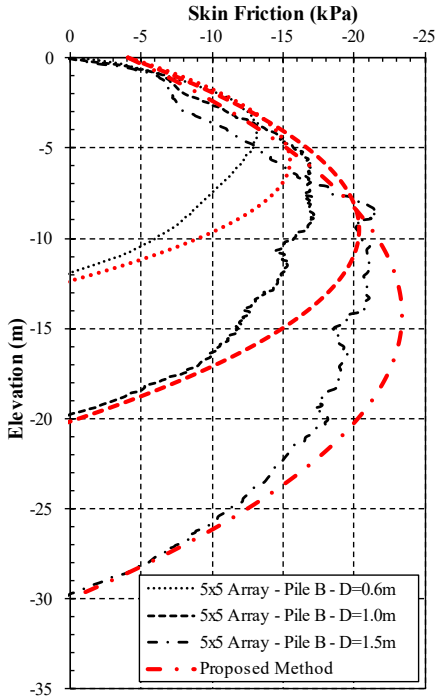

Figure 4.38 Comparison of NSF between the proposed method and FEA results for three different pile diameters – Pile B, 5x5 array, s/D=3 and surcharge load of 50kPa.

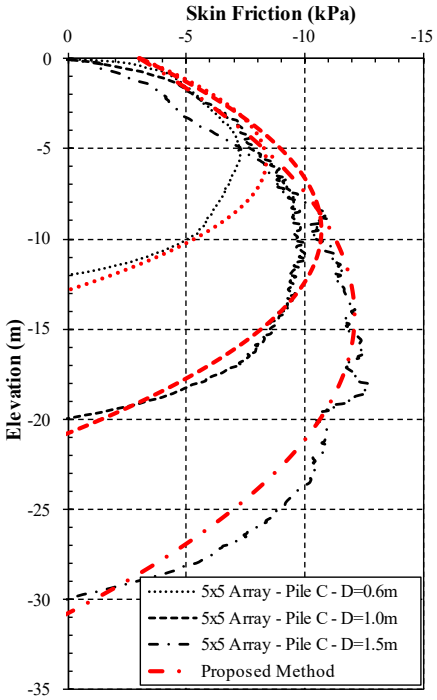

Figure 4.39 Comparison of NSF between the proposed method and FEA results for three different pile diameters – Pile C, 5x5 array, s/D=3 and surcharge load of 50kPa.

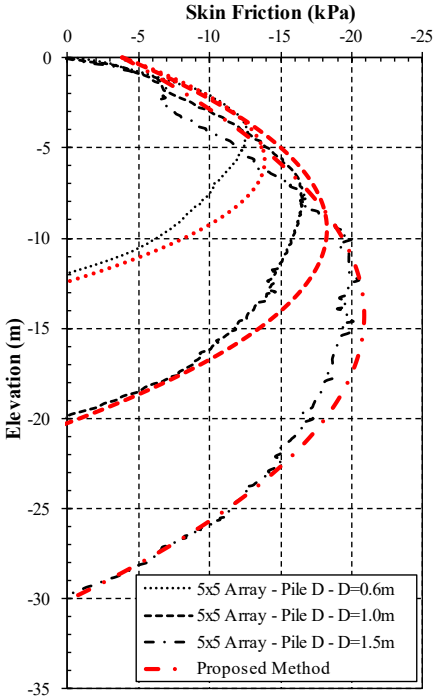

Figure 4.40 Comparison of NSF between the proposed method and FEA results for three different pile diameters – Pile D, 5x5 array, s/D=3 and surcharge load of 50kPa.

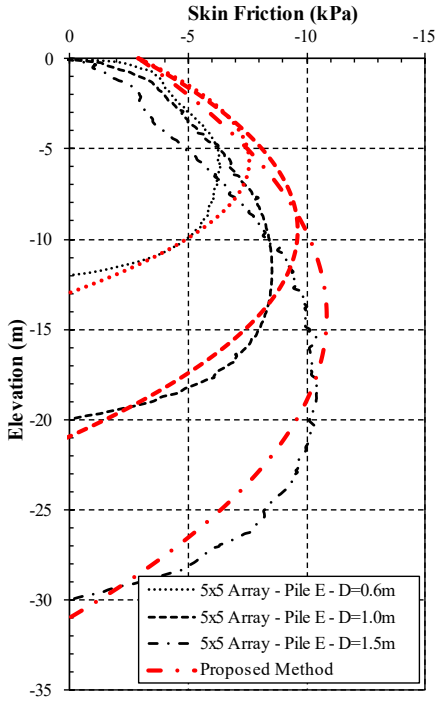

Figure 4.41 Comparison of NSF between the proposed method and FEA results for three different pile diameters – Pile E, 5x5 array, s/D=3 and surcharge load of 50kPa.

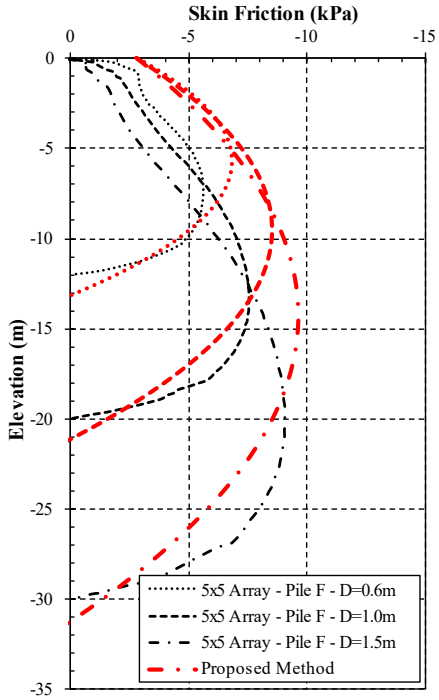

Figure 4.42 Comparison of NSF between the proposed method and FEA results for three different pile diameters – Pile F, 5x5 array, s/D=3 and surcharge load of 50kPa.

Based on the NSF distributions presented from Figure 4.37 to Figure 4.42, the total dragload exerted on each pile has been calculated for both the proposed method and the FEA results. The comparison of the results have shown in Table 4.8 along with the percentile differences.

Table 4.8 Comparison of dragload forces for each pile position for three different pile diameters between the proposed method and FEA results.

Pile-#	Dragload (kN)						Percentile Difference(%)		
	FEA Results			Suggested Method					
	D=0.6m	D=1.0m	D=1.5m	D=0.6m	D=1.0m	D=1.5m	D=0.6m	D=1.0m	D=1.5m
Pile-A	236	931	2542	291	1036	2651	23	11	4
Pile-B	202	746	2031	255	900	2298	26	21	13
Pile-C	126	471	1247	145	493	1238	15	5	-1
Pile-D	196	721	1930	230	810	2062	17	12	7
Pile-E	113	404	1049	133	448	1120	18	11	7
Pile-F	98	339	872	120	403	1002	22	19	15

As shown in Table 4.8, the new proposed method is generally in good agreement with the FEA results and it is capable of predicting the dragloads exerted on the piles better than any other conventional analytical methods.

CHAPTER 5

CONCLUSION AND RECOMMENDATIONS

In this comprehensive study, a thorough investigation was conducted to analyze the behavior of negative skin friction on the end-bearing bored pile foundations connected with a pile cap using three-dimensional finite element analysis. The research commenced validating the model by examining the behavior of a single pile with a reference case study and showing satisfactory agreement between the results of a similar three-dimensional analysis and the field measurements. Subsequent analyses explored the impact of soil parameters, pile and pile group dimensions on the negative skin friction distribution and the dragload forces exerted on the piles, revealing a significant influence of the behavior and the magnitude of negative skin friction.

Furthermore, the study touched upon the relative pile and soil settlements and their effect on the NSF behavior as well as change of the NSF distribution along the pile length and neutral plane position due to foundation loading.

Based on the conducted parametric analyses, the key findings are summarised below:

- The pile diameter has a higher impact on the magnitude of the NSF for the inner piles than the outer piles due to change in the distance between the adjacent piles with changing pile diameter.
- The length of pile in the soft compressible layer is directly related to the magnitude and distribution of the NSF along the pile length.
- The change between the pile spacing from 3D to 6D has showed that even when dealing with end-bearing piles, the NSF is still influenced by group effect and higher NSFs were observed for the increased pile spacing. Based on the findings of the various researchers there should be a limit on the

increase of the NSF due to pile spacing but this should be confirmed with further parametric analyses.

- The number of piles in pile arrays of the same size has a significant impact on the magnitude of the NSF and dragload forces based on comparison of the results of FEA between 3x3 and 5x5 pile arrays due to load contribution shared by the number of piles in an array.
- When the effect of pile position is investigated, it is observed that the dragforce and maximum unit NSF decreases going from outer to inner piles. Shape of the NSF distribution along the pile length changes from elliptical to a belly shape in the same order. However, when the surrounding surcharge load is increased, the NSF distribution of the inner piles become similar to the outer piles due to increased NSF. It is also noticed that when the surcharge load is increased the neutral point location moves towards the ground surface.
- Based on the parametric analyses of the soil parameters, it is acknowledged that the most important factors are the soil compressibility and pile-soil interface coefficient.

The normalized FEA results have been compared with the β-method which is believed to be the most accurate analytical method and with the tributary area method. The β-method overpredicts the magnitude of the NSF, hence the total dragload forces calculated on the pile shaft and tributary area method underestimates the total dragload for smaller pile spacings and overestimates for the larger ones. Therefore, a new method has been proposed to meet the needs of the industry, where time constraints disallow 3D FEA analyses. Although, there exist limitations with the suggested method, it predicts the magnitude and the distribution of the NSF reasonably well and the calculated dragloads are in a good agreement with the FEA results.

It is important to acknowledge that the quantification of negative skin friction and the dragload forces were specific to the analyzed 5x5 pile array configuration. Therefore, caution must be exercised when applying these findings to different pile

arrangements due to the observed difference in the load contribution variation between the 3x3 and 5x5 pile arrays. It should also be noted that the study does not take into account the pile driving effects and hence the findings are only applicable to bored piles.

Overall, this thesis provides valuable insights into the behavior of end-bearing pile foundations connected with a pile cap under negative skin friction, emphasizing the significance of pile group configurations, proper modelling of surcharge loads around the foundation and the choice of soil parameters in design and analysis. The outcomes contribute to the development of more accurate design approaches and mitigation strategies for negative skin friction and dragload forces, enhancing the understanding and optimization of pile foundation design in challenging geotechnical conditions.

Future research can further extend these findings by exploring different soil profiles, pile geometry, pile group configurations, different causes of NSF development such as ground water lowering scenario and floating piles to obtain a more comprehensive understanding of negative skin friction phenomena in pile foundations. Moreover, the proposed method should be extended to different end-bearing pile arrays by developing a new pile position coefficient formulation instead of using partial factors and by considering the load contribution effect when the total number of piles change in different pile arrays.

REFERENCES

Auvinet, G. and Hanell, J. J. (1981). "Negative skin friction on piles in Mexico City clay." Proceedings of 10th International Conference of Soil Mechanics and Foundation Engineering, Vol.2, pp. 599~604.

Auvinet-Guichard, G., & Rodríguez-Rebolledo, J. F. (2017). Criteria for the design of friction piles subjected to negative skin friction and transient loads. Ingeniería, investigación y tecnología, 18(3), 279-292.

Azzouz, A. S., Baligh, M. M., & Whittle, A. J. (1990). Shaft resistance of piles in clay. Journal of Geotechnical Engineering, 116(2), 205-221.

Biot MA (1941) General theory of three-dimensional consolidation. J Appl Phys 12:155–164.

Biot MA (1955) Theory of elasticity and consolidation for a porous anisotropic solid. J Appl Phys 26:182–185.

Bowles, J. E. (1997). Foundation Analysis and Design. New York: The MacGraw-Hill Companies.

Bozozuk, M. (1972). "Downdrag measurements on 160-ft floating pipe test pile in marine clay". Canadian Geotechnical Journal, Vol.9, No.2, pp. 127~136.

Bozozuk, M. (1981). "Bearing capacity of pile preloaded by downdarg." Proceedings of 10th International Conference of Soil Mechanics and Foundation Engineering, Vol.2, pp. 631~636.

Brand, E. W. and Luangdilok, N. (1975). "A long-term foundation failure caused by dragdown on piles". 4th Southeast Asian Conference on Soil Engineering, Kuala Lumpur, Malaysis, pp.4-15~4-24.

Briaud, J. L., Jeng, S. and Bush, R. (1991). “Group effect in the case of downdrag”. Proceedings of Geotechnical Engineering Congress, Boulder, U.S.A, Vol.1, pp. 505~518.

Brinkgreve, R. J. B. (2014). Pile modelling in a 2D plain strain model.

Broms, B. B., (1976). “Pile foundation-pile groups.” Proceedings of 6th European Conference of Soil Mechanics and Foundation Engineering, Vienna, Austria, Vol.2, pp. 103~132.

Brown, D. A., Reese, L. C., & O'Neill, M. W. (1987). Cyclic lateral loading of a large-scale pile group. Journal of Geotechnical Engineering, 113(11), 1326-1343.

Burland, J. B., Butler, F. G. and dunican, P. (1966). “The behaviour and design of large diameter bored piles in stiff clay”. Proceedings of the Symposium on large bored piles. ICE, London.

Burland, J. B. (1973). “Shaft friction of piles in clay”. Ground Engineering, 6(3), pp. 30~42.

Bustamante, M., & Gianeselli, L. (1982). Pile bearing capacity prediction by means of static penetrometer CPT. In Proceedings of the 2nd European symposium on penetration testing (Vol. 2, pp. 493-500). Balkema, Amsterdam, the Netherlands.

Bustamante, M., Doix, B. (1985). “Design Method for Ground Anchors and Grouted Micropiles” (In French) Bull. Liaison Labo. P. et Ch. No.140, pp.75-92.

Chellis, R. D. (1961). “Pile Foundations”. 2nd Edition. McGraw-Hill Book Company.

Chow, F. C., Jardine, R. J., Nauroy, J. F., & Brucy, F. (1997). Time-related increases in the shaft capacities of driven piles in sand. Geotechnique, 47(2), 353-361.

Chow, F. C., Jardine, R. J., Brucy, F., & Nauroy, J. F. (1998). Effects of time on capacity of pipe piles in dense marine sand. Journal of Geotechnical and Geoenvironmental Engineering, 124(3), 254-264.

Comodromos, E. M., & Bareka, S. V. (2005). Evaluation of negative skin friction effects in pile foundations using 3D nonlinear analysis. Computers and Geotechnics, 32(3), 210-221.

Cooke, R. W. (1974). "Settlement of friction pile foundations". Proc. Conf. on tall buildings, Kuala Lumpur, pp. 7~19.

Coyle, H. M., & Castello, R. R. (1981). New design correlations for piles in sand. Journal of the Geotechnical Engineering Division, 107(7), 965-986.

Davisson, M. T. (1962). Negative friction on piles in sand. Proceedings of the 5th International Conference on Soil Mechanics and Foundation Engineering, 333-337.

Davisson, M. T. (1993). "Negative skin friction in piles and design decision". Proc. 3rd Int. Conf. Case Histories Geotech. Engng, Rolla, 1792-1801.

Drbe, O., Sadrekarimi, A., El Naggar, H., & Sangiuliano, T. (2016). Modelling of negative skin friction on driven piles. In Proc., of 69th Canadian Geotechnical Conf. GeoVancouver.

Endo, M., Minou, A., Kawasaki, T. and Shibata, T. (1969). "Negative skin friction acting on steel pipe pile in clay." Proceedings of 7th International Conference of Soil Mechanics and Foundation Engineering, Mexico, Vol.2, pp.85~92.

Ergun, M. U. and Sonmez, D. (1995). "Negative skin friction from surface settlement measurements in model group tests." Canadian Geotechnical Journal, Vol.32, pp. 1075~1079.

Fellenius, B. H., (1972). “Downdrag on piles in clay due to negative skin friction.” Canadian Geotechnical Journal, Vol.9, No.4, pp. 323~327.

Fellenius, B. H. (1998). “Recent advances in the design of piles for axial loads, dragloads, downdrag, and settlement”. ASCE and Port of New York and New Jersey Seminar.

Fellenius, B. H. (2008). Effective stress analysis and set-up for shaft capacity of piles in clay. In From research to practice in geotechnical engineering (pp. 384-406).

Garlanger, J. E. (1974). “Measurement of pile downdrag beneath a bridge abutment.” Highway Research Board, Transport Research Record, No.517. pp. 61~69.

Indraratna, B., Balasubramaniam, A. S., Phamvan, P., & Wong, Y. K. (1992). Development of negative skin friction on driven piles in soft Bangkok clay. Canadian Geotechnical Journal, 29(3), 393-404.

Indraratna, B., & Balasubramaniam, A. S. (1993). Closure to “Performance of test embankment constructed to failure on soft marine clay” by B. Indraratna, AS Balasubramaniam, and S. Balachandran (January 1992, Vol. 118, No. 1). Journal of Geotechnical Engineering, 119(8), 1326-1329.

Inoue, Y., Tamaoki, K. and Ogai, T. (1977). “Settlement of building due to pile downdrag”. Proceedings of 9th International Conference of Soil Mechanics and Foundation Engineering, Tokyo, Japan, Vol.1, pp. 561~564.

Jacob, F. and Kenneth, L. C. (1997). Construction Failure. 2nd Edition, John Wiley & Sons, Inc.

Jamiolkowski, M., & Forrest, J. (1988). Research applied to geotechnical engineering. James Forrest Lecture. Proceedings of the Institution of Civil Engineers, 84(3), 571-604.

Jeong, S., & Kim, S. (1998). Interaction factors for pile groups due to downdrag. Soils and foundations, 38(2), 49-61.

Johannessen, I. J. and Bjerrum, L., (1965). “Measurement of the Compression of a Steel Pile to Rock due to Settlement of the Surrounding Clay.” Proceedings of 6th International Conference of Soil Mechanics and Foundation Engineering, Montreal, Canada, Vol.2, pp. 261~264.

Keenan, G. H. and Bozozuk, M. (1985). “Downdrag on a three-pile group of pipe piles”. Proceedings of 11th ICSMFE, Vol. 3, San Fransico, 1985.

Kézdi, Á., & Rétháti, L. (1988). Soil mechanics of earthworks, foundations, and highway engineering (Vol. 3). Elsevier.

Kim, H. J., Mission, J. L. C., & Park, I. S. (2007). Analysis of static axial load capacity of single piles and large diameter shafts using nonlinear load transfer curves. KSCE Journal of Civil Engineering, 11, 285-292.

Kim, H. J., Mission, J. L., Park, T. W., & Dinoy, P. R. (2018). Analysis of negative skin-friction on single piles by one-dimensional consolidation model test. International Journal of Civil Engineering, 16, 1445-1461.

Kog, Y. C. (1987). “A case study of downdrag and axial load on timber piles in layered soil”. Proceedings 5th International Geotechnical Seminar on Case Histories in Soft Clay, Nanyang Technological Institute, Singapore, 2~4 Dec., pp.269~276.

Kog, Y. C. (1990). “Down-drag and axial load on piles.” Ground Engineering, April, 1990, pp.24~30.

Lee, C. J., Chen, H. T. and Wang, W. H. (1998). “Negative skin friction on a pile due to excessive groundwater withdrawal”. Proc. Centrifuge 98. eds. Kimura, Kusakabe & Takemura. pp. 513~ 518. A.A. Balkema, Rotterdam.

Lee, C. J., Bolton, M. D., & Al-Tabbaa, A. (2002). Numerical modelling of group effects on the distribution of dragloads in pile foundations. Geotechnique, 52(5), 325-335.

Lee, C. J., & Ng, C. W. (2004). Development of downdrag on piles and pile groups in consolidating soil. Journal of Geotechnical and Geoenvironmental Engineering, 130(9), 905-914.

Lee, C. J., & Chen, C. Z. (2022). Negative skin friction on grouped piles. In Physical modelling in geotechnics (pp. 679-684). Routledge.

Leoni, L., & Sassu, M. (2018). Negative skin friction of axially loaded piles in clay: field tests and FEM simulations. Acta Geotechnica, 13(4), 903-917.

Leung, C. F., Liao, B. K., Chow, Y. K., Shen, R. F. and Kog, Y. C. (2004). "Behavior of pile subject to negative skin friction and axial load". Soils and Foundations, Vol. 44, No. 6, pp17~26.

Liang, R., Yin, Z. Y., Yin, J. H., & Wu, P. C. (2023). Numerical analysis of time-dependent negative skin friction on pile in soft soils. Computers and Geotechnics, 155, 105218.

Lim, C. H., Chow, Y. K., & Karunaratne, G. P. (1993). Negative skin friction on single piles in a layered half-space. International journal for numerical and analytical methods in geomechanics, 17(9), 625-645.

Little, J. A. (1989). "The Development of shaft adhesion with onset of negative skin friction for a fixed base model pile". Proc. 2nd Int'l Conf. Foundations & Tunnels Eng. pp. 111~117.

Little J. A. and Ibrahim K. (1993). "Predictions associated with the pile downdrag study at the SERC soft clay site at Bothkennar, Scotland". Proceedings of the Wroth Memorial Synmposium on Predictive Soil Mechanics, pp. 796~818.

Little, J.A. (1994). “Downdrag on piles: review and recent experimentation”. ASCE Geotechnical Special Publication, Vol. 2, No.40, pp.1805~1826.

Liu, J., Gao, H., & Liu, H. (2012). Finite element analyses of negative skin friction on a single pile. Acta Geotechnica, 7, 239-252.

Matlock, H. (1970, April). Correlation for design of laterally loaded piles in soft clay. In Offshore technology conference (pp. OTC-1204). OTC.

Meyerhof, G. G. (1963). Some recent research on the bearing capacity of foundations. Canadian geotechnical journal, 1(1), 16-26.

NAVFAC (1982). Foundation and earth structures, Design manual 7.2, U.S. Department of the Navy, Virginia.

Okabe, T. (1977). “Large negative friction and friction-free pile method”. Proceedings of 9th International Conference of Soil Mechanics and Foundation Engineering, Tokyo, Vol.1, pp. 679~682.

Poulos, H. G., & Davis, E. H. (1980). Pile foundation analysis and design (Vol. 397). New York: Wiley.

Poulos, H. G. (1989). Pile behaviour—theory and application. Geotechnique, 39(3), 365-415.

Randolph, M. F. and Wroth C. P. (1978). “An analysis of the deformation of vertically loaded piles.” Journal of Geotechnical Engineering Division, A.S.C.E., Vol.104, No.12, pp. 1465~1488.

Randolph, M. F. (2003). Science and empiricism in pile foundation design. Géotechnique, 53(10), 847-875.

Randolph, M. F., & White, D. J. (2008). Upper-bound yield envelopes for pipelines at shallow embedment in clay. Géotechnique, 58(4), 297-301.

Reese, L. C., Cox, W. R., & Koop, F. D. (1974, May). Analysis of laterally loaded piles in sand. In Offshore Technology Conference (pp. OTC-2080). OTC.

Rituraj, S. S., & Giridhar Rajesh, B. (2022). Negative skin friction on piles: State of the art. Advances in Geo-Science and Geo-Structures: Select Proceedings of GSGS 2020, 323-335.

Salas. J. A. J. & Belzunce, J. A. (1965). Resolution theorique de la distribution des forces dans les pieux. Proc. 6th Int. Conf. Soil Mech. 2, 309-313.

Schlosser F., Jacobsen H. M., and Juran I. (1984). "Le renforcement des sols (1)." Revue Frangaise de G6otechnique, No. 29, France, 7-32.

Schmertmann, J. H. (1975). Measurement of in situ shear strength, SOA Report. In Proceedings, ASCE Spec. Conference on In Situ Measurement of Soil Properties, Raleigh, NC, 1975 (Vol. 2, pp. 57-138).

Shahin, M., Farouk, A., & Saad, M. M. (2022). Numerical analysis of group effect on dragload on piles subjected to negative skin friction. Journal of Engineering Research, 6(1), 29-33.

Shen, R. F., Leung, C. F., Chow, Y. K., Kog, Y. C., & Liao, B. K. (2022). Negative skin friction on piles. In Physical Modelling in Geotechnics (pp. 673-678). Routledge.

Teh, C. I., & Wong, K. S. (1995). Discussion of “Pile Groups under Negative Skin Friction” by CY Lee. Journal of Geotechnical Engineering, 121(7), 574-575.

Terzaghi, K. and Peck, R. B. (1948). Soil Mechanics in Engineering Practice, New York: Wiley.

Vesic, A. S. (1977). Design of pile foundations. NCHRP synthesis of highway practice, (42).

Wong, K. S. and Teh, C. I. (1995). “Downdrag on single piles”. Bengt B. Broms Symposium on Geotechnical Engineering, Singapore, pp. 449~466.

Yen, T. L., Lin, H., Chin, C. T. and Wang, R. F. (1989). “Interpretation of instrumented driven steel pipe piles”. Proceedings of Congress, Foundation engineering, current principles and practices. Vol.2, pp. 1293~1308.

Zhang, Y., Zhou, L. P., Wang, M. Y., Ding, X., & Wang, C. (2021). Experimental Study on the Negative Skin Friction of the Pile Group Induced by Rising and Lowering the Groundwater Level. Advances in Civil Engineering, 2021, 1-12.

APPENDICES

A. Pile and Soil Settlements

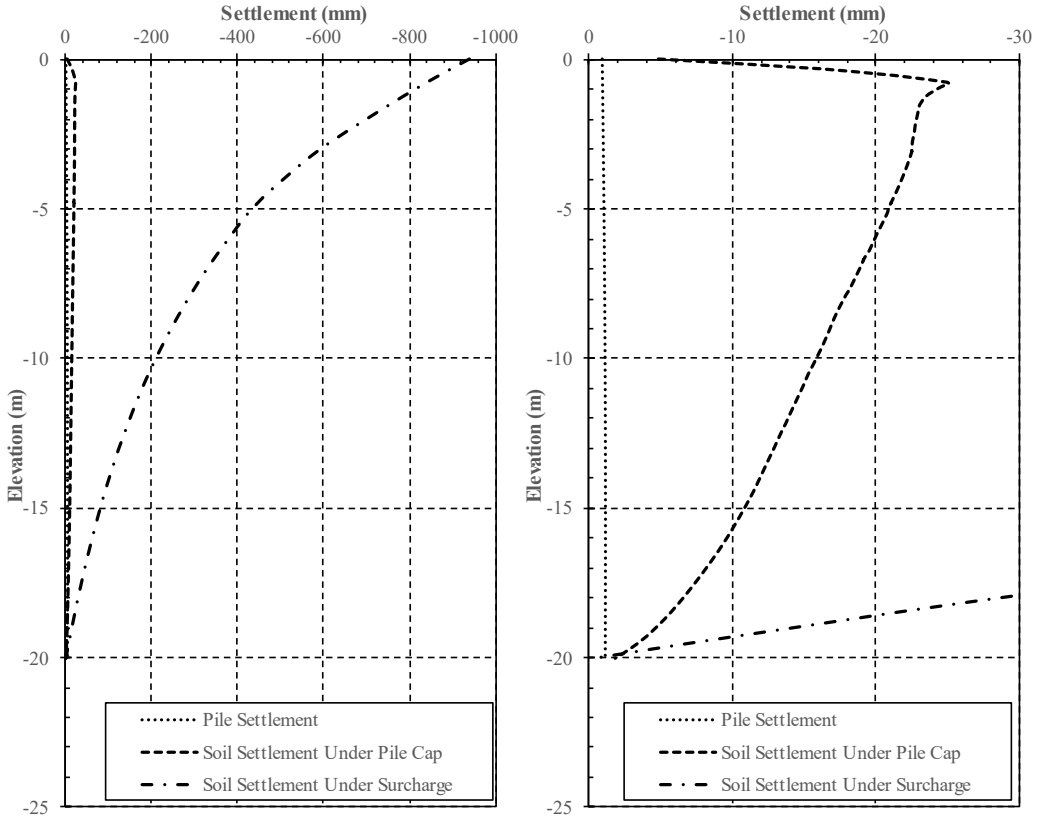

Figure A.1 Calculated pile and soil settlements from FEA where D=1.0m, s/D=3, L/D=20, surcharge load=50kPa, soil compressibility factor λ^*=0.07.

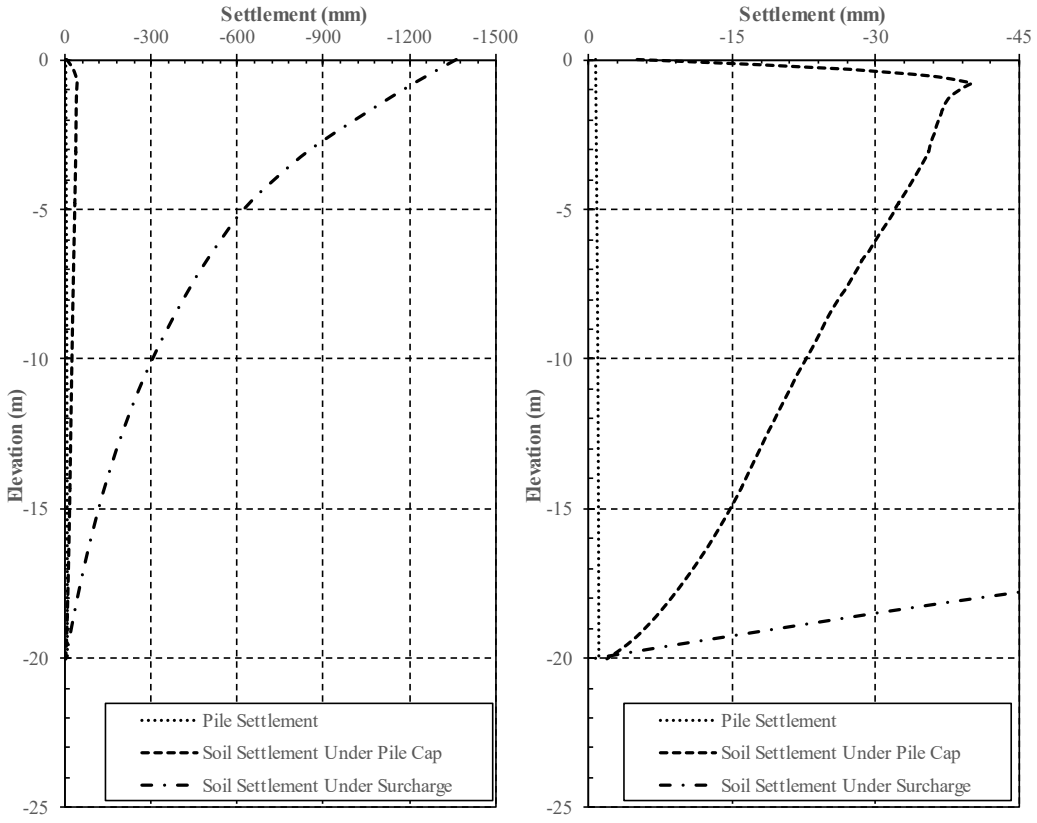

Figure A.2 Calculated pile and soil settlements from FEA where D=1.0m, s/D=3, L/D=20, surcharge load=50kPa, soil compressibility factor λ*=0.10.

B. Change of NSF and Neutral Point due to Foundation Loading

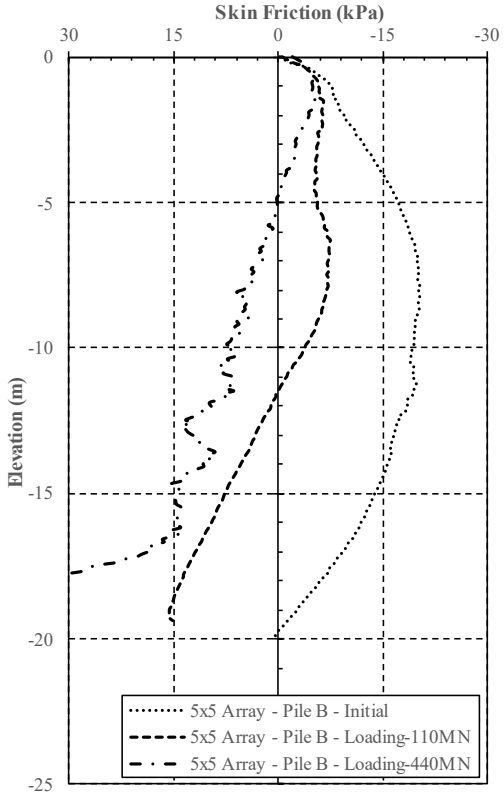

Figure A.3 Change of NSF and NP due to foundation loading for the 5x5 array, D=1m, s/D=6, L/D=20, surcharge load=50kPa – Pile B.

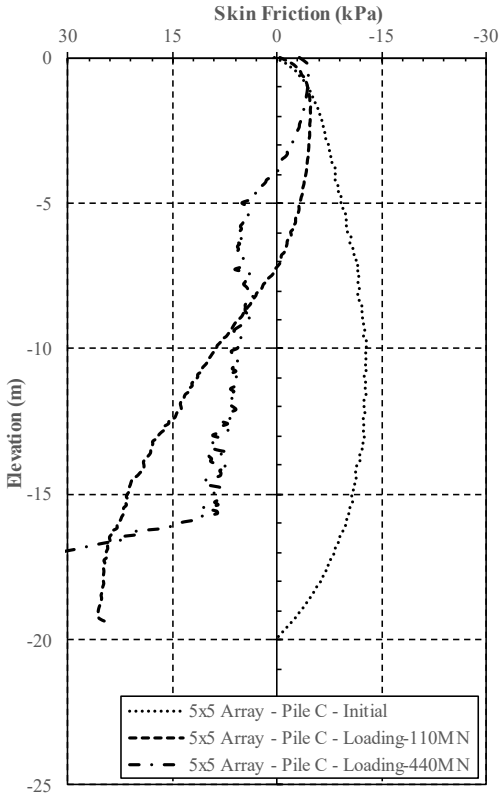

Figure A.4 Change of NSF and NP due to foundation loading for the 5x5 array, D=1m, s/D=6, L/D=20, surcharge load=50kPa – Pile C.

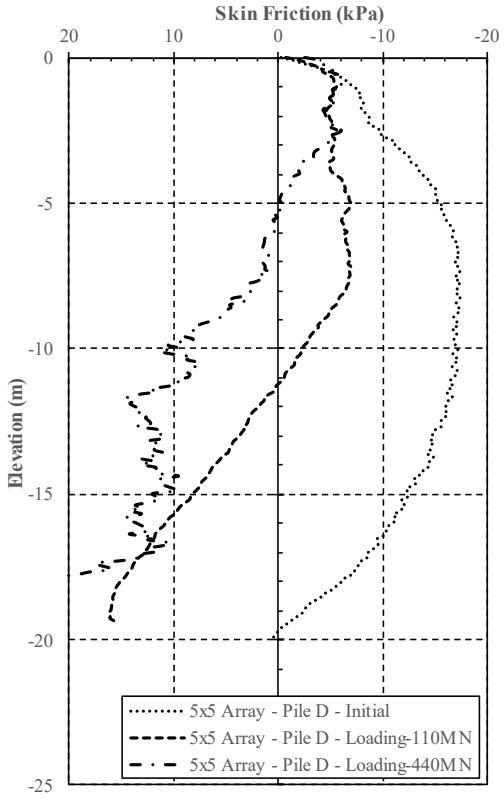

Figure A.5 Change of NSF and NP due to foundation loading for the 5x5 array, D=1m, s/D=6, L/D=20, surcharge load=50kPa – Pile D.

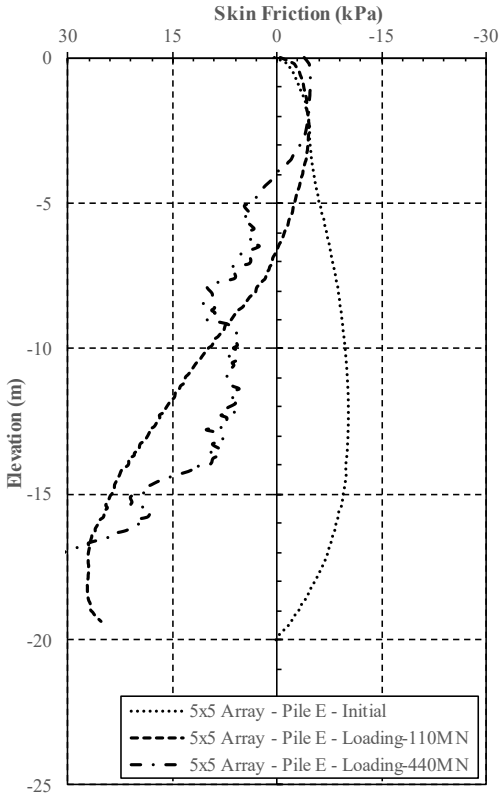

Figure A.6 Change of NSF and NP due to foundation loading for the 5x5 array, D=1m, s/D=6, L/D=20, surcharge load=50kPa – Pile E.

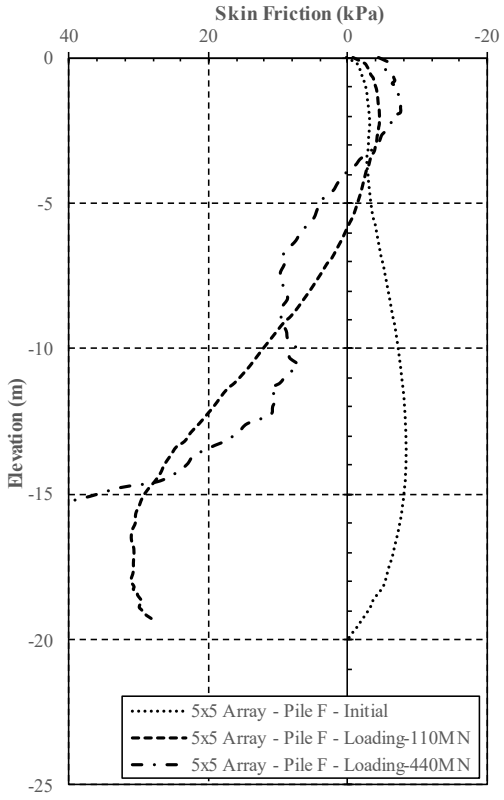

Figure A.7 Change of NSF and NP due to foundation loading for the 5x5 array, D=1m, s/D=6, L/D=20, surcharge load=50kPa – Pile F.

C. The Effect of Pile Diameter

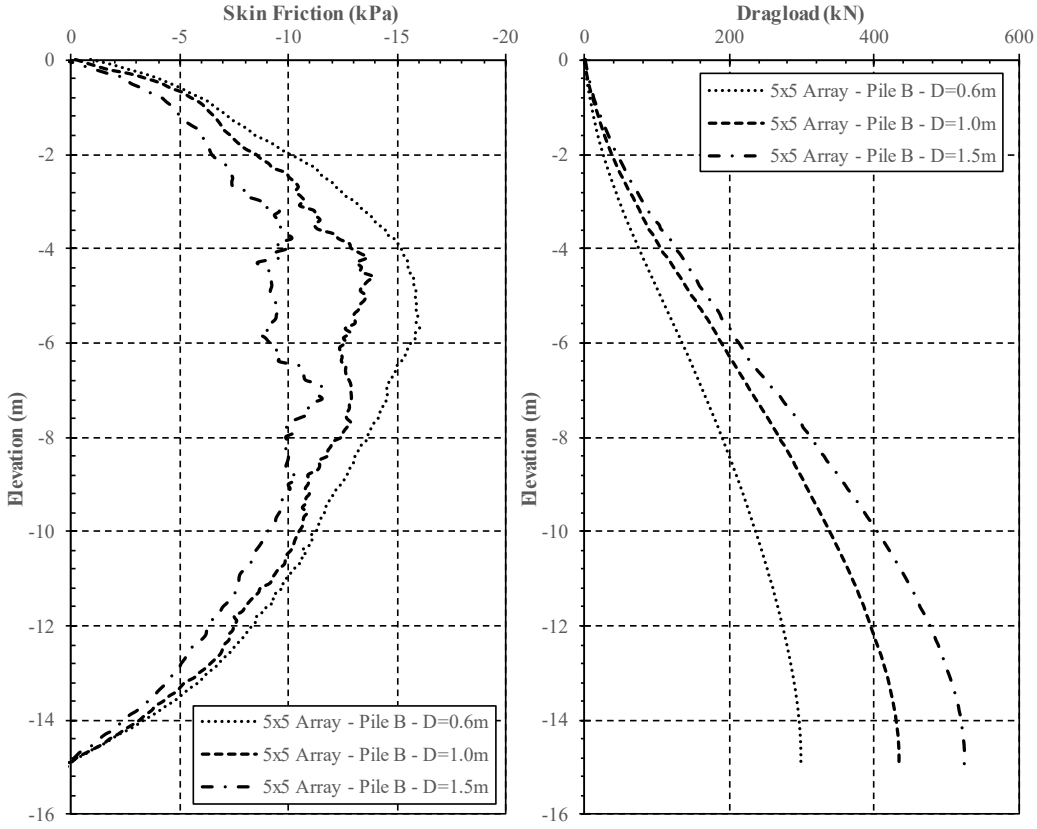

Figure A.8 NSF and dragload of Pile B in three different diameter cases for model conditions of 5x5 array, L=15m, s/D=3 and surcharge load of 50kPa.

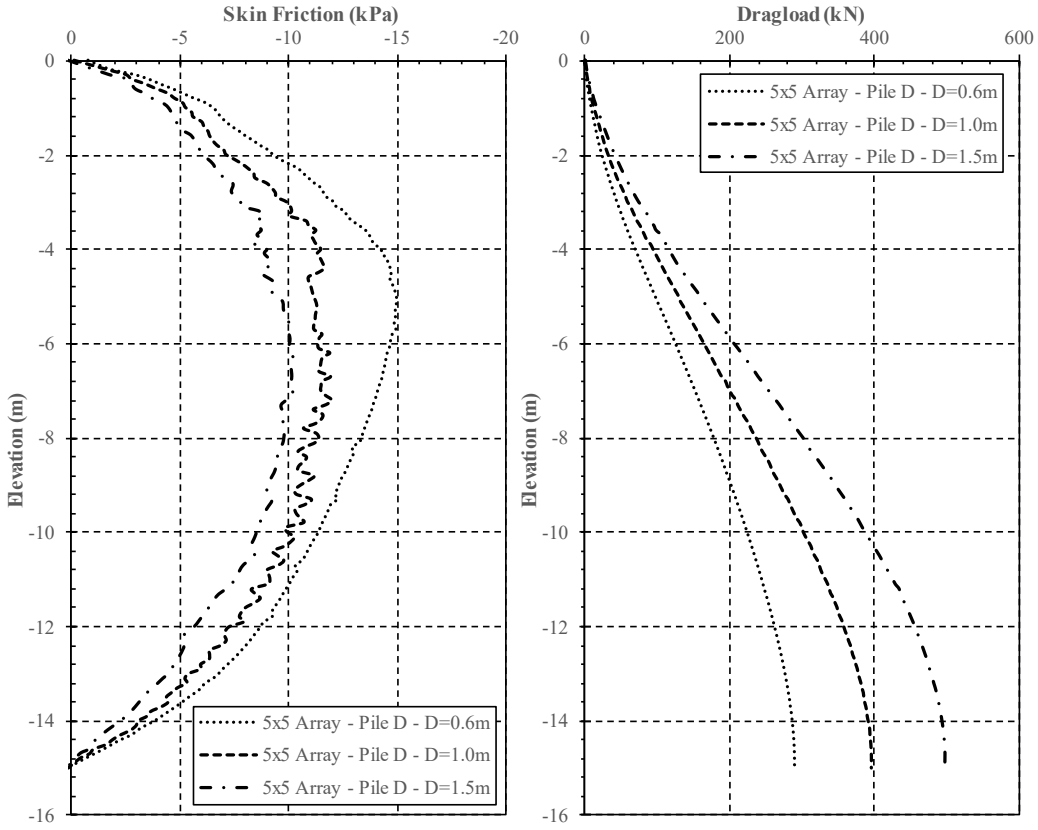

Figure A.9 NSF and dragload of Pile D in three different diameter cases for model conditions of 5x5 array, L=15m, s/D=3 and surcharge load of 50kPa.

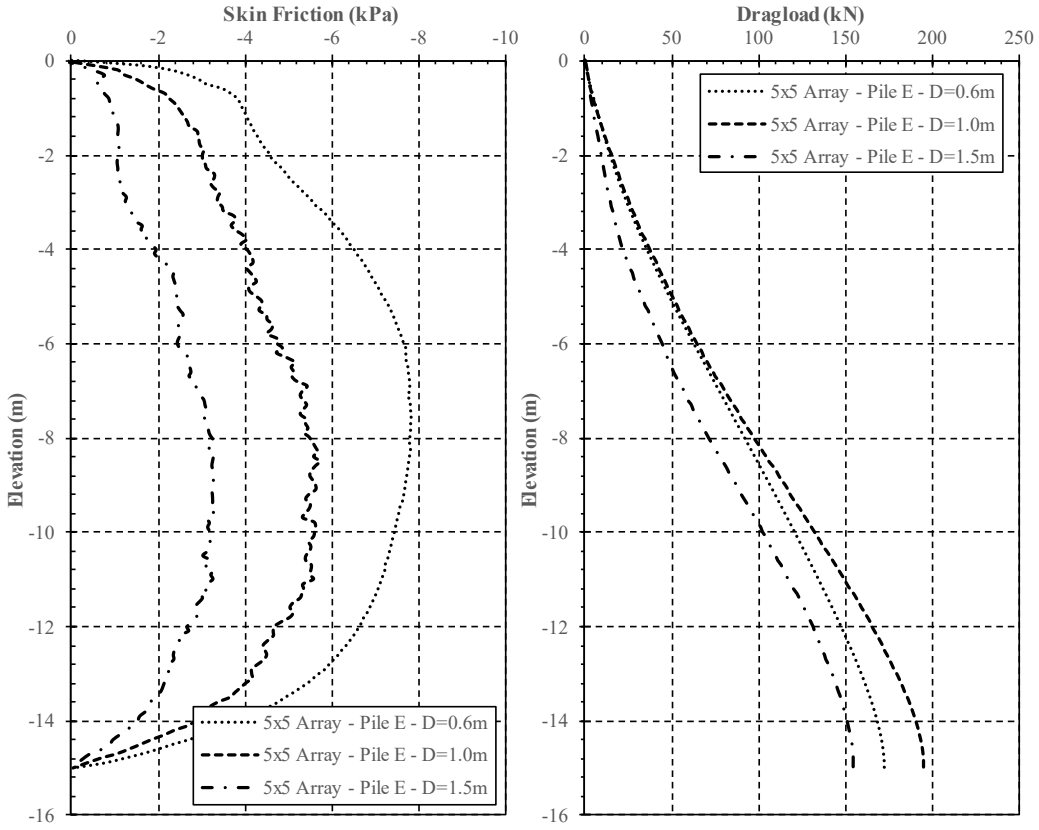

Figure A.10 NSF and dragload of Pile E in three different diameter cases for model conditions of 5x5 array, L=15m, s/D=3 and surcharge load of 50kPa.

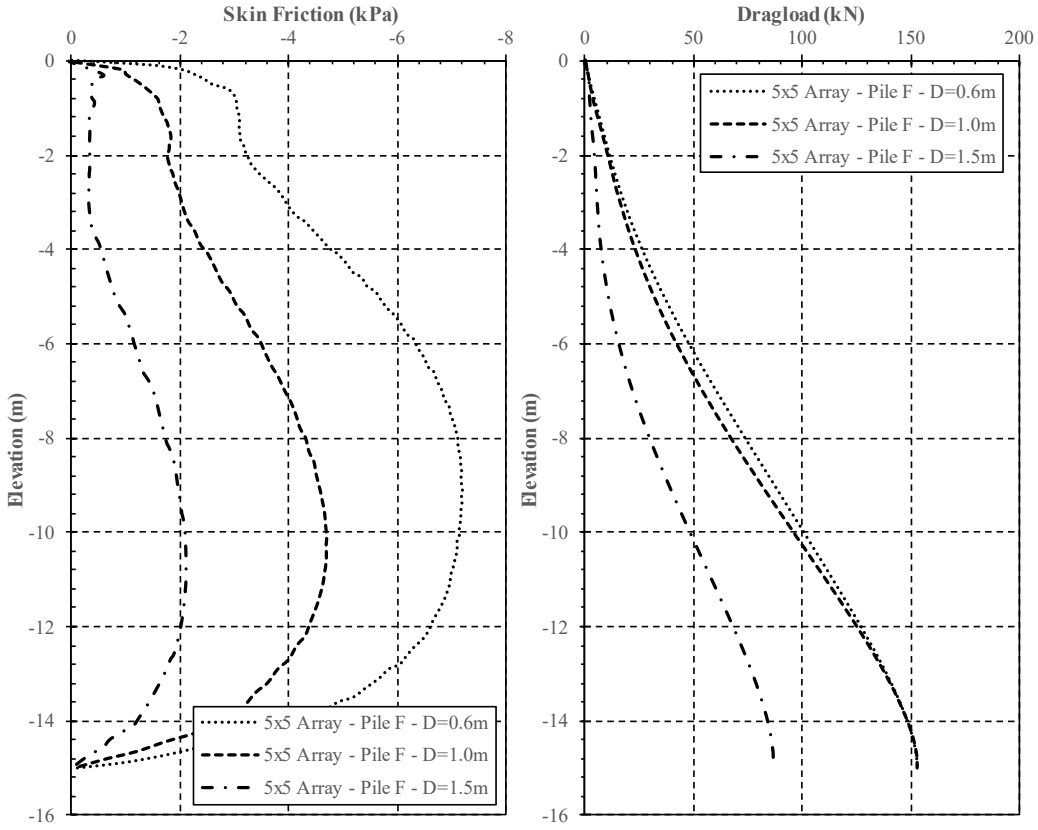

Figure A.11 NSF and dragload of Pile F in three different diameter cases for model conditions of 5x5 array, L=15m, s/D=3 and surcharge load of 50kPa.

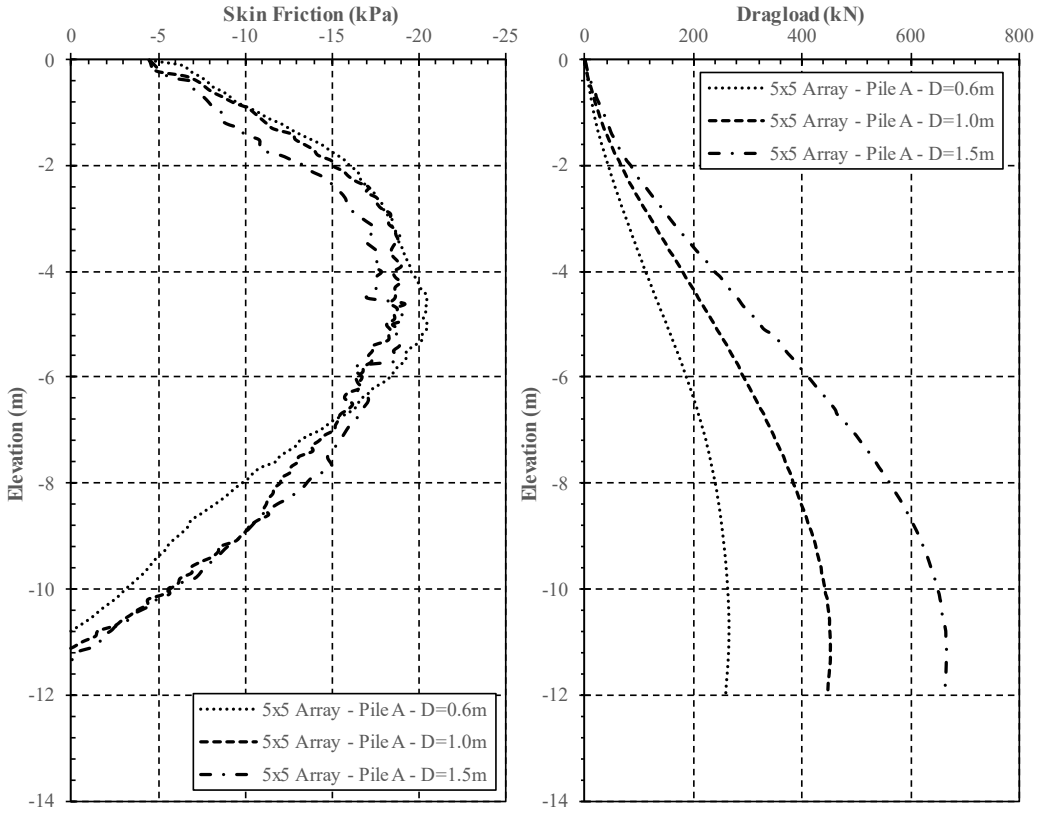

Figure A.12 NSF and dragload of Pile A in three different diameter cases for model conditions of 5x5 array, L=12m, s/D=6 and surcharge load of 100kPa.

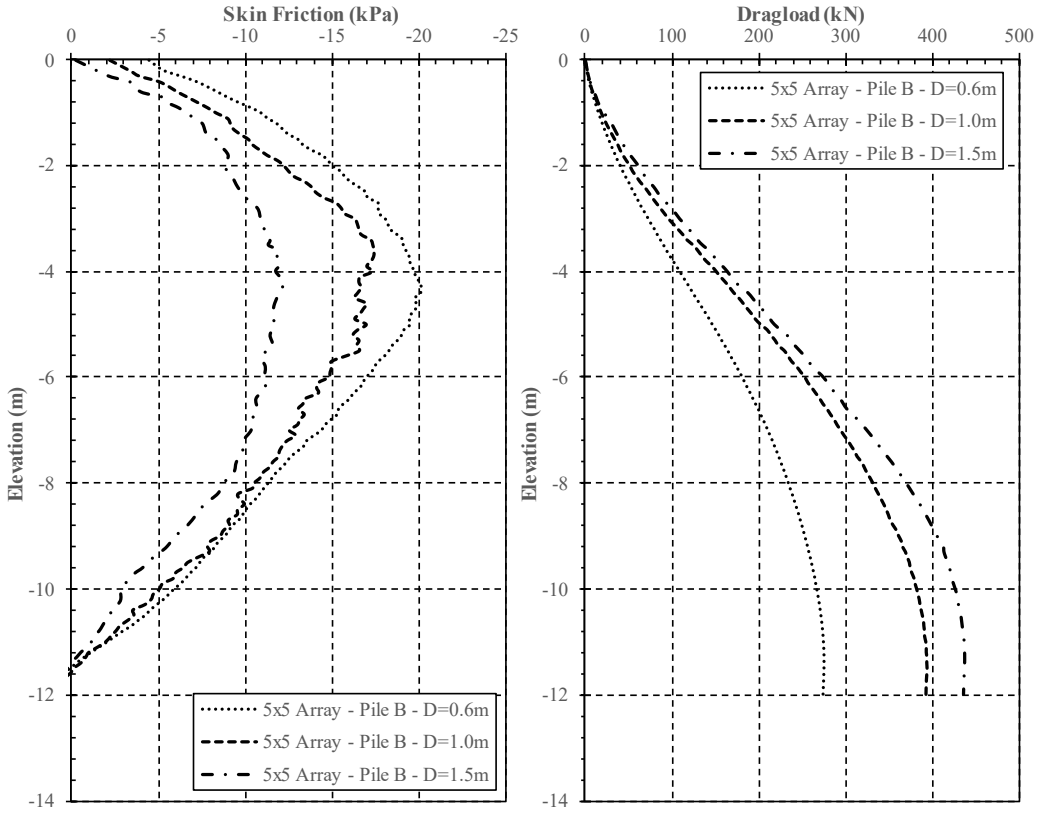

Figure A.13 NSF and dragload of Pile B in three different diameter cases for model conditions of 5x5 array, L=12m, s/D=6 and surcharge load of 100kPa.

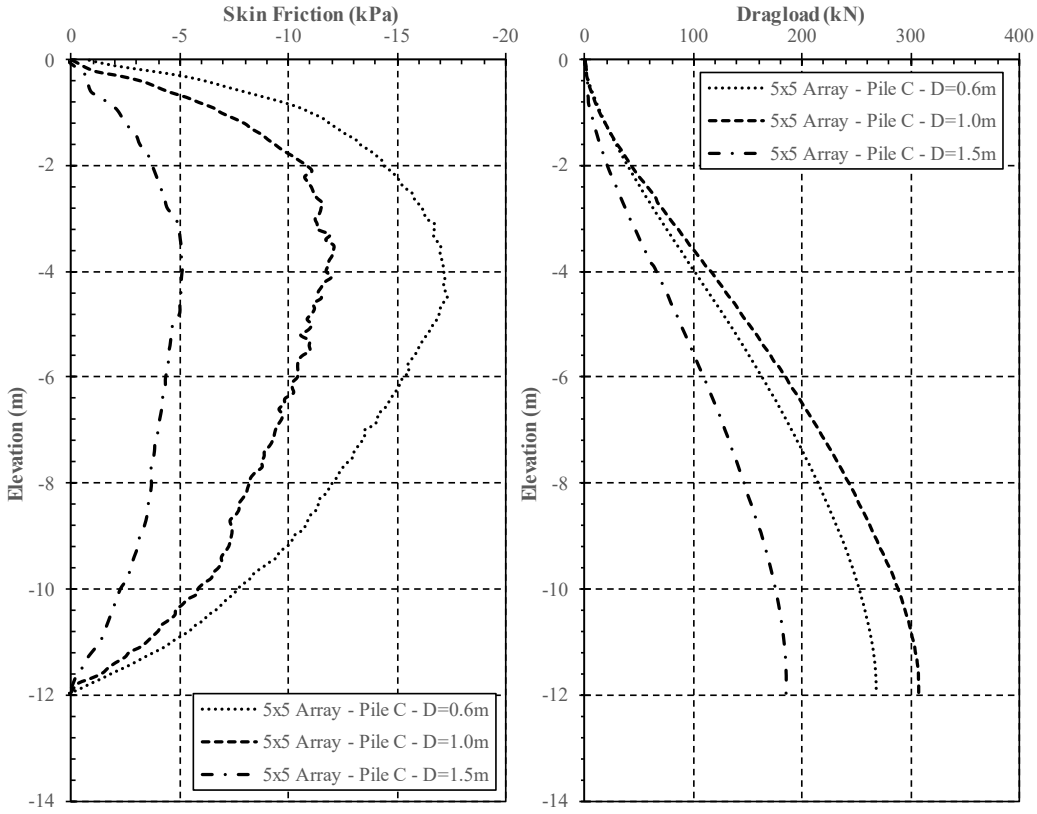

Figure A.14 NSF and dragload of Pile C in three different diameter cases for model conditions of 5x5 array, L=12m, s/D=6 and surcharge load of 100kPa.

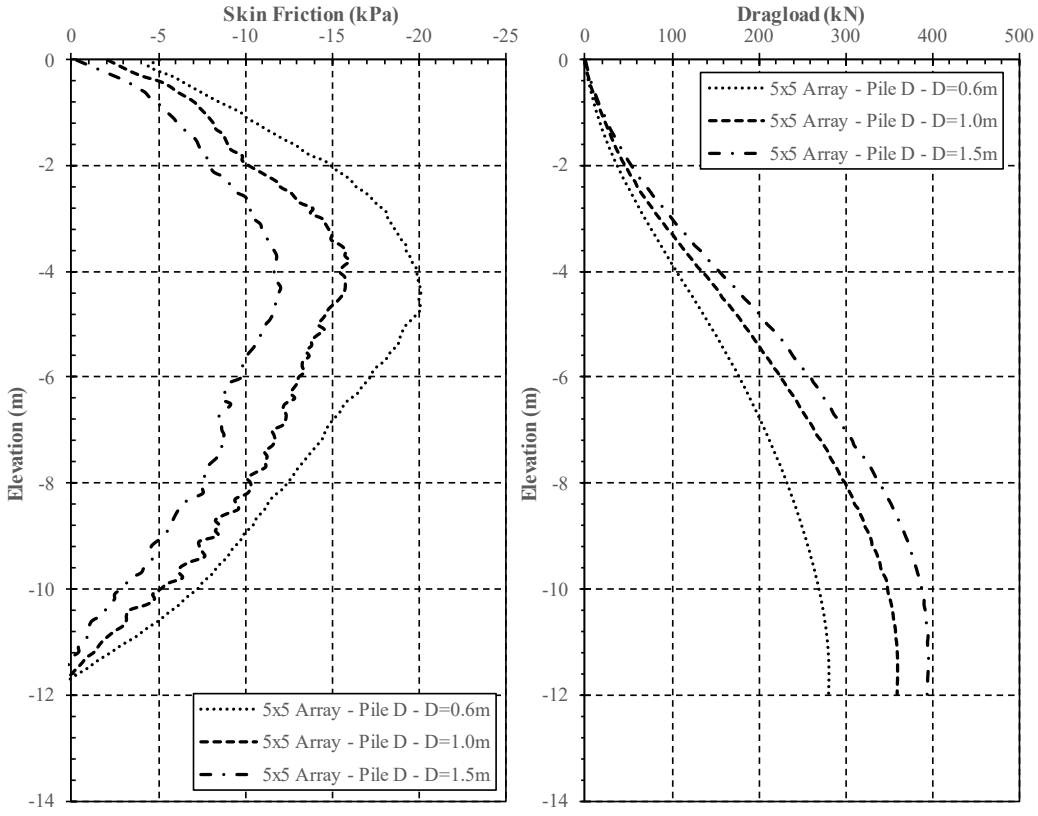

Figure A.15 NSF and dragload of Pile D in three different diameter cases for model conditions of 5x5 array, L=12m, s/D=6 and surcharge load of 100kPa.

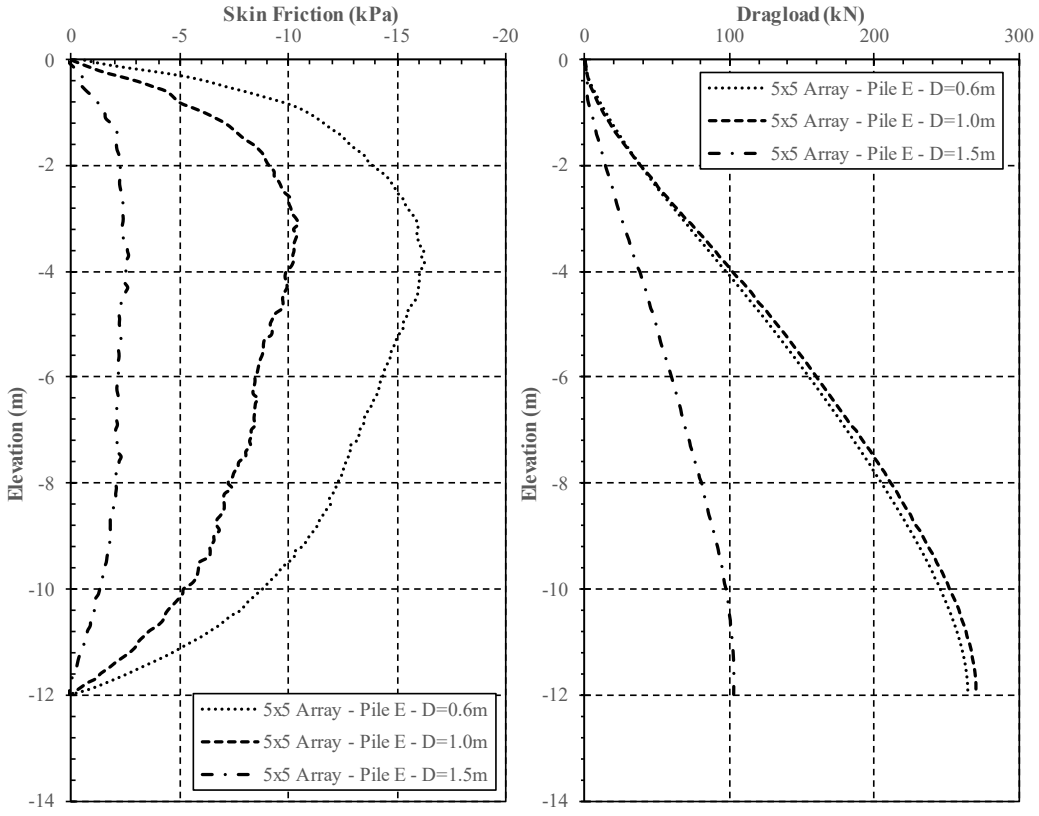

Figure A.16 NSF and dragload of Pile E in three different diameter cases for model conditions of 5x5 array, L=12m, s/D=6 and surcharge load of 100kPa.

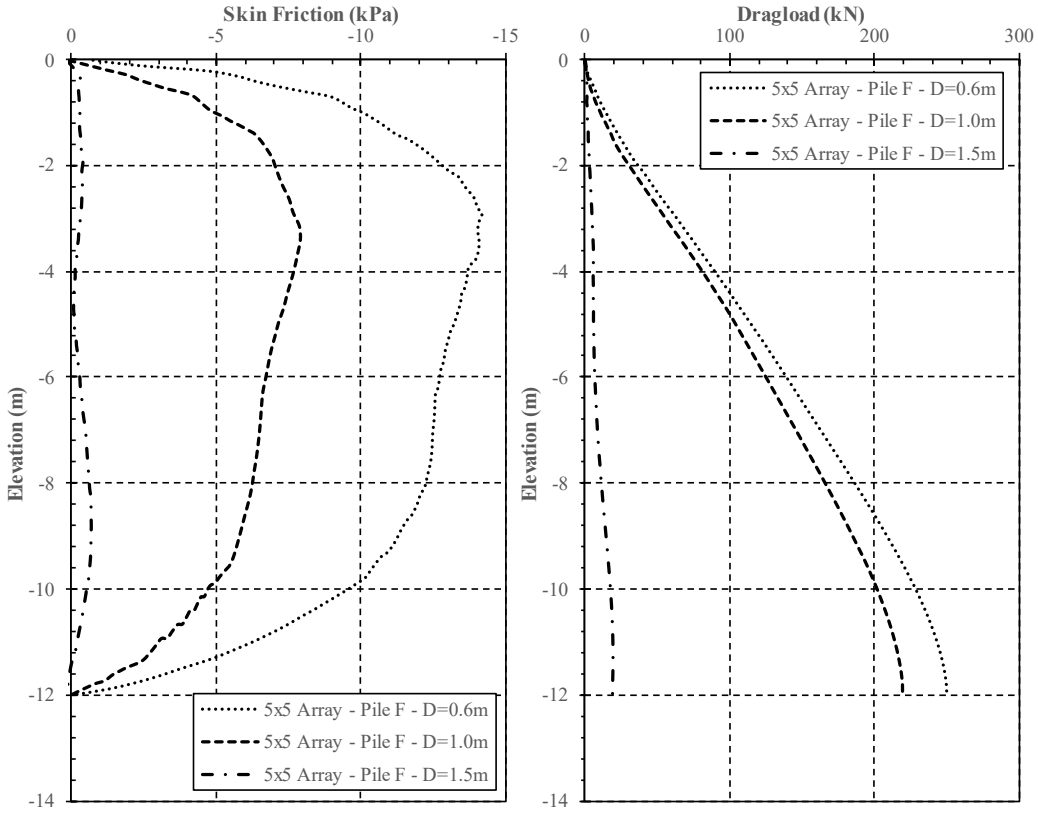

Figure A.17 NSF and dragload of Pile F in three different diameter cases for model conditions of 5x5 array, L=12m, s/D=6 and surcharge load of 100kPa.

D. The Effect of Pile Length

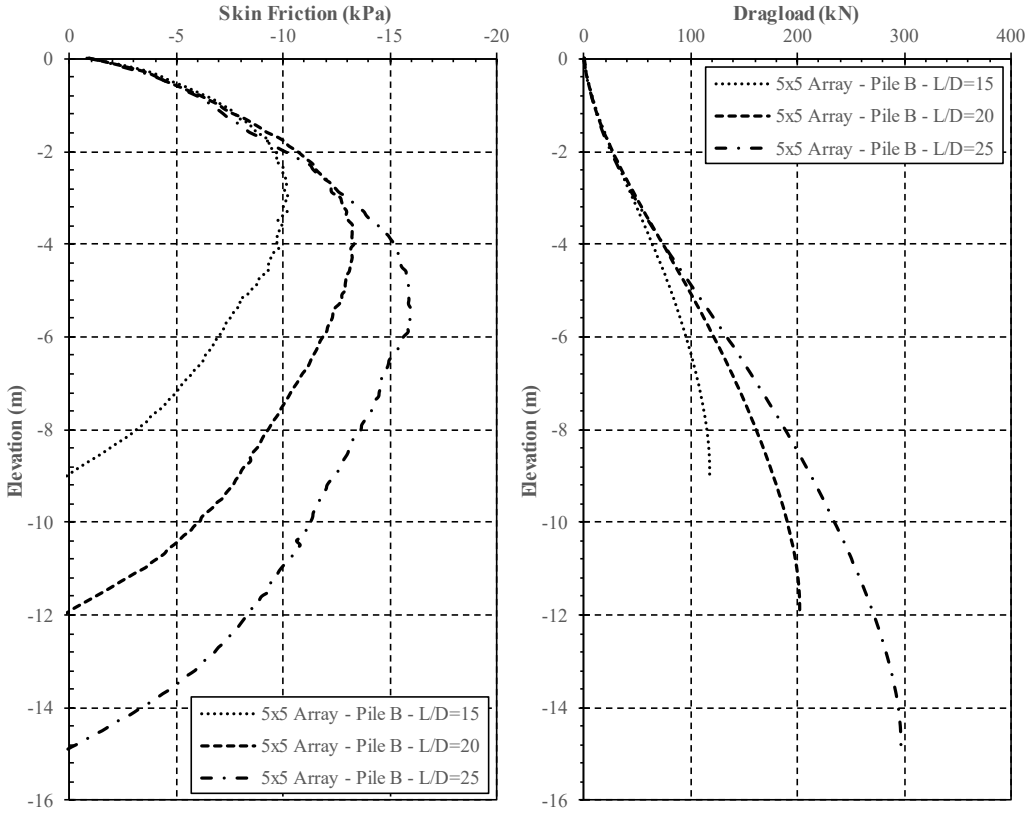

Figure A.18 NSF and dragload of Pile B in three different length cases for model conditions of 5x5 array, D=0.6m, s/D=3 and surcharge load of 50kPa.

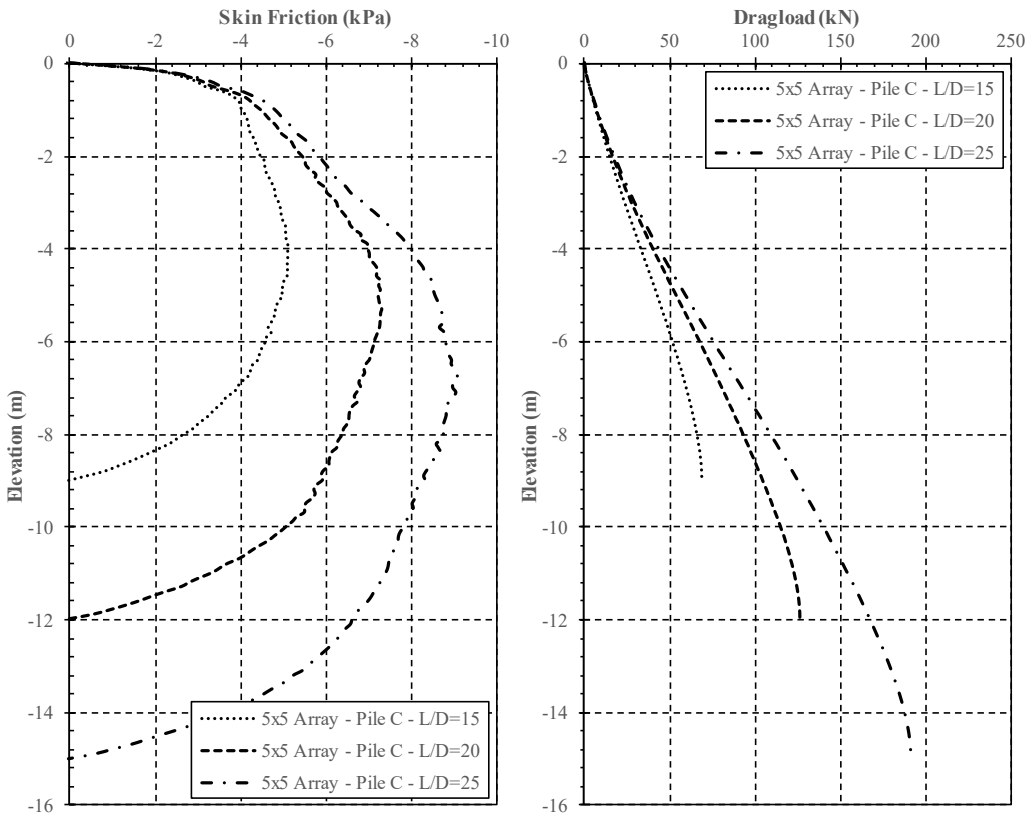

Figure A.19 NSF and dragload of Pile C in three different length cases for model conditions of 5x5 array, D=0.6m, s/D=3 and surcharge load of 50kPa.

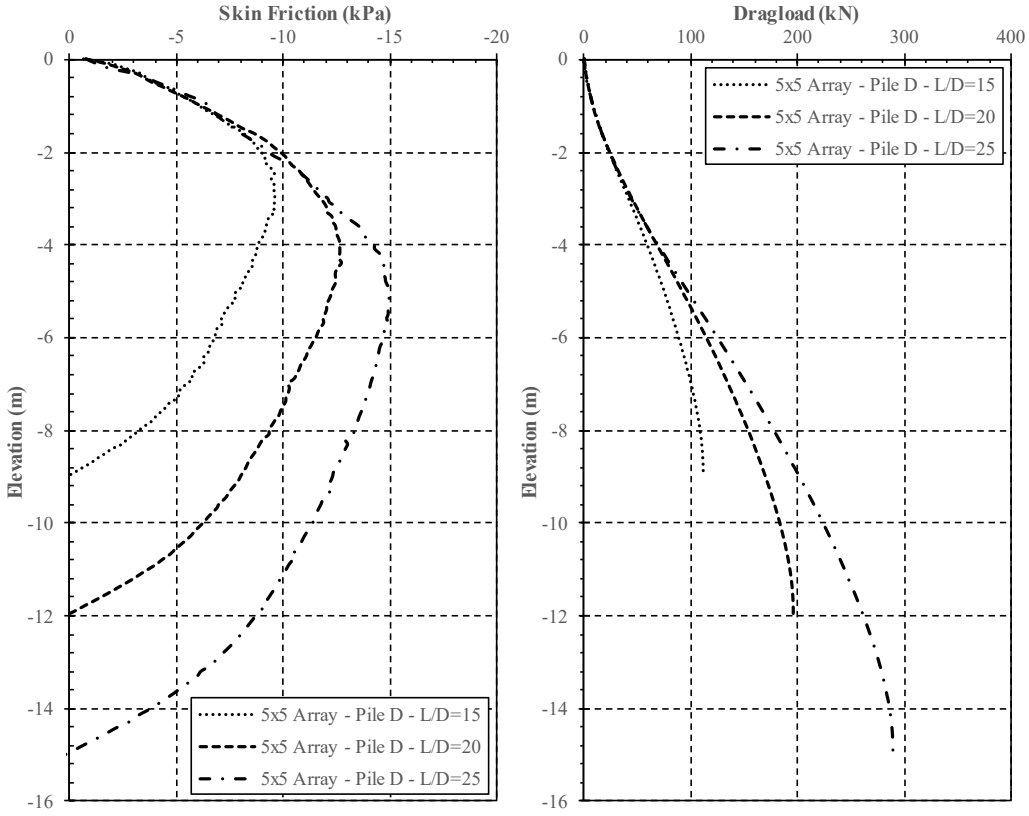

Figure A.20 NSF and dragload of Pile D in three different length cases for model conditions of 5x5 array, D=0.6m, s/D=3 and surcharge load of 50kPa.

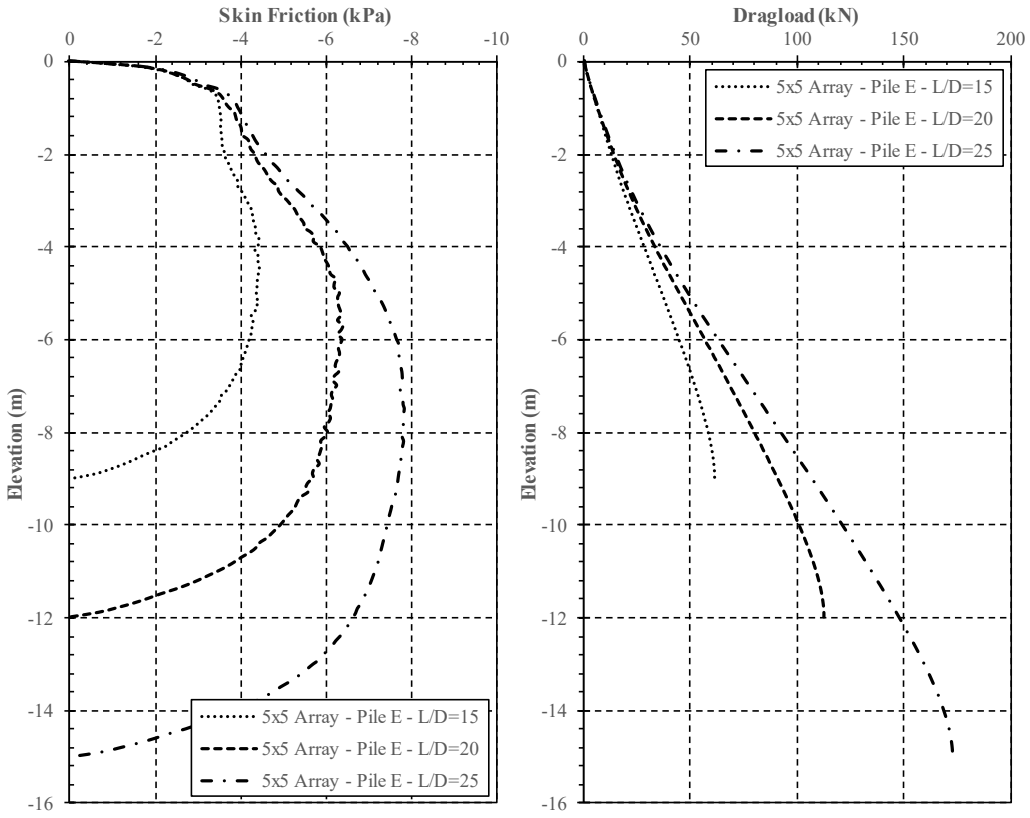

Figure A.21 NSF and dragload of Pile E in three different length cases for model conditions of 5x5 array, D=0.6m, s/D=3 and surcharge load of 50kPa.

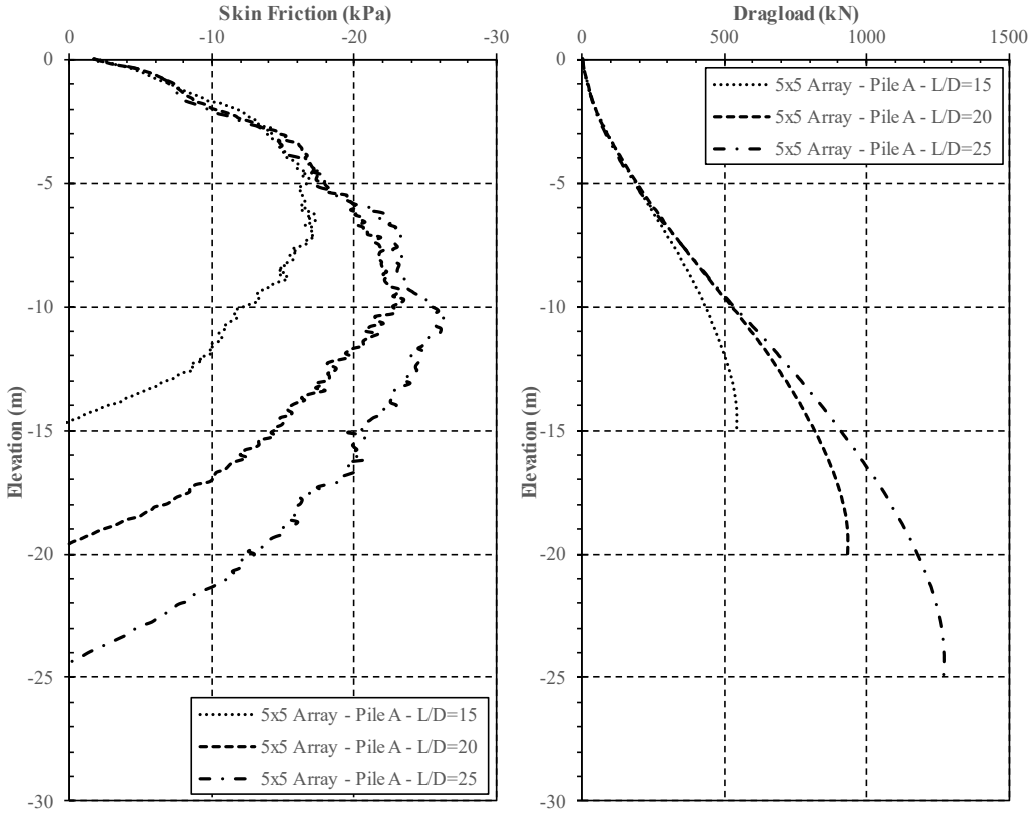

Figure A.22 NSF and dragload of Pile A in three different length cases for model conditions of 5x5 array, D=1.0m, s/D=3 and surcharge load of 50kPa.

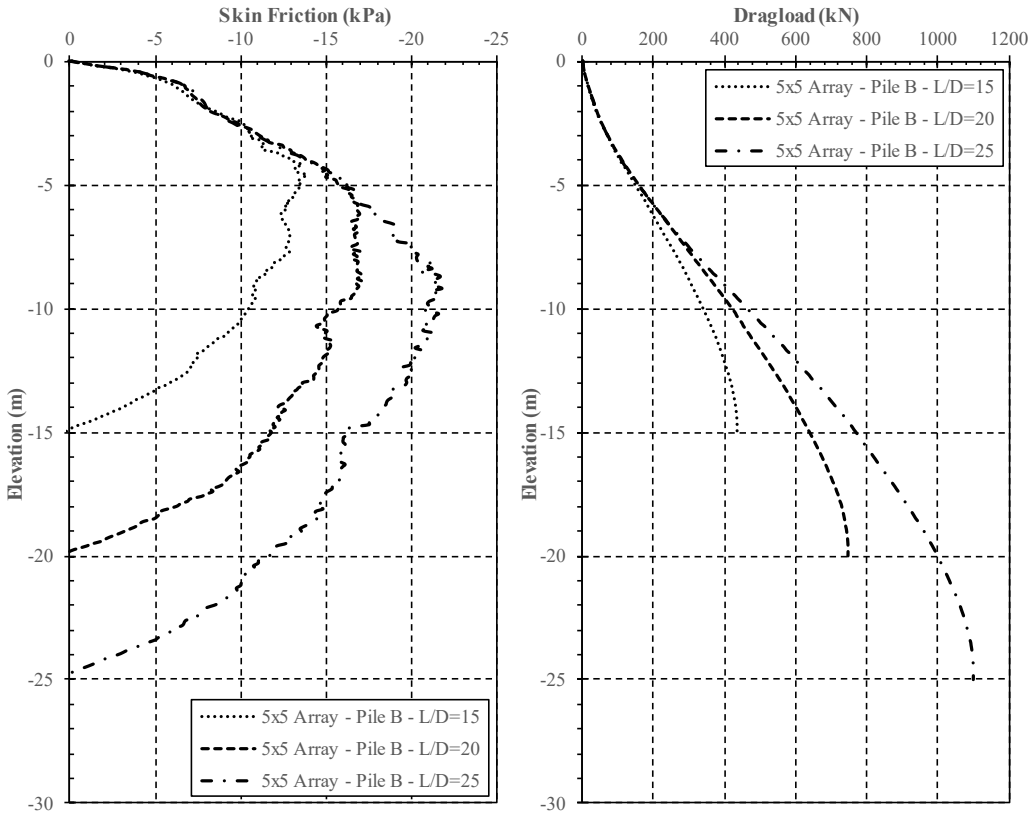

Figure A.23 NSF and dragload of Pile B in three different length cases for model conditions of 5x5 array, D=1.0m, s/D=3 and surcharge load of 50kPa.

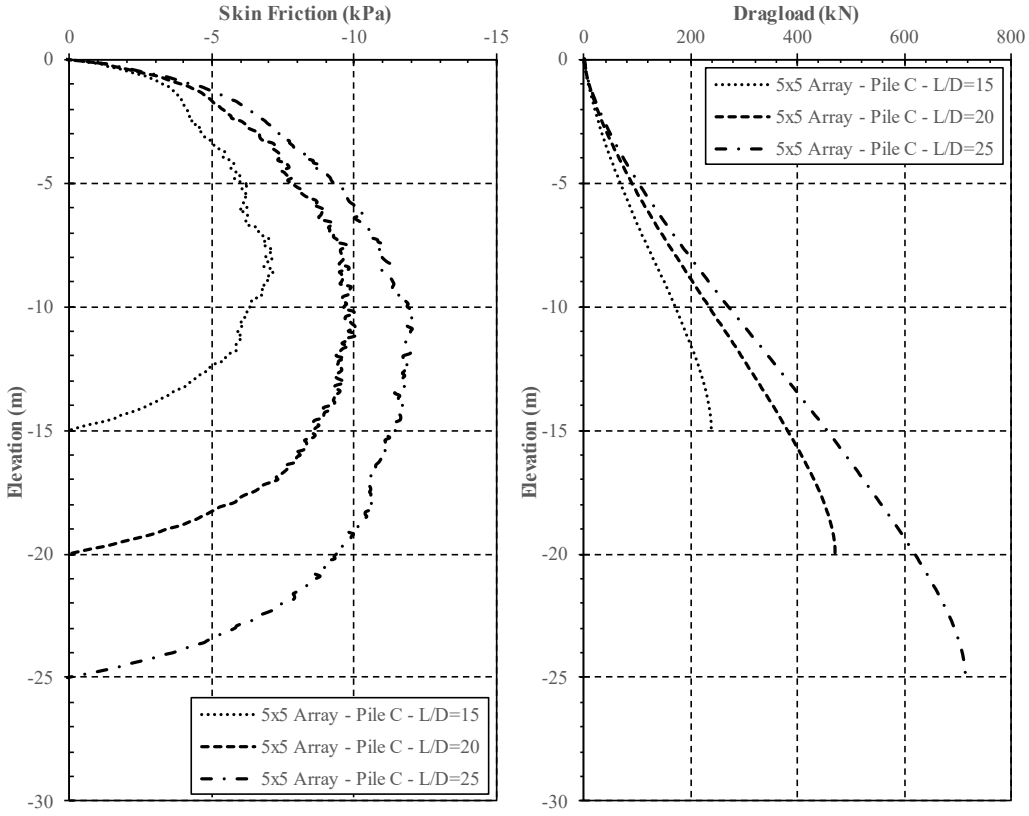

Figure A.24 NSF and dragload of Pile C in three different length cases for model conditions of 5x5 array, D=1.0m, s/D=3 and surcharge load of 50kPa.

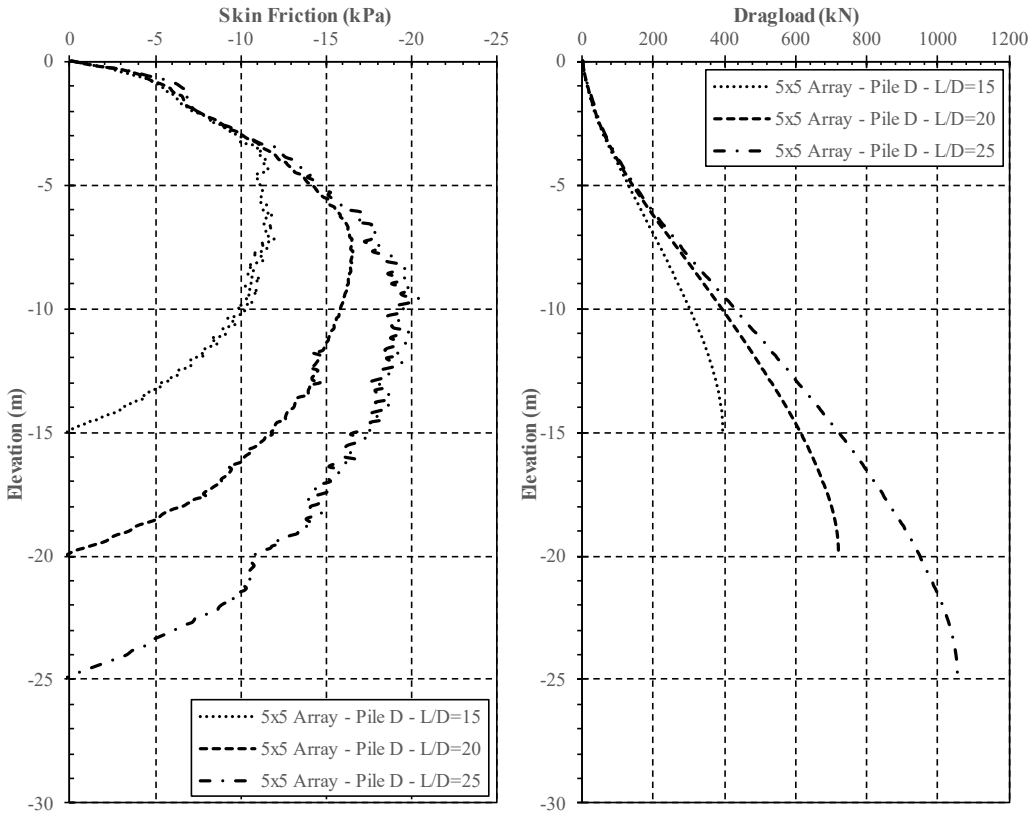

Figure A.25 NSF and dragload of Pile D in three different length cases for model conditions of 5x5 array, D=1.0m, s/D=3 and surcharge load of 50kPa.

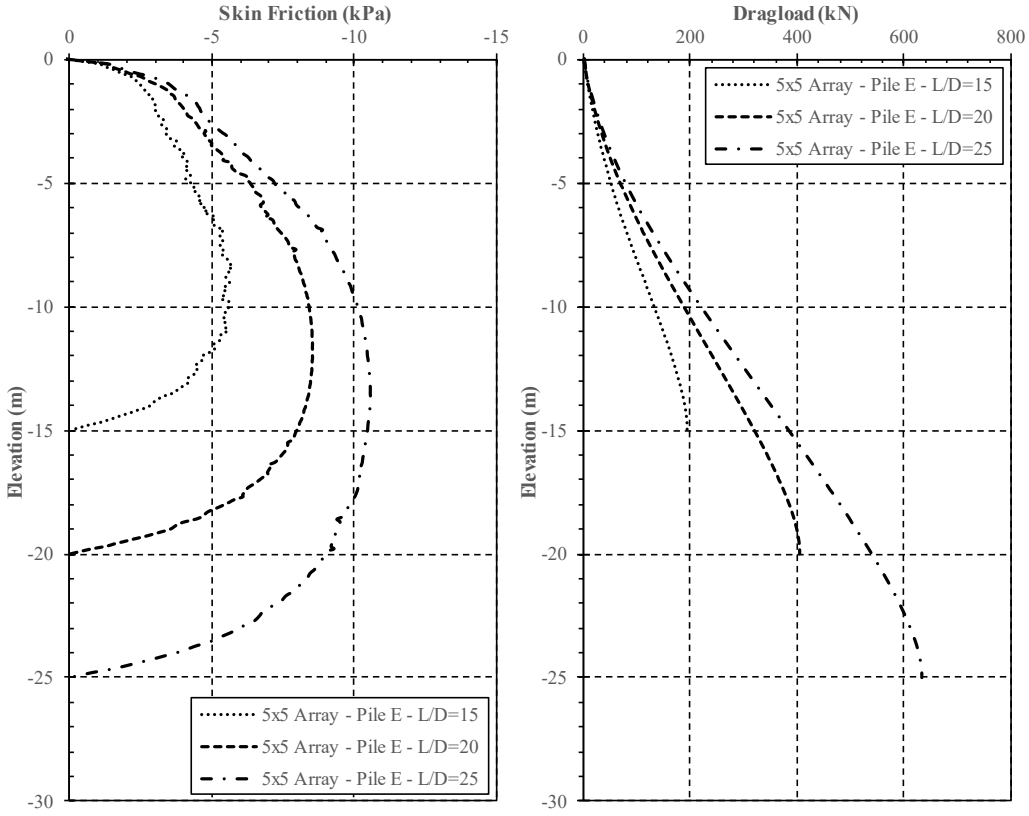

Figure A.26 NSF and dragload of Pile E in three different length cases for model conditions of 5x5 array, D=1.0m, s/D=3 and surcharge load of 50kPa.

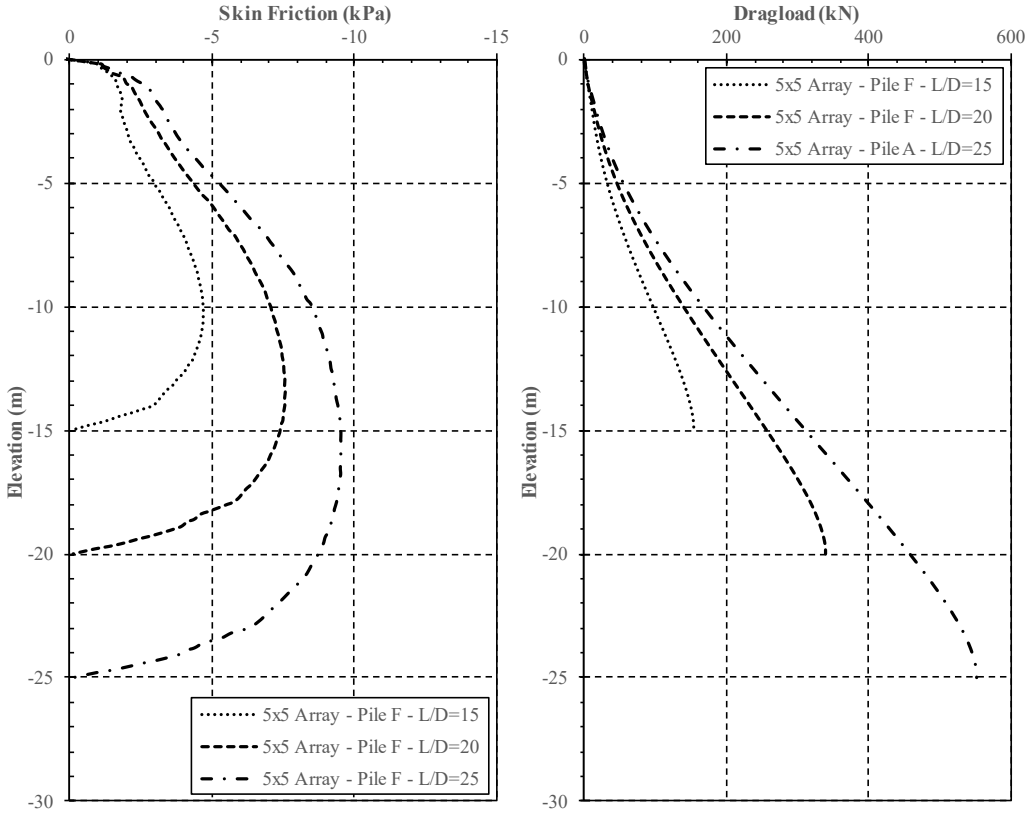

Figure A.27 NSF and dragload of Pile F in three different length cases for model conditions of 5x5 array, D=1.0m, s/D=3 and surcharge load of 50kPa.

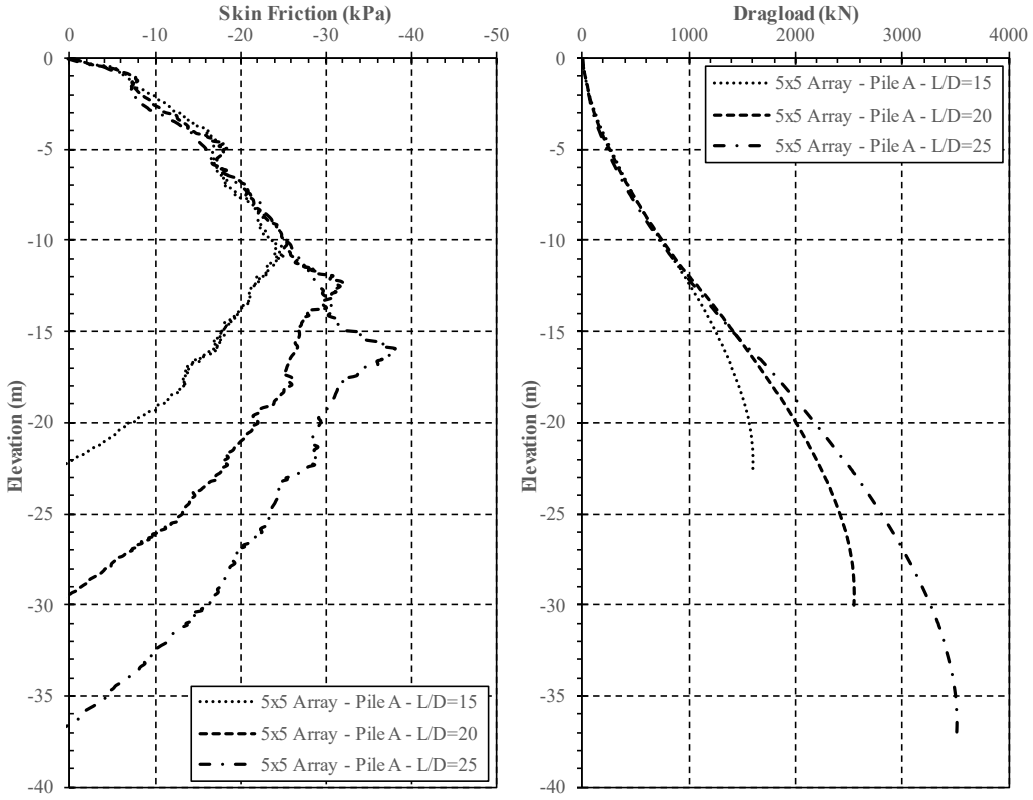

Figure A.28 NSF and dragload of Pile A in three different length cases for model conditions of 5x5 array, D=1.5m, s/D=3 and surcharge load of 50kPa.

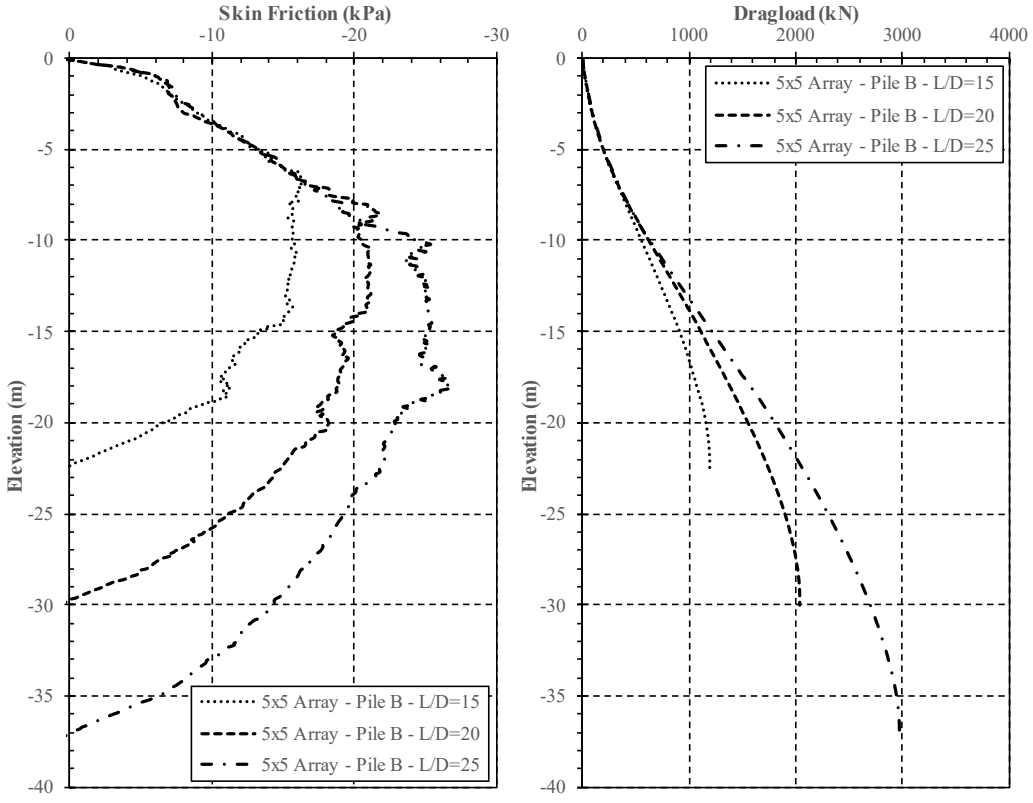

Figure A.29 NSF and dragload of Pile B in three different length cases for model conditions of 5x5 array, D=1.5m, s/D=3 and surcharge load of 50kPa.

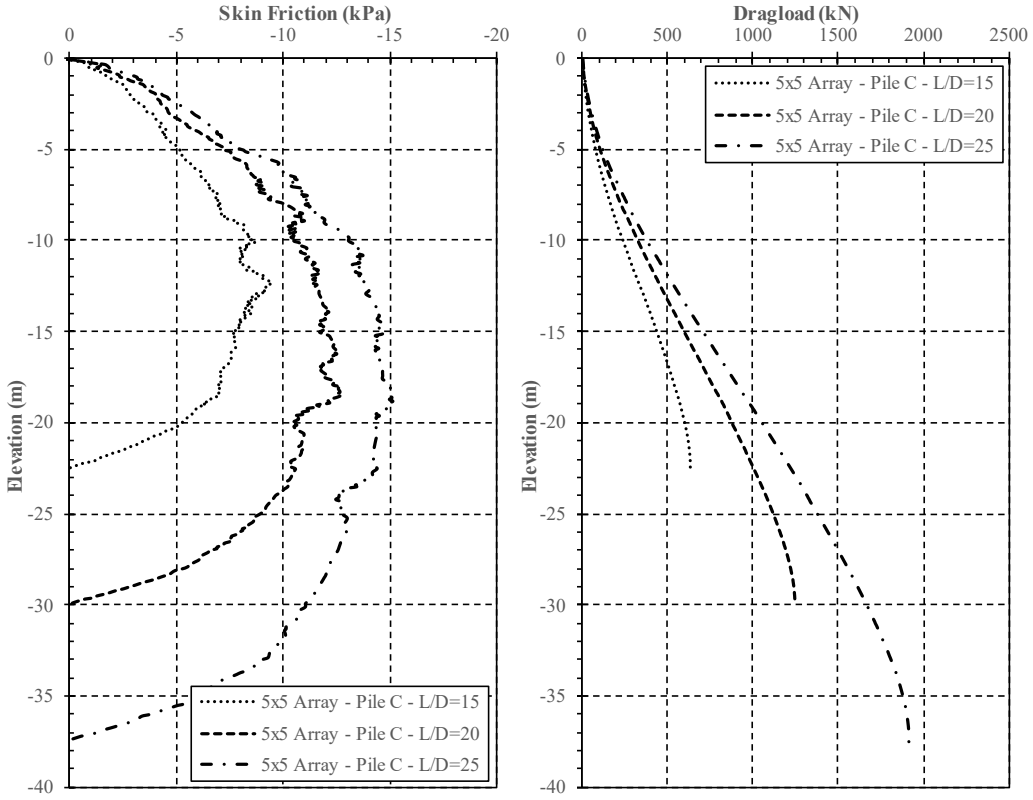

Figure A.30 NSF and dragload of Pile C in three different length cases for model conditions of 5x5 array, D=1.5m, s/D=3 and surcharge load of 50kPa.

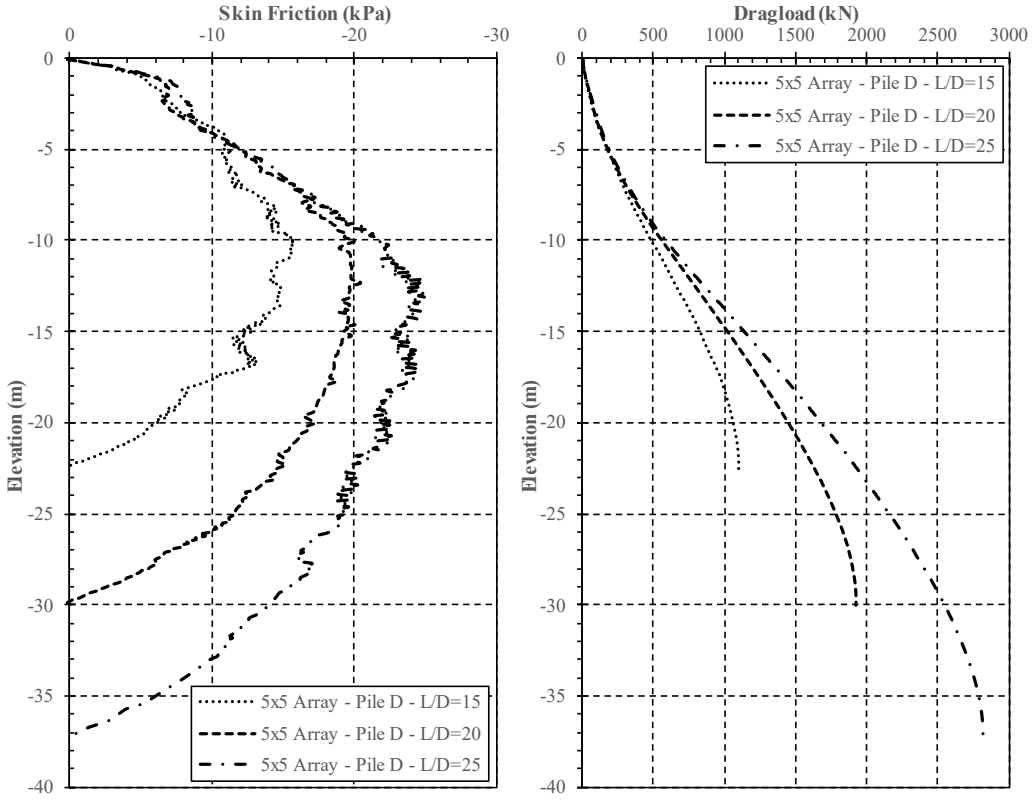

Figure A.31 NSF and dragload of Pile D in three different length cases for model conditions of 5x5 array, D=1.5m, s/D=3 and surcharge load of 50kPa.

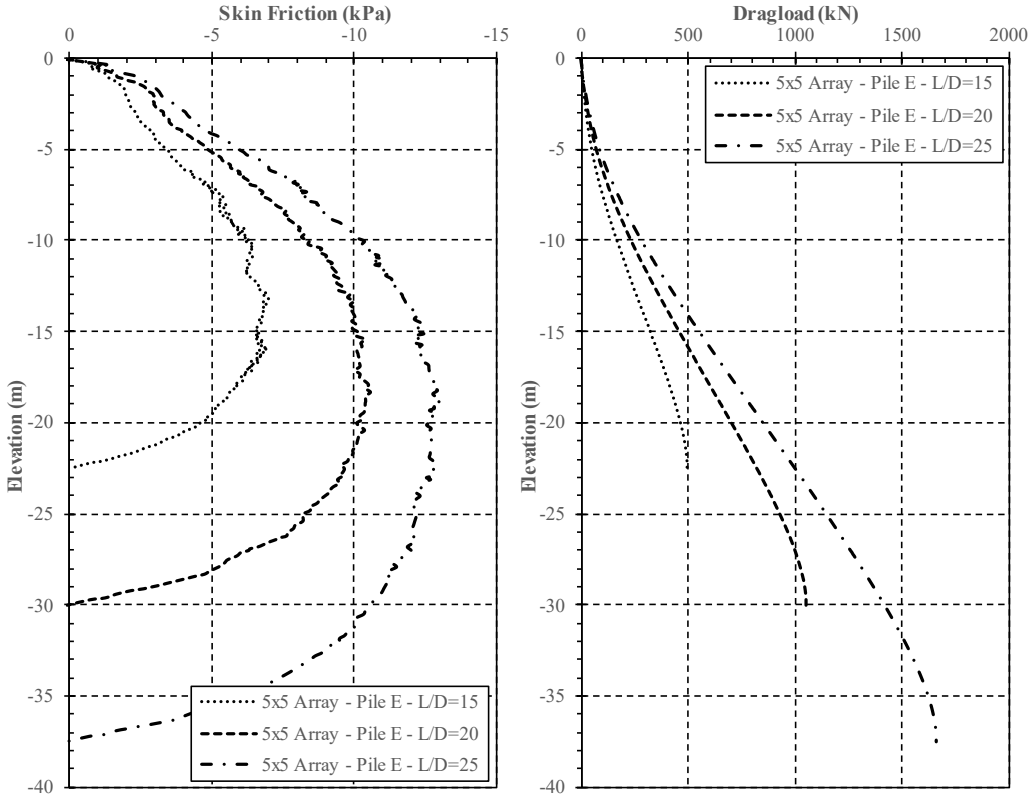

Figure A.32 NSF and dragload of Pile E in three different length cases for model conditions of 5x5 array, D=1.5m, s/D=3 and surcharge load of 50kPa.

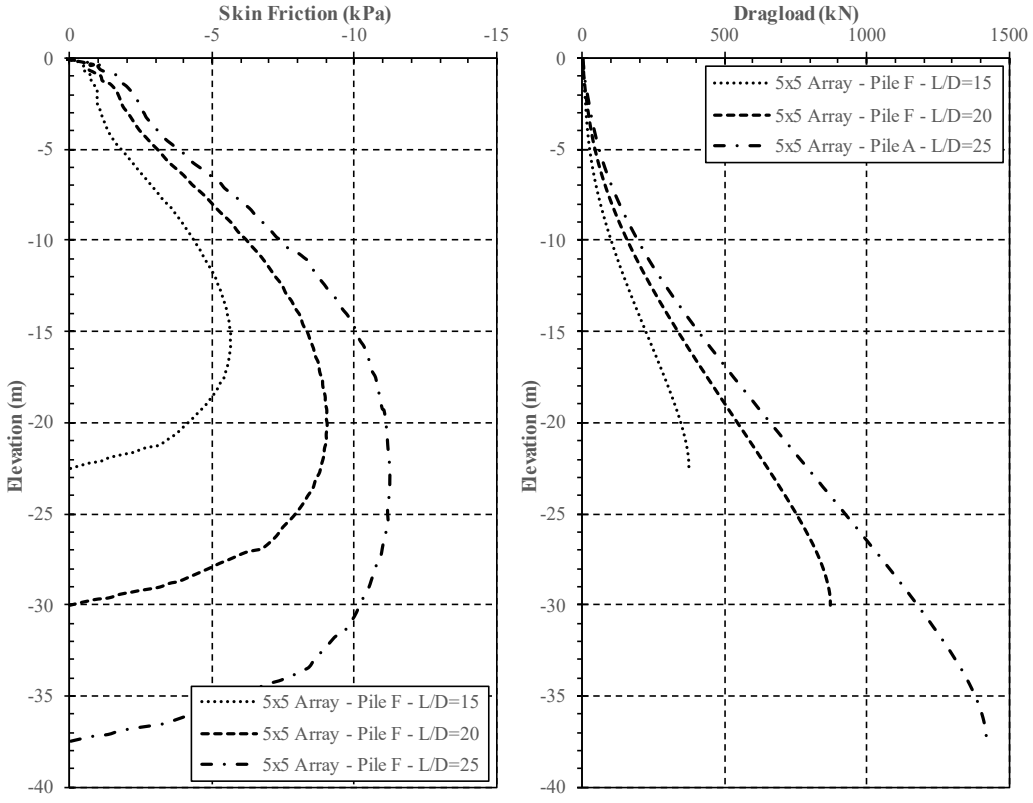

Figure A.33 NSF and dragload of Pile F in three different length cases for model conditions of 5x5 array, D=1.5m, s/D=3 and surcharge load of 50kPa.

E. The Effect of Pile Spacing

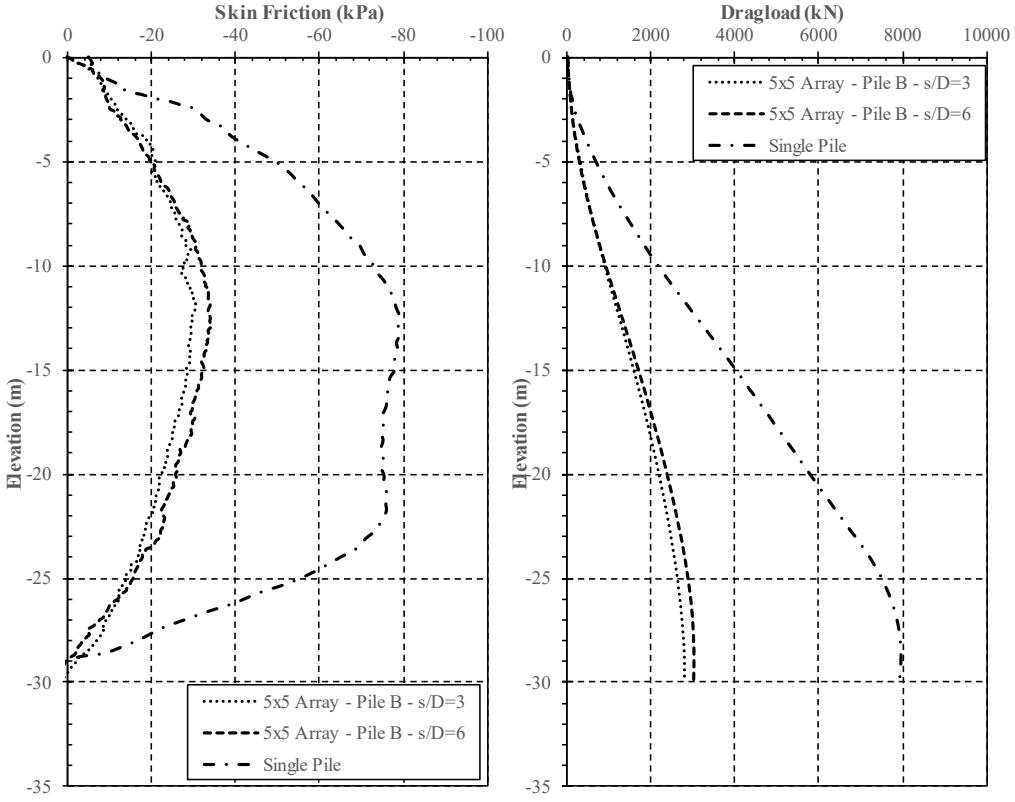

Figure A.34 NSF and dragload of Pile B in three pile spacing cases for model conditions of D=1.5m, L/D=20 and surcharge load of 100kPa.

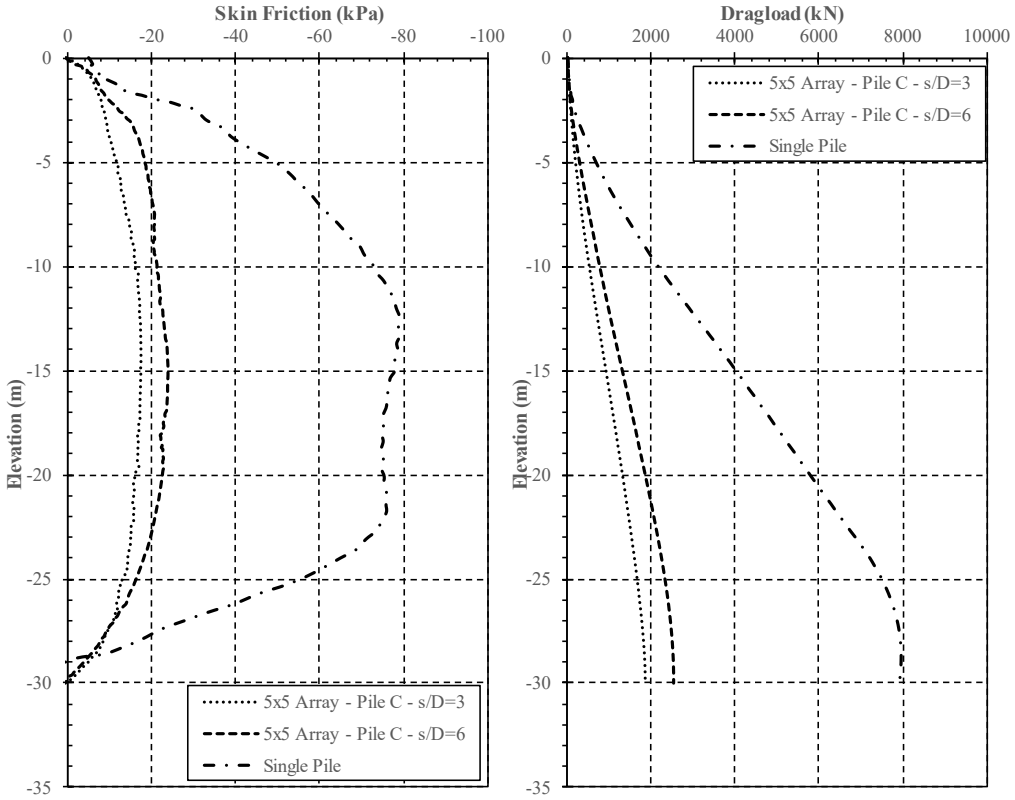

Figure A.35 NSF and dragload of Pile C in three pile spacing cases for model conditions of D=1.5m, L/D=20 and surcharge load of 100kPa.

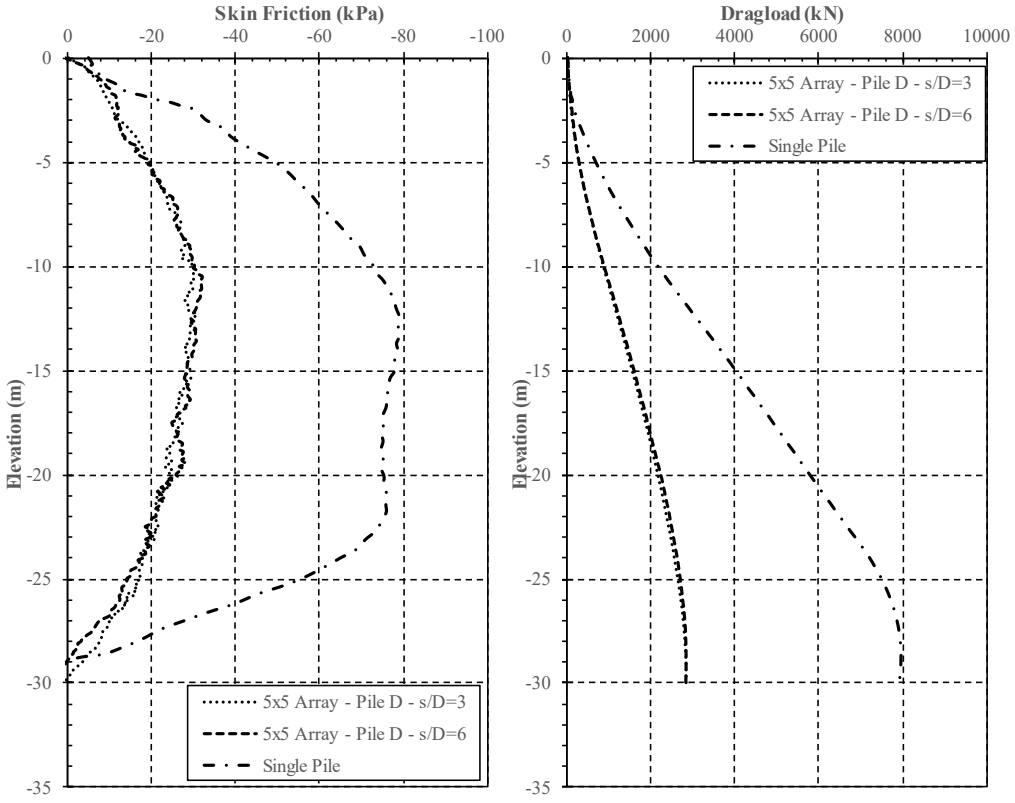

Figure A.36 NSF and dragload of Pile D in three pile spacing cases for model conditions of D=1.5m, L/D=20 and surcharge load of 100kPa.

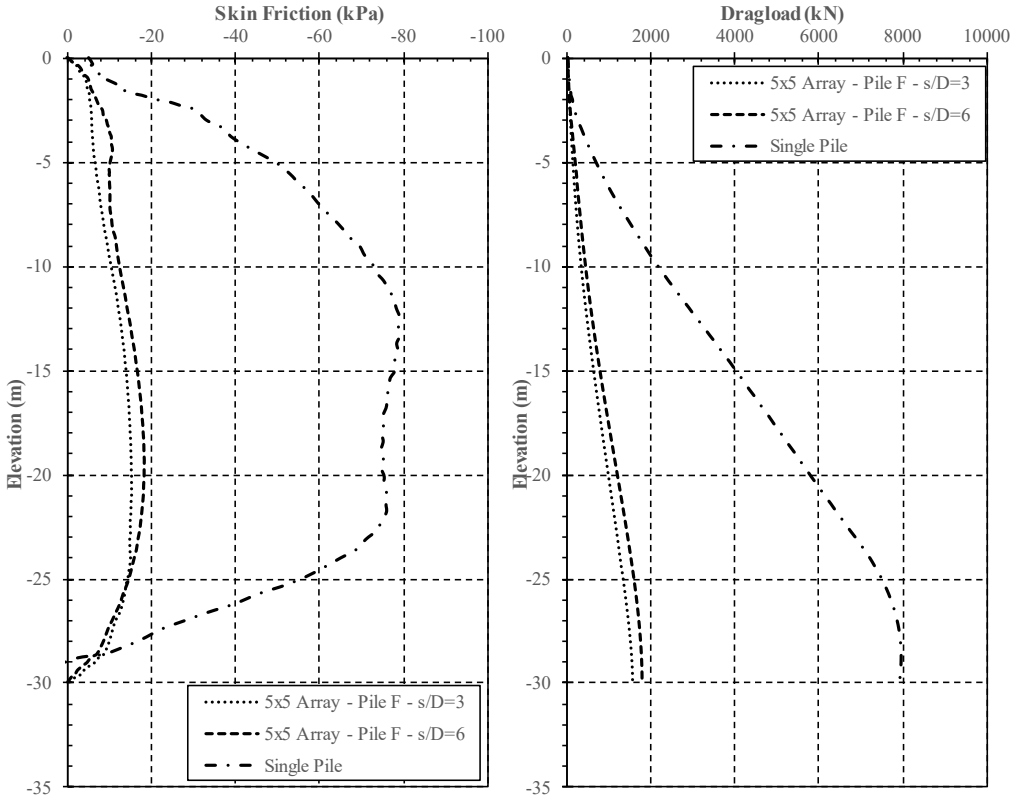

Figure A.37 NSF and dragload of Pile F in three pile spacing cases for model conditions of D=1.5m, L/D=20 and surcharge load of 100kPa.

F. The Effect of Number of Piles in a Pile Array

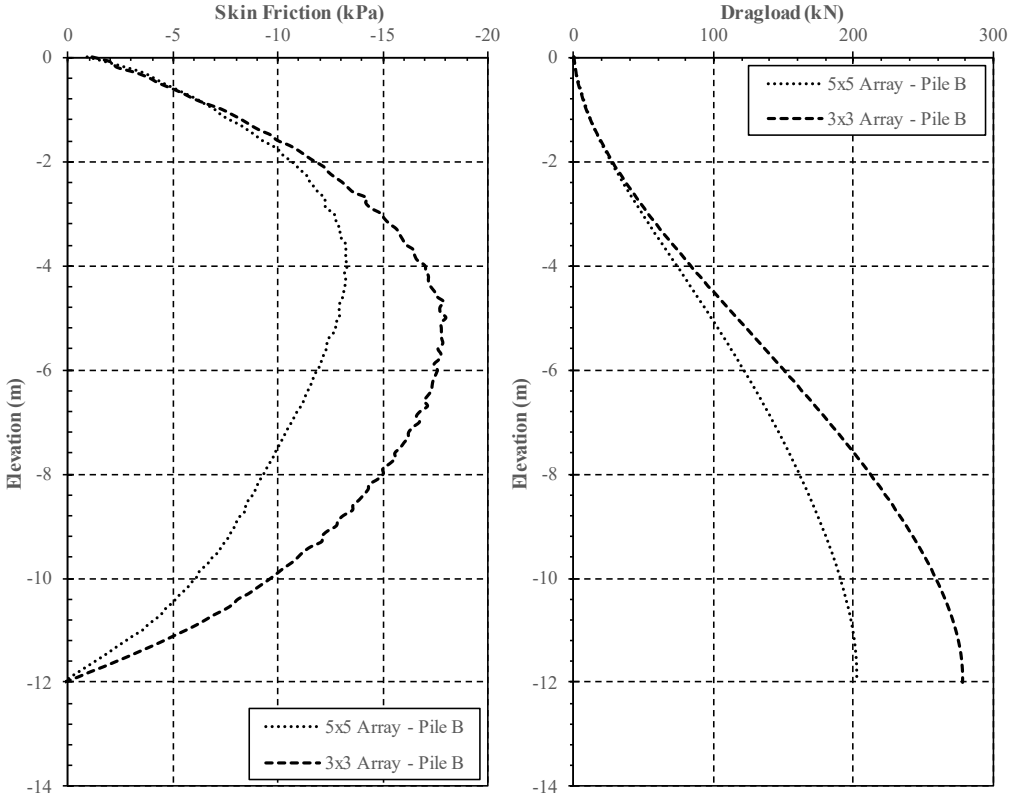

Figure A.38 NSF and dragload of Pile B in two different pile arrays for model conditions of D=0.6m, s/D=3, L/D=20 and surcharge load of 50kPa.

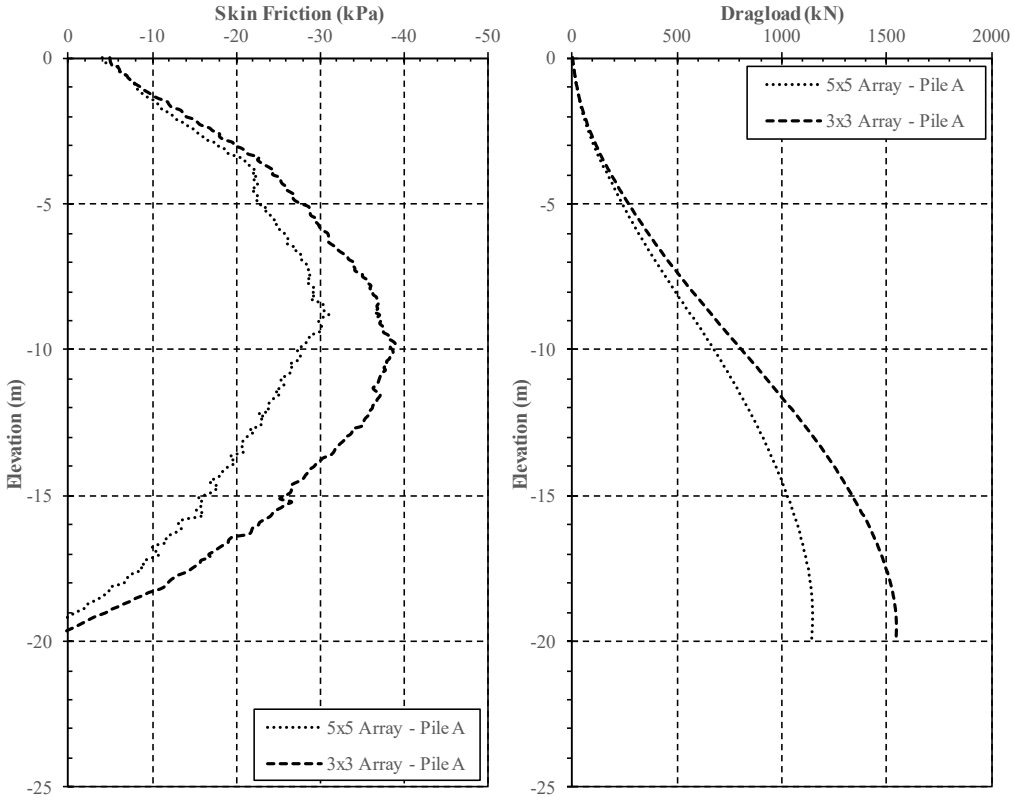

Figure A.39 NSF and dragload of Pile A in two different pile arrays for model conditions of D=1.0m, s/D=3, L/D=20 and surcharge load of 100kPa.

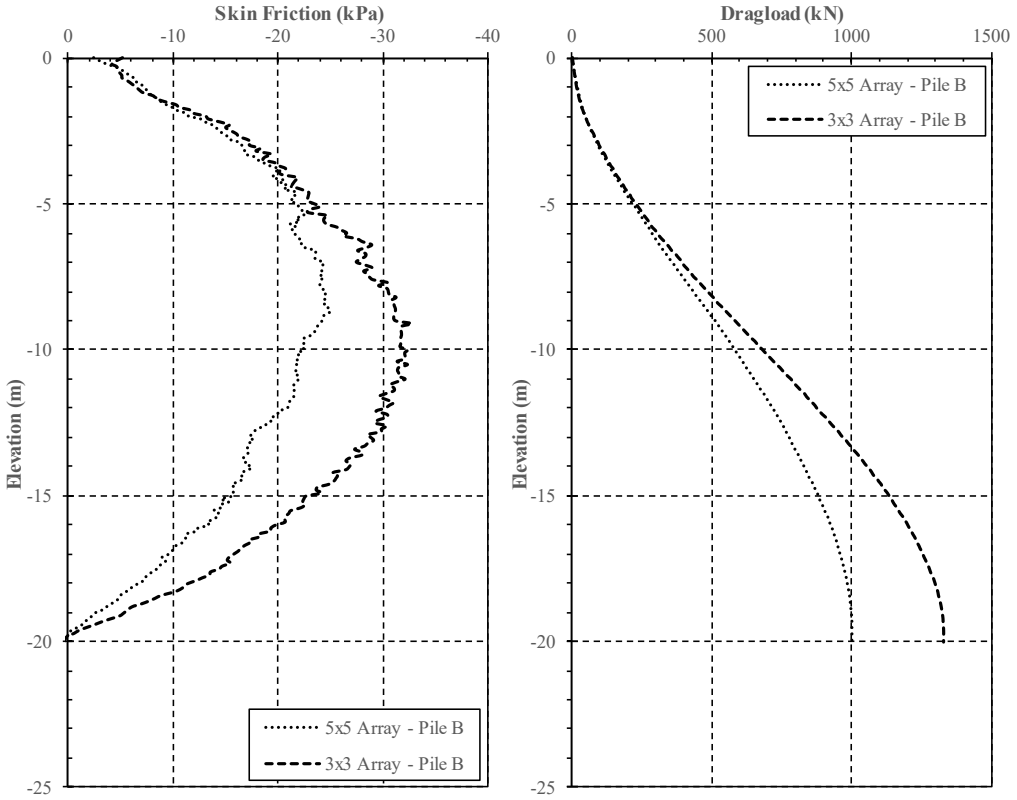

Figure A.40 NSF and dragload of Pile B in two different pile arrays for model conditions of D=1.0m, s/D=3, L/D=20 and surcharge load of 100kPa.

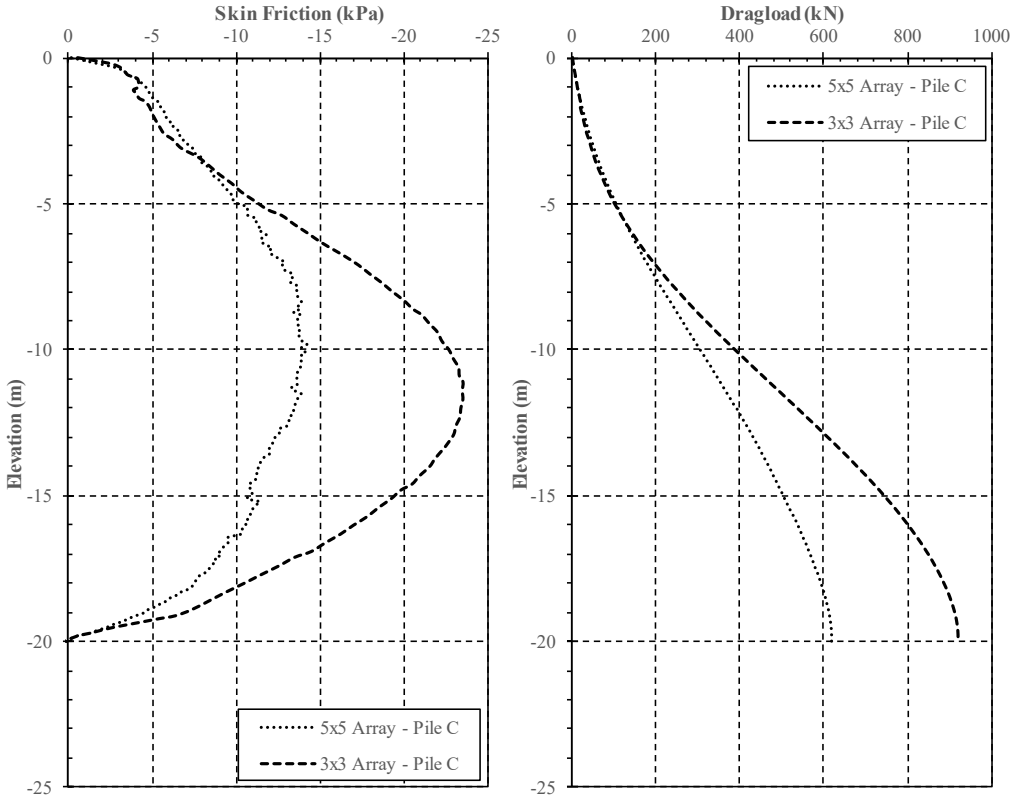

Figure A.41 NSF and dragload of Pile C in two different pile arrays for model conditions of D=1.0m, s/D=3, L/D=20 and surcharge load of 100kPa.

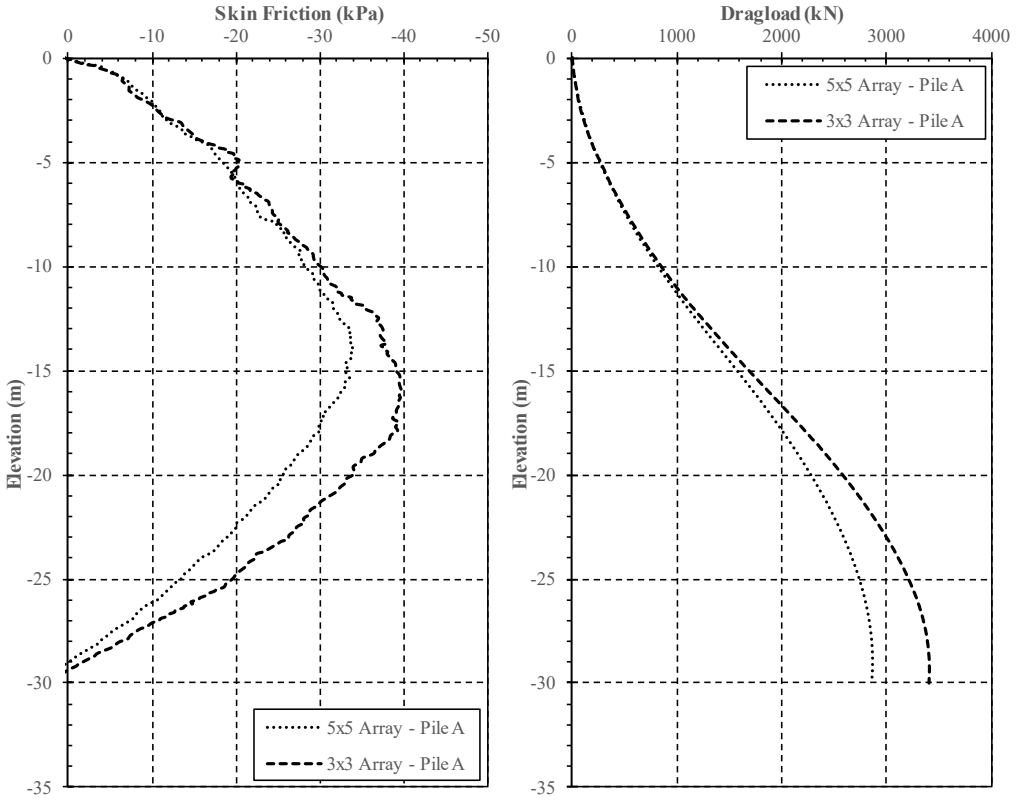

Figure A.42 NSF and dragload of Pile A in two different pile arrays for model conditions of D=1.5m, s/D=6, L/D=20 and surcharge load of 50kPa.

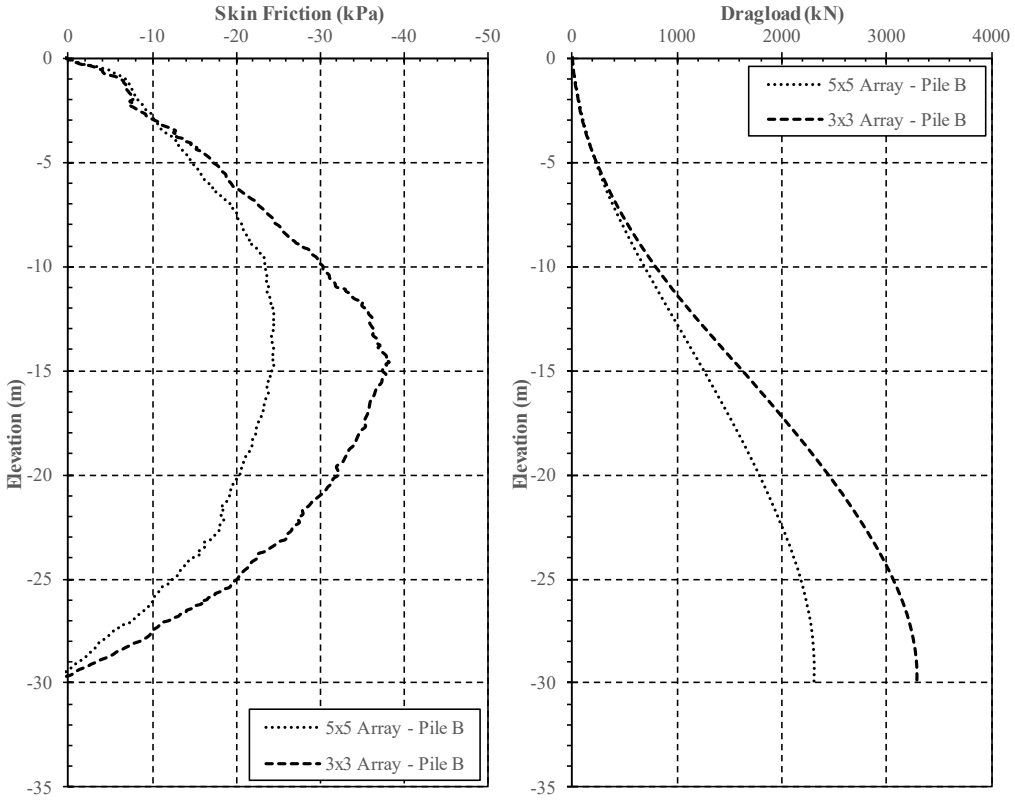

Figure A.43 NSF and dragload of Pile B in two different pile arrays for model conditions of D=1.5m, s/D=6, L/D=20 and surcharge load of 50kPa.

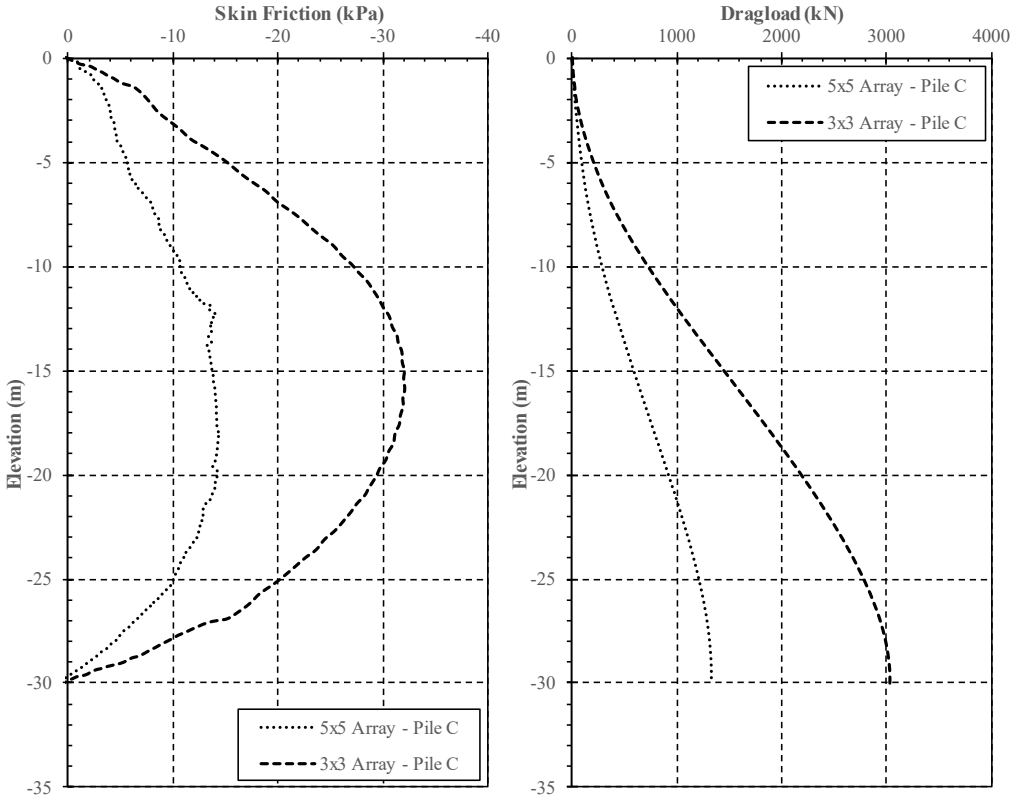

Figure A.44 NSF and dragload of Pile C in two different pile arrays for model conditions of D=1.5m, s/D=6, L/D=20 and surcharge load of 50kPa.

G. The Effect of Pile Position in a Pile Array

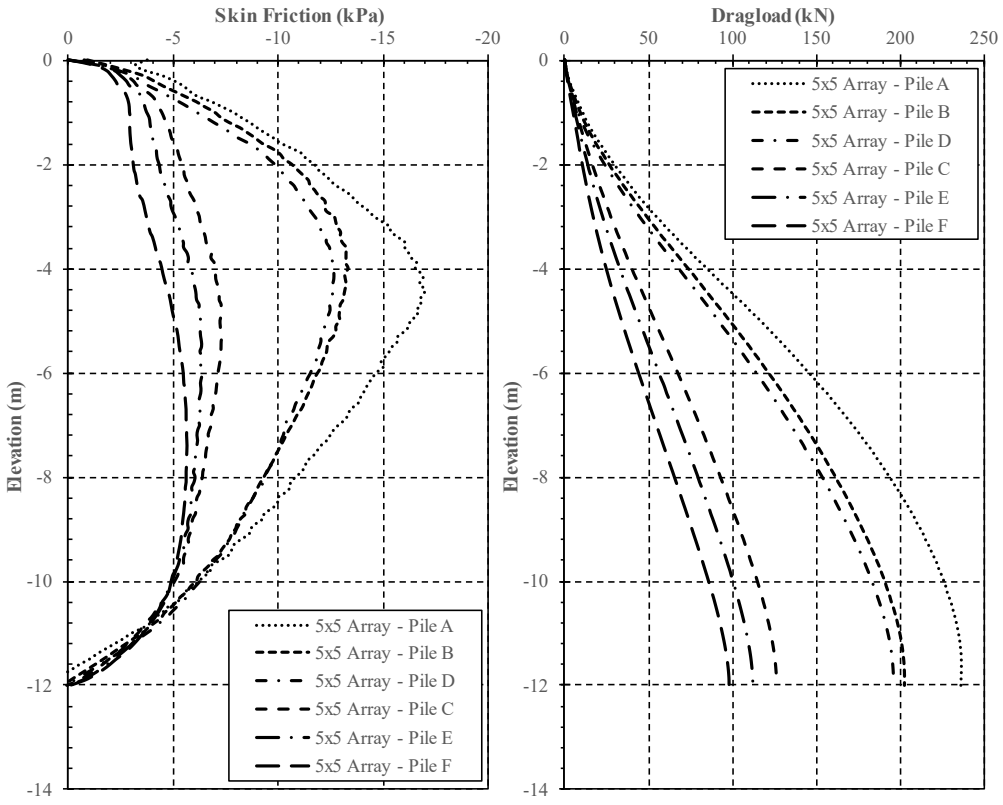

Figure A.45 NSF and dragload of different pile positions for model conditions of D=0.6m, s/D=3, L/D=20 and surcharge load of 50kPa.

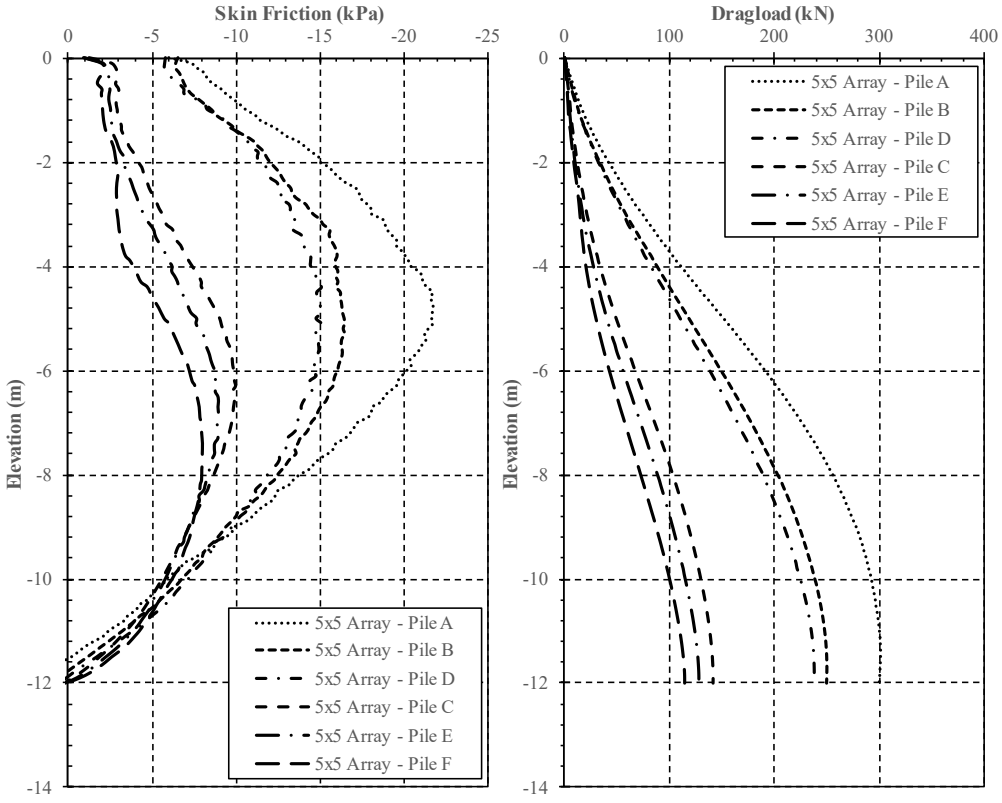

Figure A.46 NSF and dragload of different pile positions for model conditions of D=0.6m, s/D=3, L/D=20 and surcharge load of 100kPa.

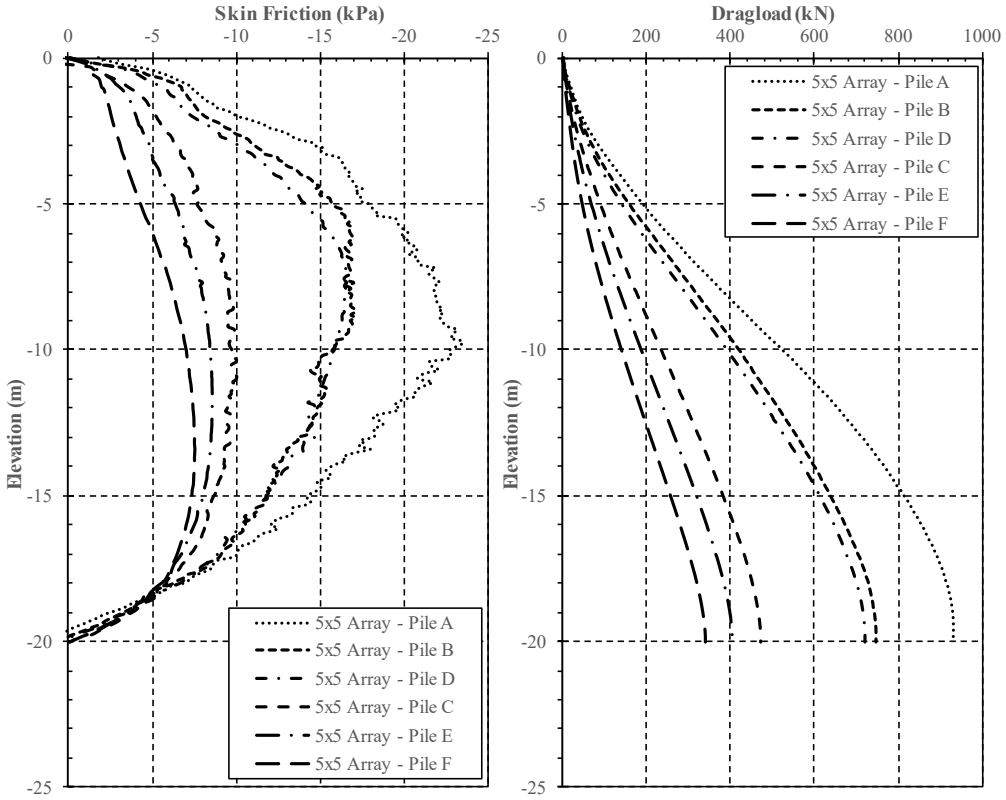

Figure A.47 NSF and dragload of different pile positions for model conditions of D=1.0m, s/D=3, L/D=20 and surcharge load of 50kPa.

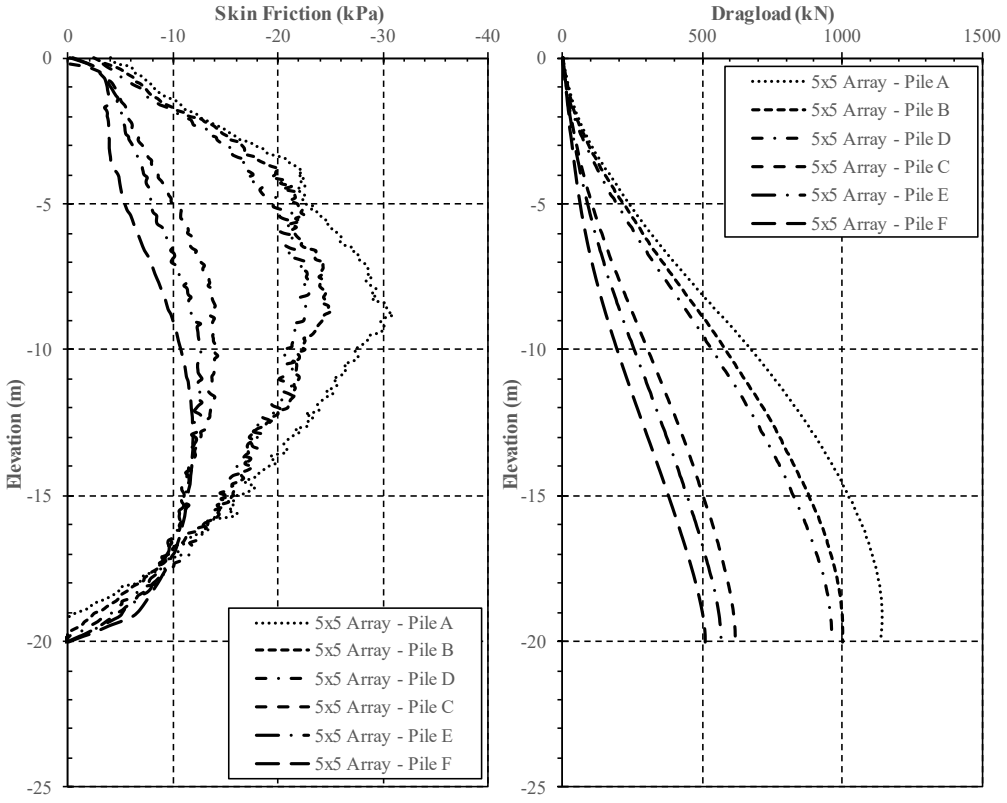

Figure A.48 NSF and dragload of different pile positions for model conditions of D=1.0m, s/D=3, L/D=20 and surcharge load of 100kPa.

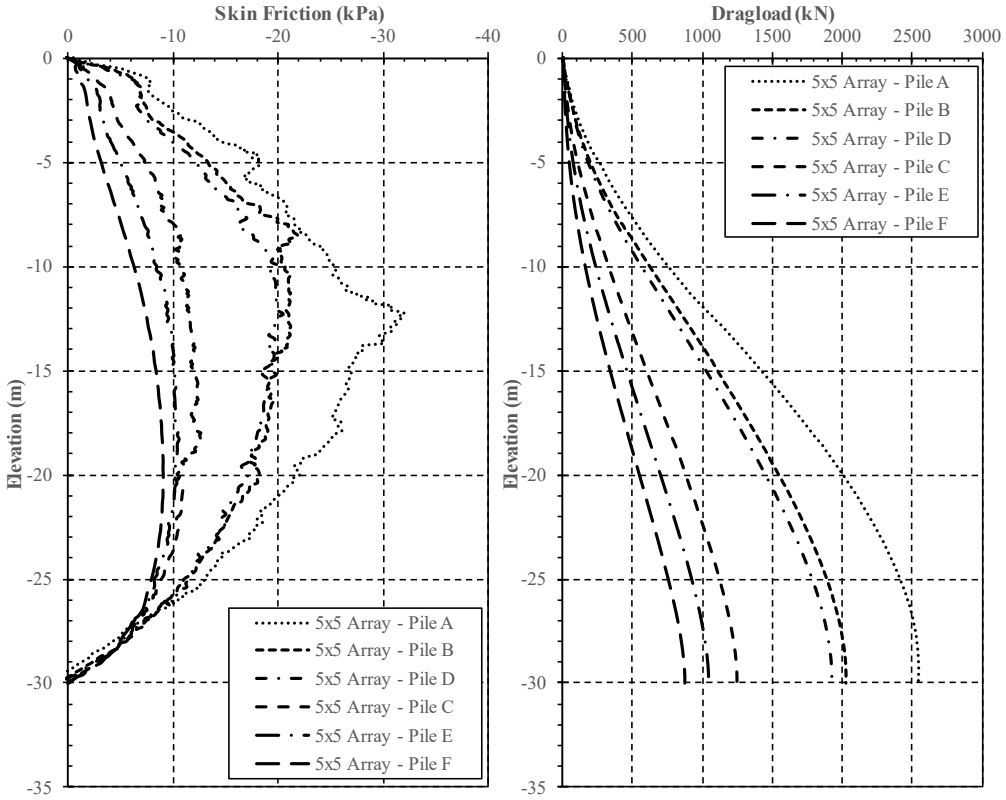

Figure A.49 NSF and dragload of different pile positions for model conditions of D=1.5m, s/D=3, L/D=20 and surcharge load of 50kPa.

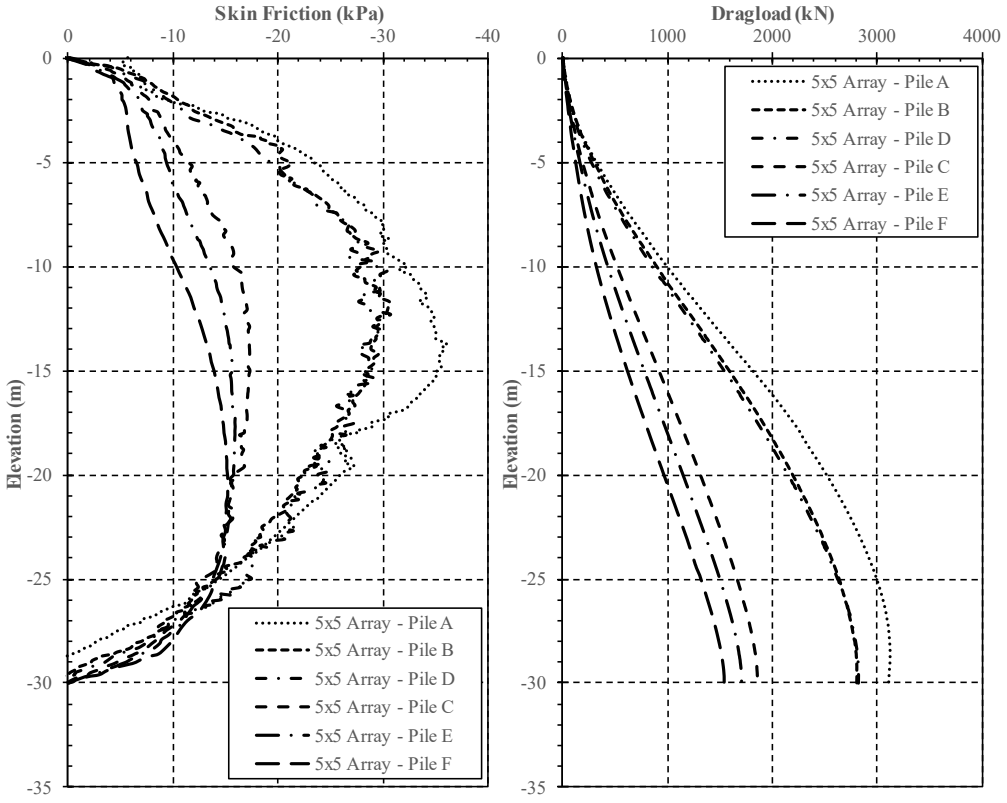

Figure A.50 NSF and dragload of different pile positions for model conditions of D=1.5m, s/D=3, L/D=20 and surcharge load of 100kPa.

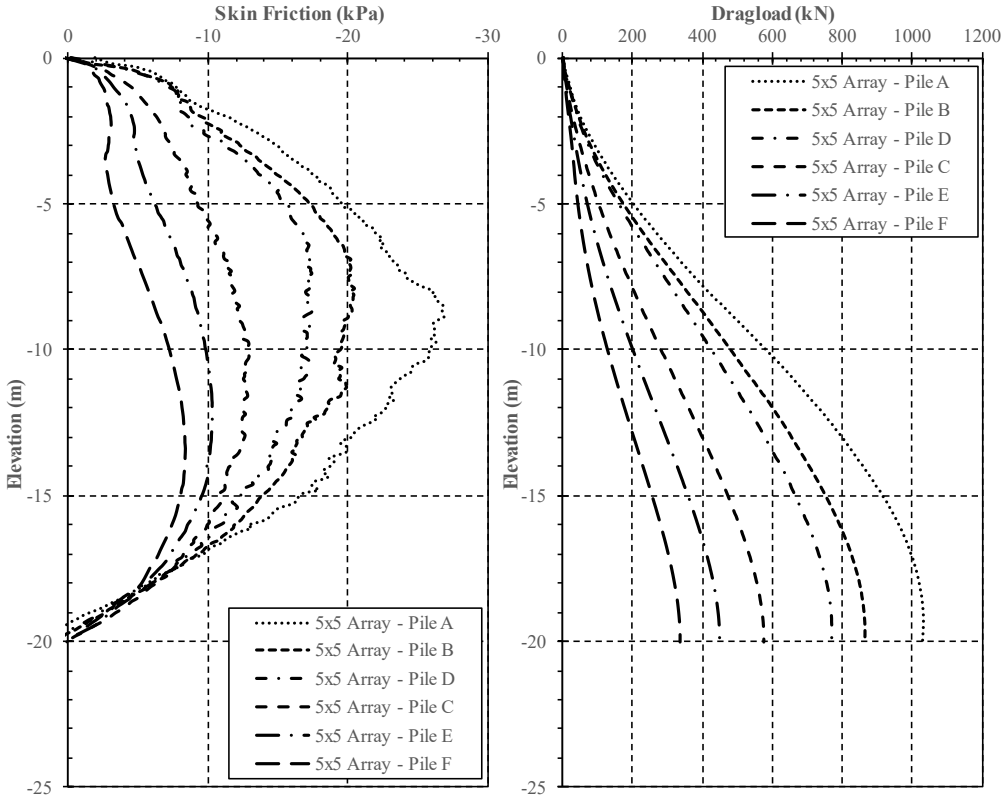

Figure A.51 NSF and dragload of different pile positions for model conditions of D=1.0m, s/D=6, L/D=20 and surcharge load of 50kPa.

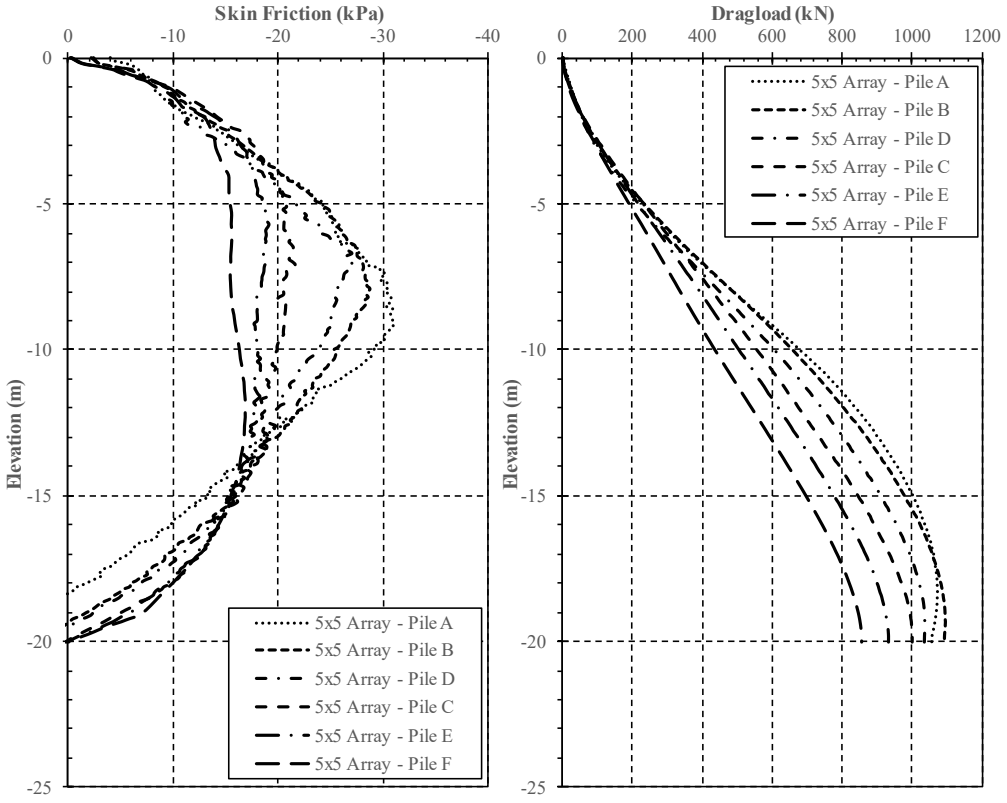

Figure A.52 NSF and dragload of different pile positions for model conditions of D=1.0m, s/D=6, L/D=20 and surcharge load of 100kPa.

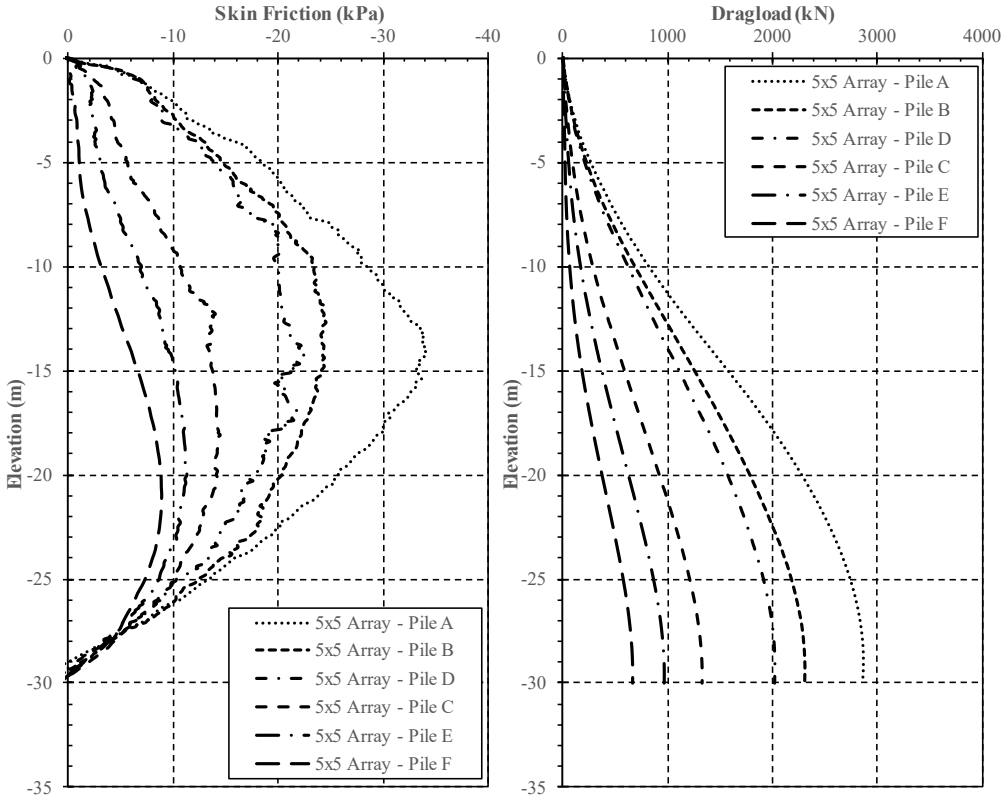

Figure A.53 NSF and dragload of different pile positions for model conditions of D=1.5m, s/D=6, L/D=20 and surcharge load of 50kPa.

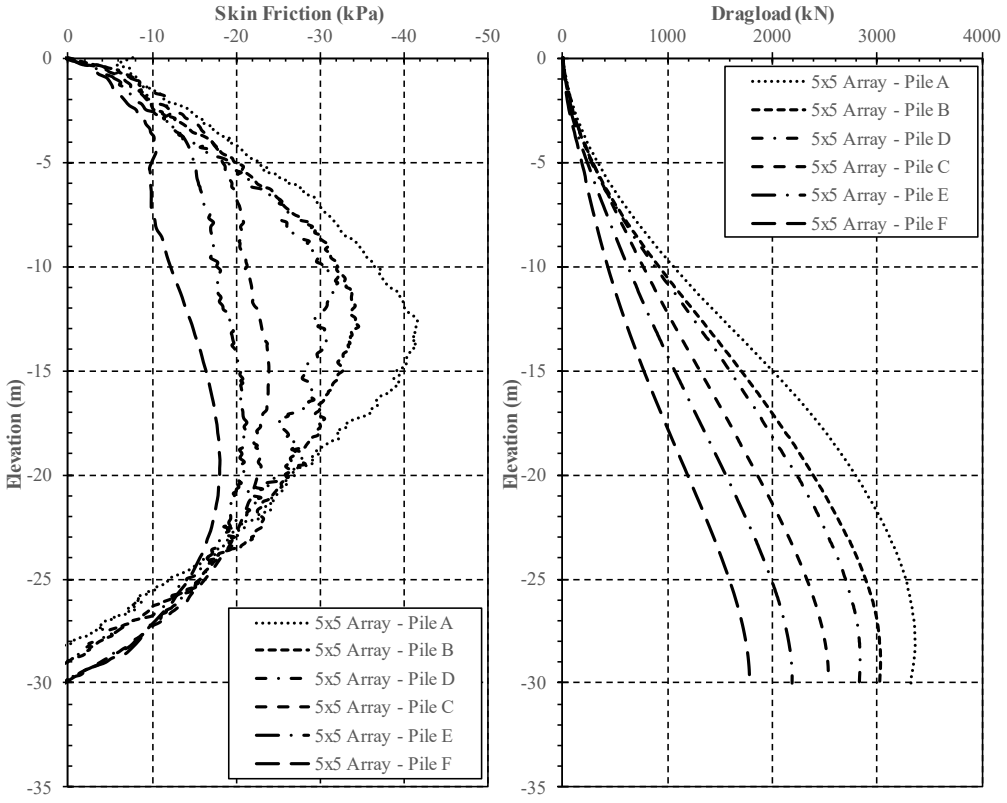

Figure A.54 NSF and dragload of different pile positions for model conditions of D=1.5m, s/D=6, L/D=20 and surcharge load of 100kPa.

H. The Effect of Soil Compressibility Factor

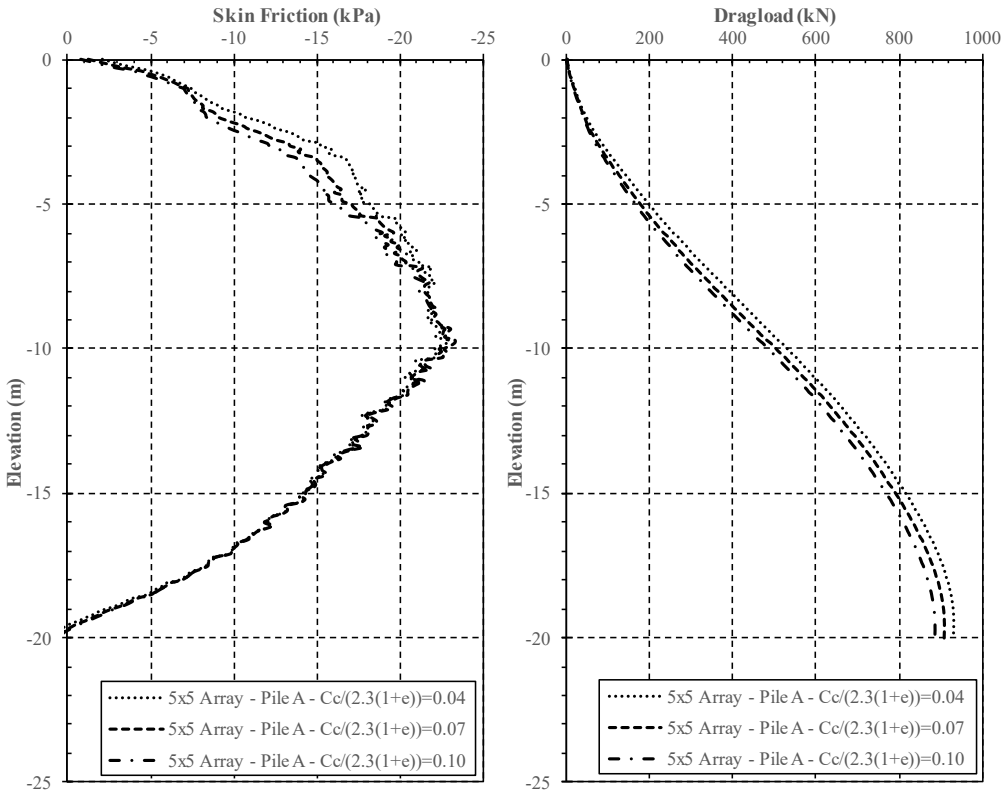

Figure A.55 NSF and dragload of three different soil compressibility factors of Pile A for model conditions of D=1.0m, s/D=3, L/D=20 and surcharge load of 50kPa.

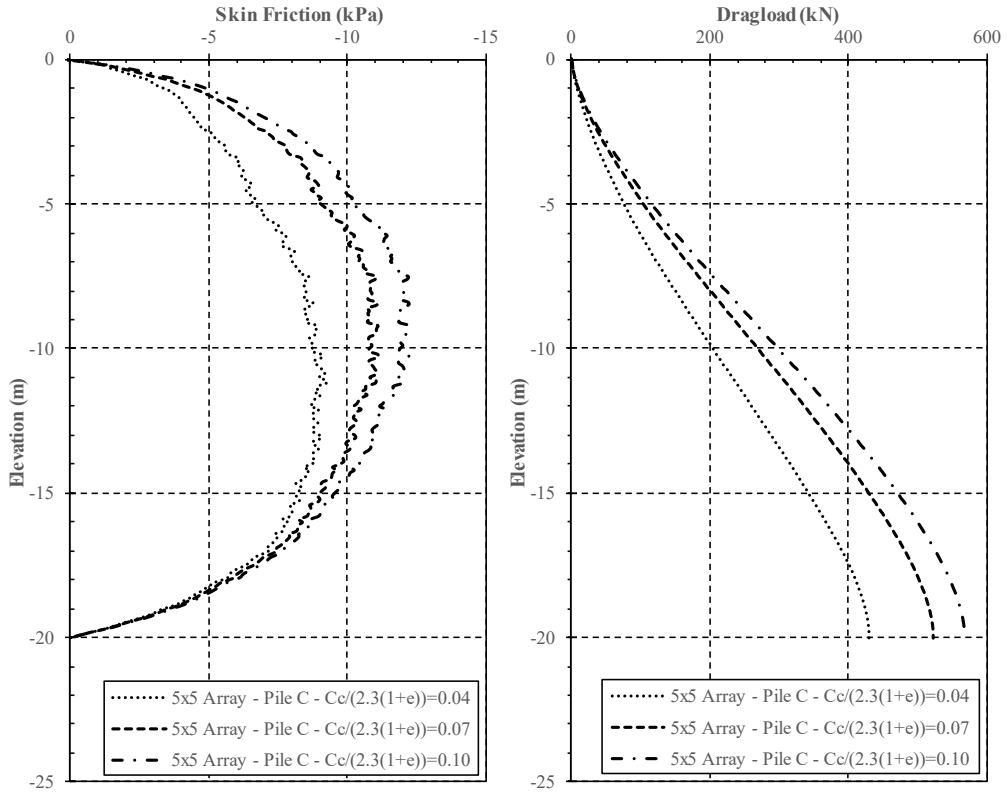

Figure A.56 NSF and dragload of three different soil compressibility factors of Pile C for model conditions of D=1.0m, s/D=3, L/D=20 and surcharge load of 50kPa.

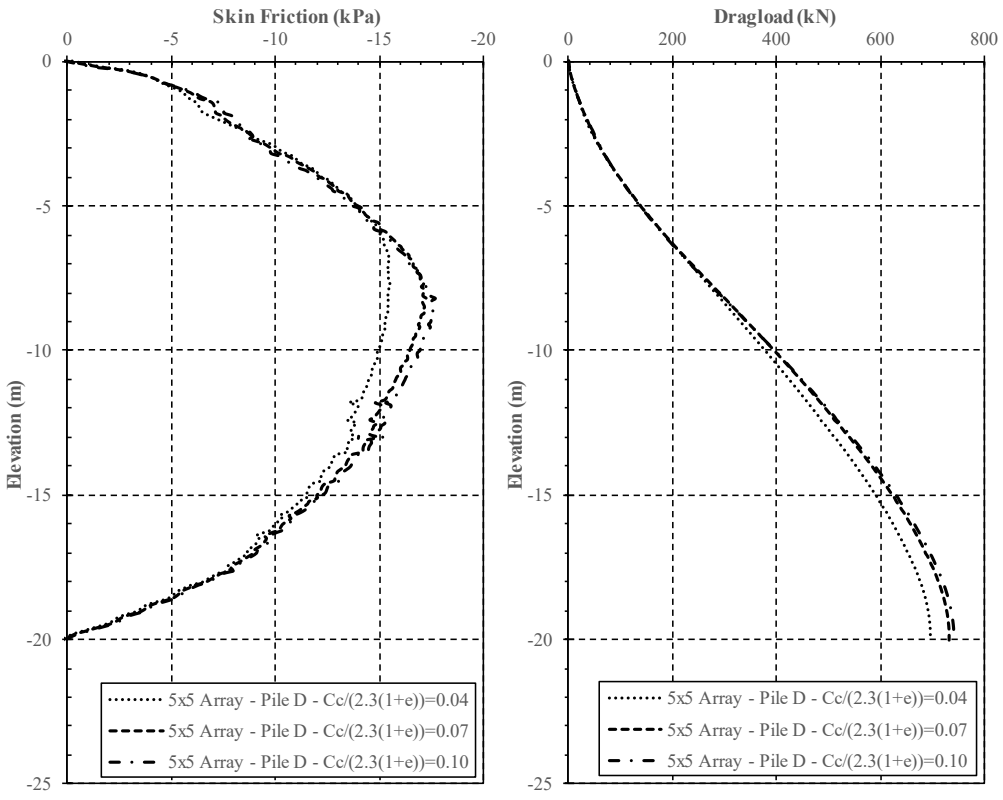

Figure A.57 NSF and dragload of three different soil compressibility factors of Pile D for model conditions of D=1.0m, s/D=3, L/D=20 and surcharge load of 50kPa.

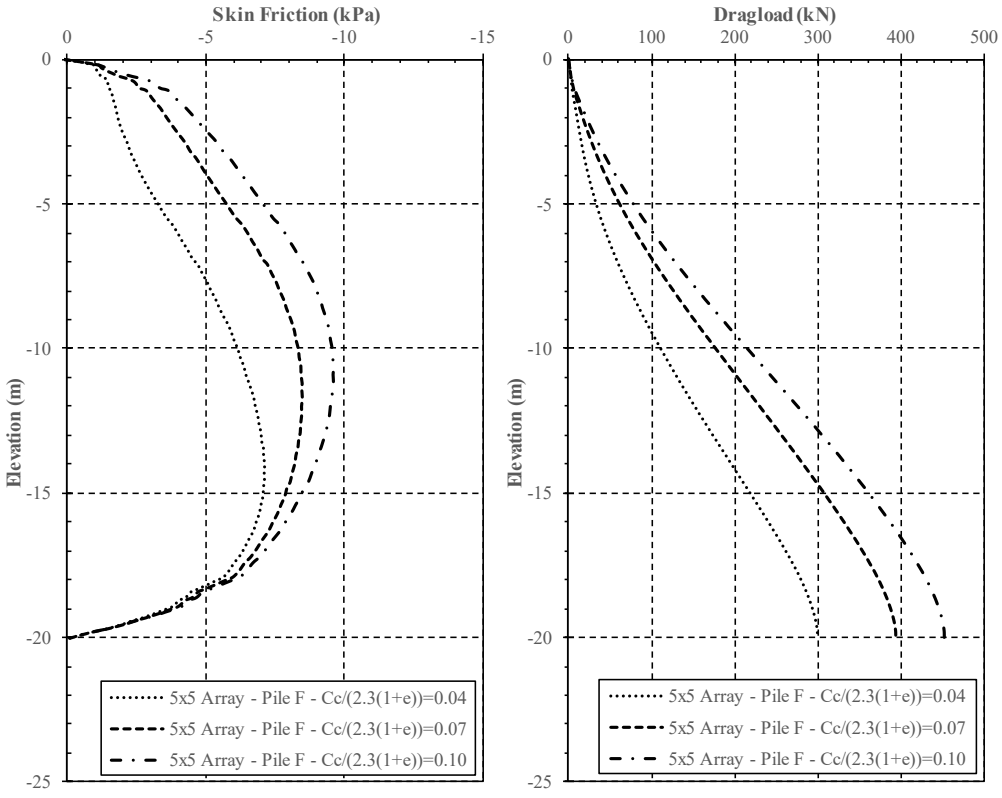

Figure A.58 NSF and dragload of three different soil compressibility factors of Pile F for model conditions of D=1.0m, s/D=3, L/D=20 and surcharge load of 50kPa.

I. The Effect of Soil Cohesion

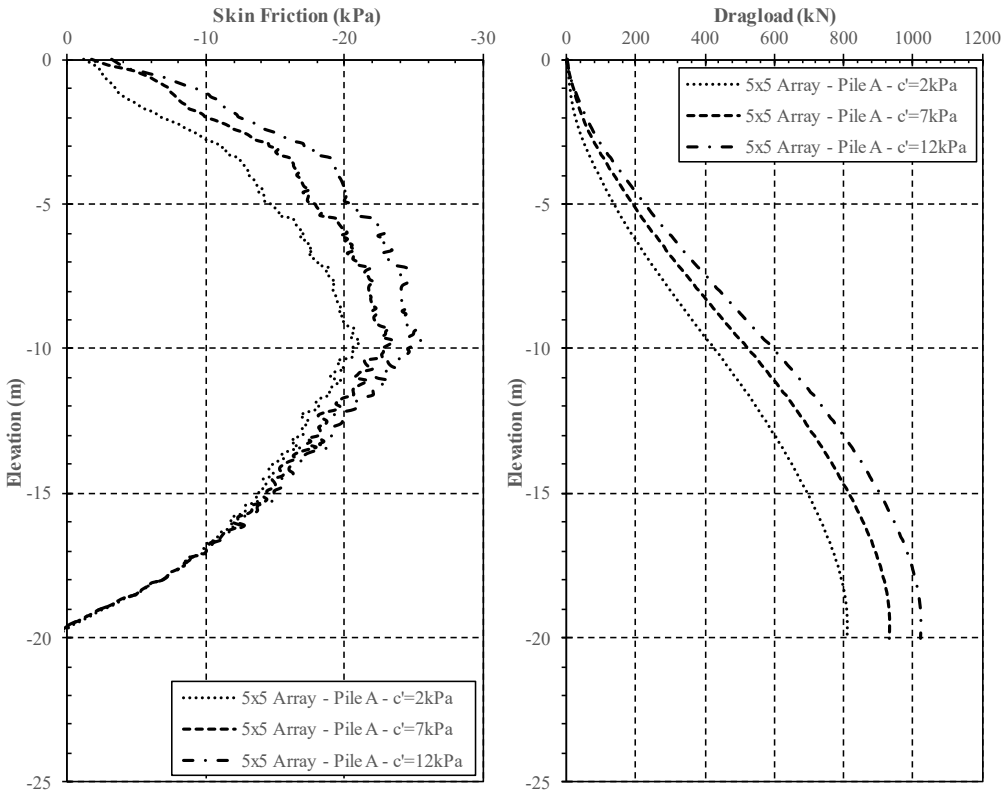

Figure A.59 NSF and dragload of three different soil cohesion of Pile A for model conditions of D=1.0m, s/D=3, L/D=20 and surcharge load of 50kPa.

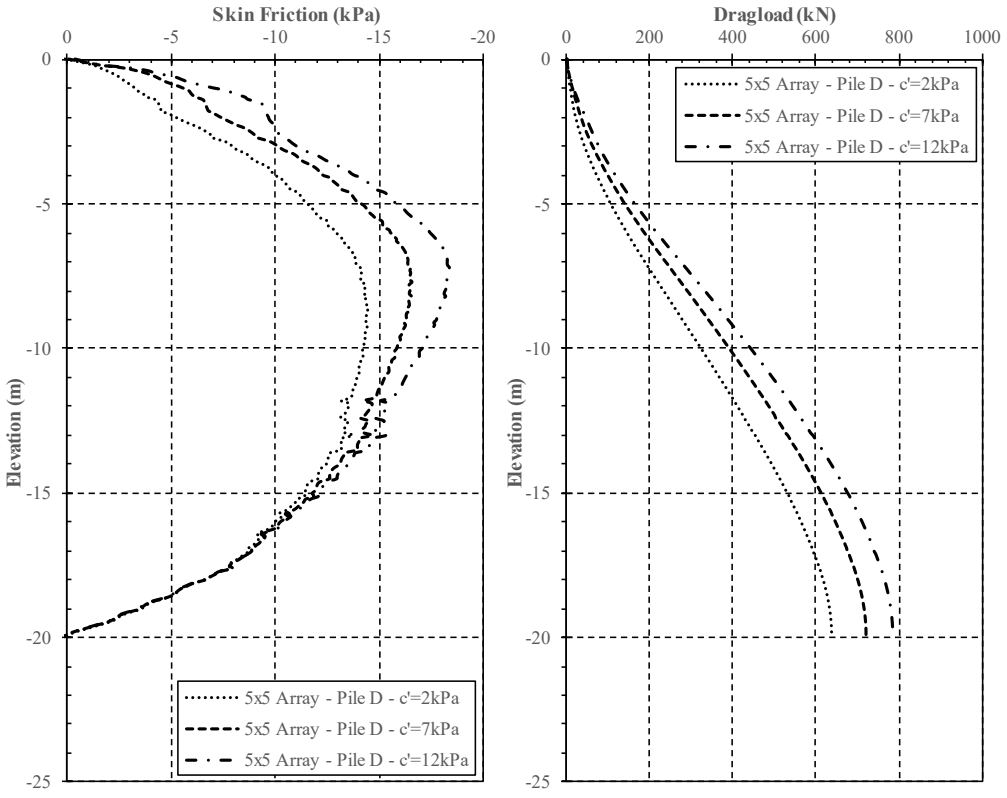

Figure A.60 NSF and dragload of three different soil cohesion of Pile D for model conditions of D=1.0m, s/D=3, L/D=20 and surcharge load of 50kPa.

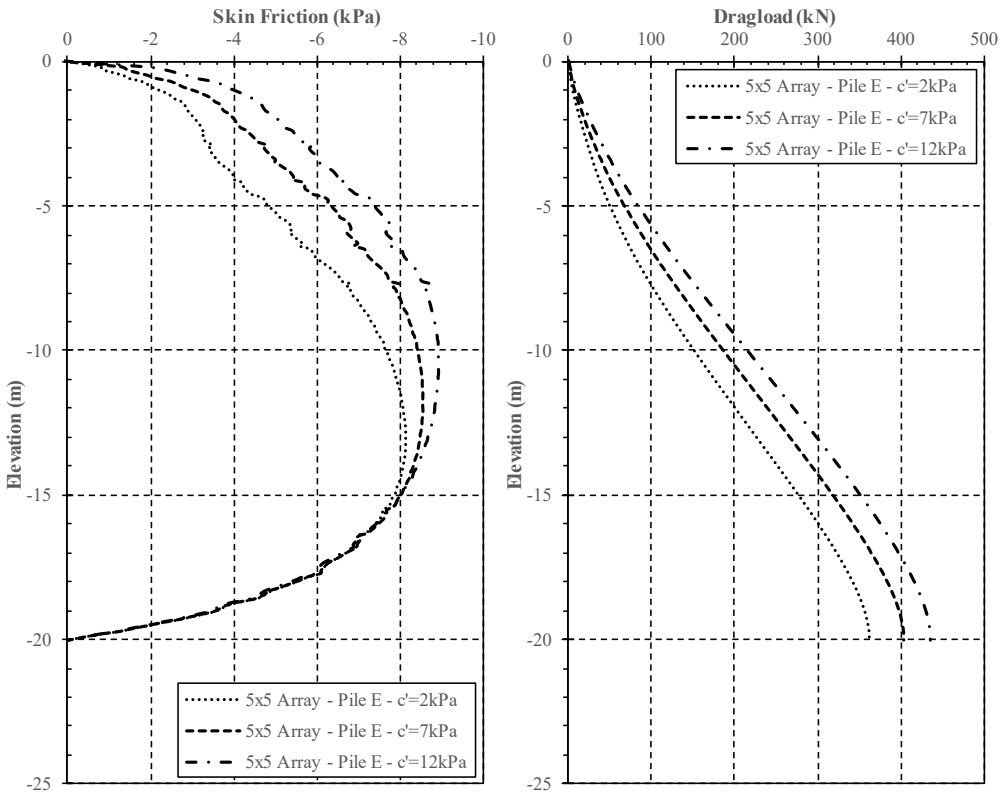

Figure A.61 NSF and dragload of three different soil cohesion of Pile E for model conditions of D=1.0m, s/D=3, L/D=20 and surcharge load of 50kPa.

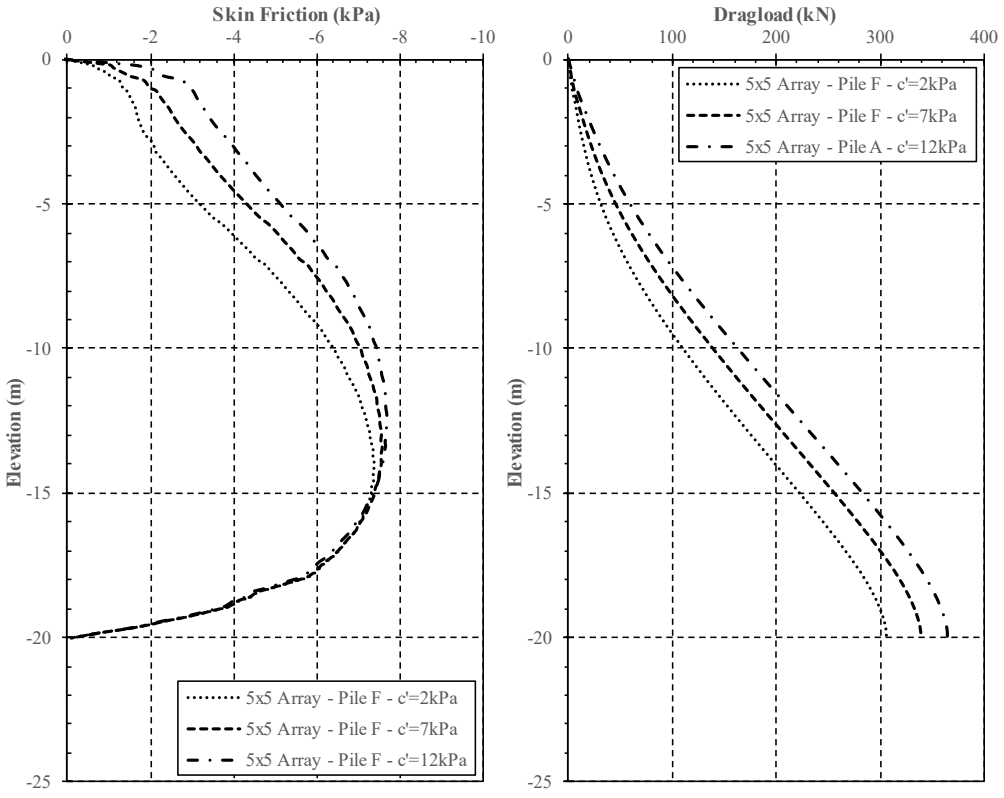

Figure A.62 NSF and dragload of three different soil cohesion of Pile F for model conditions of D=1.0m, s/D=3, L/D=20 and surcharge load of 50kPa.

J. The Effect of Soil Friction Angle

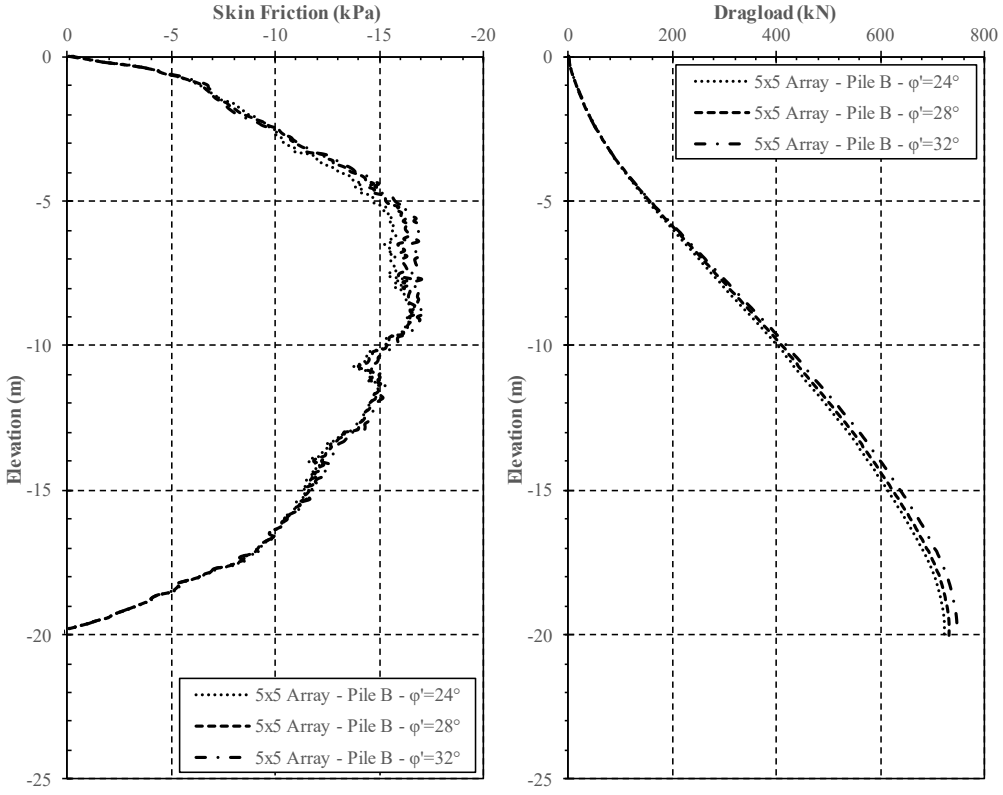

Figure A.63 NSF and dragload of three different soil friction angles of Pile B for model conditions of D=1.0m, s/D=3, L/D=20 and surcharge load of 50kPa.

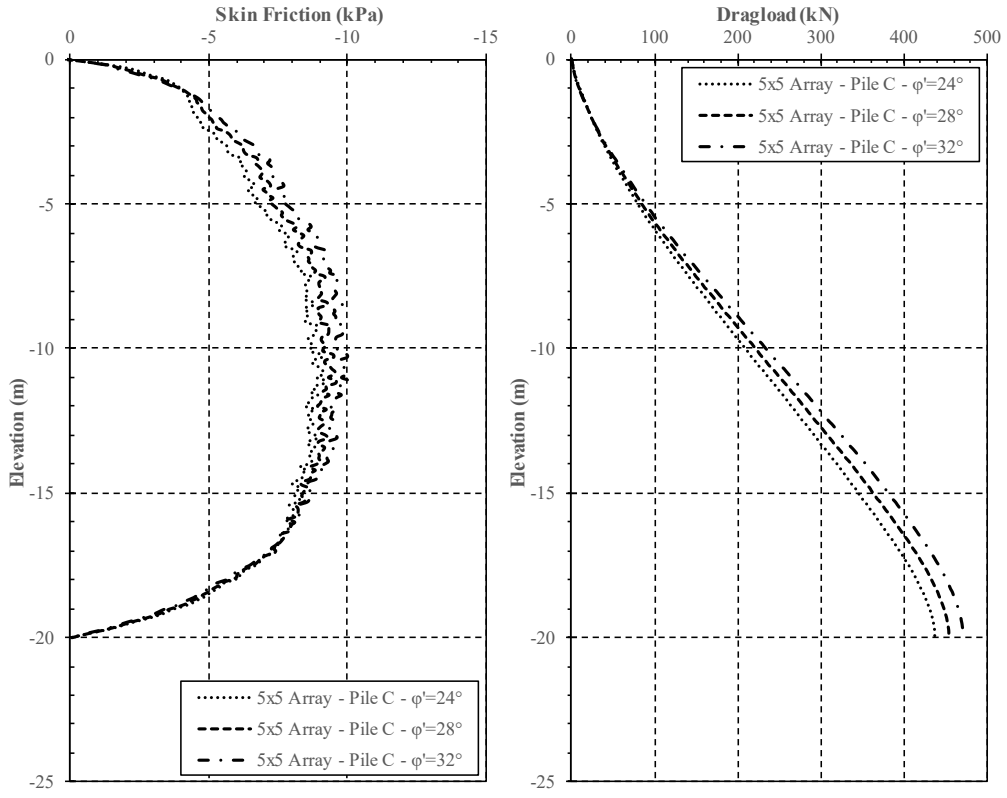

Figure A.64 NSF and dragload of three different soil friction angles of Pile C for model conditions of D=1.0m, s/D=3, L/D=20 and surcharge load of 50kPa.

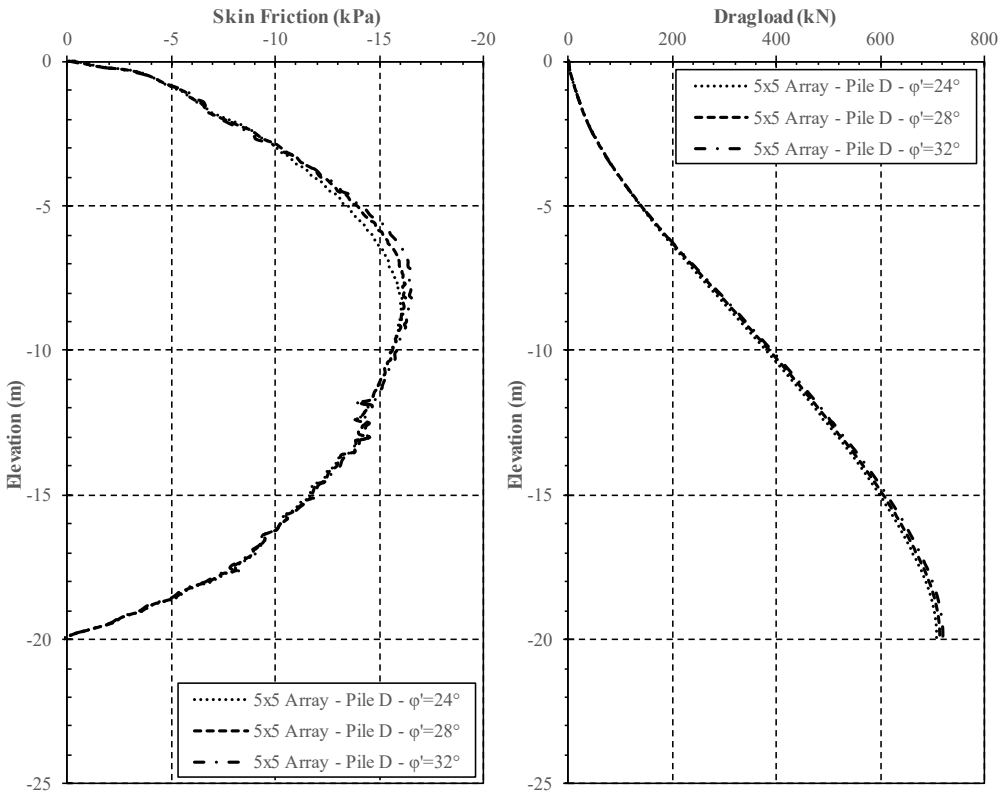

Figure A.65 NSF and dragload of three different soil friction angles of Pile D for model conditions of D=1.0m, s/D=3, L/D=20 and surcharge load of 50kPa.

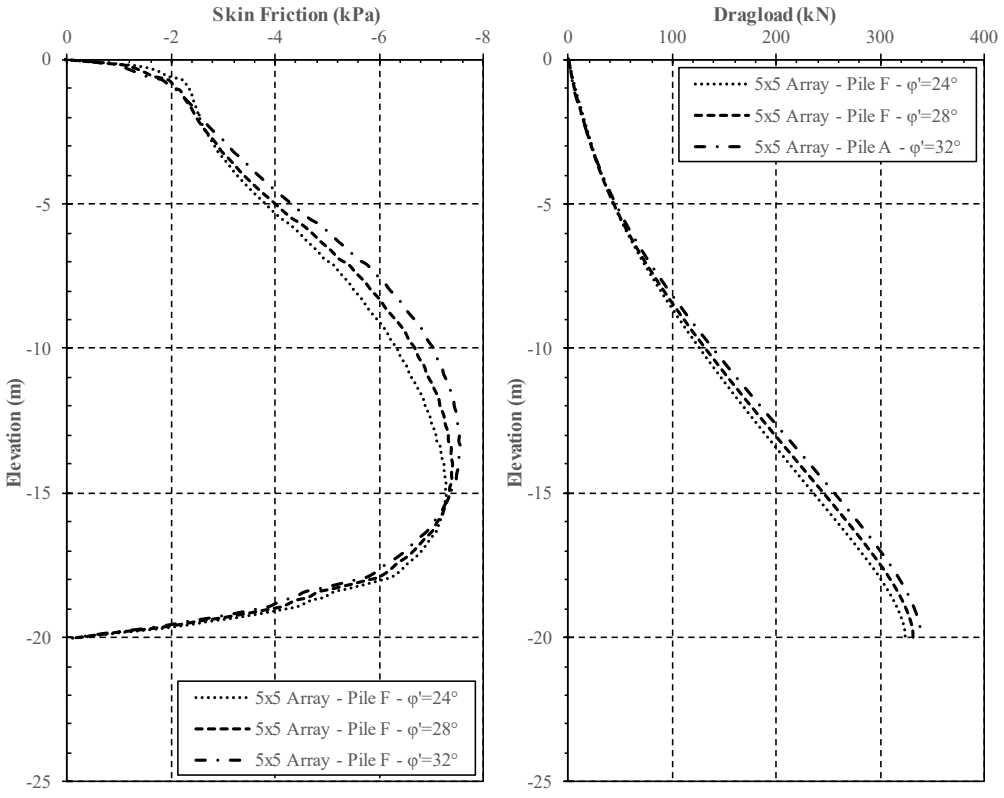

Figure A.66 NSF and dragload of three different soil friction angles of Pile F for model conditions of D=1.0m, s/D=3, L/D=20 and surcharge load of 50kPa.

K. The Effect of Interface Coefficient

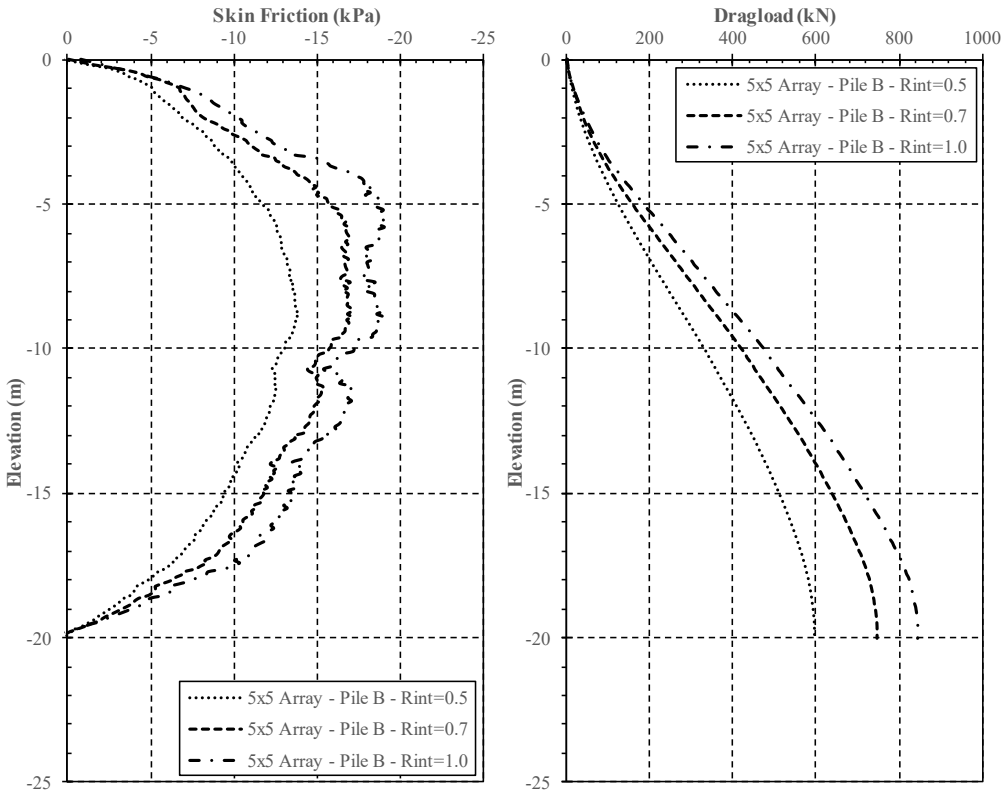

Figure A.67 NSF and dragload of three different pile-soil interface coefficients of Pile B for model conditions of D=1.0m, s/D=3, L/D=20 and surcharge load of 50kPa.

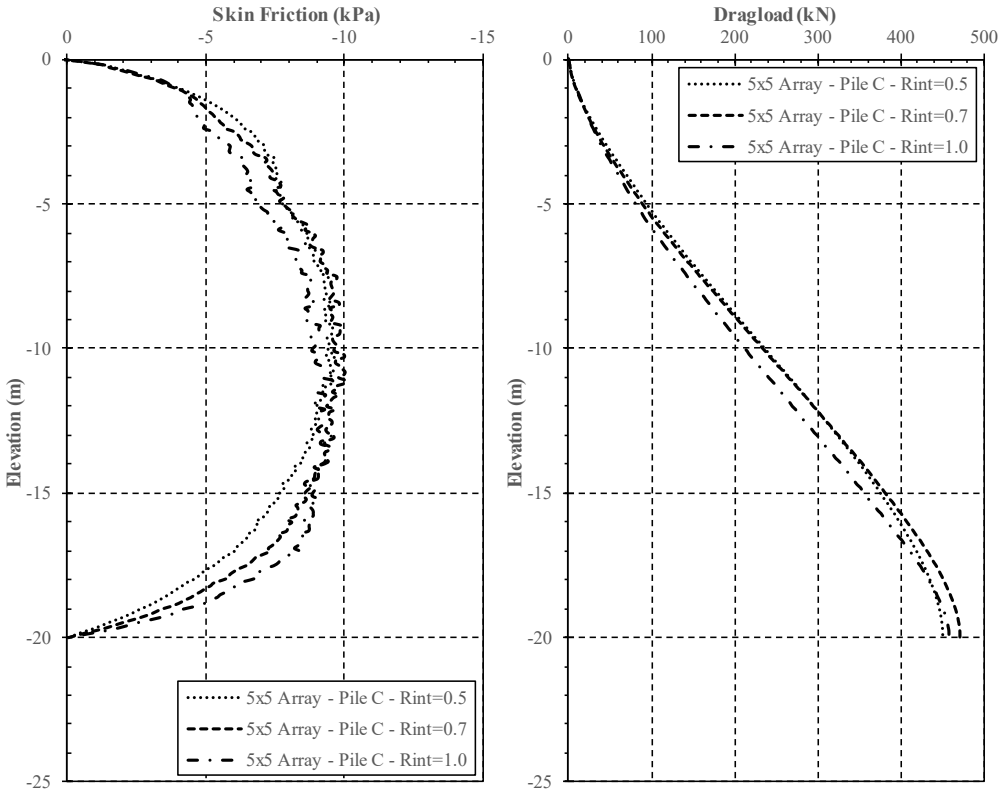

Figure A.68 NSF and dragload of three different pile-soil interface coefficients of Pile C for model conditions of D=1.0m, s/D=3, L/D=20 and surcharge load of 50kPa.

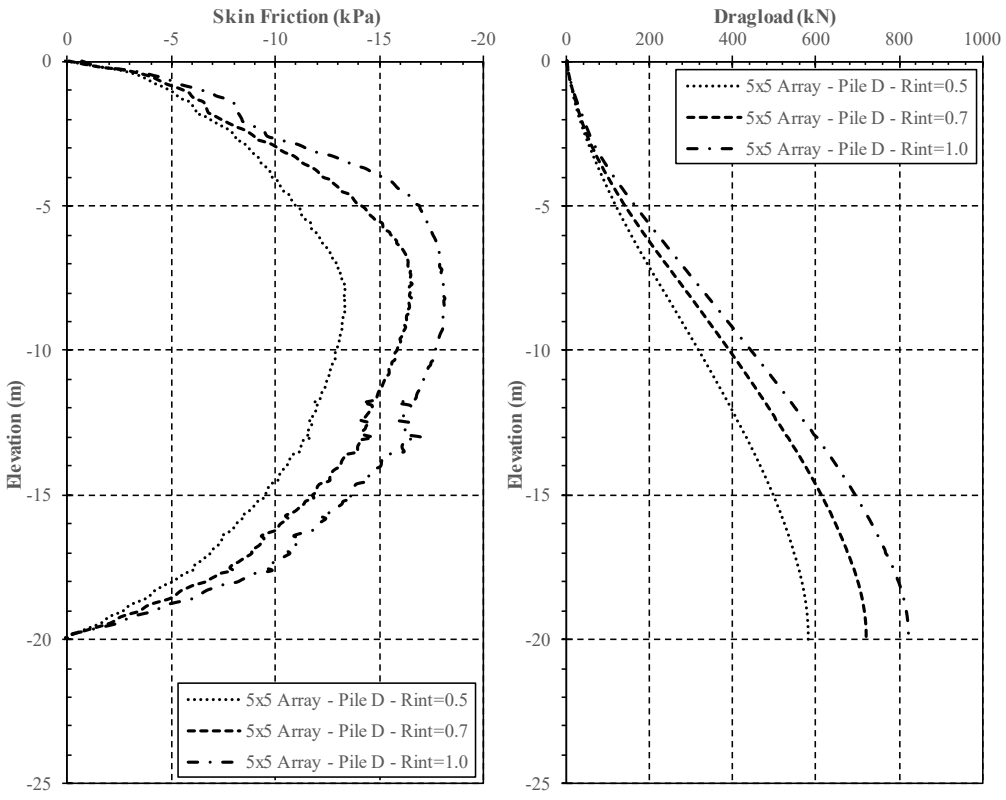

Figure A.69 NSF and dragload of three different pile-soil interface coefficients of Pile D for model conditions of D=1.0m, s/D=3, L/D=20 and surcharge load of 50kPa.

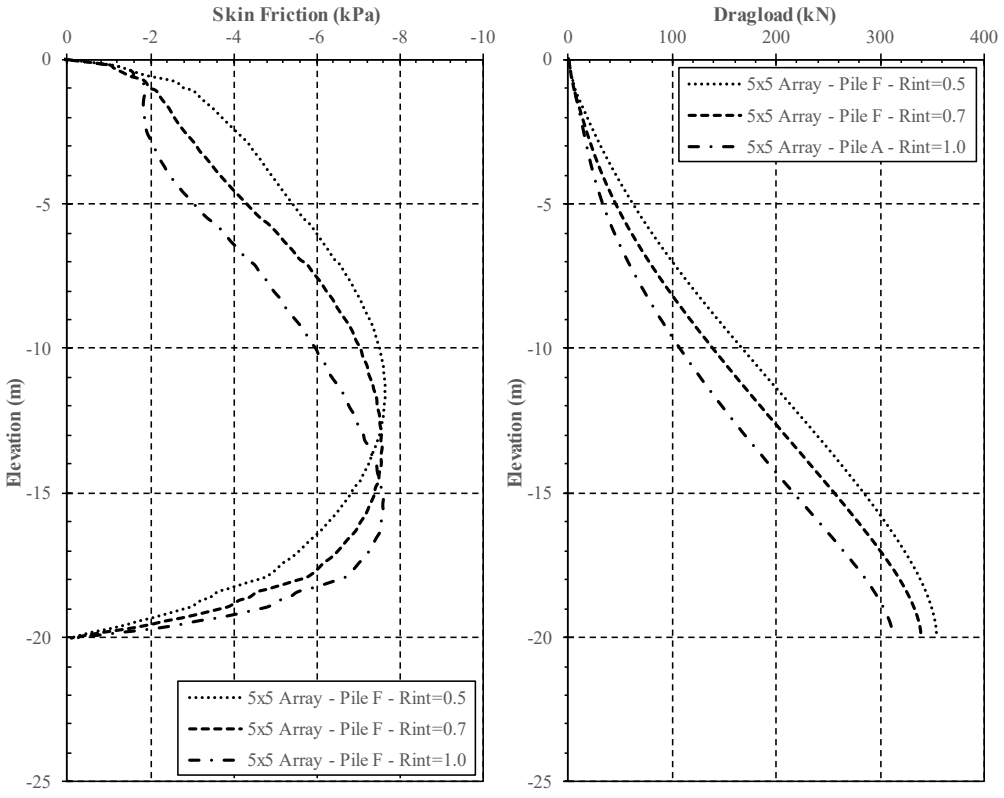

Figure A.70 NSF and dragload of three different pile-soil interface coefficients of Pile F for model conditions of D=1.0m, s/D=3, L/D=20 and surcharge load of 50kPa.

L. Comparison of the Results with Analytical Estimations

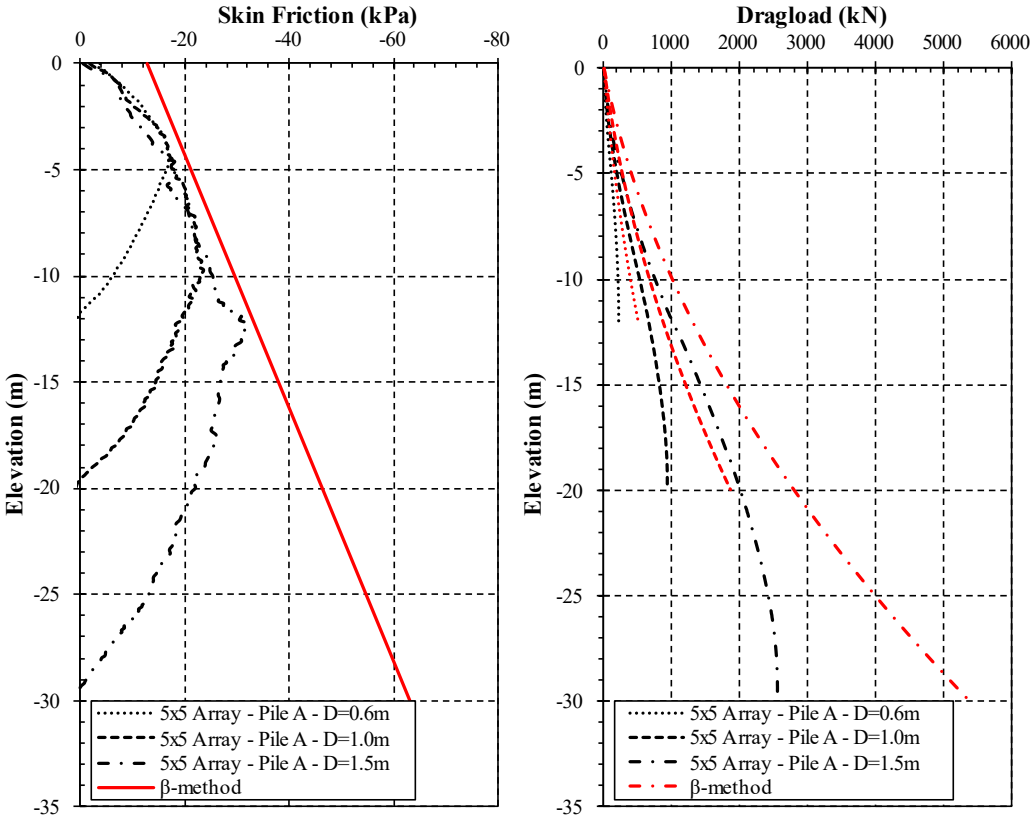

Figure A.71 Comparison of the NSF between FEA and the β-method for 5x5 pile array, s/D=3, L/D=20 and surcharge load of 50kPa – Pile A.

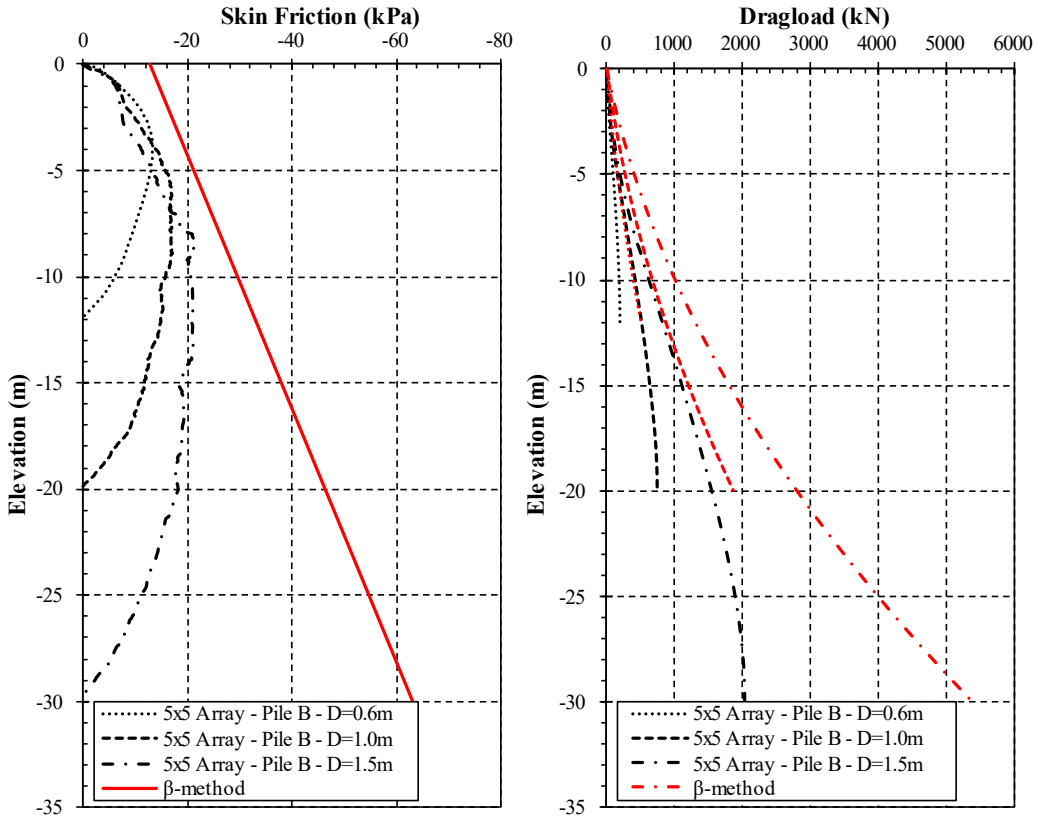

Figure A.72 Comparison of the NSF between FEA and the β-method for 5x5 pile array, s/D=3, L/D=20 and surcharge load of 50kPa – Pile B.

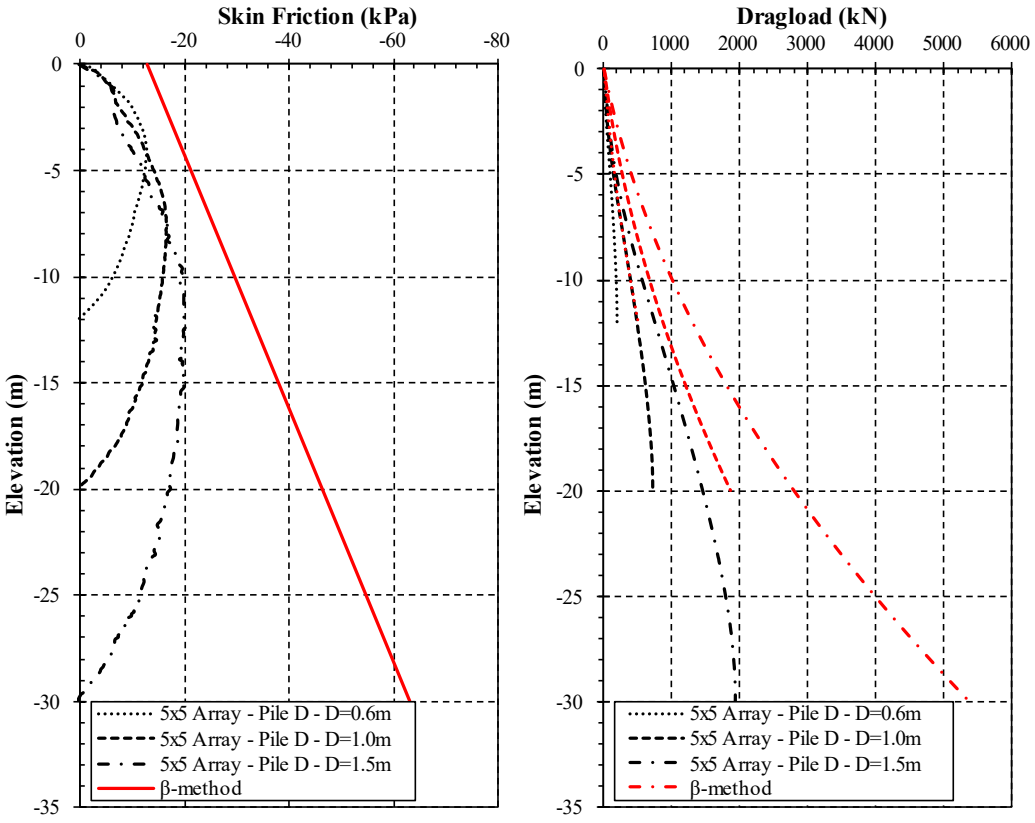

Figure A.73 Comparison of the NSF between FEA and the β-method for 5x5 pile array, s/D=3, L/D=20 and surcharge load of 50kPa – Pile D.

Table A.1 Comparison of dragload forces for each pile position for three different pile diameters between the β-method and FEA results, 5x5 array, s/D=3 and surcharge load of 50kPa.

Pile-#	Dragload (kN)						Percentile Difference (%)		
	FEA Results			Suggested Method					
	D=0.6m	D=1.0m	D=1.5m	D=0.6m	D=1.0m	D=1.5m	D=0.6m	D=1.0m	D=1.5m
Pile-A	236	931	2542	521	1867	5385	121	101	112
Pile-B	202	746	2031	521	1867	5385	158	150	165
Pile-D	196	721	1930	521	1867	5385	166	159	179

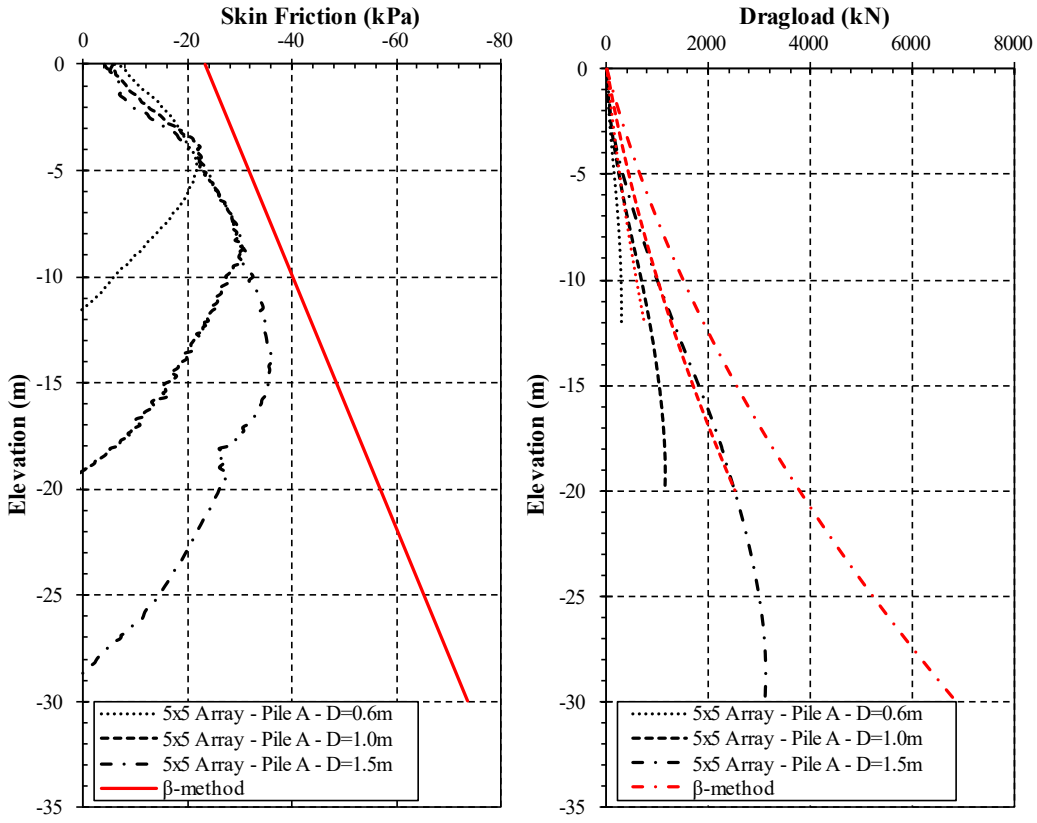

Figure A.74 Comparison of the NSF between FEA and the β-method for 5x5 pile array, s/D=3, L/D=20 and surcharge load of 100kPa – Pile A.

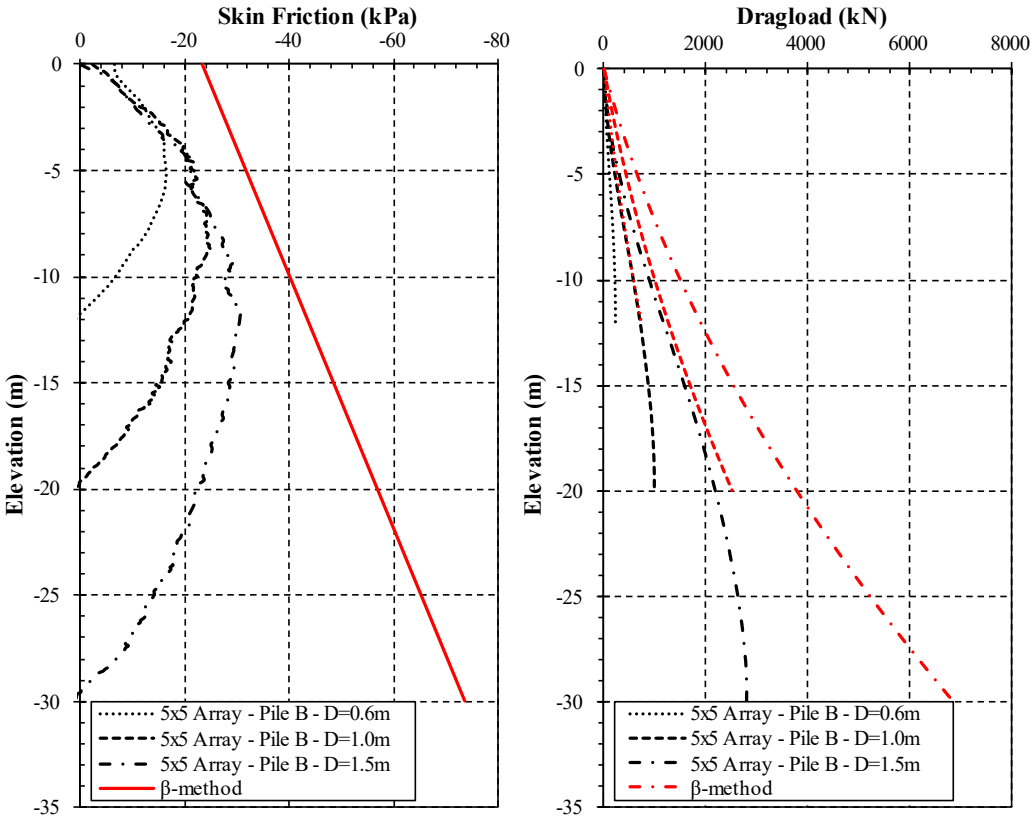

Figure A.75 Comparison of the NSF between FEA and the β-method for 5x5 pile array, s/D=3, L/D=20 and surcharge load of 100kPa – Pile B.

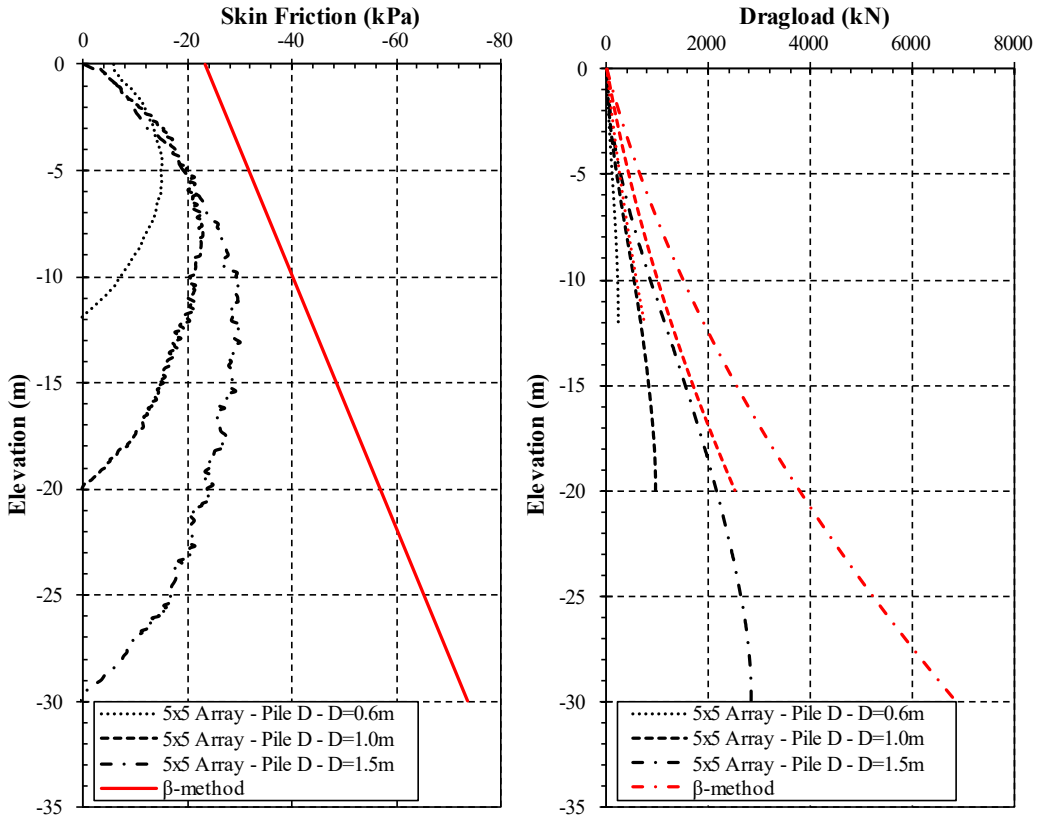

Figure A.76 Comparison of the NSF between FEA and the β-method for 5x5 pile array, s/D=3, L/D=20 and surcharge load of 100kPa – Pile D.

Table A.2 Comparison of dragload forces for each pile position for three different pile diameters between the β-method and FEA results, 5x5 array, s/D=3 and surcharge load of 100kPa.

Pile-#	Dragload (kN)						Percentile Difference (%)		
	FEA Results			Suggested Method					
	D=0.6m	D=1.0m	D=1.5m	D=0.6m	D=1.0m	D=1.5m	D=0.6m	D=1.0m	D=1.5m
Pile-A	300	1141	3113	758	2525	6864	153	121	120
Pile-B	251	1001	2804	758	2525	6864	202	152	145
Pile-D	239	962	2823	758	2525	6864	217	162	143

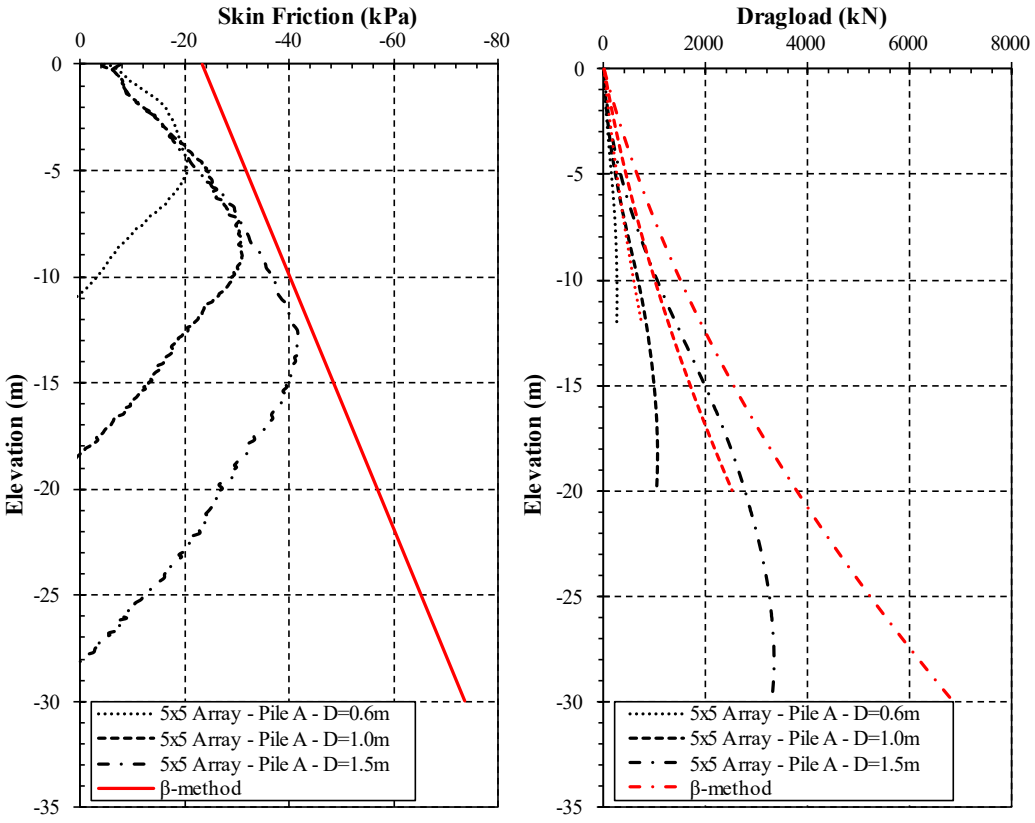

Figure A.77 Comparison of the NSF between FEA and the β-method for 5x5 pile array, s/D=6, L/D=20 and surcharge load of 100kPa – Pile A.

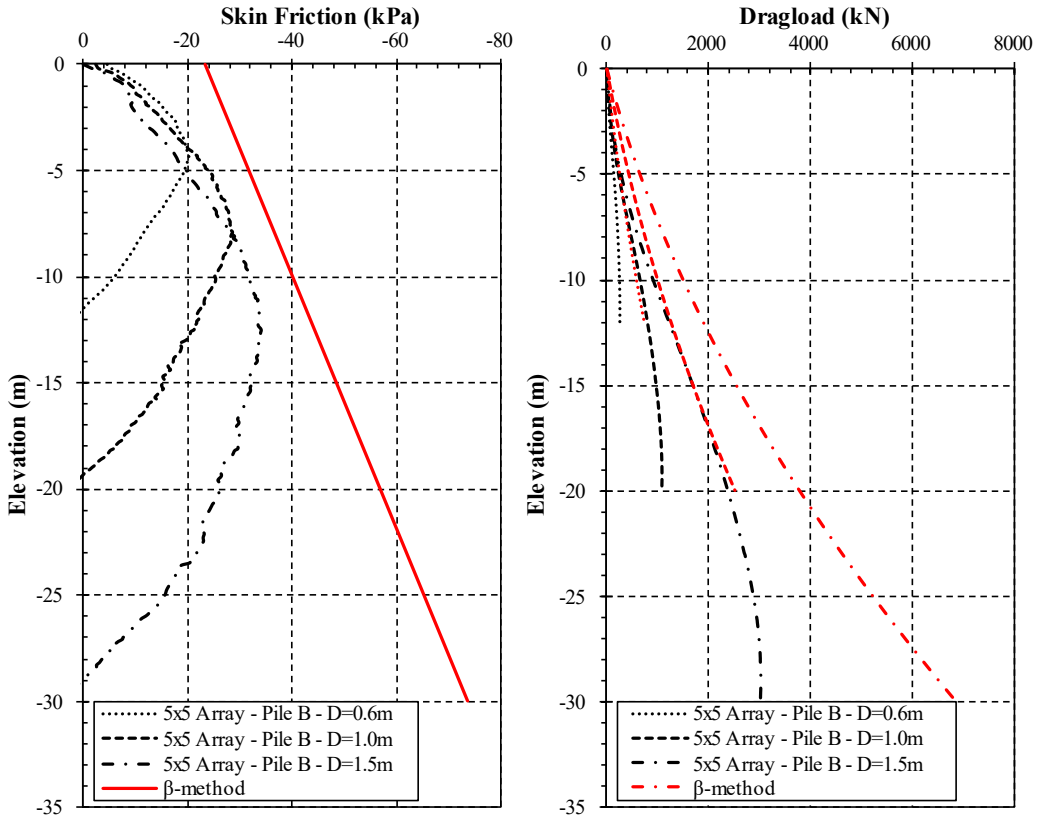

Figure A.78 Comparison of the NSF between FEA and the β-method for 5x5 pile array, s/D=6, L/D=20 and surcharge load of 100kPa – Pile B.

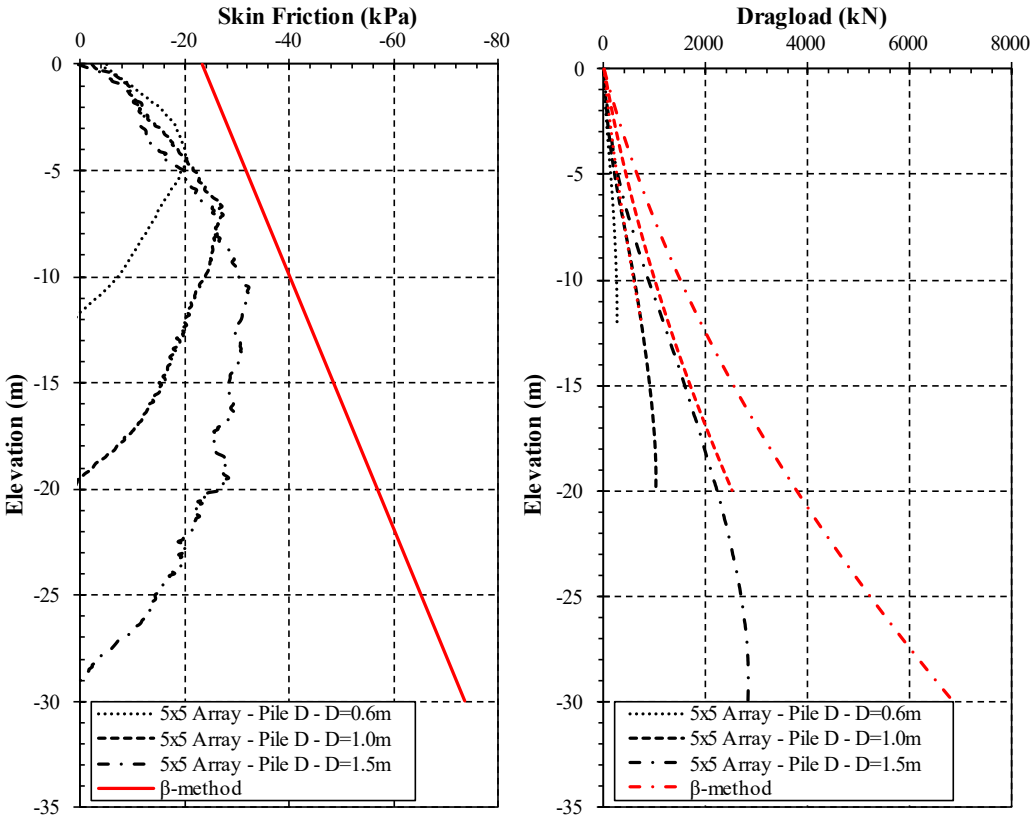

Figure A.79 Comparison of the NSF between FEA and the β-method for 5x5 pile array, s/D=6, L/D=20 and surcharge load of 100kPa – Pile D.

Table A.3 Comparison of dragload forces for each pile position for three different pile diameters between the β-method and FEA results, 5x5 array, s/D=6 and surcharge load of 100kPa.

Pile-#	Dragload (kN)						Percentile Difference (%)		
	FEA Results			Suggested Method					
	D=0.6m	D=1.0m	D=1.5m	D=0.6m	D=1.0m	D=1.5m	D=0.6m	D=1.0m	D=1.5m
Pile-A	259	1055	3317	758	2525	6864	193	139	107
Pile-B	273	1093	3024	758	2525	6864	178	131	127
Pile-D	281	1035	2827	758	2525	6864	170	144	143

M. Comparison of 3D Results with 2D Axisymmetric Simulation of Tributary Area Method

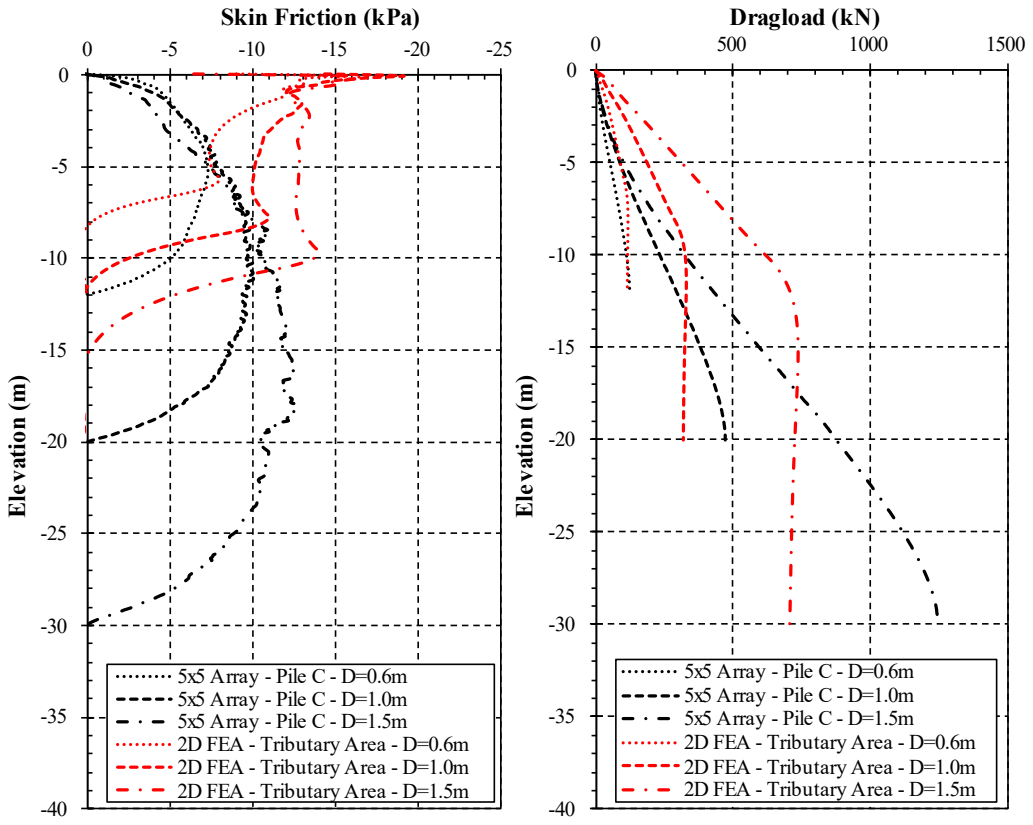

Figure A.80 Comparison of the NSF between 3D FEA and 2D axisymmetric tributary area, 5x5 pile array, s/D=3, L/D=20 and surcharge load of 50kPa – Pile C.

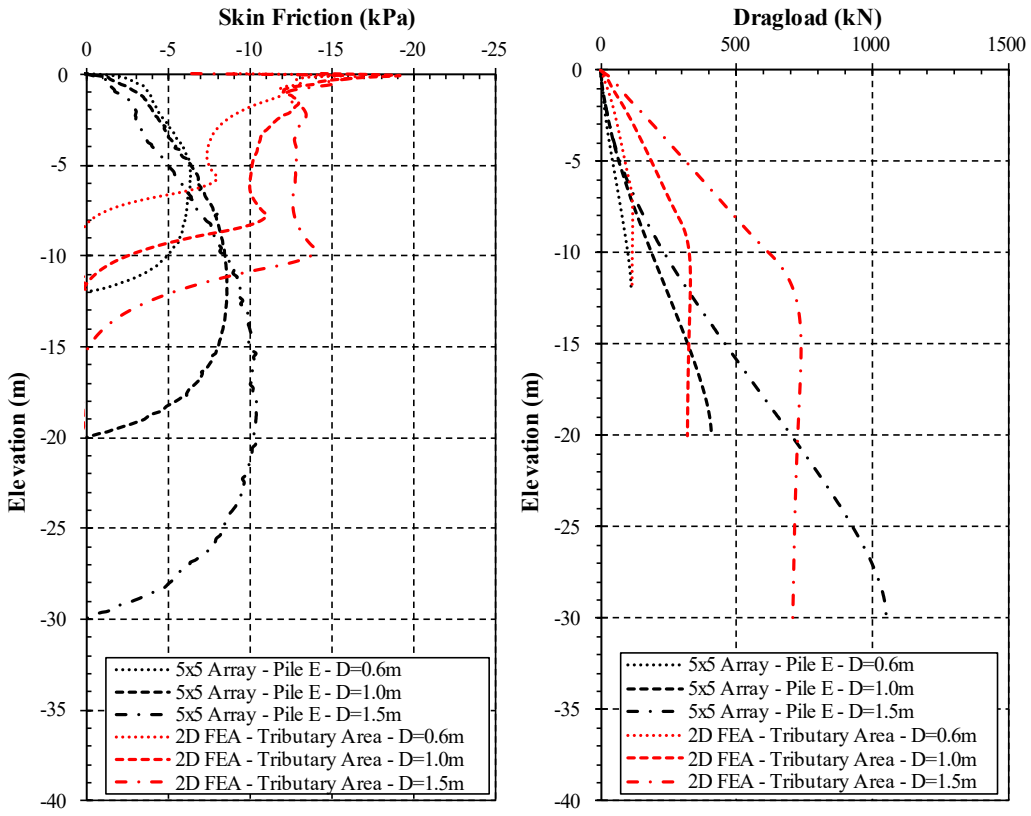

Figure A.81 Comparison of the NSF between 3D FEA and 2D axisymmetric tributary area, 5x5 pile array, s/D=3, L/D=20 and surcharge load of 50kPa – Pile E.

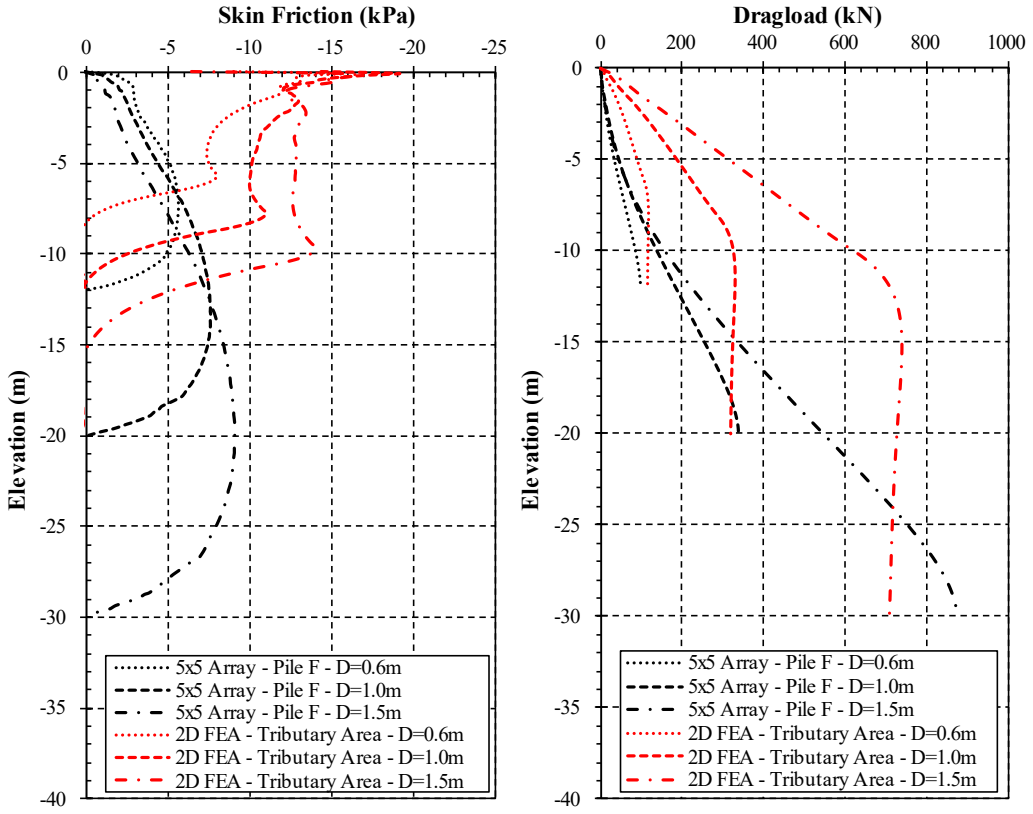

Figure A.82 Comparison of the NSF between 3D FEA and 2D axisymmetric tributary area, 5x5 pile array, s/D=3, L/D=20 and surcharge load of 50kPa – Pile F.

Table A.4 Comparison of dragload forces for each pile position for three different pile diameters between the tributary area method and FEA results, 5x5 array, s/D=3 and surcharge load of 50kPa.

Pile-#	Dragload (kN)						Percentile Difference (%)		
	3D FEA			2D Axisymmetric					
	D=0.6m	D=1.0m	D=1.5m	D=0.6m	D=1.0m	D=1.5m	D=0.6m	D=1.0m	D=1.5m
Pile-C	126	471	1247	115	318	709	-9	-32	-43
Pile-E	113	404	1049	115	318	709	2	-21	-32
Pile-F	98	339	872	115	318	709	17	-6	-19

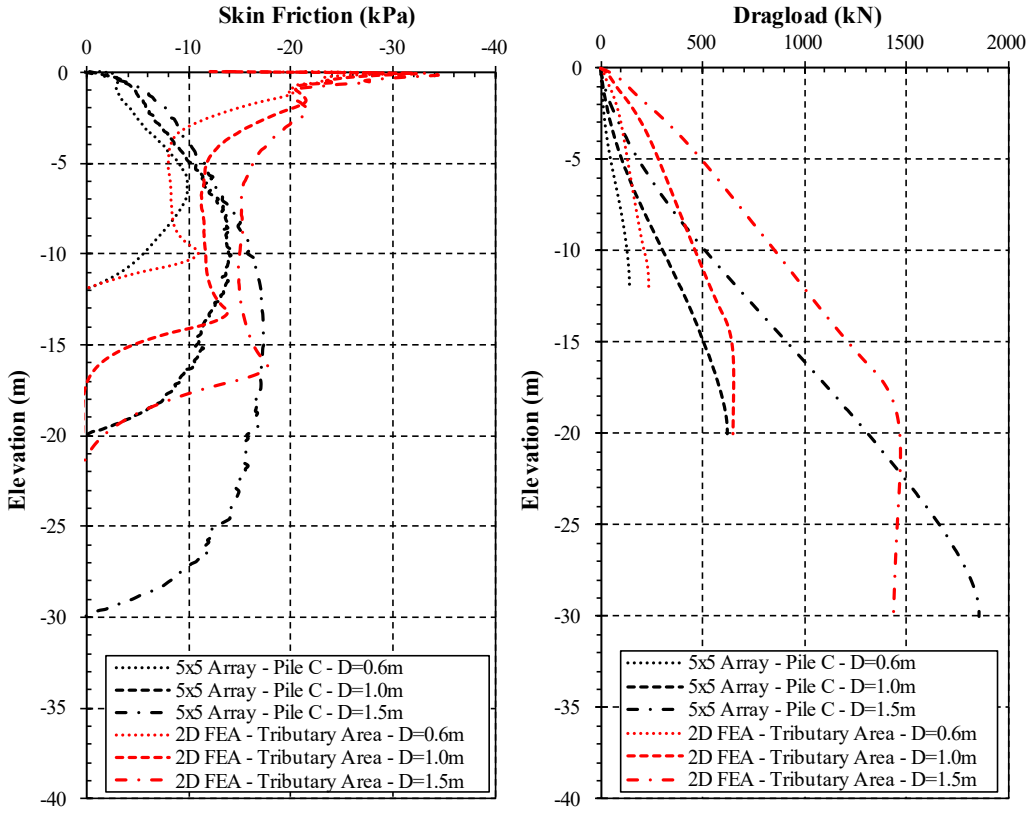

Figure A.83 Comparison of the NSF between 3D FEA and 2D axisymmetric tributary area, 5x5 pile array, s/D=3, L/D=20 and surcharge load of 100kPa – Pile C.

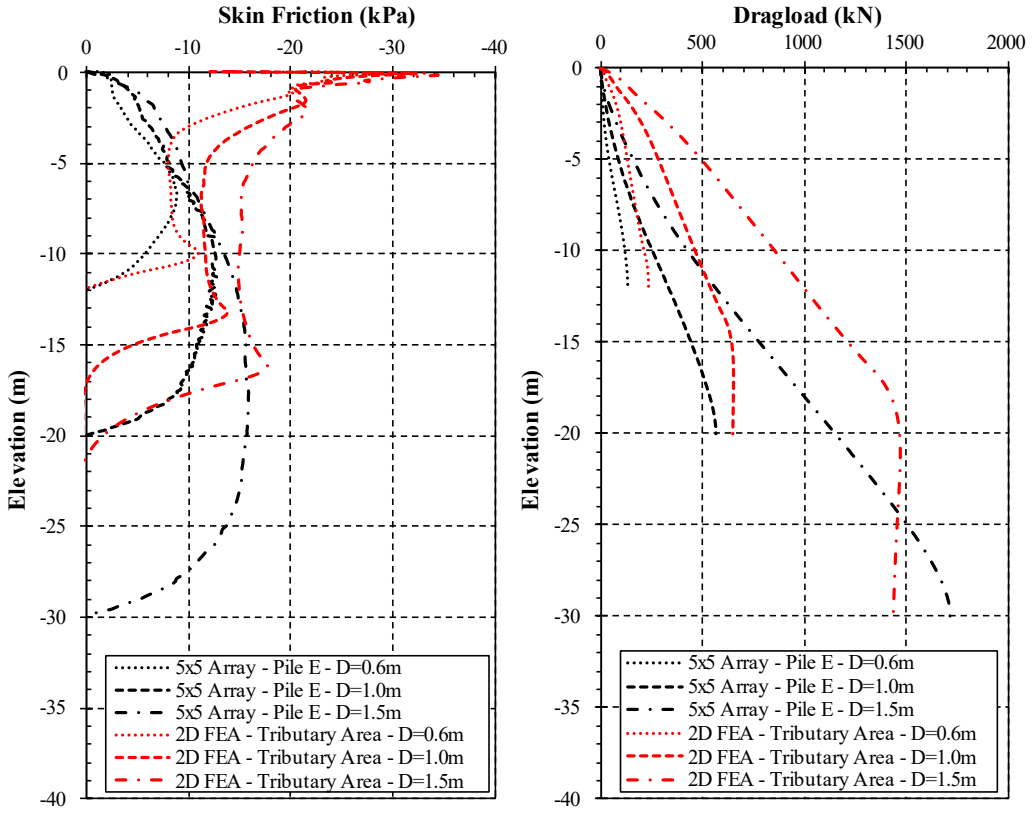

Figure A.84 Comparison of the NSF between 3D FEA and 2D axisymmetric tributary area, 5x5 pile array, s/D=3, L/D=20 and surcharge load of 100kPa – Pile E.

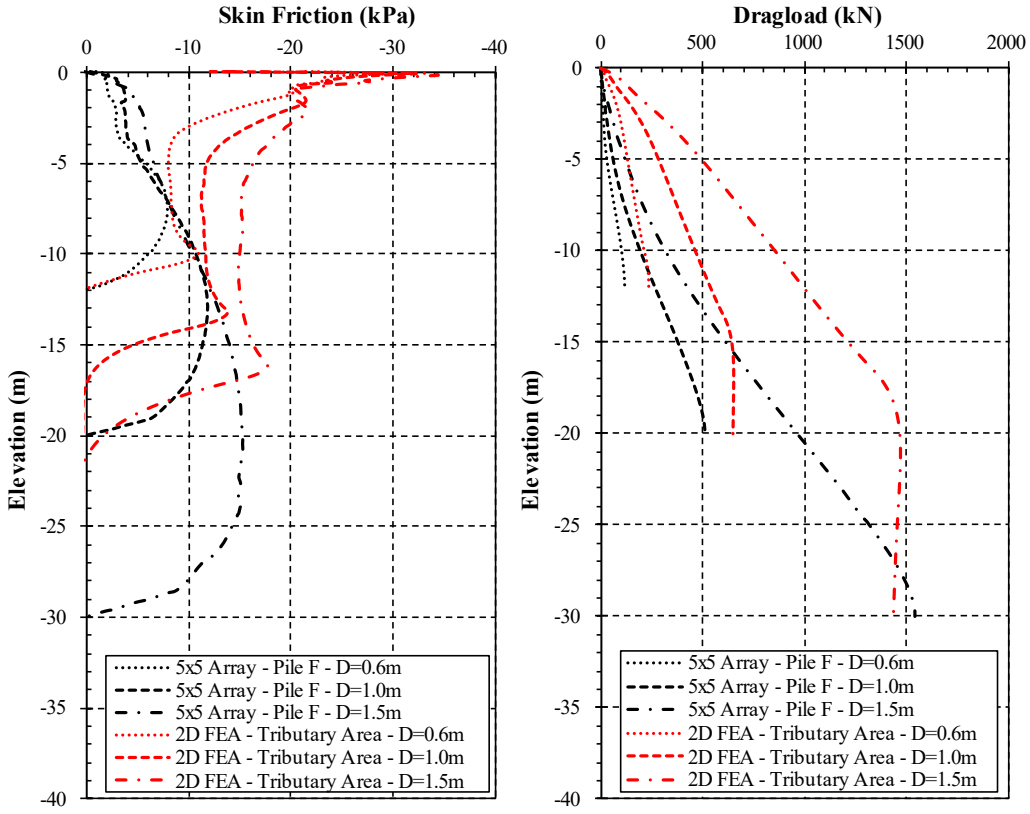

Figure A.85 Comparison of the NSF between 3D FEA and 2D axisymmetric tributary area, 5x5 pile array, s/D=3, L/D=20 and surcharge load of 100kPa – Pile F.

Table A.5 Comparison of dragload forces for each pile position for three different pile diameters between the tributary area method and FEA results, 5x5 array, s/D=3 and surcharge load of 100kPa.

Pile-#	Dragload (kN)						Percentile Difference (%)		
	3D FEA			2D Axisymmetric					
	D=0.6m	D=1.0m	D=1.5m	D=0.6m	D=1.0m	D=1.5m	D=0.6m	D=1.0m	D=1.5m
Pile-C	142	620	1855	235	647	1434	65	4	-23
Pile-E	129	566	1714	235	647	1434	82	14	-16
Pile-F	114	509	1540	235	647	1434	106	27	-7

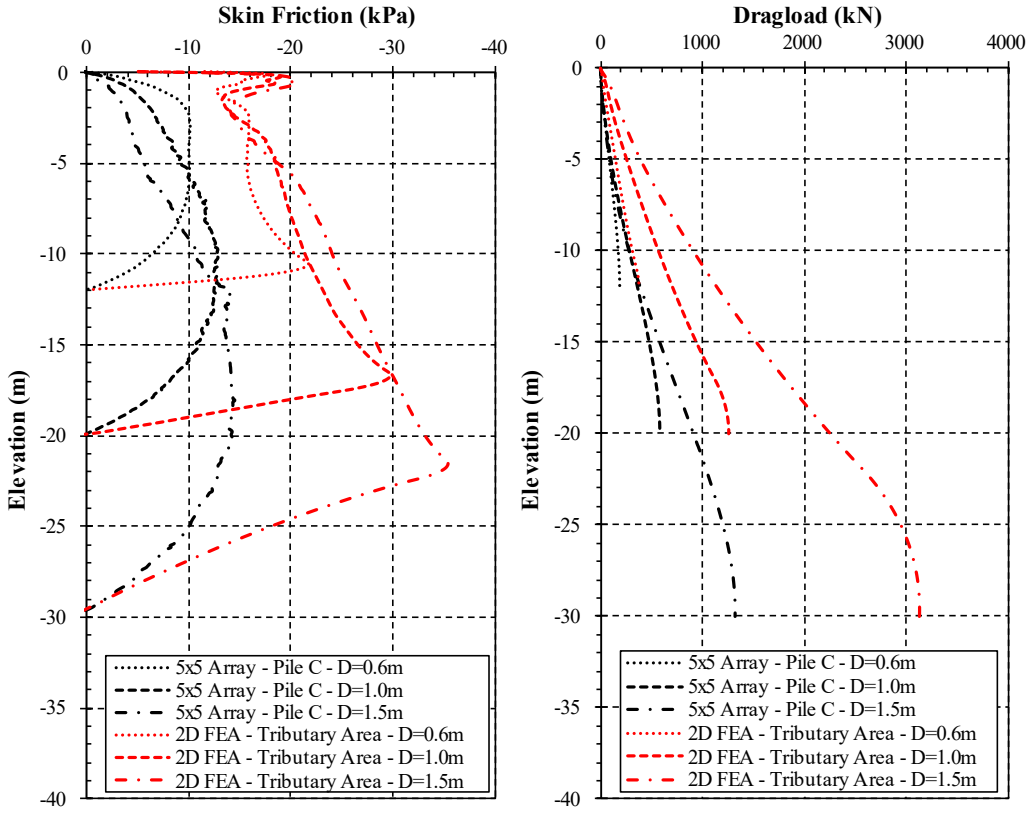

Figure A.86 Comparison of the NSF between 3D FEA and 2D axisymmetric tributary area, 5x5 pile array, s/D=6, L/D=20 and surcharge load of 50kPa – Pile C.

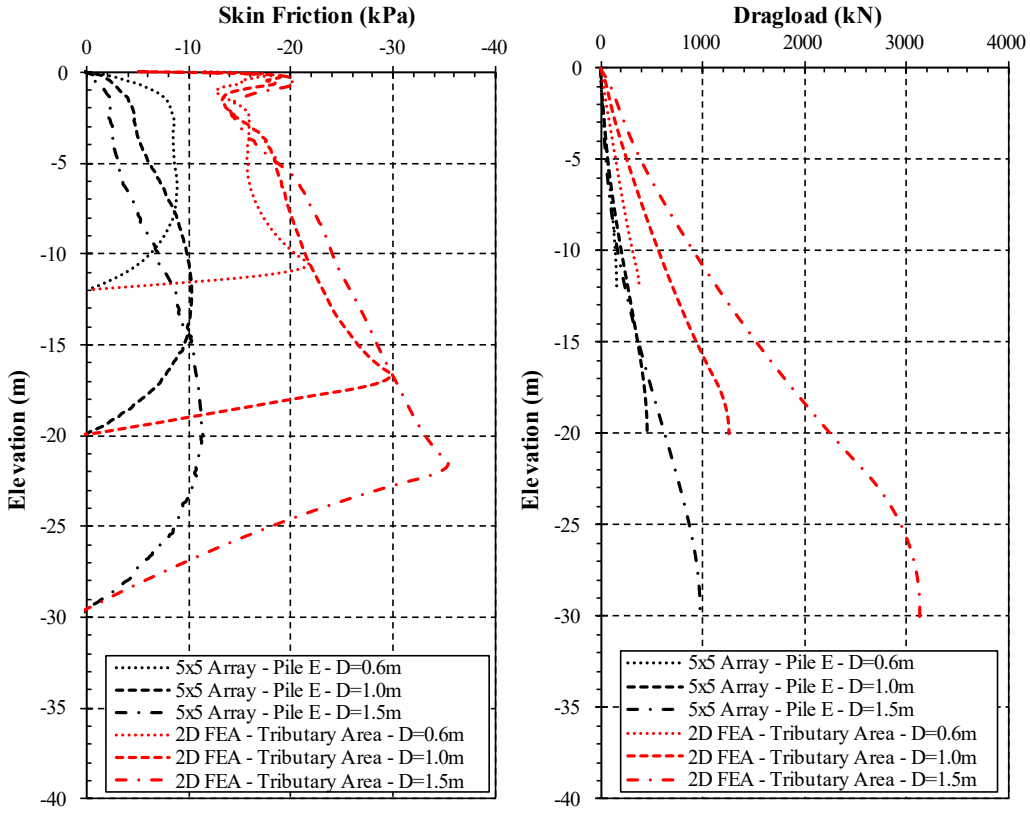

Figure A.87 Comparison of the NSF between 3D FEA and 2D axisymmetric tributary area, 5x5 pile array, s/D=6, L/D=20 and surcharge load of 50kPa – Pile E.

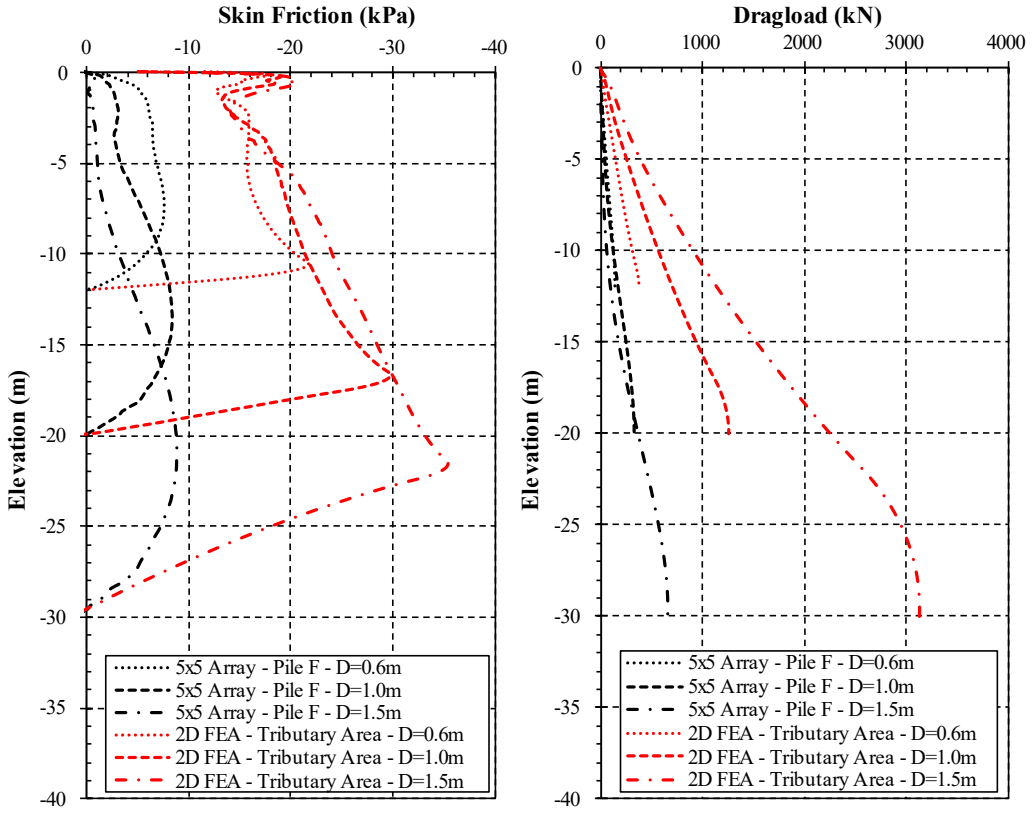

Figure A.88 Comparison of the NSF between 3D FEA and 2D axisymmetric tributary area, 5x5 pile array, s/D=6, L/D=20 and surcharge load of 50kPa – Pile F.

Table A.6 Comparison of dragload forces for each pile position for three different pile diameters between the tributary area method and FEA results, 5x5 array, s/D=6 and surcharge load of 50kPa.

Pile-#	Dragload (kN)						Percentile Difference (%)		
	3D FEA			2D Axisymmetric					
	D=0.6m	D=1.0m	D=1.5m	D=0.6m	D=1.0m	D=1.5m	D=0.6m	D=1.0m	D=1.5m
Pile-C	183	577	1326	369	1256	3123	102	118	136
Pile-E	162	450	976	369	1256	3123	128	179	220
Pile-F	135	335	661	369	1256	3123	173	275	372

N. The New Suggested Method for Predictions of NSF

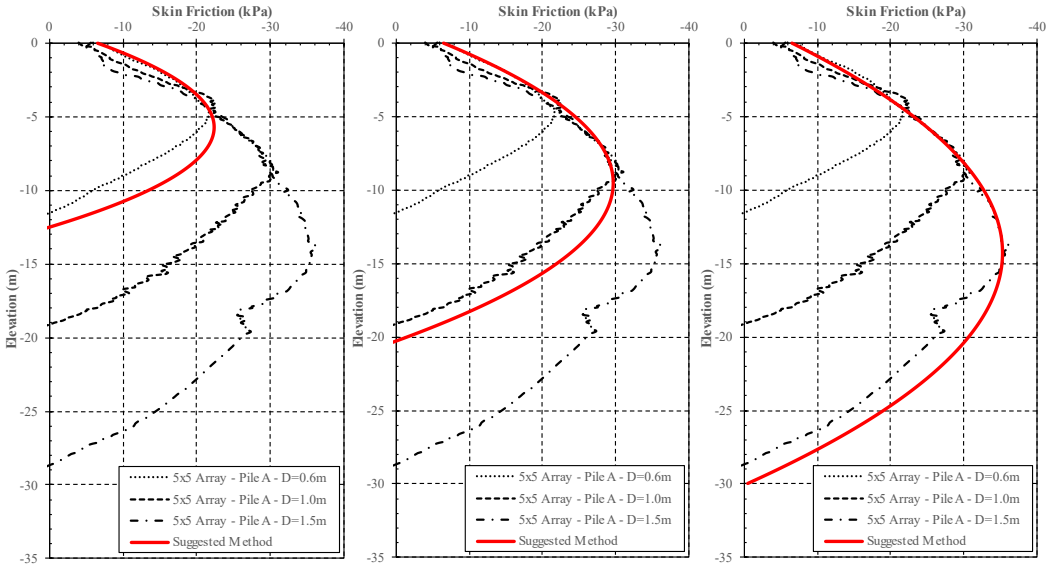

Figure A.89 Comparison of NSF between the suggested method and FEA results for three different pile diameters -Pile A, 5x5 array, s/D=3 and surcharge load of 100kPa.

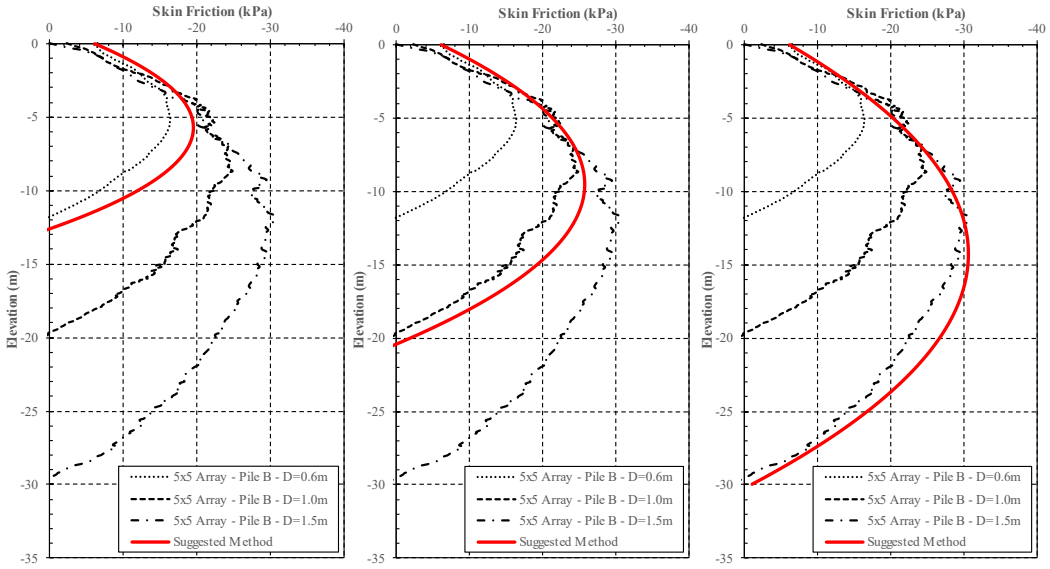

Figure A.90 Comparison of NSF between the suggested method and FEA results for three different pile diameters -Pile B, 5x5 array, s/D=3 and surcharge load of 100kPa.

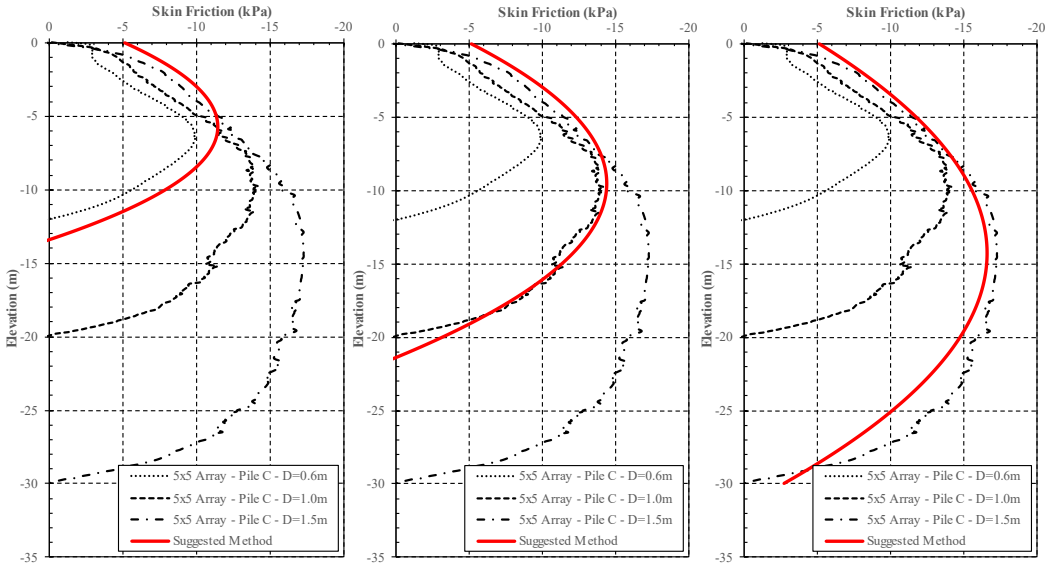

Figure A.91 Comparison of NSF between the suggested method and FEA results for three different pile diameters -Pile C, 5x5 array, s/D=3 and surcharge load of 100kPa.

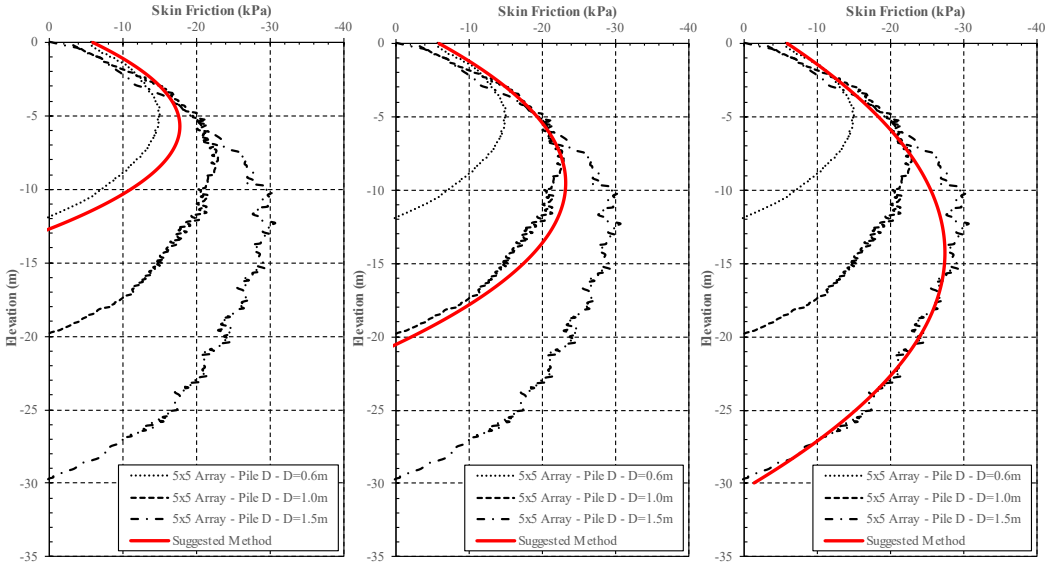

Figure A.92 Comparison of NSF between the suggested method and FEA results for three different pile diameters -Pile D, 5x5 array, s/D=3 and surcharge load of 100kPa.

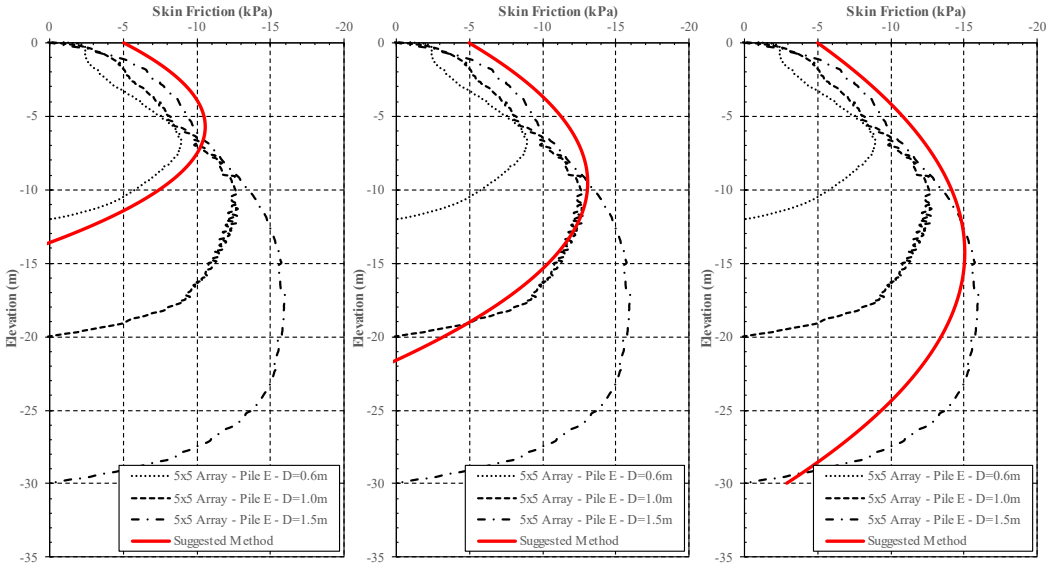

Figure A.93 Comparison of NSF between the suggested method and FEA results for three different pile diameters -Pile E, 5x5 array, s/D=3 and surcharge load of 100kPa.

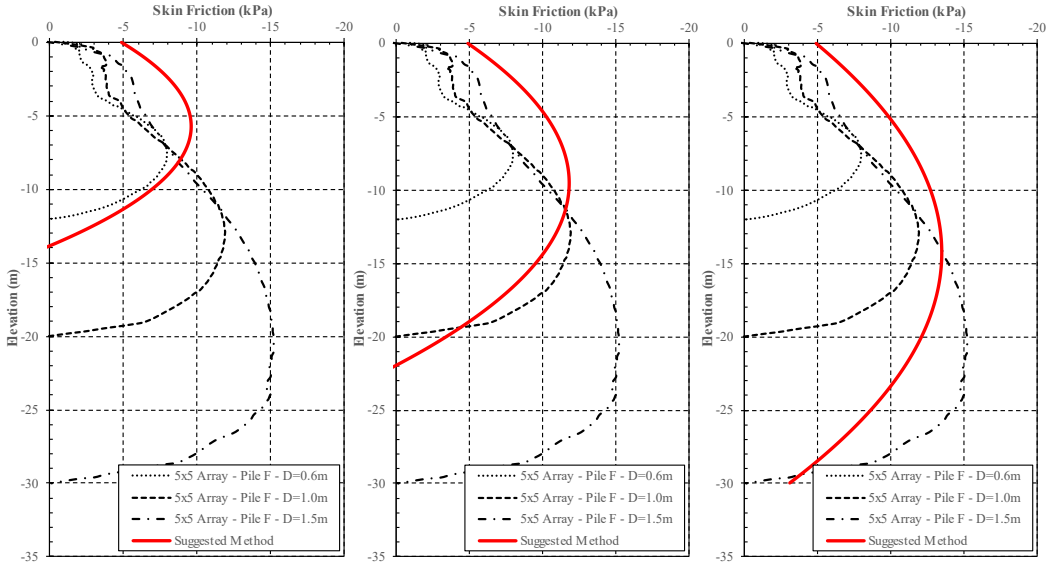

Figure A.94 Comparison of NSF between the suggested method and FEA results for three different pile diameters -Pile F, 5x5 array, s/D=3 and surcharge load of 100kPa.

Table A.7 Comparison of dragload forces for each pile position for three different pile diameters between the suggested method and FEA results, 5x5 array, s/D=3 and surcharge load of 100kPa.

Pile-#	Dragload (kN)						Percentile Difference(%)		
	FEA Results			Suggested Method					
	D=0.6m	D=1.0m	D=1.5m	D=0.6m	D=1.0m	D=1.5m	D=0.6m	D=1.0m	D=1.5m
Pile-A	300	1141	3113	373	1325	3479	24	16	12
Pile-B	251	1001	2804	331	1166	3046	32	16	9
Pile-C	142	620	1855	206	688	1747	45	11	-6
Pile-D	239	962	2823	303	1060	2758	27	10	-2
Pile-E	129	566	1714	192	635	1602	49	12	-7
Pile-F	114	509	1540	178	582	1458	56	14	-5

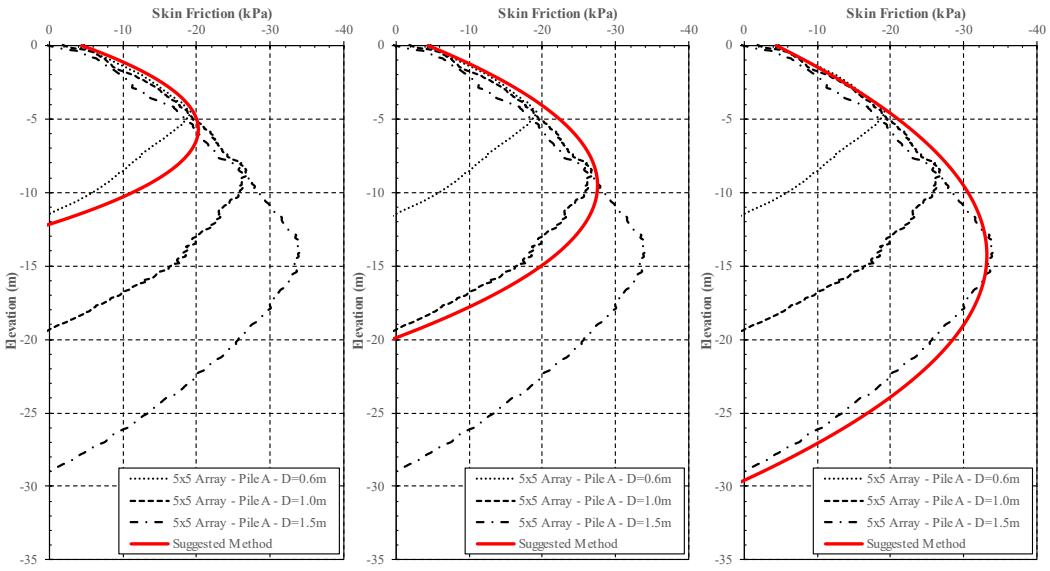

Figure A.95 Comparison of NSF between the suggested method and FEA results for three different pile diameters - Pile A, 5x5 array, s/D=6 and surcharge load of 50kPa.

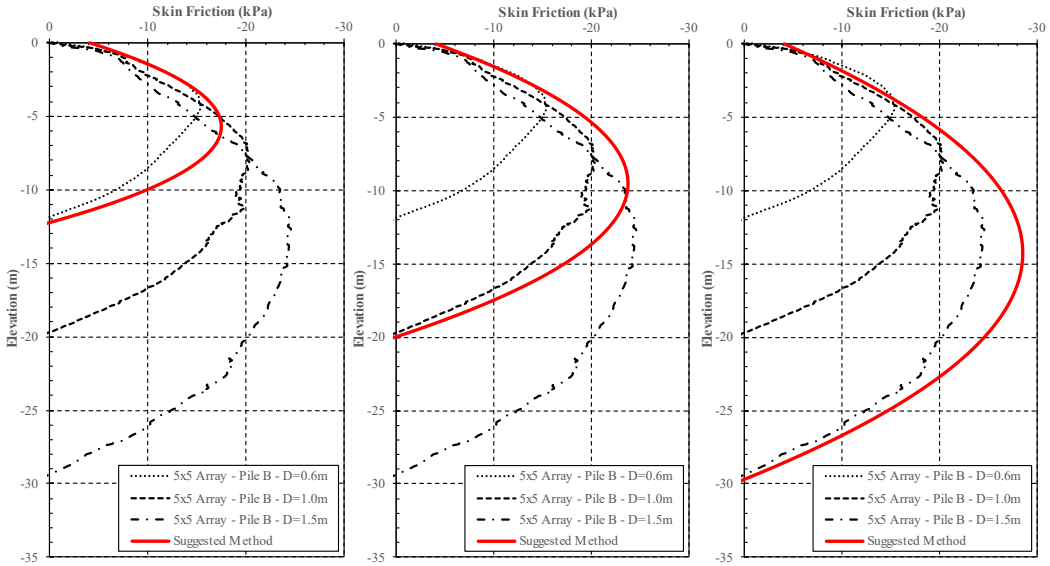

Figure A.96 Comparison of NSF between the suggested method and FEA results for three different pile diameters - Pile B, 5x5 array, s/D=6 and surcharge load of 50kPa.

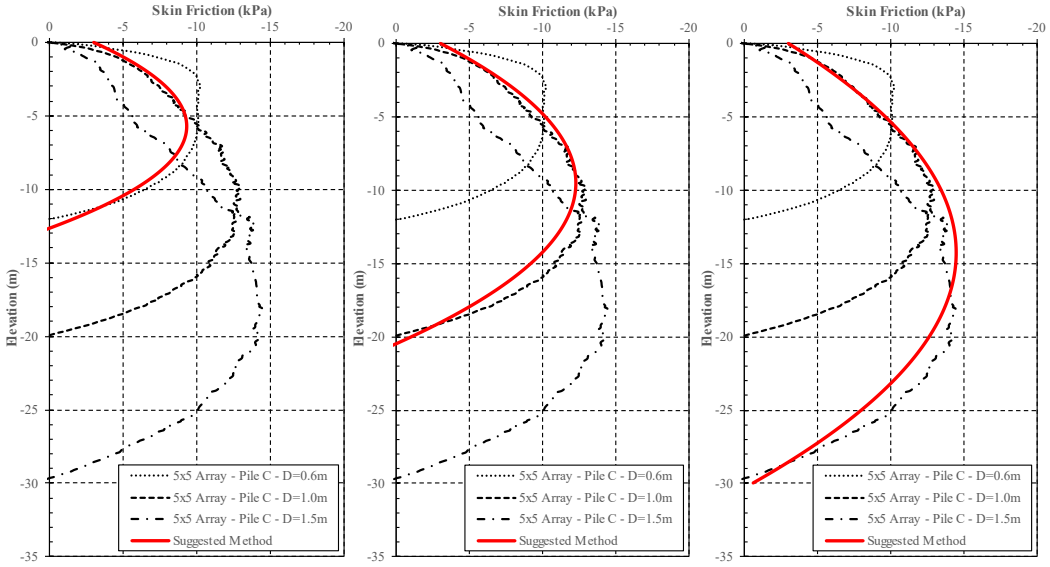

Figure A.97 Comparison of NSF between the suggested method and FEA results for three different pile diameters - Pile C, 5x5 array, s/D=6 and surcharge load of 50kPa.

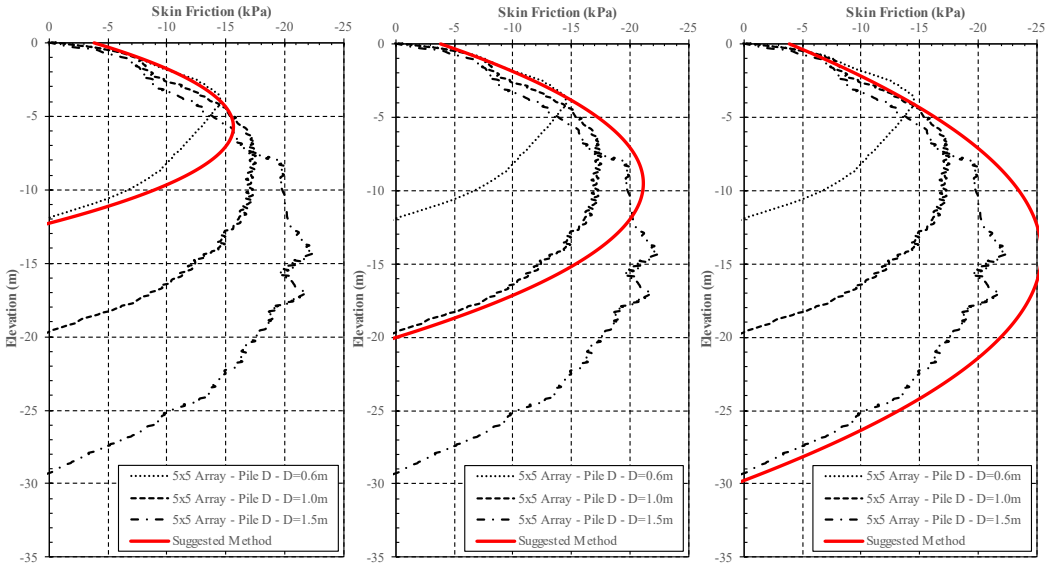

Figure A.98 Comparison of NSF between the suggested method and FEA results for three different pile diameters - Pile D, 5x5 array, s/D=6 and surcharge load of 50kPa.

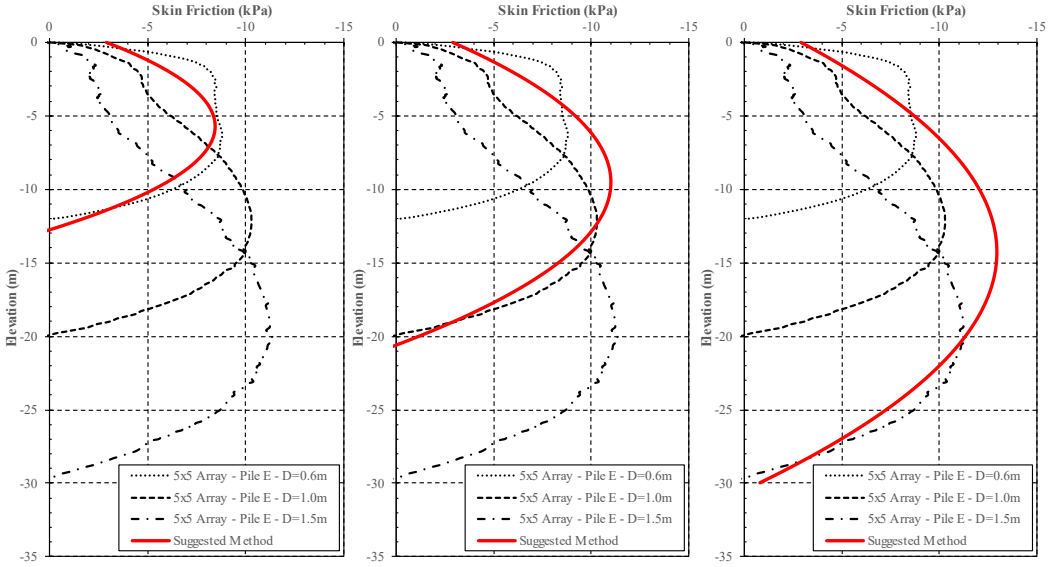

Figure A.99 Comparison of NSF between the suggested method and FEA results for three different pile diameters - Pile E, 5x5 array, s/D=6 and surcharge load of 50kPa.

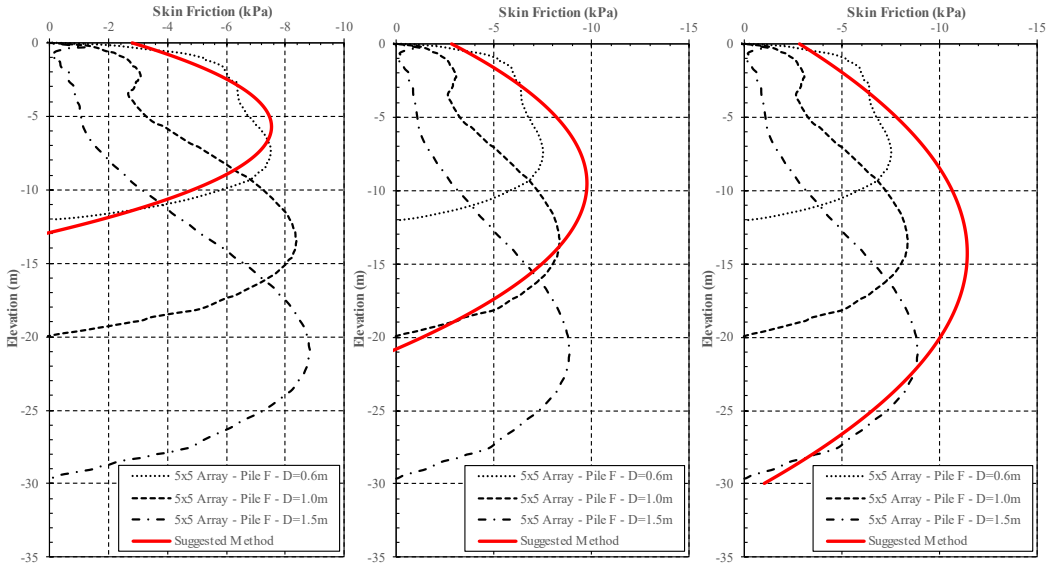

Figure A.100 Comparison of NSF between the suggested method and FEA results for three different pile diameters - Pile F, 5x5 array, s/D=6 and surcharge load of 50kPa.

Table A.8 Comparison of dragload forces for each pile position for three different pile diameters between the suggested method and FEA results, 5x5 array, s/D=6 and surcharge load of 50kPa.

Pile-#	Dragload (kN)						Percentile Difference(%)		
	FEA Results			Suggested Method					
	D=0.6m	D=1.0m	D=1.5m	D=0.6m	D=1.0m	D=1.5m	D=0.6m	D=1.0m	D=1.5m
Pile-A	250	1028	2868	325	1194	3184	30	16	11
Pile-B	230	864	2307	284	1035	2750	23	20	19
Pile-C	183	577	1326	159	556	1451	-13	-4	9
Pile-D	217	770	2022	256	928	2462	18	21	22
Pile-E	162	450	976	145	503	1307	-10	12	34
Pile-F	135	335	661	131	450	1162	-3	34	76